THE UNIVERSITY OF CHICAGO

TUMOR CELL SENESCENCE IN CANCER THERAPY

A DISSERTATION SUBMITTED TO

THE FACULTY OF THE DIVISION OF THE BIOLOGICAL SCIENCES

AND THE PRITZKER SCHOOL OF MEDICINE

IN CANDIDACY FOR THE DEGREE OF

DOCTOR OF PHILOSOPHY

COMMITTEE ON CANCER BIOLOGY

BY

YUE LIU

CHICAGO, ILLINOIS

MARCH 2022

TABLE OF CONTENTS

LIST OF FIGURES

LIST OF TABLES

ACKNOWLEDGEMENTS

I would like to sincerely thank my mentor Dr. Stephen J. Kron for being extensively engaged throughout the entirety of my Ph.D. Steve keeps open-minded and enthusiastic about almost all kinds of science. He encouraged me to find self-motivation and confidence in scientific research. He motivated me to take challenges in research and prepared me with the strategies to de-risk. He offered me opportunities to communicate and collaborate. Through the highs and lows of graduate school, Steve is always there and with me. I greatly appreciate Steve's effort in training me to become an honest, thoughtful, and independent scientific researcher.

I would like to thank all current and former members of the Kron Lab for creating a professional, collaborative, and friendly working environment. In particular, I would like to take this opportunity to thank the individuals who directly worked on the same projects as me: Elena V. Efimova, Joanna Pagacz, Ding Wu, Donald J. Wolfgeher, Aishwarya Ramamurthy, and Jacqueline Brinkman. Their thoughtful suggestions and expert assistance have benefited my projects tremendously.

I would like to thank my collaborators, Dr. Rick C. Betori and Dr. Grant B. Frost of the Scheit Lab at Northwestern University, for their generous support in developing the novel telomerase inhibitor NU-1. Their expertise in chemistry has greatly enriched my projects.

I would like to gratefully acknowledge my thesis committee, Professor Erin Adams, Wei Du, Akash Patnaik, and James Labelle for their time, insights, and support over the last five years.

I would also like to acknowledge the core facilities at the University of Chicago for the

technical support and scientific advice in the past several years. Special thanks to ni Solanki of the Animal Resource Center for assistance and suggestions with mouse works.

I would also like to thank my friends and family for their continued support and encouragement during my Ph.D. I am extremely grateful to people who helped bring joy to my life and/or to those I care about.

ABSTRACT

Cellular senescence refers to a state in which cells enter a permanent cell cycle arrest without undergoing cell death. Cells become senescent after being exposed to replicative, genotoxic, oncogenic, and/or oxidative stress. Senescence has long been considered a tumor-suppressive mechanism that prevents the malignant transformation and uncontrollable proliferation of cells carrying an unstable genome and/or activated oncogenes. Therapy-induced senescence (TIS), the induction of senescence in tumors through radiation and/or certain chemotherapy treatments, is thought to contribute to the anti-tumor effects of cancer treatments. Various mechanisms that induce tumor cell senescence are extensively examined in this thesis. I first demonstrated the DNA repair-independent role of DNA-PKcs and detailed how inhibition of DNA-PKcs accelerates senescence by resulting in persistent DNA damage foci and mitotic slippage in response to radiation. Then I explored the roles of telomerase catalytic activity in DNA damage response and senescence. According to the results, using a novel covalent TERT inhibitor NU-1 and the well-established antagonists BIBR-1532 and MST-321 to target telomerase catalytic activity enhanced cellular senescence by delaying end-joining repair of DNA double-strand breaks induced by radiation. In the syngeneic CT26 murine colon carcinoma tumor model, NU-1 did not affect the host or reduce tumor growth on its own, but it significantly enhanced activated immune infiltrate and exhibited immunogenic radiosensitization over radiation alone. This study points to TERT as an attractive target for overcoming intrinsic resistance to genotoxic therapy and potentiating anti-tumor immune response. In the next chapter, I discussed the possibility of using

senescent tumor cells as a cancer vaccine for controlling tumor growth and metastasis, including how the senescence vaccine synergizes radiation and immune checkpoint inhibitors. Senescent tumor cells have been shown to promote dendritic cell maturation/activation and T cell priming, thereby enabling dendritic cells activated by senescent tumor cells to serve as cancer vaccines for treating both local and metastatic tumors. This work may offer translational benefits from using senescent tumor cells to enhance anti-tumor immunity and improve cancer treatment. Paradoxically, a growing body of preclinical studies indicates that accumulated senescent cells in tumors may also promote tumor recurrence, metastasis, and resistance to therapy. The utilization of senolytics, a class of chemical compounds that specifically eliminate senescent cells, might be a promising approach to inhibit senescence-mediated detrimental effects. Senolytic compounds such as ABT263, a BCL-2 inhibitor, were commonly used following senescence induction in preclinical studies, referred to as the "one-two punch" strategy. Here, I demonstrated that senescent tumor cells induced by various inducers displayed varying sensitivity to ABT263-induced apoptosis. Interestingly, senescent cells displayed bystander effects, causing neighboring non-senescent cells to become more sensitive to senolytic treatment, whereas the degree of bystander effect was positively correlated with senescent cells' sensitivity to senolytic compounds. This work suggested that evaluating senescence hallmarks and/or manipulating therapy-induced senescence might be necessary to improve the efficacy of "one-two punch" cancer therapy.

LIST OF PUBLICATIONS

1. **Liu, Y.**, Efimova E. V., Ramamurthy, A., Kron, S. J. Repair-independent functions of DNA-PKcs protect irradiated cells from mitotic slippage and accelerated senescence. *Journal of cell science, 2019, 132: jcs-229385.*

2. Betori R., **Liu, Y.**, Mishra R. K., Cohen S. B., Kron, S. J., Scheidt, K.A. Targeted covalent inhibition of telomerase. *ACS chemical biology, 2020, 15.3: 706-717.*

3. Brinkman, J.*, **Liu, Y.***, Flor, A., Kron, S. J. Small-molecule drug repurposing to target DNA damage repair and response pathways. *Seminars in Cancer Biology, Academic Press, 2021, 68: 230-241. (* co-first authors)*

4. **Liu, Y.**, Betori R., Pagzac, J., Efimova, E.V., Wolfgeher, D. J., Wu, D., Cohen S.B., Scheidt, S.A., Kron, S. J. Targeting telomerase reverse transcriptase with the covalent inhibitor NU-1 confers immunogenic radiation sensitization. *Submitted, 2022*

CHAPTER 1

INTRODUCTION

This chapter consists in part of the following published manuscript:

J A Brinkman, Y Liu, S J Kron. Small-molecule drug repurposing to target DNA damage repair and response pathways. *Seminars in cancer biology*. 2020. 68: 230-241. PMID: 32113999; PMCID: PMC7483256; DOI: 10.1016/j.semcancer.2020.02.013

Brinkman and I collected references and made the tables together. I was responsible for making the figures, while the majority of the writing was done by Brinkman. All of the authors contributed to manuscript editing.

Cellular senescence was firstly discovered in vitro in the 1960s (1), which is known as replicative senescence, while it took another 30 years for researchers to eventually detect senescent cells in aged human tissue (2). In addition to replicative stress-induced telomere damage, senescence can be induced by oncogenic stresses and cancer therapeutic stresses, which may all converge on DNA damage signals to initiate the senescence program (Figure 1.1) (3). Senescent cells typically undergo irreversible cell cycle arrest and develop an enlarged and flattened morphology *in vitro*. Other common characteristics of senescence, both *in vitro* and *in vivo*, include the upregulated senescence-associated beta-galactosidase (SA-βgal) activity, elevated expression of cyclin-dependent kinase inhibitors, persistent DNA damage signals, and appearance of senescence-associated heterochromatin foci (Figure 1.1) (4-6). Although entering permeant growth arrest state, senescent cells remain metabolically active and release a plethora of bioactive proteins and extracellular vesicles, termed as senescence-associated secretory phenotype (SASP), reflecting one of the most critical features of senescence (Figure 1.1) (7, 8). Meanwhile, senescent cells are resistant to cell death mechanisms against such as apoptosis, allowing them to survive for long period and to be accumulated along with aging (Figure 1.1) (9-11).

Cellular senescence has been recently considered as one of the cancer hallmarks (12). Senescence has long been viewed as a tumor suppression mechanism due to the lack of proliferation capability (13), while cancer, on the contrary, can be viewed as the outcome of unlimited and controlled cell proliferation. In particular, the senescence driven by oncogenic stresses appears to be the initial barrier against complete malignant transformation and aberrant hyperproliferation (14). Cellular senescence is frequently detected in cancer after therapies and used to be considered a beneficial outcome of cancer therapies because of the limitation of

malignant progression. Meanwhile, senescent cancer cells have been reported to promote the immune surveillance of cancer cells (Figure 1.2). However, accumulated evidence reveals the detrimental effects of senescence in cancer progression (15). Pharmacological or genetic elimination of senescent cells delays and/or alleviates aging-related symptoms, including spontaneous tumorigenesis and cancer-associated death (9, 16, 17). In different experimental systems, senescent cells have been shown to stimulate malignant transformation, accelerate tumor growth, trigger cancer stemness, promote cancer metastasis, and suppress the anti-tumor immune response (Figure 1.2), most of which has been reported as hallmarks of cancer (18-21). The SASP has been considered the key player in mediating senescence-associated pro-tumor effects, which modulates tumor cells tumor microenvironment in an autocrine and/or paracrine manner and therefore supports the other hallmarks of cancer (7, 8, 12, 22, 23).

This chapter will discuss the complexity of cellular senescence, highlighting the recent discoveries illustrating the dual roles of senescence in the context of cancer and underlining that there is no universal description of senescence and its functions. The genetic background and the microenvironment of senescent cells must be carefully considered when conducting research in cellular senescence.

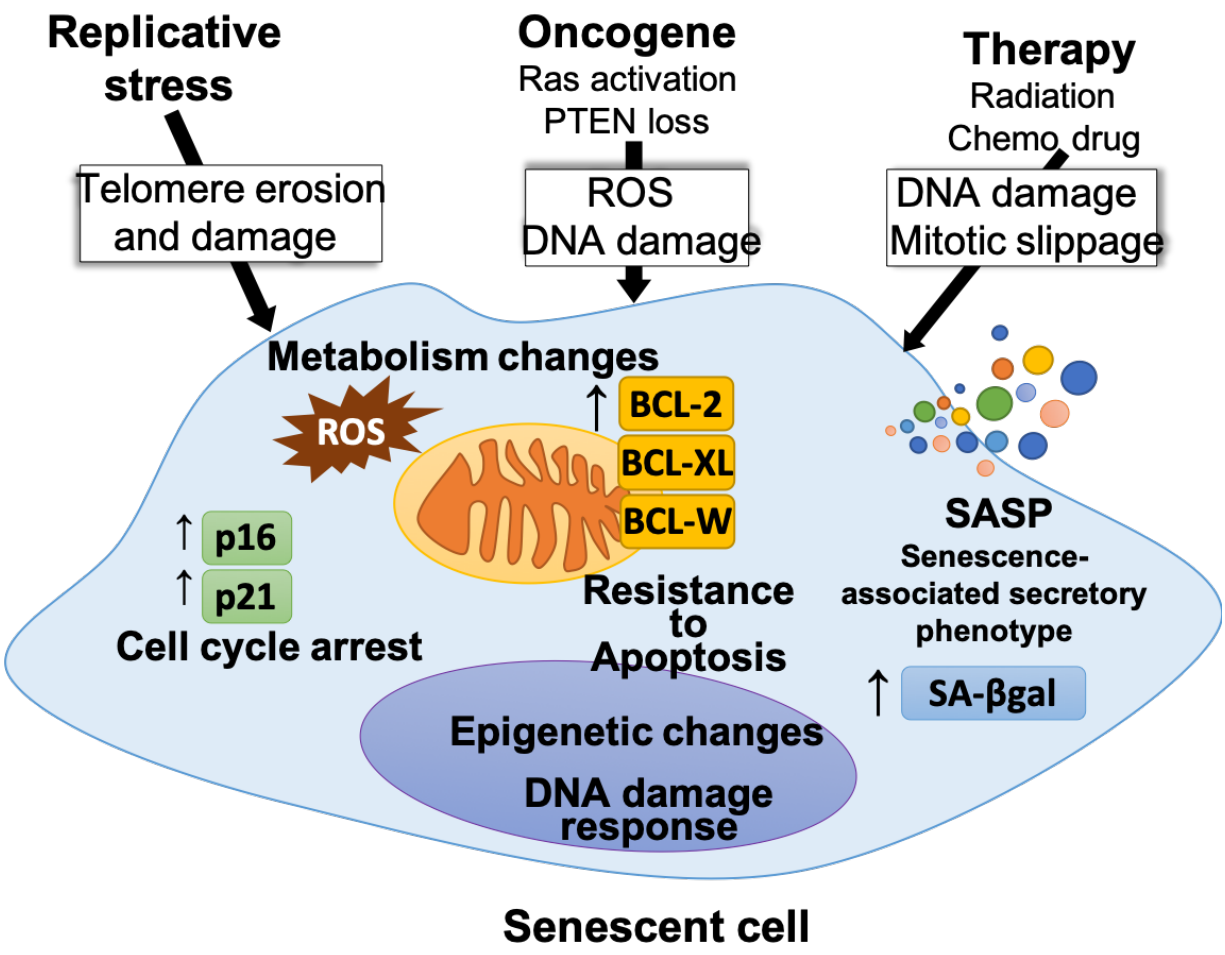

Figure 1.1: The induction and hallmarks of cellular senescence.
In a simplified model, cellular senescence is induced by replicative stresses, oncogenic stresses and therapeutic stresses including radio- and chemo-therapy. Most of these stresses will converge on DNA damage signals to initiate senescence program. Therefore, the persistent DNA damage response is generally detected in senescent cells. In culture, senescent cells usually develop enlarged and flattened morphology, representing a direct method to distinguish senescent cells from non- senescent cells. The upregulated activity of senescence-associated beta-galactosidase is widely used as a biomarker for cellular senescence both *in vitro* and *in vivo*. Another commonly use maker is senescence-associated heterochromatin foci (SAHF). Due to the stable cell cycle arrest, the cyclin-dependent kinase inhibitors, such as p16INK14A and p21CIP, are found to be increased in senescent cells. The accumulation of dysfunctional mitochondria and increased level of reactive oxygen species are often observed in senescent cells as well. Another critical features of senescence is the senescence-associated secretory phenotype (SASP), which is consisted of a wide spectrum of proteins and extracellular vesicles and plays critical roles in senescence associated effects. Meanwhile, senescent cells have developed apoptosis resistant mechanisms including upregulation of anti-apoptotic proteins (e.g., BCL2 family members) but downregulation of pro-apoptotic proteins.

1.1 Induction of cellular senescence (Figure 1.1)

1.1.1 Replicative senescence (telomere shortening and damage)

Replicative senescence is refers to the incapability of proliferation after multiple cell divisions (1). The mechanism of replicative senescence has been long ascribed to telomere shortening, one of the first and best characterized mechanisms of senescence induction (24). As most somatic cells lack the telomere maintenance machinery, such as telomerase expression or recombination of telomeres, telomeres shorten within each round of DNA replication. Below a certain length, the loss of telomere capping proteins and/or protective structures triggers a DNA damage response (DDR) that is very similar to that triggered by DNA double strand breaks (DSBs), leading to cell cycle arrest, and eventually cellular senescence (25). The mice with disrupted telomere maintenance mechanism, either through genetic knockout of telomerase reverse transcriptase (TERT) (26) or the RNA template (TR) (27), displayed shortened life span and progeria phenotype including progressive tissue atrophy, stem cell depletion, organ system failure and impaired tissue injury responses, which is associated with short dysfunctional telomere and increased endogenous DNA damage signaling.

1.1.2 Oncogene induced senescence (OIS)

Oncogene activation is a powerful inducer of cellular senescence. Oncogene induced senescence (OIS) was initially demonstrated in primary mammalian cells with overexpression of Ras in a p53 dependent manner (28) and was further shown to occur *in vivo* (29). Later on, other oncogenes, including mos,cdc6, and cyclin E, were described as senescence inducers, reinforcing the notion that OIS provides a barrier to malignant progression (30). The mechanisms of OIS have been linked to DNA damage signaling (30, 31). Indeed, Ras activation triggers DNA hyper-

replication that is intrinsically associated with replicative stress, leading to stalled replication forks (32) and rapid telomere attrition (33), which eventually engages DNA damage response and causes senescence. Moreover, oncogene-induced reactive oxygen species (ROS) which have been proposed to fuel cell proliferation also cause DNA damage, cell cycle arrest, and eventually cellular senescence (34, 35). The inactivation of tumor suppressors, such as PTEN, also induce cellular senescence (36, 37). Although initially it has been reported that PTEN loss induced senescence is independent of DNA damage but associated with enhanced p53 translation (36). Later on, it has been found that PTEN loss in protatic epithelial cells incudes DDR, leading to p53 stabilization, and cellular senescence (37).

1.1.3 DNA damage induced and therapy induced senescence (TIS)

Nuclear DNA damage is often considered as underlying mechanism of cellular senescence. The DNA damage response (DDR) is initiated through a kinase cascade, including ATM, ATR, CHK1, and CHK2. These signals converge on the tumor suppressor p53, whose activation will drive the expression of the cyclin-dependent kinase inhibitor p21 and p16. Both p21 and p16 play critical roles in mediating cell cycle arrest through interacting with CDK4 and/or CDK6. The cell cycle checkpoint is release once the DNA damage has been repaired. However, the irreparable DNA damage induces prolonged DDR and extended growth arrest in the form of cellular senescence (38). Inhibition of DDR signaling kinases such as ATM may allow senescent cells to re-enter the cell cycle (39).

Multiple DNA damaging agents, including radiation (ionizing and UV) and genotoxic chemical compounds, are able to induce this type of senescence. Senescence occurs after treatment with radiation and/or chemotherapies, which is termed as therapy induced senescence

(TIS) (18, 40). Many senescence-inducing therapies generate DNA single- and/or double-strand breaks on telomeres (41) or other region of chromosomes (42), displaying the close relationship between TIS and genotoxic stress (43). Although the DDR and its associated cell cycle checkpoint play a central role in TIS, TIS can be induced through other mechanisms. Targeting mitosis processes by inhibition of Aurora A kinase induces senescence in tumor cell regardless of p53 status (44). The reagents modifying epigenetic modification are also known to cause senescence, probably due to the alterations on chromosome structures. These reagents include histone deacetylase inhibitors (HDACIs) such as sodium dibutyrate (SDB) and trichostatin A (TSA) (45), and DNA methylases inhibitor such as 5-aza-2′-deoxycytidine (46). Due to the limitation of cancer cell proliferation, TIS supports anti-tumor effects and benefits treatment outcomes (47). However, the genotoxic therapies also induce senescence in other types of cells, including immune cells, which contributes to the adverse effects of cancer therapies (48, 49). In the meantime, accumulated evidence indicates that senescent tumor cells can promote to tumor relapse and metastasis (21, 49). Both beneficial and detrimental effects of TIS have been reported to be highly dependent on cell and tissue context and the senescence-associated secretory phenotype (SASP) (8, 50), which will be described in detail in the *SASP session*.

1.1.4 DNA damage induction and repair in general

An important consideration is that normal cellular DNA is under constant challenge initiated by exogenous and endogenous stresses that affect its integrity. Cellular respiration and resulting production of reactive oxygen species (ROS) along with other metabolic stresses may result in 10^4-10^5 DNA base and strand lesions per day per diploid genome. Environmental exposures such as ingested, absorbed or inhaled genotoxins add to this load. Topoisomerases

occasionally become trapped on cleaved DNA. Replication forks may mis-incorporate bases, leading to mismatch repair, or stall and collapse, leading to transient gaps and breaks. Normal cells are capable of activating adaptive pathways that resolve the vast majority of spontaneous DNA lesions without suffering mutations or aneuploidy. As such, drugs under development that dramatically added to endogenous damage levels by preventing cleansing of the nucleotide pool or markedly suppressed basal DNA repair, mediated principally by mismatch repair, base excision repair (BER), nucleotide excision repair (NER), single strand re-ligation and replication restart, might display toxicities such as myelosuppression, photosensitivity and/or carcinogenicity, preventing further clinical development. This constraint likely limits opportunities for repurposing to target base, nucleotide and single strand repair pathways.

Importantly, while cells must continuously contend with nucleotide, base and single strand damage, DNA double-strand breaks (DSBs) are far more rare and potentially lethal even in small numbers, as they result in aneuploidy, apoptosis, senescence and mitotic catastrophe. Exogenous stresses such as chemotherapy or ionizing radiation can induce complex DSBs characterized by chemical damage and strand gaps that prevents simple re-ligation. Indeed, a single clinical dose of radiation may yield fifty complex DSBs per cell. Cells express a network of hundreds of proteins involved in DSB detection, signal transduction and checkpoint arrest, DNA and chromatin modification along with the many enzymes that repair DSBs by diverse mechanisms that reflect the kind of damage and the availability of the sister chromatid as a repair template. This provides diverse targets for repurposing otherwise non-toxic drugs as sensitizers to genotoxic therapy. While several drugs appear to block multiple DNA repair pathways, many of these are DNA damaging on their own. As examples, diverse hedgehog pathway inhibitors such as mebendazole, itraconazole (non-specific) (51-53) and vismodegib (targeted) (54) appear

to block multiple DNA repair pathways and also modulate DNA damage checkpoint responses, although many of these effects might be linked to increased oxidative stress.

Mismatch repair

Colorectal and other cancers are commonly deficient for DNA mismatch repair (MMR) (55), leading to so-called microsatellite instability. While MMR deficient cells are commonly resistant to chemotherapy, their repair deficiency suggests potential for repurposing to exploit the resulting Achilles heel. The flavonoid natural product baicalein binds mismatches, producing toxicity in MMR deficient cells by inducing DSBs (56). Inhibition of dihydrofolate reductase (DHFR) with antifolates such as the chemotherapy agent methotrexate limits deoxythymidine biosynthesis, resulting in deoxyuracil mis-incorporation, genomic instability and cellular toxicity. The potassium-sparing diuretic triamterene has long been recognized as an anti-folate, mediating some of its side effects. MMR-deficient cells are specifically sensitized to triamterene, resulting in cell death due to DSBs (57).

Nucleotide excision repair

A recent cell based screen for drugs that prevent repair of UV-mediated DNA damage identified spironolactone, a potassium-sparing diuretic that blocks the effects of aldosterone, as a selective inhibitor of transcription-coupled nucleotide excision repair (NER) (58, 59). Thereby, spironolactone potentiates the effects of platinum chemotherapy agents by preventing removal of DNA adducts. The mechanism is ascribed to ubiquitin/proteasome-mediated degradation of XPB, a component of TFIIH. Strikingly, spironolactone appears to also block homologous recombination DSB repair (60), potentially reflecting impacts on transcription. The resulting block to DNA damage response appears to selectively target cancer cells and, more specifically, cancer stem cells (61).

Interstrand crosslinks

Multiple DNA repair mechanisms can recognize and repair the interstrand cross-links (ICLs) induced by platinum chemotherapy agents, but this is a particular responsibility of the multi-subunit Fanconi Anemia (FA) pathway (62). Like DSBs, ICLs are comparatively rare, making their repair an attractive target for repurposing. Cell-based screens (63, 64) identified small molecules that block FANCD2 foci formation, a reporter of FA pathway activation. Hits included the polyphenol natural product curcumin, with the caveat that this is a common pan-assay interference compound (65), but also the PI3K kinase inhibitor wortmannin, the PKC inhibitor H-9, and CDK inhibitor alsterpaullone, the HSP90 inhibitor 17-AAG, the cathepsin B inhibitor CA-074-Me, and the proteasome inhibitor bortezomib, each appearing to sensitize cells to cisplatin by blocking FA pathway function.

End joining repair of DSBs

The primary pathway for DSB repair throughout the cell cycle is re-ligation by Ku protein-dependent, conventional non-homologous end-joining (NHEJ) (66). Relying primarily on the relatively precise NHEJ pathway, it can take less than an hour for half of the DSBs induced by a dose of ionizing radiation to be rejoined. Then along with conventional NHEJ, remaining DSBs may be repaired by slower, Ku-independent pathways dubbed alternative, backup or microhomology mediated end-joining (MMEJ) (67) and/or single strand annealing that process and ligate free ends.

How the chromatin context of DNA damage impacts its repair remains poorly understood, but a wide range of epigenetic drugs have been found to slow overall DSB repair, suggesting opportunities for repurposing. Many drugs that target chromatin assembly or remodeling and/or inhibit enzymes that mediate histone acetylation, methylation,

phosphorylation, ubiquitylation, sumoylation or removal of these modifications appear to impact DSB repair (68, 69). Though often ascribed to altered expression of DNA repair genes, some of the effects are likely direct as the targets include chromatin modifiers that localize to and/or are active at DSBs. As examples, targeting PRC1/2 polycomb repressive complexes with ubiquitin ligase inhibitor PRT4165 for the PRC1 catalytic subunit BMI-1 (70, 71), or GSK126 and BRD4770 methyltransferase inhibitors for PRC2 catalytic subunits EZH2 and EHMT2/G9a, respectively (71), blocks end-joining DSB repair. Suggesting additional complexity, the fluoroquinolone antibiotic enoxacin was shown to enhance NHEJ at the expense of HR by promoting accumulation of damage-related lncRNAs and, thereby, 53BP1 at DSBs by stimulating DICER (72).

Despite its key role throughout the cell cycle, there have been surprisingly few efforts to apply repurposing to suppress NHEJ repair. A cell-based screen of repurposing libraries for drugs that could delay DSB repair after irradiation (73) identified dozens of existing drugs, natural products, and cellular metabolites, though specificity to NHEJ, MMEJ or other repair mechanisms was not determined. Of 18 hits selected for low toxicity, chemical diversity and distinct bioactivities, 17 displayed radiosensitization in mice bearing transplanted tumors (74). Choosing representative hits for further analysis, the beta-lactam antibiotic cephalexin, calcium channel blocker nisoldipine, antidepressant trazodone, and HMG-CoA reductase inhibitor pitavastatin each demonstrated a dramatic delay in DSB repair (74, 75). In the case of pitavastatin, the mechanism was linked to reduced protein farnesylation, a downstream effect of blocking HMG-CoA reductase. In the clinic, targeting NHEJ may have value in reducing resistance to genotoxic therapy. Among mechanisms for radiosensitization by the EGFR

inhibiting antibody cetuximab may be reduced DSB repair, potentially mediated by cytoplasmic sequestration of the NHEJ regulatory kinase DNA-PKcs (76, 77).

Though NHEJ is fast and often precise, MMEJ will leave behind a small insertion or deletions (indel). In CRISPR/Cas9 genome editing, the targeted DNA breaks often result in indels rather than completing site-directed mutation via homology-directed repair (HDR) from an artificial template. Thus, there has been considerable interest in suppressing end-joining to favor HDR, leading to efforts to prolong S and G2 or directly target known end-joining factors (78). A screen for increased HDR identified the β3-adrenergic receptor agonist L755507 and the ER-to-Golgi transport inhibitor brefeldin A (79). Among other modulators, the natural product flavonoid resveratrol (80) has also been reported to increase the HDR/indel ratio.

Homologous recombination (HR) and HR deficiency

In S phase or G2, the sister chromatid provides a precisely matched repair template enabling DSB repair by homologous recombination (HR) (81). NHEJ is suppressed and DNA resection is induced on at least one free end. The exposed single strand assembles a RAD51 nucleofilament that searches the repair template for homology, and then serves as primer. The resulting D loop resolves and the newly replicated strand binds to the complementary sequence on the other free end, catalyzing rejoining.

Homologous recombination deficiency (HRD) is common in cancer, associated with mutations in HR genes such as RAD51, Fanconi Anemia genes, DNA damage signaling genes, or regulators like BRCA1 and BRCA2 (82). The loss of HR repair appears to shift the repair balance toward the error-prone rejoining mechanisms. Most efforts to leverage HRD as an Achilles heel (aka synthetic lethality) have used targeted agents directed at error-prone end-joining repair factors such as poly(ADP-ribose) polymerase (PARP) or Polymerase θ (Polθ) (83).

Leveraging the synthetic lethality strategy, PARP inhibitors have recently been approved to target the HRD phenotype of BRCA1 or BRCA2 mutated tumors (83, 84). However, repurposing also offers an attractive path to synthetic lethality with HRD.

Along the HR pathway from resection to resolution, RAD51 has been the major target for both *de novo* drug development (85) and repurposing. RAD51 expression is significantly decreased by histone deacetylase inhibitors such as suberoylanilide hydroxamic acid (SAHA or vorinostat) (86), conferring PARP inhibitor sensitivity (87, 88). BET bromodomain inhibitors such as JQ1 similarly decrease expression of BRCA1 and RAD51 (89, 90), thereby enhancing effects of PARP inhibition. Targeting RAD51 function, CDK1/2 inhibitor dinaciclib can block the assembly of RAD51 nucleofilaments to reduce HR (91). The mTOR inhibitor rapamycin has a similar effect (92). The HSP90 inhibitor ganetespib destabilizes BRCA1, BRCA2 and RAD51, sensitizing cells to PARP inhibitors (93). The AKT inhibitor perifosine targets the deubiquitinase UCHL3, increasing RAD51 degradation and sensitizing cells to PARP inhibitors (94).

1.1.5 Cellular response to DNA damage other than cellular senescence

Early events in the signal transduction pathway that senses DNA damage and triggers an organized response are mediated by the PI3K related family of protein kinases (PIKKs) ATR, ATM, and DNA-PKcs that serve overlapping roles in DNA damage recognition and signaling (95-98). Small-molecule kinase inhibitors targeting one or more of these enzymes have largely failed on their own as cancer drugs, but remain under evaluation in combination with genotoxic agents including radiotherapy. The methylxanthine alkaloid caffeine long known to block DNA repair and cell cycle arrest after DNA damage was eventually identified as a weak ATM, ATR (99) and DNA-PKcs (100) inhibitor. A second radiosensitizer that blocks DNA-damage induced

cell cycle arrest, the protein kinase C inhibitor UCN-01 (7-hydroxystaurosporine), was found to inhibit CHK1 (101).

The tumor suppressor p53, the gene most commonly mutated in cancer, is a key signal transducer mediating the response to DNA damage. ATM-dependent DNA damage signaling stabilizes p53, inducing gene expression that impacts DNA repair, cell cycle checkpoint arrest in G1 and G2/M, metabolism, oxidative stress, apoptosis, autophagy, and cellular senescence. Drug screens to reactivate, stabilize or block p53 have identified diverse novel molecules but repurposing efforts have lagged behind. However, repurposed drugs that target one or more p53 effector pathways are well described, as detailed in the following:

Apoptosis

Activation of p53 promotes apoptosis by several mechanisms, principally via inducing pro-apoptotic BH3-only proteins and apoptosis effectors along with sensitization to apoptotic signaling (Figure 1.3). Adjusting the apoptotic threshold can potentiate or counter activated p53 to modulate cell death. The HIV protease inhibitors (HPIs) are well-tolerated peptidomimetics that inhibit the HIV aspartyl protease, a retroviral enzyme that is necessary for viral particle production (102). HPIs such as nelfinavir, have been shown to downregulate the PI3K-Akt pathway as well as cause radiosensitization *in vivo* (103). *In vitro* implicate decreased Cyclin D1 and CDK4, inducing cell cycle arrest and ultimately apoptosis (104, 105).

Opposing p53, nuclear factor-kappa B (NF-KB) transcription factors regulate genes which participate in DNA damage responses to promote cell survival. As such, diverse small molecules that target NF-KB, ranging from nutraceuticals to approved drugs, also affect DNA-damaged induced apoptosis (106, 107). As an example, the proteasome inhibitor bortezomib can

suppress degradation of IKBα, reduce radiation-induced NF-KB activity and promote apoptosis (108-110).

The janus kinases (JAKs) are cytosolic tyrosine kinases linked to signaling receptors like G-protein coupled receptors and cytokine receptors that activate the signal transducer and activator of transcription (STAT) family transcription factors to alter gene expression (111). The STAT3 transcription factor is a well-known anti-apoptotic factor and cells deficient in STAT3 have reduced activity of the ATM-Chk2 and ATR-Chk1 pathways (112). The Bruton's tyrosine kinase (BTK) inhibitor ibrutinib and the JAK inhibitor ruxolitinib are radiosensitizers (113, 114), presumably by targeting this pathway. Ibrutinib blocks STAT3 activation (113, 115) and may chemosensitize cells to cisplatin via JAK2 inhibition (116). Targeting the JAK/STAT pathway with ruxolitinib enhances apoptosis in cells treated with cisplatin (117).

Autophagy

Autophagy is considered a target (and feedback regulator) of p53 that modulates DNA repair and survival after DNA damage (Figure 1.3). Along with other phenothiazines, the dopamine antagonist trifluoperazine (TFP) is a common hit in repurposing screens, including studies of chemo- and radiosensitizers. Among diverse mechanisms that have been proposed, TFP may impair autophagy, potentially linked to blocking calmodulin signaling (118-120). Autophagy may be a common target of the anti-psychotics (121). Although connections to DNA damage response are complex and indirect, potentially conflating cell survival with DNA repair, autophagy has been considered an attractive target to enhance genotoxic therapy (122-124). In turn, the very broad range of natural products and existing drugs that have been recognized as autophagy modulators (125-127), provides a rich source of candidates for repurposing to sensitize cancer cells to radiation and/or chemotherapy.

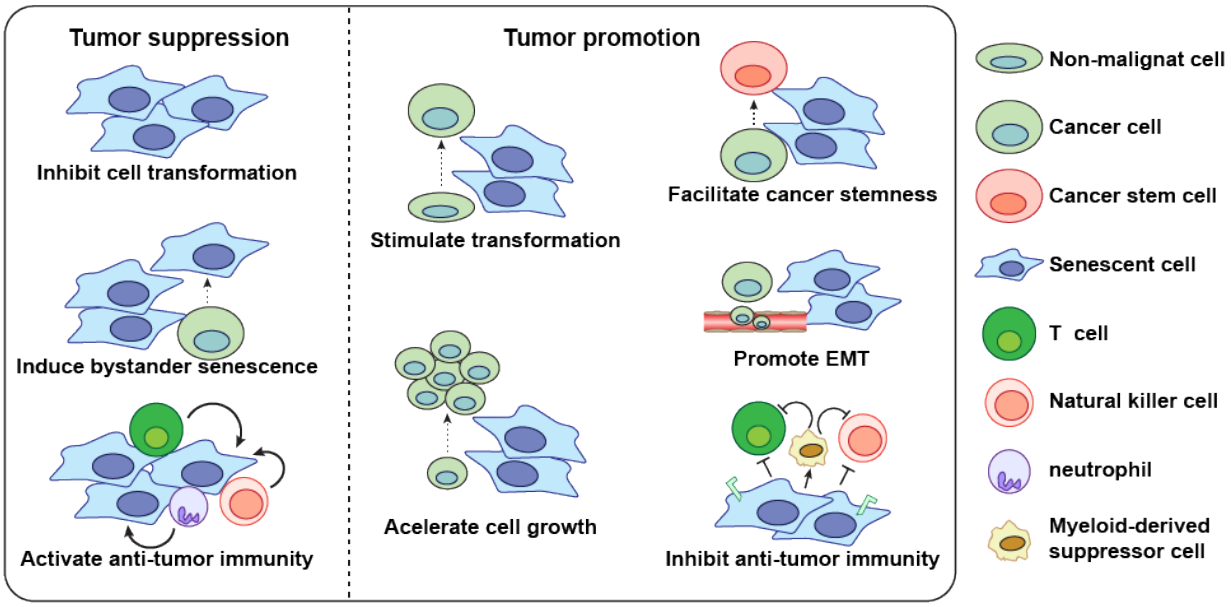

Figure 1.2: The effects of cellular senescence in cancer progression.
Senescent cells paly both beneficial and detrimental roles in tumor progression. The oncogene induced senescence has been considered a tumor barrier due to the irreversible growth arrest, preventing the fully transformation of pre-malignant cells. While senescent cells display the cell-autonomous self-reinforcement impacts, they also trigger their neighboring cells into senescence stage through paracrine effects, termed as bystander senescence or paracrine senescence. Meanwhile, senescent cells promote the recruitment and activation of both innate and adaptive immune cells, including NK cells, neutrophils, and T cells, through SASP-dependent or -independent signaling pathways. However, senescent stromal cells have been reported to promote cell transformation and cancer cell proliferation through SASP. Senescent cells also contribute to cancer metastasis through multiple mechanisms, including promoting cell migration, facilitating EMT, accelerating angiogenesis and etc. The SASP factors are associated with cancer cell reprogramming as well, leading to therapy resistance. The chronic inflammatory microenvironment created by senescent cells is associated with the upregulation of immune suppressors but downregulation of effector cells, causing the inhibition of anti-tumor immune response.

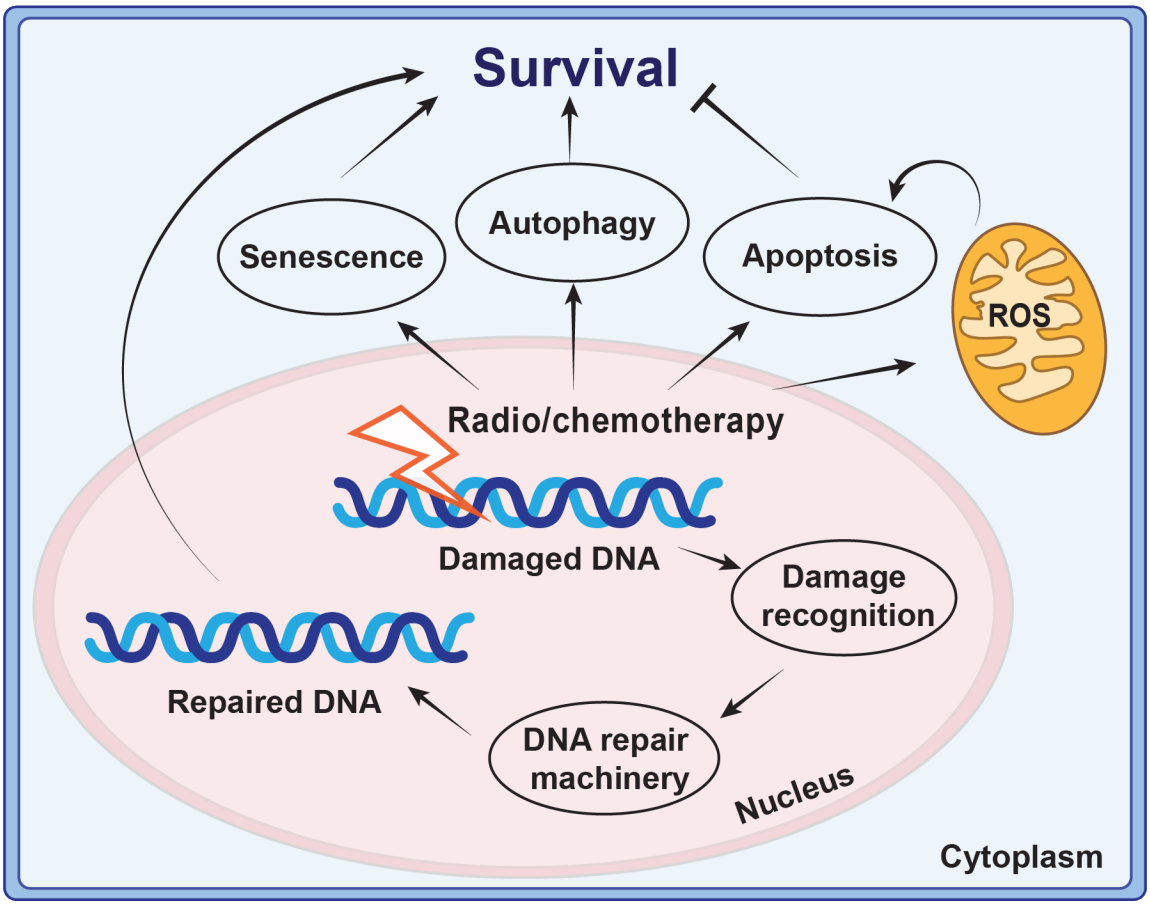

Figure 1.3: Overview of DNA repair and response pathways in cancer cells.
DNA single-strand and double-strand breaks occur when a cell is exposed to genotoxic stress like radiation or chemotherapy. This damage initiates a series of signaling pathways which aim at damage recognition and DNA repair. Simultaneously, the damaged DNA initiates a signaling cascade, ultimately increasing reactive oxygen species (ROS) and promoting apoptosis, or activating autophagy and senescence as a survival mechanism. Cancer cells exhibit resistance to DNA damage driven cell death through the enhancement of DNA damage repair mechanisms. Additionally, these cells are particularly adapted to genotoxic environments by adopting additional resistance mechanisms exploited post-DNA damage including the upregulation of anti-apoptotic signals.

1.2 Hallmarks of cellular senescence (Figure 1.1)

1.2.1 DNA damage response (DDR)

Senescent cells are associated with stable DNA damage response (DDR), which is frequently detected though the staining of phosphorylated histone H2AX (γH2AX), p53-binding protein (53BP1 or TP53BP1), and ATM (38). DDR can be initiated by a variety of DNA damaging stimuli such as radiation and chemotherapy drugs as described above (128). The intrinsic factors that induce DDR include DNA replication errors and replication folk collapse during S phase. The oncogenic stress induced upregulation of reactive oxygen species causes DNA damage probably through disrupting normal DNA replication (31). Telomeric damage due to serious attrition is detected in replicative senescence (25), while DNA damage foci on non-telomeric regions are also persistent in many senescent cells. The unrepaired DNA double strand break (DSB) is one of the powerful triggers for DDR, which has been demonstrated in both senescent cells in culture and tissues from aging animals (129). In certain senescent cells, the DNA damage foci are also observed on undamaged chromatin, which is probably due to unleashed ATM activity (130). One of the major substrates of DDR signaling cascade is p53, which can be phosphorylated on multiple serine sites by the kinases involved in DDR, such as ATM, CHK1 and CHK2. The phosphorylation of p53 leads to a decrease in its binding affinity of the E3 ubiquitin ligase MDM2, and therefore enhancing p53 level in cells (128). The transcription activity of p53 plays important roles in mediating and reinforcing senescence phenotype (131), including $p16^{INK4a}$/$p21^{CIP}$ driven cell cycle arrest. The phosphorylation on CDC25 by CHK1 downregulates its activity and blocks G2-M transition, leading to G2 cell cycle arrest (132). The other signals that can be regulated by DDR include NF-κB, STING, MAPK,

and STAT signaling pathways, which are essential for other senescence features in addition to controlling cell cycle (133, 134).

1.2.2 Cyclin-dependent kinase (CDK) inhibitor and cell cycle arrest

One commonly used marker in senescence detection is the expression level of cyclin dependent kinase inhibitors, including $p16^{INK4a}$ (encoded by *CDKN2A*) and $p21^{CIP}$(encoded by *CDKN1A*) (135). $p16^{INK4A}$ is considered as a senescence marker due to its capability in selectively inhibiting cyclin D-dependent protein CDK4 and CDK6, and therefore inducing cell cycle arrest (136, 137). The expression of $p16^{INK4A}$ is highly dynamic according to cell cycle stages . Interesting, it was found that $p16^{INK4A}$ is highly expressed in tissues under certain stresses such as wounding and aging, but is generally absent in unstressed, healthy and young tissues (138). Indeed, elimination of $p16^{INK4A}$ positive senescent cells delays age related pathologies and extends life and/or health span in INK-ATTAC mice (139). An alternate reading frame protein product of the CDKN2A gene is $p14^{ARF}$ in human, or $p19^{ARF}$ in mouse, which shares exons 2 and 3 with $p16^{INK4A}$ (140). It has been reported $p19^{ARF}$ expression triggers senescence in mouse fibroblasts (137). Although the exact contribution of ARF in cellular senescence is still puzzling, one possible mechanism is that ARF mediates cell cycle though directly binding to MDM2 protein and therefore promoting p53-mediated gene transcription (141, 142). Under certain circumstances, another INK4 family member, $p15^{INK4B}$, encoded by *CDKN2C*, compensates for the function of $p16^{INK4A}$ (143). In prostate cancer cells, the expression of $p15^{INK4B}$ is mediated Akt signaling and is necessary for androgen induced senescence (144).

The expression level of $p21^{CIP}$ is also found to be increased in response to senescence stimuli (145). Although it is able to inhibit all cyclin/CDK complexes, $p21^{CIP}$ confers G1 cell

cycle arrest mainly through blocking the activation of both cyclin E/CDK2 and cyclin A/CDK2 in a p53 dependent manner after ionizing radiation (146). Expression of $p21^{CIP}$ can be also induced by p53 independent signaling pathways, including stress associated TGF-β, Rb, and integrin, while these signals converge on the recruitment of Sp1/Sp3 transcription factor to the p21 promoter (147). Unlike $p16^{INK4A}$, the level of $p21^{CIP}$ is dynamically changed in senescent cells, making $p21^{CIP}$ a controversial marker for cellular senescence. By contrary, p21 stabilizes and promotes active cyclin–CDK complex formation in a dose-dependent manner, which is required for cell proliferation (148). Human fibroblasts lack $p21^{CIP}$ are able to develop senescent morphology even with damaged G1 cell cycle checkpoint (149). These scenarios indicate that $p21^{CIP}$ might be critical in the initial of cellular senescence by inducing G1 cell cycle arrest, but it is not necessary for maintaining senescence phenotype, which suggests that $p21^{CIP}$ upregulation may not be a reliable marker for cellular senescence.

1.2.3 Chromatin and nuclear changes

The alterations of chromosome structures and epigenetic modifications are commonly observed in senescent cells. Senescence-associated heterochromatic foci (SAHF), visualized by large nucleolus and punctate DNA foci after DAPI staining, is a distinct heterochromatic structure associated with stable gene repression, particularly for E2F targeted genes (150). This feature is mostly observed in oncogene induced human cell senescence in a ATR dependent manner, but is not detected in replicative senescence or in mouse cells (135, 151). The formation of SAHF requires histone chaperone proteins ASF1A and HIRA (152). Signaling pathways such as retinoblastoma (Rb) and NOTCH-HMGA1 axis are essentials mediators for SAHF and its associated chromatin architecture (150, 153). The chromatin changes in senescent cells are

closely correlated with senescence-associated gene expression. Histone H3K9 mono- and di-methyltransferases G9a and GLP were found to be downregulated in senescent cells through DDR induced activation of APC/C (Cdh1) ubiquitin ligase and proteasome degradation, causing a global decrease in H3K9 di-methylation that benefits the expression of IL-6 and IL-8, two major players of senescence-associated secretory phenotype (SASP) (154). Histone acetyltransferase p300 induces a dynamic hyper-acetylated chromatin state and drives a senescent-specific gene expression program (155). The recruitment of chromatin reader protein BRD4 to senescence activated super-enhancers controls SASP expression and its downstream paracrine signaling (156). Except for chromatin modifications, DNA methylation at promoter CpG islands in senescent cells changes into a pattern which contributes to protecting cells from transformation (157).

Another common feature of senescent cells is loss of Lamin B1, a key component in building up nuclear inner membrane (158, 159). The reduction of Lamin B1 in senescent cells has been linked with the large scale changes of chromatin, including the spatial re-localization of H3K9me3 positive heterochromatin into SAHF (160) and the redistribution of both H3K4me3 and H3K27me3 marks (161), suggesting a direct mechanism for global transcriptome alteration. Down-regulation of Lamin B1 also is associated with nuclear envelope instability, which facilitates the releasing of cytoplasmic chromatin fragments (CCFs) (162). Theses CCFs activates cytosolic DNA-sensing cyclic GMP-AMP synthase linked to stimulator of interferon genes (cGAS-STING) pathway and therefore enhancing SASP and inflammation (163).

1.2.4 Accumulation of dysfunctional mitochondria

Mitochondrial dysfunction has been described as a feature of cellular senescence (164). Mitochondria fission proteins Fis1 and Drp are downregulated in senescent cells, leading to the disruption of fission and fusion dynamic. The hyper-fused mitochondria, at least partially, explains the mechanism for its changes in morphology and function (165). Another driver for the increased dysfunctional mitochondria is the decreased turnover of mitochondria, term as mitophagy, in senescent cells (166). The dysfunctional mitochondrial is associated with increased level of reactive oxygen species (ROS) (167), which might the key driver of replicative senescence (168). Indeed, mitochondria depletion prevents senescence both *in vitro* and *in vivo* (169). The mitochondrial dysfunction-associated senescence (MiDAS) displays a distinct SASP pattern through the suppression of NF-κB activity and loss of IL-1 signaling loop (170), suggesting that mitochondria dysfunction can also contribute to the other feature of cellular senescence.

1.2.5 Resistance to apoptosis

Many stimuli leading to cellular senescence can also triggers apoptosis (9). It has been long observed that senescent human fibroblasts are resistant to undergo p53 dependent apoptosis (171). Upon apoptosis stress, the level of anti-apoptotic protein Bcl-2 in senescent cells fails to be downregulated, providing the direct mechanism for apoptosis resistance (172). The chromatin immunoprecipitation studies demonstrated remarked upregulation of H4K16 acetylation but depletion with H4K20Me3 on the *Bcl-2* gene with H4K16Ac in senescent fibroblasts, justifying the high level of BCL2 protein. BAX, a pro-apoptotic BH-3 protein, is regulated in the opposite way (173). Other members of BCL2 family proteins, particularly BCL-W and BCL-XL, are also

upregulated in replicative senescence (174) and oncogene induced senescent cells (175). Other than BCL2 family members, FOXO4 is upregulated in senescent cells and restrains p53 dependent apoptosis (176). The CDK inhibitor p21 suppresses NF-κB activation and the downstream JNK- and caspase signaling (177). The heat shock protein 90 (HSP90) contribute to cell survival through stabilizing PI3K/AKT signals (178). Other pro-survival proteins in senescent cells include Eephrins (EFNB1 or 3), PI3Kδ, and plasminogen-activated inhibitor-2 (PAI-2) (179). Many senolytic drugs, which are used to specifically eliminate senescent cells, have been designed based on targeting the mechanisms for apoptotic resistance (175, 178-180).

1.2.6 Senescence-associated secretory phenotype (SASP)

Although senescent cells are arrested in cell cycle, they remain metabolically active. Cells undergo senescence display hyper secretory phenotype, which is termed as senescence-associated secretory phenotype (SASP) or senescence messaging secretome (SMS). The SASP confers autocrine and paracrine effects on senescent cells themselves and their microenvironment, and is considered an important feature of cellular senescence. The SASP is consisted of a wide range of bioactive factors, including numerous soluble signaling molecules such as cytokines, chemokines, growth factors, proteases, lipids, extracellular components, matrix metalloproteinases (MMP), and even nucleic acid. Many soluble proteins can be directly secreted into extracellular environment, while the proteins synthesized as transmembrane precursors require ectodomain shedding to be converted into soluble counterparts. Enzymes such as metalloprotease A disintegrin and metalloproteinase 17 (ADAM17) are increased and responsible for the cleavage and releasing of the transmembrane proteins in many senescent cells (181, 182). In addition, proteins enclosed in exosome-like extracellular vesicles were also reported as components in SASP, which are important mediators of cell proliferation (183).

The expression of SASP is associated with stress response in senescent cells. Consistently, senescent cells driven by ectopic expression of $p16^{INK4A}$ or $p21^{CIP}$ appear not to express SASP, although display other features of cellular senescence (184). Persistent DDR signaling is necessary for the expression of several SASP factors, including IL-6 and IL-8. Genetic depletion of DDR proteins such as ATM, NBS1, or CHK2 suppresses the expression of these SASP components (133, 185). Meanwhile, the stress-inducible kinase p38MAPK also plays critical roles in regulating SASP. Inhibition of p38MAPK markedly reduced the secretion of most SASP factors (186). Most of the stress associated signals converge on nuclear factor κB (NF-κB) and CCAAT enhancer binding protein-β (C/EBP-β), which cooperatively contribute to the expression of proinflammatory cytokines such as IL-1α, IL-6, and IL-8 (16, 187-190). Interestingly, the surface-bound IL-1α meditates senescence-associated secretion of IL-6 and IL-8, which forms a self-amplification signaling and reinforces the senescence phenotype (191). In the meantime, the signaling through IL-1 receptor also initiates the upregulation of micro RNAs 146a and 146b, which serve as part of the negative feedback loop restraining IL-1 receptor signal transduction through IRAK1dwoenregulation and restrains excessive SASP expression (192).

NOTCH1, which was found to be significantly upregulate in senescent cells, is another key factor in mediating the composition of SASP (193). It has been demonstrated that NOTCH1 negatively regulates the proinflammatory transcription factor C/EBP-β and therefore reprogramming SASP from classic inflammatory phenotype toward tumor growth factor β (TGF-β) rich secretome (194). TGF-β is an important SASP factor which confers diverse functions by modulating the expression of downstream target genes in a context-dependent manner (195). It appears that upregulation of the TGF-β signaling is required for p21-mediated programmed senescence during embryonic development (196). Moreover, TGF-β promotes the expression of

NAPDH oxidase Nox4, causing increased ROS and DDR in cells and supporting paracrine senescence (197). A self-enforced positive reciprocal regulatory loop between TGF-β and Notch has been discovered (198). Indeed, TGF-β stimulation induces an acute activation of Notch signaling in non-transformed cells, which appears to be partially essential for G1 cell cycle arrest and cellular senescence (199).

The mammalian TOR (mTOR) signaling has been extensively discussed as regulator of lifespan and aging (200). The mTOR activity is required for SASP production in senescent cells (201, 202). In particular, inhibition of mTOR using rapamycin selectively suppresses the translation IL-1A and therefore reduces NF-κB transcriptional activity, leading to the decreased expression of inflammatory cytokines such as IL-6 and IL-8 while the other senescence phenotype are unaffected (203). Additionally, mTOR initiates the translation of the mitogen-activated protein kinase-activated protein kinase 2 (MAPKAPK2) through 4EBP1 phosphorylation. Then MAPKAPK2 phosphorylates the RNA-binding protein ZFP36L1 during senescence, inhibiting its ability to degrade the transcripts of numerous SASP components (204). Therefore, mTOR inhibitor serves as a potent SASP suppressor, which provides a direct mechanism for using rapamycin to ameliorate age-related pathologies trigged by SASP (205).

Recent findings have suggested that cyclic GMP-AMP synthase (cGAS), a critical indicator of innate immune sensing of cytoplasmic DNA (cytoplasmic chromatin fragments, mtDNA and cDNA), is activated in senescent cells and triggers the production of the second messenger cGAMP, which binds and activates the adaptor protein, stimulator of interferon genes (STING) (206, 207). STING then TANK-binding kinase 1 (TBK1) and IκB kinase to activate IFN regulatory factor 3 (IRF3) (208) and NF-κB (209), respectively, leading to the production of type I interferons and inflammatory cytokines (210). The upregulation of Toll-like receptor 2

(TLR2) is also mediated by cGAS-STING signaling, which controls the SASP and reinforces the cell cycle arrest program in oncogene induced senescence (OIS) mainly through NF-κB activation (211). The blockade of STING signaling pathway abolishes SASP production and many SASP associated functions of senescent cells (207, 212). Loss of cGAS even comprises others senescence phenotype while the mechanisms has been ascribed to lack of SASP reinforcement on senescence (206, 210), other possibilities are remined to be examined.

Metabolism also influences SASP and cellular senescence. It has been reported that nicotinamide phosphoribosyltransferase (NAMPT), the master enzyme responsible for NAD+ formation, is upregulated through high mobility group A (HMGA) proteins during senescence. The resulted high NAD^+/NADH ratio restrains AMPK activity but unleashes p38 MAPK activity and therefore enhancing NF-κB mediated expression of proinflammatory SASP. Therefore, the addition of nicotinamide mononucleotide (NMN) further enhances the secretion of inflammatory cytokines through increasing NAD+/NADH ratio in senescent fibroblasts induced by replicative or oncogenic stress (213). However, increasing NAD+ levels in mouse brain through nicotinamide riboside (NR) supplementation has been reported as a strategy which reduces neuroinflammation by suppressing cGAS–STING signaling and cellular senescence (214). These paradoxical results indicated that the effects of NAD metabolism on SASP modulation may be highly context dependent, which requires further investigation.

SASP can also be regulated through epigenetic mechanisms (215). The two major histone H3K9 mono- and dimethyltransferases, G9a and G9a-like protein (GLP), are decreased upon DDR, which leads to a global decrease in H3K9 dimethylation, an epigenetic mark for euchromatic gene silencing. The decline of H3K9 dimethylation at SASP gene promoters is correlated with the induction of IL-6 and IL-8 (154). Inhibition of histone deacetylase (HDAC) is

sufficient to activate pro-inflammatory SASP in the absence of DNA breaks, suggesting a direct mechanism between histone hyperacetylation associated chromatin remodeling and SASP factors (216). Consistently, SIRT1 (NAD-dependent deacetylase sirtuin-1), which is downregulated in senescent cells, has been reported to repress the expression of SASP factors through the deacetylation of H3K9 and H4K16 in their promoter regions (217). The component of SAHF, histone variant macroH2A1, on SASP genes creates a positive feedback loop that maintaining SASP expression (218). Other epigenetic factors, including BRD4, HMGB2, GATA4 and MLL1, have also been demonstrated in regulating SASP factors (215).

1.3 Cellular senescence in cancer progression (Figure 1.2)

1.3.1 Cellular senescence as a tumor suppressor

Cellular senescence is initially considered a tumor suppression mechanism. The expression of oncogenic ras in primary human or rodent cells results in p53/p16 dependent G1 cell cycle arrest and cellular senescence, forming an early barrier to prevent transformed cells from excessive proliferation (28). Lymphoma cells which fail to enter senescent stage due to SUV39H1 inactivation display rapid proliferation and develop aggressive but apoptosis-competent lymphomas *in vivo* in response to oncogenic Ras (219). Acute PTEN inactivation induces growth arrest and senescence in a p53-dependent manner both *in vitro* and *in vivo*, while double inactivation of PTEN and p53 The triggers invasive prostate cancer, suggesting the critical role of cellular senescence in restricting tumorigenesis (220). Senescence program can also contribute to cancer therapy. *INK4a* mutations appear to compromise the outcome of the treatment of alkylating agent cyclophosphamide in murine lymphomas, while tumors with WT *INK4a* but harboring a Bcl2-mediated apoptotic block display senescence markers and better

response than tumors with senescence defects after chemotherapy (47). The high level of Aurora A kinase, a member of a family of mitotic serine/threonine kinases playing important roles in mitosis was found to be responsible for Cisplatin resistance in epithelial ovarian cancer, which has been ascribed to the suppression of senescence through downregulation of senescent genes by direct binding to the transcription factor sex determining region Y-box 8 (SOX8) (221).

The SASP has also been reported as anti-tumor program through reinforce growth arrest and induce paracrine senescence (222, 223). The signaling from IL-1 receptor is one of the most well-studied mechanisms that creates a self-amplification loop of SASP production and underpins senescence (191, 224). The NF- κB and C/EBP-β dependent SASP factors, such as IL-8 and GROα, are also able to drive a self-amplifying secretory network through activating CXCR2. The activated CXCR2 signals are correlated with production of reactive oxygen species (ROS) and therefore inducing cell cycle arrest and eventually senescence. The increased expression of CXCR2 has been detected in preneoplastic lesions, while CXCR2 was found to be mutated or loss in advanced cancers, supporting the perspective that malignancy reflects escape from senescence (225). IL-6 was also required for the of OIS in a cell-autonomous mode, which will also further amplify inflammatory network through C/EBP-β (226). Furthermore, the SASP factors may also stimulate the expression of the tumor suppressor promyelocytic leukemia protein (PML) via by JAK/STAT signaling (227).

The senescent cells can spread senescence phenotype towards their neighbors both i*n vitro* and *in vivo*, termed as paracrine senescence or bystander senescence (224, 228, 229). It has been reported that senescent cells may induce DDR in their neighboring cells via gap junction and ROS upregulation (229). The upregulation of ROS due to mitochondrial dysfunction in senescent cells was found to be necessary and sufficient to activate NF-κB signals, which causes

the 53BP1 involved DNA damage response in bystander cells (228). The SASP is also able to induce non-senescent cells into senescent stage. The soluble SASP components that are able to induce paracrine senescence include TGF-β family ligands, VEGF, CCL2 and CCL20. Indeed, TGF-β target genes are remarkably upregulated during OIS and paracrine senescence, while TGFBR1 inhibitors partially prevent the appearance of paracrine senescence. This p16INK4a and p21CIP1 dependent paracrine senescence confers tumor suppression effects both *in vitro* and *in vivo* (224). Another SASP factor IGFBP7 secreted by $BRAFV^{600E}$ driven senescent cell was also found to induce senescence and apoptosis through MEK-ERK signaling, while loss of IGFBP7 expression might represent a critical step in melanoma genesis (230).

Although the anti-tumor effects of senescent cells are mostly attributed to the lack of proliferation capacity, accumulated evidences indicate that senescent cells are able to activate immune surveillance of senescent and non-senescent tumor cells (20, 222, 231). Decades ago, it has been reported that the primary response of p53 reactivation in p53-deficient tumors is senescence program instead of apoptosis. The p53 dependent senescent cells are closely associated with an neutrophil and nature killer cell involved innate immune response in liver that targeting tumor cells, indicating that senescence program can act together with innate immunity as a potent tumor suppression mechanism (232). Consistently, pre-malignant senescent hepatocytes induced by N-Ras have been found to stimulate a monocytes/macrophages dependent $CD4^+$ T cell mediated clearance of tumor cells through SASP, further supporting that oncogenic senescence associated immune surveillance represents an important extrinsic component anti-tumor barrier (233). In the presence of chronic liver damage and chemical carcinogenic stress, the hepatic stellate cells develop p53-depedent senescence and produce NF-κB mediated SASP. These SASP factors promote macrophage polarization toward a tumor

inhibiting M1 state which is capable of eliminating of premalignant senescent and non-senescent cells (234). Indeed, p53 signals appear to play critical roles in senescence associated anti-tumor immune response particularly in the context of murine liver. The senescence in liver carcinoma driven by expression of p53 and H-Ras^{G12V} secrete chemokines such as CCL2 to promote the NK cell infiltrate in liver which conducts tumor suppression effects (235). The SASP factors modulated by the chromatin reader BRD4 in OIS have also been reported to promote antitumor M1 polarization of macrophages and recruit NK cells, leading to senescent cell elimination and a tumor-suppressive program (156). Addition of OIS, the aneuploid senescent cells have induced by inhibition of Monopolar spindle 1 kinase (Mps1) been reported to meditate NK cell clearance in a NF-κB signaling dependent manner, suggesting a possible anti-tumor mechanism during cancer evolution (236). The senescent cancer cells induced by radiation and the PARP inhibitor verliparib have been confirmed as cancer vaccine which drives T cells and NK cell dependent anti-tumor immune response in multiple syngeneic mouse models (237).

1.3.2 Cellular senescence as a tumor promotor

It has been reported that senescent cells may contribute to malignancy transformation. The non-malignant epithelial cells cocultured with senescent fibroblasts displayed neoplastic development, increased migration, and nuclear atypia, suggesting a possibility for becoming invasive and undergoing full malignant transformation (238, 239). Considering that the conditioned medium from senescent cells is able to for confer the similar effects, the tumor initiation roles of cellular senescence has been ascribed to the SASP factors such as matrix metalloproteinase-3 (MMP-3) (238). The clearance of p16^{INK4a} positive cells, representing senescent cells, in the transgenic INK-ATTAC mouse model causes diminished tumorigenesis

during aging, further proving that the accumulation of senescent cells in animals is responsible for age associated tumor development (240). Co-injection of epithelial cells and senescent cells into mice significantly increased the tumor taken rate of nude mice compared to injection of epithelial cells alone, indicating that senescent cells created a microenvironment that favors tumorigenesis (241). The tumors developed after co-injection appeared to grow much faster compared to tumors caused by epithelial cells alone, suggesting a growth stimulation effects of cellular senescence. Strikingly, senescent cells induced by p16 ectopic expression, Ras oncogenic stress, or H_2O_2 are all capable of promoting the proliferation of their neighboring cells in a non-cell autonomous manner through coculture experiments, illustrating that the growth boosting effects are independent of senescence inducers (241).

The growth stimulation effects of senescent cells have been reported in multiple models both *in vitro* and *in vivo*. In a 3D culture system, conditioned medium from senescent fibroblasts promoted anchorage-independent growth of immortalized ovarian surface epithelial cells (239). Interestingly, senescent fibroblasts induced by tobacco extracts appeared to increase proliferation only in partially transformed epithelial cells instead of the normal epithelial cells, indicating that the response of cells to senescent cells might highly context dependent (242). Cytokines have been long considered crucial players in tumor initiation and progression. For instance, interleukin (IL)-6, which is also a major SASP factor triggered by NF-κB signals, has been reported as a key factor in activating STAT3 signals and therefore driving many aspects of carcinogenesis including transformation, proliferation, and invasion. Indeed, depletion of IL-6 from senescent mesenchymal stem cells partially blocked their stimulatory effects on the proliferation and migration of breast tumor cells (243). Other than IL-6, osteopontin (OPN), a protein secreted by senescent fibroblasts, also promote preneoplastic cell growth *in vitro* and *in vivo* (244). The

matrix metalloproteinase (MMP) is another SASP factor that was reported to promote the proliferation of breast cancer cells in culture and in xenograft model (245). Chemerin, a recently discovered SASP factor, can promote cutaneous squamous cell carcinoma (cSCC) cell migration through CCRL2 and GPR1 receptor signals with subsequent MAPK activation (246).

Senescent stromal and tumor cells also contribute to tumor metastasis. Disruption of cellular senescence or suppression of SASP using anti-inflammatory compound such as metformin reduce exacerbated pathological neovascularization triggered by senescence in a mouse ischemic retinopathy model (247). The SASP was shown to alter the morphology and migration of breast cancer cells toward an aggressive stage through targeting microtubule integrity and dynamics (248). Along with the similar system, senescent fibroblasts promote the membrane invading capability of vein endothelial cells in culture through secreted vascular endothelial growth factor (VEGF), suggesting a role of senescence in angiogenesis (249), while the senescent prostate stromal cells promote angiogenesis and prostate cancer tumorigenesis through, at least partially, TGF- β1 mediated secretion of connective tissue growth factor (CTGF) (250). Additionally, senescent tumor cells lead to increased tumor invasion and epithelial-mesenchymal transition (EMT). CXCL12 has been considered an critical SASP factor which mediates tumor survival and EMT via CXCR4 signaling. Co-transplantation with senescent and proliferating cancer cells in mouse develops more lymphatic vessel networks (251). The SASP secreted by senescent mesothelioma (Ras induced) can trigger the development of a EMT (epithelial-to-mesenchymal)-like, clonogenic and chemoresistant cell subpopulation of cancer cells, which has been ascribed to SASP mediated STAT3 activation though it is unclear which SASP factor plays the key roles (252). In colon and rectal cancer cell lines, chemotherapy induced senescent cells produce a SASP that is capable of inducing EMT (253), while the

constitutive activated HER2 signals in senescent breast epithelial cells elicits a complex secretome and promotes metastasis *in vivo through* paracrine effects driven by (254). IL-6 secreted by senescent osteoblasts was found to increase osteoclastogenesis and the localization of breast cancer metastatic to bone (255). The matrix metalloproteinases MMP1 and MMP secreted by senescent fibroblasts contribute to the early EMT of keratinocytes and initiation of skin carcinoma through activating protease-activated receptor 1 (PAR-1) signaling pathways (256). The secreted frizzled related protein 2 (SFRP2), secreted by senescent melanoma cells, serves as Wnt antagonist and leads to the downregulation of stress responses but upregulation of angiogenesis of melanoma cells, which contributes to melanoma metastasis and progression (257).

The accumulation of senescent cells in cancer has been considered a critical factor in mediating therapy resistance. Senescent endothelial cells induced by doxorubicin in thymus create a chemo-resistant niche and therefore promoting the residual tumor survival and relapse, which is believed to be mediated by the SASP factor IL-6 and Timp-1 (258). Later on, it has been reported that acute IL-6 secretion, which is controlled by PI3K/AKT signals in senescent endothelial cells, is sufficient to confer chemoprotective effects (259). Consistently, p53-dependent senescence in breast cancer protects cancer cells from apoptosis and attenuates the efficacy of doxorubicin through SASP mediated autocrine/paracrine activity (260). Senescent cells have been extensively studied in tissue remodeling, particularly through SASP mediated paracrine effects (261). In the context of cancer, it has been reported that senescence is involved in tumor cell reprogramming and stemness, which contributes to tumor recurrence and therapy resistance. The ectopic expression of reprogramming factors OCT4, SOX2, KLF4, and cMYC (OSKM) in mice simultaneously leads to senescence and reprogramming, while blocking SASP

factor such as IL-6 diminishes stem cell reprogramming, suggesting an enhancement effect of senescence in cell reprogramming *in vivo* (262). Indeed, cellular senescence in blood cancers displays critical roles in the induction of maintenance of cancer stem cells. Senescent myeloma cells induced by DNA damage contribute to the emergence, maintenance and migration of cancer stem-like cells through CHK2 dependent SASP both *in vitro* and *in vivo* (263). The similar effects of senescence in caner stemness have been discovered in B-cell lymphoma, B cell chronic lymphocytic leukemia (B-CLL), and acute myeloid leukemia (AML) models as well (264). Interestingly, the key signaling components of senescence machinery, such as $p16^{INK4A}$, $p21^{CIP1}$, p53, and histone H3 trimethylation (H3K9me3) are also considered critical regulators of stemness, providing the direct correlation between senescence and stemness (264). The impacts of senescence on stemness reprogramming recently have been reported in solid tumor cell lines. Both stem and non-stem hepatocellular carcinoma cells cocultured with doxorubicin induced senescent hepatocellular carcinoma cells displayed increased expression of reprograming genes and liver stemness genes, suggesting a direct role of senescence in stemness initiation and maintenance (265). Consistently, the breast cancer MCF-7 cells treated with either senescence-conditioned medium or key SASP factors IL-6 and IL-8 revels the characteristics of stemness, including increased CD44 expression, self-renewal and multilineage differentiation capacity in culture (266).

Many studies have reported the senescence mediated immunosuppression is also responsible for tumor promotion, although we have discussed the positive impacts of senescence in immune surveillance of cancer cells earlier (7, 8, 23, 50). The exact effects of cellular senescence on anti-tumor immune response appear to be highly dependent on the stage of tumorigenesis and the tissue microenvironment. The premalignant senescent hepatocytes secrete

CCL2 and thus promoting liver infiltrate of immature CCR2$^+$ myeloid cells, which will further differentiate into macrophages and eliminate premalignant cells. When hepatocellular carcinoma cells already exist in liver, they block the maturation of recruited CCR2$^+$myeloid precursors, leading to tumor promotion through inhibiting NK cell function. Therefore, senescent hepatocytes suppress the initiation of hepatocellular carcinoma (HCC) but accelerate growth of fully established HCC through the dual roles in modulating anti-tumor immunity (267). The senescent hepatic stellate cells (HSCs) triggered by lipoteichoic acid (LTA), a major component of the cell wall of Gram-positive bacteria in gut, produce a Toll-like receptor 2 (TLR2) mediated secretome, which upregulates the ratio of regulatory T cells (Treg) in liver. As a result, senescent HSCs suppress cytotoxic T cell involved anti-tumor immunity and therefore promoting HCC progression (268). The senescent cells in Pten null prostate cancer promote the infiltration of myeloid derived suppressor cells (CD11b$^+$/ Gr-1$^+$, MDSCs) through JAK2/STAT3 mediated secretion of immune suppressive cytokines (269, 270). Interestingly, pharmacological inhibition of JAK2 reprograms the SASP and reveals immune-stimulatory effects of senescent prostate cancer cells (269), while the inhibition of NOTCH might represent another strategy to promote immune surveillance of premalignant cells in liver (194). Notably, the MDSCs recruited in prostate tumors protects cells from therapy induced senescence and the efficacy of chemotherapies in general (270). The senescence associated upregulation of MDSCs is also observed in skin models, where the stromal-derived SASP, particularly IL-6, is sufficient to enhance MDSCs recruitment and their capability in blocking anti-tumor T cell response (271). A recent study in colorectal cancer model revealed that senescent tumor cells are accompanied with highly secretion of C-X-C motif chemokine ligand 12 (CXCL12) and colony stimulating factor 1 (CSF1), while CXCL12 directly suppresses T cell infiltrate through downregulating CXCR4 on

T cells and CSF1 promotes the differentiation of M2 macrophage which further inhibits $CD8^+$ T cell activity (272). Therefore, pharmacological neutralizing the immune suppressive SASP factors or reprogramming SASP have been investigated ass promising ways to rebuild the anti-tumor immune response and diminish the detrimental effects of senescence in cancers (269, 272). Addition of SASP, senescent dermal fibroblasts displayed increased surface expression of the non-classical MHC molecule HLA-E, which drives immune suppressive effects through triggering NKG2A mediated inhibitory signals in NK and cytotoxic CD8+ T cells (273). The expression of HLA-E can be upregulated in a proinflammatory SASP dependent manner through cell autonomous or non-autonomous mechanisms (273). Meanwhile, therapy induced senescence has been associated with immune cell senescence, especially T cells, which contributes to both side effects and cancer relapse during/after therapies (49).

1.4 Conclusions

The studies about cellular senescence and its functions under physiological and pathological conditions have exploded in the last decade, which has facilitated the development of better models for the senescence research and novel strategies to alleviate senescence-associated diseases. Cellular senescence is frequently observed after current cancer therapies and emerged as one of the hallmarks of cancer (12), while it conducts both beneficial and detrimental impacts on cancer progression and treatment efficacy. Throughout this chapter, we have discussed how senescent cells are diverse due to the variances in the senescence inducers, genetic background, tissue context, and stages of senescence. One of the most critical factors reflecting the differences among senescence is the SASP, whose composition is highly dynamic and coordinately regulated by both intrinsic and extrinsic signals. While many efforts have been

made to profile SASP factors through low-/ high-throughput methods, it is still challenging to timely and/or geographically illustrate the components in SASP and their corresponding functions and/or targeted cells. The development of the chemical biology tools, including APEX (274) and TurboID (275), which are initially designed for protein labeling and enrichment and have been confirmed useful in studying secreted proteins both *in vitro* and *in vivo*, may benefit the future exploration of SASP characteristics. This chapter also illustrated that senescent cells even with the same genetic background and senescent stimulus can display opposite effects on cancer progression, suggesting a significant heterogeneity of cellular senescence. As described in this chapter, current studies have indicated that multiple factors, including epigenetic modification, paracrine signals from the neighboring cells, and stages of senescence, might contribute to senescence heterogeneity, while future studies are required to further explain the mechanisms controlling heterogenous senescent cells. Advanced technologies such as single-cell RNA sequencing and proteomic profiling have been utilized to dissect the heterogeneity of cellular senescence in culture or in aging tissues, which have displayed promising outcomes (276-279). Such approaches and studies with tumors may contribute to the understanding of the triggers and roles of senescence heterogeneity, leading to better control and/or utilization of cellular senescence in cancer and eventually the improvement of cancer therapies.

1.5 References

1. Hayflick L, and Moorhead PS. The serial cultivation of human diploid cell strains. *Exp Cell Res.* 1961;25:585-621.

2. Dimri GP, Lee X, Basile G, Acosta M, Scott G, Roskelley C, et al. A biomarker that identifies senescent human cells in culture and in aging skin in vivo. *Proc Natl Acad Sci U S A.* 1995;92(20):9363-7.

3. Campisi J. Aging, cellular senescence, and cancer. *Annu Rev Physiol.* 2013;75:685-705.

4. Dodig S, Cepelak I, and Pavic I. Hallmarks of senescence and aging. *Biochem Med (Zagreb).* 2019;29(3):030501.

5. Hernandez-Segura A, Nehme J, and Demaria M. Hallmarks of Cellular Senescence. *Trends Cell Biol.* 2018;28(6):436-53.

6. Gorgoulis V, Adams PD, Alimonti A, Bennett DC, Bischof O, Bishop C, et al. Cellular Senescence: Defining a Path Forward. *Cell.* 2019;179(4):813-27.

7. Coppe JP, Desprez PY, Krtolica A, and Campisi J. The senescence-associated secretory phenotype: the dark side of tumor suppression. *Annu Rev Pathol.* 2010;5:99-118.

8. Faget DV, Ren Q, and Stewart SA. Unmasking senescence: context-dependent effects of SASP in cancer. *Nat Rev Cancer.* 2019;19(8):439-53.

9. Childs BG, Baker DJ, Kirkland JL, Campisi J, and van Deursen JM. Senescence and apoptosis: dueling or complementary cell fates? *EMBO Rep.* 2014;15(11):1139-53.

10. Kirkland JL, Tchkonia T, Zhu Y, Niedernhofer LJ, and Robbins PD. The Clinical Potential of Senolytic Drugs. *J Am Geriatr Soc.* 2017;65(10):2297-301.

11. Dolgin E. Send in the senolytics. *Nat Biotechnol.* 2020;38(12):1371-7.

12. Hanahan D. Hallmarks of Cancer: New Dimensions. *Cancer Discov.* 2022;12(1):31-46.

13. Campisi J. Senescent cells, tumor suppression, and organismal aging: good citizens, bad neighbors. *Cell.* 2005;120(4):513-22.

14. Campisi J, and d'Adda di Fagagna F. Cellular senescence: when bad things happen to good cells. *Nat Rev Mol Cell Biol.* 2007;8(9):729-40.

15. Lee S, and Schmitt CA. The dynamic nature of senescence in cancer. *Nat Cell Biol.* 2019;21(1):94-101.

16. Tchkonia T, Zhu Y, van Deursen J, Campisi J, and Kirkland JL. Cellular senescence and the senescent secretory phenotype: therapeutic opportunities. *J Clin Invest.* 2013;123(3):966-72.

17. Amor C, Feucht J, Leibold J, Ho YJ, Zhu C, Alonso-Curbelo D, et al. Senolytic CAR T cells reverse senescence-associated pathologies. *Nature.* 2020;583(7814):127-32.

18. Ewald JA, Desotelle JA, Wilding G, and Jarrard DF. Therapy-induced senescence in cancer. *J Natl Cancer Inst.* 2010;102(20):1536-46.

19. Schosserer M, Grillari J, and Breitenbach M. The Dual Role of Cellular Senescence in Developing Tumors and Their Response to Cancer Therapy. *Front Oncol.* 2017;7:278.

20. Mavrogonatou E, Pratsinis H, and Kletsas D. The role of senescence in cancer development. *Semin Cancer Biol.* 2020;62:182-91.

21. Ohtani N, Takahashi A, Mann DJ, and Hara E. Cellular senescence: a double-edged sword in the fight against cancer. *Exp Dermatol.* 2012;21 Suppl 1:1-4.

22. Birch J, and Gil J. Senescence and the SASP: many therapeutic avenues. *Genes Dev.* 2020;34(23-24):1565-76.

23. Prasanna PG, Citrin DE, Hildesheim J, Ahmed MM, Venkatachalam S, Riscuta G, et al. Therapy-Induced Senescence: Opportunities to Improve Anticancer Therapy. *J Natl Cancer Inst.* 2021;113(10):1285-98.

24. Harley CB, Futcher AB, and Greider CW. Telomeres shorten during ageing of human fibroblasts. *Nature.* 1990;345(6274):458-60.

25. d'Adda di Fagagna F, Reaper PM, Clay-Farrace L, Fiegler H, Carr P, Von Zglinicki T, et al. A DNA damage checkpoint response in telomere-initiated senescence. *Nature.* 2003;426(6963):194-8.

26. Jaskelioff M, Muller FL, Paik JH, Thomas E, Jiang S, Adams AC, et al. Telomerase reactivation reverses tissue degeneration in aged telomerase-deficient mice. *Nature.* 2011;469(7328):102-6.

27. Rudolph KL, Chang S, Lee HW, Blasco M, Gottlieb GJ, Greider C, et al. Longevity, stress response, and cancer in aging telomerase-deficient mice. *Cell.* 1999;96(5):701-12.

28. Serrano M, Lin AW, McCurrach ME, Beach D, and Lowe SW. Oncogenic ras provokes premature cell senescence associated with accumulation of p53 and p16INK4a. *Cell.* 1997;88(5):593-602.

29. Sarkisian CJ, Keister BA, Stairs DB, Boxer RB, Moody SE, and Chodosh LA. Dose-dependent oncogene-induced senescence in vivo and its evasion during mammary tumorigenesis. *Nat Cell Biol.* 2007;9(5):493-505.

30. Bartkova J, Rezaei N, Liontos M, Karakaidos P, Kletsas D, Issaeva N, et al. Oncogene-induced senescence is part of the tumorigenesis barrier imposed by DNA damage checkpoints. *Nature.* 2006;444(7119):633-7.

31. Mallette FA, and Ferbeyre G. The DNA damage signaling pathway connects oncogenic stress to cellular senescence. *Cell Cycle.* 2007;6(15):1831-6.

32. Di Micco R, Fumagalli M, Cicalese A, Piccinin S, Gasparini P, Luise C, et al. Oncogene-induced senescence is a DNA damage response triggered by DNA hyper-replication. *Nature.* 2006;444(7119):638-42.

33. Suram A, Kaplunov J, Patel PL, Ruan H, Cerutti A, Boccardi V, et al. Oncogene-induced telomere dysfunction enforces cellular senescence in human cancer precursor lesions. *EMBO J.* 2012;31(13):2839-51.

34. Heeren G, Jarolim S, Laun P, Rinnerthaler M, Stolze K, Perrone GG, et al. The role of respiration, reactive oxygen species and oxidative stress in mother cell-specific ageing of yeast strains defective in the RAS signalling pathway. *FEMS Yeast Res.* 2004;5(2):157-67.

35. Ogrunc M, Di Micco R, Liontos M, Bombardelli L, Mione M, Fumagalli M, et al. Oncogene-induced reactive oxygen species fuel hyperproliferation and DNA damage response activation. *Cell Death Differ.* 2014;21(6):998-1012.

36. Alimonti A, Nardella C, Chen Z, Clohessy JG, Carracedo A, Trotman LC, et al. A novel type of cellular senescence that can be enhanced in mouse models and human tumor xenografts to suppress prostate tumorigenesis. *J Clin Invest.* 2010;120(3):681-93.

37. Parisotto M, Grelet E, El Bizri R, Dai Y, Terzic J, Eckert D, et al. PTEN deletion in luminal cells of mature prostate induces replication stress and senescence in vivo. *J Exp Med.* 2018;215(6):1749-63.

38. Fumagalli M, Rossiello F, Mondello C, and d'Adda di Fagagna F. Stable cellular senescence is associated with persistent DDR activation. *PLoS One.* 2014;9(10):e110969.

39. Zhang X, Li J, Sejas DP, and Pang Q. The ATM/p53/p21 pathway influences cell fate decision between apoptosis and senescence in reoxygenated hematopoietic progenitor cells. *J Biol Chem.* 2005;280(20):19635-40.

40. Wu PC, Wang Q, Grobman L, Chu E, and Wu DY. Accelerated cellular senescence in solid tumor therapy. *Exp Oncol.* 2012;34(3):298-305.

41. Hewitt G, Jurk D, Marques FD, Correia-Melo C, Hardy T, Gackowska A, et al. Telomeres are favoured targets of a persistent DNA damage response in ageing and stress-induced senescence. *Nat Commun.* 2012;3:708.

42. Bonner WM, Redon CE, Dickey JS, Nakamura AJ, Sedelnikova OA, Solier S, et al. GammaH2AX and cancer. *Nat Rev Cancer.* 2008;8(12):957-67.

43. Shay JW, and Roninson IB. Hallmarks of senescence in carcinogenesis and cancer therapy. *Oncogene.* 2004;23(16):2919-33.

44. Huck JJ, Zhang M, McDonald A, Bowman D, Hoar KM, Stringer B, et al. MLN8054, an inhibitor of Aurora A kinase, induces senescence in human tumor cells both in vitro and in vivo. *Mol Cancer Res.* 2010;8(3):373-84.

45. Munro J, Barr NI, Ireland H, Morrison V, and Parkinson EK. Histone deacetylase inhibitors induce a senescence-like state in human cells by a p16-dependent mechanism that is independent of a mitotic clock. *Exp Cell Res.* 2004;295(2):525-38.

46. Petrova NV, Velichko AK, Razin SV, and Kantidze OL. Small molecule compounds that induce cellular senescence. *Aging Cell.* 2016;15(6):999-1017.

47. Schmitt CA, Fridman JS, Yang M, Lee S, Baranov E, Hoffman RM, et al. A senescence program controlled by p53 and p16INK4a contributes to the outcome of cancer therapy. *Cell.* 2002;109(3):335-46.

48. Shao L, Feng W, Li H, Gardner D, Luo Y, Wang Y, et al. Total body irradiation causes long-term mouse BM injury via induction of HSC premature senescence in an Ink4a- and Arf-independent manner. *Blood.* 2014;123(20):3105-15.

49. Demaria M, O'Leary MN, Chang J, Shao L, Liu S, Alimirah F, et al. Cellular Senescence Promotes Adverse Effects of Chemotherapy and Cancer Relapse. *Cancer Discov.* 2017;7(2):165-76.

50. Munoz-Espin D, and Serrano M. Cellular senescence: from physiology to pathology. *Nat Rev Mol Cell Biol.* 2014;15(7):482-96.

51. Zhang L, Bochkur Dratver M, Yazal T, Dong K, Nguyen A, Yu G, et al. Mebendazole Potentiates Radiation Therapy in Triple-Negative Breast Cancer. *Int J Radiat Oncol Biol Phys.* 2019;103(1):195-207.

52. Zhang F, Li Y, Zhang H, Huang E, Gao L, Luo W, et al. Anthelmintic mebendazole enhances cisplatin's effect on suppressing cell proliferation and promotes differentiation of head and neck squamous cell carcinoma (HNSCC). *Oncotarget.* 2017;8(8):12968-82.

53. Tsubamoto H, Sonoda T, Ikuta S, Tani S, Inoue K, and Yamanaka N. Combination Chemotherapy with Itraconazole for Treating Metastatic Pancreatic Cancer in the Second-line or Additional Setting. *Anticancer Res.* 2015;35(7):4191-6.

54. Hehlgans S, Booms P, Gullulu O, Sader R, Rodel C, Balermpas P, et al. Radiation Sensitization of Basal Cell and Head and Neck Squamous Cell Carcinoma by the Hedgehog Pathway Inhibitor Vismodegib. *Int J Mol Sci.* 2018;19(9).

55. Jiricny J. The multifaceted mismatch-repair system. *Nat Rev Mol Cell Biol.* 2006;7(5):335-46.

56. Zhang Y, Fox JT, Park YU, Elliott G, Rai G, Cai M, et al. A Novel Chemotherapeutic Agent to Treat Tumors with DNA Mismatch Repair Deficiencies. *Cancer Res.* 2016;76(14):4183-91.

57. Guillotin D, Austin P, Begum R, Freitas MO, Merve A, Brend T, et al. Drug-Repositioning Screens Identify Triamterene as a Selective Drug for the Treatment of DNA Mismatch Repair Deficient Cells. *Clin Cancer Res.* 2017;23(11):2880-90.

58. Alekseev S, Ayadi M, Brino L, Egly JM, Larsen AK, and Coin F. A small molecule screen identifies an inhibitor of DNA repair inducing the degradation of TFIIH and the chemosensitization of tumor cells to platinum. *Chem Biol.* 2014;21(3):398-407.

59. Marteijn JA, Lans H, Vermeulen W, and Hoeijmakers JH. Understanding nucleotide excision repair and its roles in cancer and ageing. *Nat Rev Mol Cell Biol.* 2014;15(7):465-81.

60. Shahar OD, Kalousi A, Eini L, Fisher B, Weiss A, Darr J, et al. A high-throughput chemical screen with FDA approved drugs reveals that the antihypertensive drug Spironolactone impairs cancer cell survival by inhibiting homology directed repair. *Nucleic Acids Res.* 2014;42(9):5689-701.

61. Gold A, Eini L, Nissim-Rafinia M, Viner R, Ezer S, Erez K, et al. Spironolactone inhibits the growth of cancer stem cells by impairing DNA damage response. *Oncogene.* 2019;38(17):3103-18.

62. Moldovan GL, and D'Andrea AD. How the fanconi anemia pathway guards the genome. *Annu Rev Genet.* 2009;43:223-49.

63. Chirnomas D, Taniguchi T, de la Vega M, Vaidya AP, Vasserman M, Hartman AR, et al. Chemosensitization to cisplatin by inhibitors of the Fanconi anemia/BRCA pathway. *Mol Cancer Ther.* 2006;5(4):952-61.

64. Jacquemont C, Simon JA, D'Andrea AD, and Taniguchi T. Non-specific chemical inhibition of the Fanconi anemia pathway sensitizes cancer cells to cisplatin. *Mol Cancer.* 2012;11:26.

65. Baell J, and Walters MA. Chemistry: Chemical con artists foil drug discovery. *Nature.* 2014;513(7519):481-3.

66. Chang HHY, Pannunzio NR, Adachi N, and Lieber MR. Non-homologous DNA end joining and alternative pathways to double-strand break repair. *Nat Rev Mol Cell Biol.* 2017;18(8):495-506.

67. Sallmyr A, and Tomkinson AE. Repair of DNA double-strand breaks by mammalian alternative end-joining pathways. *J Biol Chem.* 2018;293(27):10536-46.

68. Rossetto D, Truman AW, Kron SJ, and Cote J. Epigenetic modifications in double-strand break DNA damage signaling and repair. *Clin Cancer Res.* 2010;16(18):4543-52.

69. House NC, Koch MR, and Freudenreich CH. Chromatin modifications and DNA repair: beyond double-strand breaks. *Front Genet.* 2014;5:296.

70. Ismail IH, McDonald D, Strickfaden H, Xu Z, and Hendzel MJ. A small molecule inhibitor of polycomb repressive complex 1 inhibits ubiquitin signaling at DNA double-strand breaks. *J Biol Chem.* 2013;288(37):26944-54.

71. Efimova EV, Takahashi S, Shamsi NA, Wu D, Labay E, Ulanovskaya OA, et al. Linking Cancer Metabolism to DNA Repair and Accelerated Senescence. *Mol Cancer Res.* 2016;14(2):173-84.

72. Gioia U, Francia S, Cabrini M, Brambillasca S, Michelini F, Jones-Weinert CW, et al. Pharmacological boost of DNA damage response and repair by enhanced biogenesis of DNA damage response RNAs. *Scientific reports.* 2019;9(1):6460.

73. Labay E, Efimova EV, Quarshie BK, Golden DW, Weichselbaum RR, and Kron SJ. Ionizing radiation-induced foci persistence screen to discover enhancers of accelerated senescence. *Int J High Throughput Screen.* 2011;2:1-13.

74. Labay E, Mauceri HJ, Efimova EV, Flor AC, Sutton HG, Kron SJ, et al. Repurposing cephalosporin antibiotics as pro-senescent radiosensitizers. *Oncotarget.* 2016;7(23):33919-33.

75. Efimova EV, Ricco N, Labay E, Mauceri HJ, Flor AC, Ramamurthy A, et al. HMG-CoA Reductase Inhibition Delays DNA Repair and Promotes Senescence After Tumor Irradiation. *Mol Cancer Ther.* 2018;17(2):407-18.

76. Dittmann K, Mayer C, and Rodemann H-P. Inhibition of radiation-induced EGFR nuclear import by C225 (Cetuximab) suppresses DNA-PK activity. *Radiotherapy and Oncology.* 2005;76(2):157-61.

77. Bandyopadhyay D, Mandal M, Adam L, Mendelsohn J, and Kumar R. Physical interaction between epidermal growth factor receptor and DNA-dependent protein kinase in mammalian cells. *Journal of Biological Chemistry.* 1998;273(3):1568-73.

78. Pawelczak KS, Gavande NS, VanderVere-Carozza PS, and Turchi JJ. Modulating DNA Repair Pathways to Improve Precision Genome Engineering. *ACS Chem Biol.* 2018;13(2):389-96.

79. Yu C, Liu Y, Ma T, Liu K, Xu S, Zhang Y, et al. Small molecules enhance CRISPR genome editing in pluripotent stem cells. *Cell Stem Cell.* 2015;16(2):142-7.

80. Li G, Zhang X, Zhong C, Mo J, Quan R, Yang J, et al. Small molecules enhance CRISPR/Cas9-mediated homology-directed genome editing in primary cells. *Sci Rep.* 2017;7(1):8943.

81. San Filippo J, Sung P, and Klein H. Mechanism of eukaryotic homologous recombination. *Annu Rev Biochem.* 2008;77:229-57.

82. Heeke AL, Pishvaian MJ, Lynce F, Xiu J, Brody JR, Chen WJ, et al. Prevalence of Homologous Recombination-Related Gene Mutations Across Multiple Cancer Types. *JCO Precis Oncol.* 2018;2018.

83. Lord CJ, and Ashworth A. PARP inhibitors: Synthetic lethality in the clinic. *Science.* 2017;355(6330):1152-8.

84. Rouleau M, Patel A, Hendzel MJ, Kaufmann SH, and Poirier GG. PARP inhibition: PARP1 and beyond. *Nat Rev Cancer.* 2010;10(4):293-301.

85. Budke B, Lv W, Kozikowski AP, and Connell PP. Recent Developments Using Small Molecules to Target RAD51: How to Best Modulate RAD51 for Anticancer Therapy? *ChemMedChem.* 2016;11(22):2468-73.

86. Ladd B, Ackroyd JJ, Hicks JK, Canman CE, Flanagan SA, and Shewach DS. Inhibition of homologous recombination with vorinostat synergistically enhances ganciclovir cytotoxicity. *DNA Repair (Amst).* 2013;12(12):1114-21.

87. Adimoolam S, Sirisawad M, Chen J, Thiemann P, Ford JM, and Buggy JJ. HDAC inhibitor PCI-24781 decreases RAD51 expression and inhibits homologous recombination. *Proc Natl Acad Sci U S A.* 2007;104(49):19482-7.

88. Konstantinopoulos PA, Wilson AJ, Saskowski J, Wass E, and Khabele D. Suberoylanilide hydroxamic acid (SAHA) enhances olaparib activity by targeting homologous recombination DNA repair in ovarian cancer. *Gynecologic oncology.* 2014;133(3):599-606.

89. Yang L, Zhang Y, Shan W, Hu Z, Yuan J, Pi J, et al. Repression of BET activity sensitizes homologous recombination–proficient cancers to PARP inhibition. *Science translational medicine.* 2017;9(400):eaal1645.

90. Miller AL, Fehling SC, Garcia PL, Gamblin TL, Council LN, van Waardenburg R, et al. The BET inhibitor JQ1 attenuates double-strand break repair and sensitizes models of pancreatic ductal adenocarcinoma to PARP inhibitors. *EBioMedicine.* 2019;44:419-30.

91. Neri P, Ren L, Gratton K, Stebner E, Johnson J, Klimowicz A, et al. Bortezomib-induced "BRCAness" sensitizes multiple myeloma cells to PARP inhibitors. *Blood.* 2011;118(24):6368-79.

92. Osoegawa A, Gills JJ, Kawabata S, and Dennis PA. Rapamycin sensitizes cancer cells to growth inhibition by the PARP inhibitor olaparib. *Oncotarget.* 2017;8(50):87044-53.

93. Jiang J, Lu Y, Li Z, Li L, Niu D, Xu W, et al. Ganetespib overcomes resistance to PARP inhibitors in breast cancer by targeting core proteins in the DNA repair machinery. *Invest New Drugs.* 2017;35(3):251-9.

94. Song Z, Tu X, Zhou Q, Huang J, Chen Y, Liu J, et al. A novel UCHL3 inhibitor, perifosine, enhances PARP inhibitor cytotoxicity through inhibition of homologous

recombination-mediated DNA double strand break repair. *Cell Death Dis.* 2019;10(6):398.

95. Blackford AN, and Jackson SP. ATM, ATR, and DNA-PK: the trinity at the heart of the DNA damage response. *Molecular cell.* 2017;66(6):801-17.

96. Goldstein M, and Kastan MB. The DNA damage response: implications for tumor responses to radiation and chemotherapy. *Annual review of medicine.* 2015;66:129-43.

97. Ciccia A, and Elledge SJ. The DNA damage response: making it safe to play with knives. *Molecular cell.* 2010;40(2):179-204.

98. Harper JW, and Elledge SJ. The DNA damage response: ten years after. *Molecular cell.* 2007;28(5):739-45.

99. Sarkaria JN, Busby EC, Tibbetts RS, Roos P, Taya Y, Karnitz LM, et al. Inhibition of ATM and ATR kinase activities by the radiosensitizing agent, caffeine. *Cancer Res.* 1999;59(17):4375-82.

100. Block WD, Merkle D, Meek K, and Lees-Miller SP. Selective inhibition of the DNA-dependent protein kinase (DNA-PK) by the radiosensitizing agent caffeine. *Nucleic Acids Res.* 2004;32(6):1967-72.

101. Graves PR, Yu L, Schwarz JK, Gales J, Sausville EA, O'Connor PM, et al. The Chk1 protein kinase and the Cdc25C regulatory pathways are targets of the anticancer agent UCN-01. *J Biol Chem.* 2000;275(8):5600-5.

102. Deeks SG, Smith M, Holodniy M, and Kahn JO. HIV-1 protease inhibitors: a review for clinicians. *Jama.* 1997;277(2):145-53.

103. Gupta AK, Cerniglia GJ, Mick R, McKenna WG, and Muschel RJ. HIV protease inhibitors block Akt signaling and radiosensitize tumor cells both in vitro and in vivo. *Cancer Res.* 2005;65(18):8256-65.

104. Gills JJ, LoPiccolo J, Tsurutani J, Shoemaker RH, Best CJ, Abu-Asab MS, et al. Nelfinavir, A lead HIV protease inhibitor, is a broad-spectrum, anticancer agent that induces endoplasmic reticulum stress, autophagy, and apoptosis in vitro and in vivo. *Clinical cancer research.* 2007;13(17):5183-94.

105. Jensen K, Bikas A, Patel A, Kushchayeva Y, Costello J, McDaniel D, et al. Nelfinavir inhibits proliferation and induces DNA damage in thyroid cancer cells. *Endocrine-related cancer.* 2017;24(3):147-56.

106. Deorukhkar A, and Krishnan S. Targeting inflammatory pathways for tumor radiosensitization. *Biochem Pharmacol.* 2010;80(12):1904-14.

107. Li G, Wang Z, Chong T, Yang J, Li H, and Chen H. Curcumin enhances the radiosensitivity of renal cancer cells by suppressing NF-kappaB signaling pathway. *Biomed Pharmacother.* 2017;94:974-81.

108. Cui H, Qin Q, Yang M, Zhang H, Liu Z, Yang Y, et al. Bortezomib enhances the radiosensitivity of hypoxic cervical cancer cells by inhibiting HIF-1alpha expression. *Int J Clin Exp Pathol.* 2015;8(8):9032-41.

109. Tamatani T, Takamaru N, Hara K, Kinouchi M, Kuribayashi N, Ohe G, et al. Bortezomib-enhanced radiosensitization through the suppression of radiation-induced nuclear factor-kappaB activity in human oral cancer cells. *Int J Oncol.* 2013;42(3):935-44.

110. Cron KR, Zhu K, Kushwaha DS, Hsieh G, Merzon D, Rameseder J, et al. Proteasome inhibitors block DNA repair and radiosensitize non-small cell lung cancer. *PLoS One.* 2013;8(9):e73710.

111. Ihle JN. Cytokine receptor signalling. *Nature.* 1995;377(6550):591.

112. Barry SP, Townsend PA, Knight RA, Scarabelli TM, Latchman DS, and Stephanou A. STAT3 modulates the DNA damage response pathway. *Int J Exp Pathol.* 2010;91(6):506-14.

113. Shi Y, Guryanova OA, Zhou W, Liu C, Huang Z, Fang X, et al. Ibrutinib inactivates BMX-STAT3 in glioma stem cells to impair malignant growth and radioresistance. *Sci Transl Med.* 2018;10(443).

114. Reeves PM, Abbaslou MA, Kools FRW, Vutipongsatorn K, Tong X, Gavegnano C, et al. Ruxolitinib sensitizes ovarian cancer to reduced dose Taxol, limits tumor growth and improves survival in immune competent mice. *Oncotarget.* 2017;8(55):94040-53.

115. Wang ML, Rule S, Martin P, Goy A, Auer R, Kahl BS, et al. Targeting BTK with ibrutinib in relapsed or refractory mantle-cell lymphoma. *New England Journal of Medicine.* 2013;369(6):507-16.

116. Zucha MA, Wu AT, Lee WH, Wang LS, Lin WW, Yuan CC, et al. Bruton's tyrosine kinase (Btk) inhibitor ibrutinib suppresses stem-like traits in ovarian cancer. *Oncotarget.* 2015;6(15):13255-68.

117. Hu Y, Hong Y, Xu Y, Liu P, Guo DH, and Chen Y. Inhibition of the JAK/STAT pathway with ruxolitinib overcomes cisplatin resistance in non-small-cell lung cancer NSCLC. *Apoptosis.* 2014;19(11):1627-36.

118. Zhang L, Yu J, Pan H, Hu P, Hao Y, Cai W, et al. Small molecule regulators of autophagy identified by an image-based high-throughput screen. *Proc Natl Acad Sci U S A.* 2007;104(48):19023-8.

119. Tsvetkov AS, Miller J, Arrasate M, Wong JS, Pleiss MA, and Finkbeiner S. A small-molecule scaffold induces autophagy in primary neurons and protects against toxicity in a Huntington disease model. *Proc Natl Acad Sci U S A.* 2010;107(39):16982-7.

120. Høyer-Hansen M, Bastholm L, Szyniarowski P, Campanella M, Szabadkai G, Farkas T, et al. Control of macroautophagy by calcium, calmodulin-dependent kinase kinase-β, and Bcl-2. *Molecular cell.* 2007;25(2):193-205.

121. Vucicevic L, Misirkic-Marjanovic M, Harhaji-Trajkovic L, Maric N, and Trajkovic V. Mechanisms and therapeutic significance of autophagy modulation by antipsychotic drugs. *Cell Stress.* 2018;2(11):282-91.

122. Levy JMM, Towers CG, and Thorburn A. Targeting autophagy in cancer. *Nat Rev Cancer.* 2017;17(9):528-42.

123. Gomes LR, Menck CFM, and Leandro GS. Autophagy Roles in the Modulation of DNA Repair Pathways. *Int J Mol Sci.* 2017;18(11).

124. Galluzzi L, Bravo-San Pedro JM, Demaria S, Formenti SC, and Kroemer G. Activating autophagy to potentiate immunogenic chemotherapy and radiation therapy. *Nat Rev Clin Oncol.* 2017;14(4):247-58.

125. Morel E, Mehrpour M, Botti J, Dupont N, Hamai A, Nascimbeni AC, et al. Autophagy: A Druggable Process. *Annu Rev Pharmacol Toxicol.* 2017;57:375-98.

126. Yoshida GJ. Therapeutic strategies of drug repositioning targeting autophagy to induce cancer cell death: from pathophysiology to treatment. *J Hematol Oncol.* 2017;10(1):67.

127. Panda PK, Fahrner A, Vats S, Seranova E, Sharma V, Chipara M, et al. Chemical Screening Approaches Enabling Drug Discovery of Autophagy Modulators for Biomedical Applications in Human Diseases. *Front Cell Dev Biol.* 2019;7:38.

128. Jackson SP, and Bartek J. The DNA-damage response in human biology and disease. *Nature.* 2009;461(7267):1071-8.

129. Galbiati A, Beausejour C, and d'Adda di Fagagna F. A novel single-cell method provides direct evidence of persistent DNA damage in senescent cells and aged mammalian tissues. *Aging Cell.* 2017;16(2):422-7.

130. Liu Y, Efimova EV, Ramamurthy A, and Kron SJ. Repair-independent functions of DNA-PKcs protect irradiated cells from mitotic slippage and accelerated senescence. *J Cell Sci.* 2019;132(13).

131. Beausejour CM, Krtolica A, Galimi F, Narita M, Lowe SW, Yaswen P, et al. Reversal of human cellular senescence: roles of the p53 and p16 pathways. *EMBO J.* 2003;22(16):4212-22.

132. Furnari B, Rhind N, and Russell P. Cdc25 mitotic inducer targeted by chk1 DNA damage checkpoint kinase. *Science.* 1997;277(5331):1495-7.

133. Malaquin N, Carrier-Leclerc A, Dessureault M, and Rodier F. DDR-mediated crosstalk between DNA-damaged cells and their microenvironment. *Front Genet.* 2015;6:94.

134. Dunphy G, Flannery SM, Almine JF, Connolly DJ, Paulus C, Jonsson KL, et al. Non-canonical Activation of the DNA Sensing Adaptor STING by ATM and IFI16 Mediates NF-kappaB Signaling after Nuclear DNA Damage. *Mol Cell.* 2018;71(5):745-60 e5.

135. Sharpless NE, and Sherr CJ. Forging a signature of in vivo senescence. *Nat Rev Cancer.* 2015;15(7):397-408.

136. Robles SJ, and Adami GR. Agents that cause DNA double strand breaks lead to p16INK4a enrichment and the premature senescence of normal fibroblasts. *Oncogene.* 1998;16(9):1113-23.

137. Capparelli C, Chiavarina B, Whitaker-Menezes D, Pestell TG, Pestell RG, Hulit J, et al. CDK inhibitors (p16/p19/p21) induce senescence and autophagy in cancer-associated fibroblasts, "fueling" tumor growth via paracrine interactions, without an increase in neo-angiogenesis. *Cell Cycle.* 2012;11(19):3599-610.

138. Burd CE, Sorrentino JA, Clark KS, Darr DB, Krishnamurthy J, Deal AM, et al. Monitoring tumorigenesis and senescence in vivo with a p16(INK4a)-luciferase model. *Cell.* 2013;152(1-2):340-51.

139. Baker DJ, Wijshake T, Tchkonia T, LeBrasseur NK, Childs BG, van de Sluis B, et al. Clearance of p16Ink4a-positive senescent cells delays ageing-associated disorders. *Nature.* 2011;479(7372):232-6.

140. Ko A, Han SY, and Song J. Dynamics of ARF regulation that control senescence and cancer. *BMB Rep.* 2016;49(11):598-606.

141. Sherr CJ. The INK4a/ARF network in tumour suppression. *Nat Rev Mol Cell Biol.* 2001;2(10):731-7.

142. Sherr CJ. Tumor surveillance via the ARF-p53 pathway. *Genes Dev.* 1998;12(19):2984-91.

143. Krimpenfort P, Ijpenberg A, Song JY, van der Valk M, Nawijn M, Zevenhoven J, et al. p15Ink4b is a critical tumour suppressor in the absence of p16Ink4a. *Nature.* 2007;448(7156):943-6.

144. Mirzakhani K, Kallenbach J, Rasa SMM, Ribaudo F, Ungelenk M, Ehsani M, et al. The androgen receptor-lncRNASAT1-AKT-p15 axis mediates androgen-induced cellular senescence in prostate cancer cells. *Oncogene.* 2021.

145. Wiley CD, Flynn JM, Morrissey C, Lebofsky R, Shuga J, Dong X, et al. Analysis of individual cells identifies cell-to-cell variability following induction of cellular senescence. *Aging Cell.* 2017;16(5):1043-50.

146. Dulic V, Kaufmann WK, Wilson SJ, Tlsty TD, Lees E, Harper JW, et al. p53-dependent inhibition of cyclin-dependent kinase activities in human fibroblasts during radiation-induced G1 arrest. *Cell.* 1994;76(6):1013-23.

147. Jung YS, Qian Y, and Chen X. Examination of the expanding pathways for the regulation of p21 expression and activity. *Cell Signal.* 2010;22(7):1003-12.

148. Besson A, and Yong VW. Involvement of p21(Waf1/Cip1) in protein kinase C alpha-induced cell cycle progression. *Mol Cell Biol.* 2000;20(13):4580-90.

149. Dulic V, Beney GE, Frebourg G, Drullinger LF, and Stein GH. Uncoupling between phenotypic senescence and cell cycle arrest in aging p21-deficient fibroblasts. *Mol Cell Biol.* 2000;20(18):6741-54.

150. Narita M, Nunez S, Heard E, Narita M, Lin AW, Hearn SA, et al. Rb-mediated heterochromatin formation and silencing of E2F target genes during cellular senescence. *Cell.* 2003;113(6):703-16.

151. Di Micco R, Sulli G, Dobreva M, Liontos M, Botrugno OA, Gargiulo G, et al. Interplay between oncogene-induced DNA damage response and heterochromatin in senescence and cancer. *Nat Cell Biol.* 2011;13(3):292-302.

152. Zhang R, Poustovoitov MV, Ye X, Santos HA, Chen W, Daganzo SM, et al. Formation of MacroH2A-containing senescence-associated heterochromatin foci and senescence driven by ASF1a and HIRA. *Dev Cell.* 2005;8(1):19-30.

153. Chandra T, Kirschner K, Thuret JY, Pope BD, Ryba T, Newman S, et al. Independence of repressive histone marks and chromatin compaction during senescent heterochromatic layer formation. *Mol Cell.* 2012;47(2):203-14.

154. Takahashi A, Imai Y, Yamakoshi K, Kuninaka S, Ohtani N, Yoshimoto S, et al. DNA damage signaling triggers degradation of histone methyltransferases through APC/C(Cdh1) in senescent cells. *Mol Cell.* 2012;45(1):123-31.

155. Sen P, Lan Y, Li CY, Sidoli S, Donahue G, Dou Z, et al. Histone Acetyltransferase p300 Induces De Novo Super-Enhancers to Drive Cellular Senescence. *Mol Cell.* 2019;73(4):684-98 e8.

156. Tasdemir N, Banito A, Roe JS, Alonso-Curbelo D, Camiolo M, Tschaharganeh DF, et al. BRD4 Connects Enhancer Remodeling to Senescence Immune Surveillance. *Cancer Discov.* 2016;6(6):612-29.

157. Xie W, Kagiampakis I, Pan L, Zhang YW, Murphy L, Tao Y, et al. DNA Methylation Patterns Separate Senescence from Transformation Potential and Indicate Cancer Risk. *Cancer Cell.* 2018;33(2):309-21 e5.

158. Freund A, Laberge RM, Demaria M, and Campisi J. Lamin B1 loss is a senescence-associated biomarker. *Mol Biol Cell.* 2012;23(11):2066-75.

159. Hernandez-Segura A, de Jong TV, Melov S, Guryev V, Campisi J, and Demaria M. Unmasking Transcriptional Heterogeneity in Senescent Cells. *Curr Biol.* 2017;27(17):2652-60 e4.

160. Sadaie M, Salama R, Carroll T, Tomimatsu K, Chandra T, Young AR, et al. Redistribution of the Lamin B1 genomic binding profile affects rearrangement of heterochromatic domains and SAHF formation during senescence. *Genes Dev.* 2013;27(16):1800-8.

161. Shah PP, Donahue G, Otte GL, Capell BC, Nelson DM, Cao K, et al. Lamin B1 depletion in senescent cells triggers large-scale changes in gene expression and the chromatin landscape. *Genes Dev.* 2013;27(16):1787-99.

162. Ivanov A, Pawlikowski J, Manoharan I, van Tuyn J, Nelson DM, Rai TS, et al. Lysosome-mediated processing of chromatin in senescence. *J Cell Biol.* 2013;202(1):129-43.

163. Dou Z, Ghosh K, Vizioli MG, Zhu J, Sen P, Wangensteen KJ, et al. Cytoplasmic chromatin triggers inflammation in senescence and cancer. *Nature.* 2017;550(7676):402-6.

164. Chapman J, Fielder E, and Passos JF. Mitochondrial dysfunction and cell senescence: deciphering a complex relationship. *FEBS Lett.* 2019;593(13):1566-79.

165. Mai S, Klinkenberg M, Auburger G, Bereiter-Hahn J, and Jendrach M. Decreased expression of Drp1 and Fis1 mediates mitochondrial elongation in senescent cells and enhances resistance to oxidative stress through PINK1. *J Cell Sci.* 2010;123(Pt 6):917-26.

166. Korolchuk VI, Miwa S, Carroll B, and von Zglinicki T. Mitochondria in Cell Senescence: Is Mitophagy the Weakest Link? *EBioMedicine.* 2017;21:7-13.

167. Tai H, Wang Z, Gong H, Han X, Zhou J, Wang X, et al. Autophagy impairment with lysosomal and mitochondrial dysfunction is an important characteristic of oxidative stress-induced senescence. *Autophagy.* 2017;13(1):99-113.

168. Passos JF, Saretzki G, Ahmed S, Nelson G, Richter T, Peters H, et al. Mitochondrial dysfunction accounts for the stochastic heterogeneity in telomere-dependent senescence. *PLoS Biol.* 2007;5(5):e110.

169. Correia-Melo C, Marques FD, Anderson R, Hewitt G, Hewitt R, Cole J, et al. Mitochondria are required for pro-ageing features of the senescent phenotype. *EMBO J.* 2016;35(7):724-42.

170. Wiley CD, Velarde MC, Lecot P, Liu S, Sarnoski EA, Freund A, et al. Mitochondrial Dysfunction Induces Senescence with a Distinct Secretory Phenotype. *Cell Metab.* 2016;23(2):303-14.

171. Seluanov A, Gorbunova V, Falcovitz A, Sigal A, Milyavsky M, Zurer I, et al. Change of the death pathway in senescent human fibroblasts in response to DNA damage is caused by an inability to stabilize p53. *Mol Cell Biol.* 2001;21(5):1552-64.

172. Ryu SJ, Oh YS, and Park SC. Failure of stress-induced downregulation of Bcl-2 contributes to apoptosis resistance in senescent human diploid fibroblasts. *Cell Death Differ.* 2007;14(5):1020-8.

173. Sanders YY, Liu H, Zhang X, Hecker L, Bernard K, Desai L, et al. Histone modifications in senescence-associated resistance to apoptosis by oxidative stress. *Redox Biol.* 2013;1:8-16.

174. Rochette PJ, and Brash DE. Progressive apoptosis resistance prior to senescence and control by the anti-apoptotic protein BCL-xL. *Mech Ageing Dev.* 2008;129(4):207-14.

175. Yosef R, Pilpel N, Tokarsky-Amiel R, Biran A, Ovadya Y, Cohen S, et al. Directed elimination of senescent cells by inhibition of BCL-W and BCL-XL. *Nat Commun.* 2016;7:11190.

176. Baar MP, Brandt RMC, Putavet DA, Klein JDD, Derks KWJ, Bourgeois BRM, et al. Targeted Apoptosis of Senescent Cells Restores Tissue Homeostasis in Response to Chemotoxicity and Aging. *Cell.* 2017;169(1):132-47 e16.

177. Yosef R, Pilpel N, Papismadov N, Gal H, Ovadya Y, Vadai E, et al. p21 maintains senescent cell viability under persistent DNA damage response by restraining JNK and caspase signaling. *EMBO J.* 2017;36(15):2280-95.

178. Fuhrmann-Stroissnigg H, Ling YY, Zhao J, McGowan SJ, Zhu Y, Brooks RW, et al. Identification of HSP90 inhibitors as a novel class of senolytics. *Nat Commun.* 2017;8(1):422.

179. Zhu Y, Tchkonia T, Pirtskhalava T, Gower AC, Ding H, Giorgadze N, et al. The Achilles' heel of senescent cells: from transcriptome to senolytic drugs. *Aging Cell.* 2015;14(4):644-58.

180. Kirkland JL, and Tchkonia T. Senolytic drugs: from discovery to translation. *J Intern Med.* 2020;288(5):518-36.

181. Morancho B, Martinez-Barriocanal A, Villanueva J, and Arribas J. Role of ADAM17 in the non-cell autonomous effects of oncogene-induced senescence. *Breast Cancer Res.* 2015;17:106.

182. Effenberger T, von der Heyde J, Bartsch K, Garbers C, Schulze-Osthoff K, Chalaris A, et al. Senescence-associated release of transmembrane proteins involves proteolytic processing by ADAM17 and microvesicle shedding. *FASEB J.* 2014;28(11):4847-56.

183. Takasugi M, Okada R, Takahashi A, Virya Chen D, Watanabe S, and Hara E. Small extracellular vesicles secreted from senescent cells promote cancer cell proliferation through EphA2. *Nat Commun.* 2017;8:15729.

184. Coppe JP, Rodier F, Patil CK, Freund A, Desprez PY, and Campisi J. Tumor suppressor and aging biomarker p16(INK4a) induces cellular senescence without the associated inflammatory secretory phenotype. *J Biol Chem.* 2011;286(42):36396-403.

185. Rodier F, Munoz DP, Teachenor R, Chu V, Le O, Bhaumik D, et al. DNA-SCARS: distinct nuclear structures that sustain damage-induced senescence growth arrest and inflammatory cytokine secretion. *J Cell Sci.* 2011;124(Pt 1):68-81.

186. Freund A, Patil CK, and Campisi J. p38MAPK is a novel DNA damage response-independent regulator of the senescence-associated secretory phenotype. *EMBO J.* 2011;30(8):1536-48.

187. Huggins CJ, Malik R, Lee S, Salotti J, Thomas S, Martin N, et al. C/EBPgamma suppresses senescence and inflammatory gene expression by heterodimerizing with C/EBPbeta. *Mol Cell Biol.* 2013;33(16):3242-58.

188. Salminen A, Kauppinen A, and Kaarniranta K. Emerging role of NF-kappaB signaling in the induction of senescence-associated secretory phenotype (SASP). *Cell Signal.* 2012;24(4):835-45.

189. Chien Y, Scuoppo C, Wang X, Fang X, Balgley B, Bolden JE, et al. Control of the senescence-associated secretory phenotype by NF-kappaB promotes senescence and enhances chemosensitivity. *Genes Dev.* 2011;25(20):2125-36.

190. Mongi-Bragato B, Grondona E, Sosa LDV, Zlocowski N, Venier AC, Torres AI, et al. Pivotal role of NF-kappaB in cellular senescence of experimental pituitary tumours. *J Endocrinol.* 2020;245(2):179-91.

191. Orjalo AV, Bhaumik D, Gengler BK, Scott GK, and Campisi J. Cell surface-bound IL-1alpha is an upstream regulator of the senescence-associated IL-6/IL-8 cytokine network. *Proc Natl Acad Sci U S A.* 2009;106(40):17031-6.

192. Bhaumik D, Scott GK, Schokrpur S, Patil CK, Orjalo AV, Rodier F, et al. MicroRNAs miR-146a/b negatively modulate the senescence-associated inflammatory mediators IL-6 and IL-8. *Aging (Albany NY).* 2009;1(4):402-11.

193. Ito Y, Hoare M, and Narita M. Spatial and Temporal Control of Senescence. *Trends Cell Biol.* 2017;27(11):820-32.

194. Hoare M, Ito Y, Kang TW, Weekes MP, Matheson NJ, Patten DA, et al. NOTCH1 mediates a switch between two distinct secretomes during senescence. *Nat Cell Biol.* 2016;18(9):979-92.

195. Tominaga K, and Suzuki HI. TGF-beta Signaling in Cellular Senescence and Aging-Related Pathology. *Int J Mol Sci.* 2019;20(20).

196. Munoz-Espin D, Canamero M, Maraver A, Gomez-Lopez G, Contreras J, Murillo-Cuesta S, et al. Programmed cell senescence during mammalian embryonic development. *Cell.* 2013;155(5):1104-18.

197. Hubackova S, Krejcikova K, Bartek J, and Hodny Z. IL1- and TGFbeta-Nox4 signaling, oxidative stress and DNA damage response are shared features of replicative, oncogene-induced, and drug-induced paracrine 'bystander senescence'. *Aging (Albany NY).* 2012;4(12):932-51.

198. Valdez JM, Zhang L, Su Q, Dakhova O, Zhang Y, Shahi P, et al. Notch and TGFbeta form a reciprocal positive regulatory loop that suppresses murine prostate basal stem/progenitor cell activity. *Cell Stem Cell.* 2012;11(5):676-88.

199. Kagawa S, Natsuizaka M, Whelan KA, Facompre N, Naganuma S, Ohashi S, et al. Cellular senescence checkpoint function determines differential Notch1-dependent oncogenic and tumor-suppressor activities. *Oncogene.* 2015;34(18):2347-59.

200. Weichhart T. mTOR as Regulator of Lifespan, Aging, and Cellular Senescence: A Mini-Review. *Gerontology.* 2018;64(2):127-34.

201. Chandrasekaran A, Lee MY, Zhang X, Hasan S, Desta H, Tenenbaum SA, et al. Redox and mTOR-dependent regulation of plasma lamellar calcium influx controls the senescence-associated secretory phenotype. *Exp Biol Med (Maywood).* 2020;245(17):1560-70.

202. van Vliet T, Varela-Eirin M, Wang B, Borghesan M, Brandenburg SM, Franzin R, et al. Physiological hypoxia restrains the senescence-associated secretory phenotype via AMPK-mediated mTOR suppression. *Mol Cell.* 2021;81(9):2041-52 e6.

203. Laberge RM, Sun Y, Orjalo AV, Patil CK, Freund A, Zhou L, et al. MTOR regulates the pro-tumorigenic senescence-associated secretory phenotype by promoting IL1A translation. *Nat Cell Biol.* 2015;17(8):1049-61.

204. Herranz N, Gallage S, Mellone M, Wuestefeld T, Klotz S, Hanley CJ, et al. mTOR regulates MAPKAPK2 translation to control the senescence-associated secretory phenotype. *Nat Cell Biol.* 2015;17(9):1205-17.

205. Tomimatsu K, and Narita M. Translating the effects of mTOR on secretory senescence. *Nat Cell Biol.* 2015;17(10):1230-2.

206. Gluck S, Guey B, Gulen MF, Wolter K, Kang TW, Schmacke NA, et al. Innate immune sensing of cytosolic chromatin fragments through cGAS promotes senescence. *Nat Cell Biol.* 2017;19(9):1061-70.

207. Loo TM, Miyata K, Tanaka Y, and Takahashi A. Cellular senescence and senescence-associated secretory phenotype via the cGAS-STING signaling pathway in cancer. *Cancer Sci.* 2020;111(2):304-11.

208. Sun L, Wu J, Du F, Chen X, and Chen ZJ. Cyclic GMP-AMP synthase is a cytosolic DNA sensor that activates the type I interferon pathway. *Science.* 2013;339(6121):786-91.

209. Wu J, Sun L, Chen X, Du F, Shi H, Chen C, et al. Cyclic GMP-AMP is an endogenous second messenger in innate immune signaling by cytosolic DNA. *Science.* 2013;339(6121):826-30.

210. Yang H, Wang H, Ren J, Chen Q, and Chen ZJ. cGAS is essential for cellular senescence. *Proc Natl Acad Sci U S A.* 2017;114(23):E4612-E20.

211. Hari P, Millar FR, Tarrats N, Birch J, Quintanilla A, Rink CJ, et al. The innate immune sensor Toll-like receptor 2 controls the senescence-associated secretory phenotype. *Sci Adv.* 2019;5(6):eaaw0254.

212. Takahashi A, Loo TM, Okada R, Kamachi F, Watanabe Y, Wakita M, et al. Downregulation of cytoplasmic DNases is implicated in cytoplasmic DNA accumulation and SASP in senescent cells. *Nat Commun.* 2018;9(1):1249.

213. Nacarelli T, Lau L, Fukumoto T, Zundell J, Fatkhutdinov N, Wu S, et al. NAD(+) metabolism governs the proinflammatory senescence-associated secretome. *Nat Cell Biol.* 2019;21(3):397-407.

214. Hou Y, Wei Y, Lautrup S, Yang B, Wang Y, Cordonnier S, et al. NAD(+) supplementation reduces neuroinflammation and cell senescence in a transgenic mouse model of Alzheimer's disease via cGAS-STING. *Proc Natl Acad Sci U S A.* 2021;118(37).

215. Nacarelli T, Liu P, and Zhang R. Epigenetic Basis of Cellular Senescence and Its Implications in Aging. *Genes (Basel).* 2017;8(12).

216. Pazolli E, Alspach E, Milczarek A, Prior J, Piwnica-Worms D, and Stewart SA. Chromatin remodeling underlies the senescence-associated secretory phenotype of tumor stromal fibroblasts that supports cancer progression. *Cancer Res.* 2012;72(9):2251-61.

217. Hayakawa T, Iwai M, Aoki S, Takimoto K, Maruyama M, Maruyama W, et al. SIRT1 suppresses the senescence-associated secretory phenotype through epigenetic gene regulation. *PLoS One.* 2015;10(1):e0116480.

218. Chen H, Ruiz PD, McKimpson WM, Novikov L, Kitsis RN, and Gamble MJ. MacroH2A1 and ATM Play Opposing Roles in Paracrine Senescence and the Senescence-Associated Secretory Phenotype. *Mol Cell.* 2015;59(5):719-31.

219. Braig M, Lee S, Loddenkemper C, Rudolph C, Peters AH, Schlegelberger B, et al. Oncogene-induced senescence as an initial barrier in lymphoma development. *Nature.* 2005;436(7051):660-5.

220. Chen Z, Trotman LC, Shaffer D, Lin HK, Dotan ZA, Niki M, et al. Crucial role of p53-dependent cellular senescence in suppression of Pten-deficient tumorigenesis. *Nature.* 2005;436(7051):725-30.

221. Sun H, Wang H, Wang X, Aoki Y, Wang X, Yang Y, et al. Aurora-A/SOX8/FOXK1 signaling axis promotes chemoresistance via suppression of cell senescence and induction of glucose metabolism in ovarian cancer organoids and cells. *Theranostics.* 2020;10(15):6928-45.

222. Lecot P, Alimirah F, Desprez PY, Campisi J, and Wiley C. Context-dependent effects of cellular senescence in cancer development. *Br J Cancer.* 2016;114(11):1180-4.

223. Capece D, Verzella D, Tessitore A, Alesse E, Capalbo C, and Zazzeroni F. Cancer secretome and inflammation: The bright and the dark sides of NF-kappaB. *Semin Cell Dev Biol.* 2018;78:51-61.

224. Acosta JC, Banito A, Wuestefeld T, Georgilis A, Janich P, Morton JP, et al. A complex secretory program orchestrated by the inflammasome controls paracrine senescence. *Nat Cell Biol.* 2013;15(8):978-90.

225. Acosta JC, O'Loghlen A, Banito A, Guijarro MV, Augert A, Raguz S, et al. Chemokine signaling via the CXCR2 receptor reinforces senescence. *Cell.* 2008;133(6):1006-18.

226. Kuilman T, Michaloglou C, Vredeveld LC, Douma S, van Doorn R, Desmet CJ, et al. Oncogene-induced senescence relayed by an interleukin-dependent inflammatory network. *Cell.* 2008;133(6):1019-31.

227. Hubackova S, Novakova Z, Krejcikova K, Kosar M, Dobrovolna J, Duskova P, et al. Regulation of the PML tumor suppressor in drug-induced senescence of human normal and cancer cells by JAK/STAT-mediated signaling. *Cell Cycle.* 2010;9(15):3085-99.

228. Nelson G, Kucheryavenko O, Wordsworth J, and von Zglinicki T. The senescent bystander effect is caused by ROS-activated NF-kappaB signalling. *Mech Ageing Dev.* 2018;170:30-6.

229. Nelson G, Wordsworth J, Wang C, Jurk D, Lawless C, Martin-Ruiz C, et al. A senescent cell bystander effect: senescence-induced senescence. *Aging Cell.* 2012;11(2):345-9.

230. Wajapeyee N, Serra RW, Zhu X, Mahalingam M, and Green MR. Oncogenic BRAF induces senescence and apoptosis through pathways mediated by the secreted protein IGFBP7. *Cell.* 2008;132(3):363-74.

231. von Kobbe C. Cellular senescence: a view throughout organismal life. *Cell Mol Life Sci.* 2018;75(19):3553-67.

232. Xue W, Zender L, Miething C, Dickins RA, Hernando E, Krizhanovsky V, et al. Senescence and tumour clearance is triggered by p53 restoration in murine liver carcinomas. *Nature.* 2007;445(7128):656-60.

233. Kang TW, Yevsa T, Woller N, Hoenicke L, Wuestefeld T, Dauch D, et al. Senescence surveillance of pre-malignant hepatocytes limits liver cancer development. *Nature.* 2011;479(7374):547-51.

234. Lujambio A, Akkari L, Simon J, Grace D, Tschaharganeh DF, Bolden JE, et al. Non-cell-autonomous tumor suppression by p53. *Cell.* 2013;153(2):449-60.

235. Iannello A, Thompson TW, Ardolino M, Lowe SW, and Raulet DH. p53-dependent chemokine production by senescent tumor cells supports NKG2D-dependent tumor elimination by natural killer cells. *J Exp Med.* 2013;210(10):2057-69.

236. Wang RW, Vigano S, Ben-David U, Amon A, and Santaguida S. Aneuploid senescent cells activate NF-kappaB to promote their immune clearance by NK cells. *EMBO Rep.* 2021;22(8):e52032.

237. Meng Y, Efimova EV, Hamzeh KW, Darga TE, Mauceri HJ, Fu YX, et al. Radiation-inducible immunotherapy for cancer: senescent tumor cells as a cancer vaccine. *Mol Ther.* 2012;20(5):1046-55.

238. Parrinello S, Coppe JP, Krtolica A, and Campisi J. Stromal-epithelial interactions in aging and cancer: senescent fibroblasts alter epithelial cell differentiation. *J Cell Sci.* 2005;118(Pt 3):485-96.

239. Lawrenson K, Grun B, Benjamin E, Jacobs IJ, Dafou D, and Gayther SA. Senescent fibroblasts promote neoplastic transformation of partially transformed ovarian epithelial cells in a three-dimensional model of early stage ovarian cancer. *Neoplasia.* 2010;12(4):317-25.

240. Baker DJ, Childs BG, Durik M, Wijers ME, Sieben CJ, Zhong J, et al. Naturally occurring p16(Ink4a)-positive cells shorten healthy lifespan. *Nature.* 2016;530(7589):184-9.

241. Krtolica A, Parrinello S, Lockett S, Desprez PY, and Campisi J. Senescent fibroblasts promote epithelial cell growth and tumorigenesis: a link between cancer and aging. *Proc Natl Acad Sci U S A.* 2001;98(21):12072-7.

242. Coppe JP, Boysen M, Sun CH, Wong BJ, Kang MK, Park NH, et al. A role for fibroblasts in mediating the effects of tobacco-induced epithelial cell growth and invasion. *Mol Cancer Res.* 2008;6(7):1085-98.

243. Di GH, Liu Y, Lu Y, Liu J, Wu C, and Duan HF. IL-6 secreted from senescent mesenchymal stem cells promotes proliferation and migration of breast cancer cells. *PLoS One.* 2014;9(11):e113572.

244. Pazolli E, Luo X, Brehm S, Carbery K, Chung JJ, Prior JL, et al. Senescent stromal-derived osteopontin promotes preneoplastic cell growth. *Cancer Res.* 2009;69(3):1230-9.

245. Liu D, and Hornsby PJ. Senescent human fibroblasts increase the early growth of xenograft tumors via matrix metalloproteinase secretion. *Cancer Res.* 2007;67(7):3117-26.

246. Farsam V, Basu A, Gatzka M, Treiber N, Schneider LA, Mulaw MA, et al. Senescent fibroblast-derived Chemerin promotes squamous cell carcinoma migration. *Oncotarget.* 2016;7(50):83554-69.

247. Oubaha M, Miloudi K, Dejda A, Guber V, Mawambo G, Germain MA, et al. Senescence-associated secretory phenotype contributes to pathological angiogenesis in retinopathy. *Sci Transl Med.* 2016;8(362):362ra144.

248. Aifuwa I, Giri A, Longe N, Lee SH, An SS, and Wirtz D. Senescent stromal cells induce cancer cell migration via inhibition of RhoA/ROCK/myosin-based cell contractility. *Oncotarget.* 2015;6(31):30516-31.

249. Coppe JP, Kauser K, Campisi J, and Beausejour CM. Secretion of vascular endothelial growth factor by primary human fibroblasts at senescence. *J Biol Chem.* 2006;281(40):29568-74.

250. Yang F, Tuxhorn JA, Ressler SJ, McAlhany SJ, Dang TD, and Rowley DR. Stromal expression of connective tissue growth factor promotes angiogenesis and prostate cancer tumorigenesis. *Cancer Res.* 2005;65(19):8887-95.

251. Kim YH, Choi YW, Lee J, Soh EY, Kim JH, and Park TJ. Senescent tumor cells lead the collective invasion in thyroid cancer. *Nat Commun.* 2017;8:15208.

252. Canino C, Mori F, Cambria A, Diamantini A, Germoni S, Alessandrini G, et al. SASP mediates chemoresistance and tumor-initiating-activity of mesothelioma cells. *Oncogene.* 2012;31(26):3148-63.

253. Tato-Costa J, Casimiro S, Pacheco T, Pires R, Fernandes A, Alho I, et al. Therapy-Induced Cellular Senescence Induces Epithelial-to-Mesenchymal Transition and Increases Invasiveness in Rectal Cancer. *Clin Colorectal Cancer.* 2016;15(2):170-8 e3.

254. Angelini PD, Zacarias Fluck MF, Pedersen K, Parra-Palau JL, Guiu M, Bernado Morales C, et al. Constitutive HER2 signaling promotes breast cancer metastasis through cellular senescence. *Cancer Res.* 2013;73(1):450-8.

255. Luo X, Fu Y, Loza AJ, Murali B, Leahy KM, Ruhland MK, et al. Stromal-Initiated Changes in the Bone Promote Metastatic Niche Development. *Cell Rep.* 2016;14(1):82-92.

256. Malaquin N, Vercamer C, Bouali F, Martien S, Deruy E, Wernert N, et al. Senescent fibroblasts enhance early skin carcinogenic events via a paracrine MMP-PAR-1 axis. *PLoS One.* 2013;8(5):e63607.

257. Kaur A, Webster MR, Marchbank K, Behera R, Ndoye A, Kugel CH, 3rd, et al. sFRP2 in the aged microenvironment drives melanoma metastasis and therapy resistance. *Nature.* 2016;532(7598):250-4.

258. Gilbert LA, and Hemann MT. DNA damage-mediated induction of a chemoresistant niche. *Cell.* 2010;143(3):355-66.

259. Bent EH, Gilbert LA, and Hemann MT. A senescence secretory switch mediated by PI3K/AKT/mTOR activation controls chemoprotective endothelial secretory responses. *Genes Dev.* 2016;30(16):1811-21.

260. Jackson JG, Pant V, Li Q, Chang LL, Quintas-Cardama A, Garza D, et al. p53-mediated senescence impairs the apoptotic response to chemotherapy and clinical outcome in breast cancer. *Cancer Cell.* 2012;21(6):793-806.

261. Taguchi J, and Yamada Y. Unveiling the Role of Senescence-Induced Cellular Plasticity. *Cell Stem Cell.* 2017;20(3):293-4.

262. Mosteiro L, Pantoja C, Alcazar N, Marion RM, Chondronasiou D, Rovira M, et al. Tissue damage and senescence provide critical signals for cellular reprogramming in vivo. *Science.* 2016;354(6315).

263. Cahu J, Bustany S, and Sola B. Senescence-associated secretory phenotype favors the emergence of cancer stem-like cells. *Cell Death Dis.* 2012;3:e446.

264. Milanovic M, Fan DNY, Belenki D, Dabritz JHM, Zhao Z, Yu Y, et al. Senescence-associated reprogramming promotes cancer stemness. *Nature.* 2018;553(7686):96-100.

265. Karabicici M, Alptekin S, Firtina Karagonlar Z, and Erdal E. Doxorubicin-induced senescence promotes stemness and tumorigenicity in EpCAM-/CD133- nonstem cell population in hepatocellular carcinoma cell line, HuH-7. *Mol Oncol.* 2021;15(8):2185-202.

266. Ortiz-Montero P, Londono-Vallejo A, and Vernot JP. Senescence-associated IL-6 and IL-8 cytokines induce a self- and cross-reinforced senescence/inflammatory milieu strengthening tumorigenic capabilities in the MCF-7 breast cancer cell line. *Cell Commun Signal.* 2017;15(1):17.

267. Eggert T, Wolter K, Ji J, Ma C, Yevsa T, Klotz S, et al. Distinct Functions of Senescence-Associated Immune Responses in Liver Tumor Surveillance and Tumor Progression. *Cancer Cell.* 2016;30(4):533-47.

268. Loo TM, Kamachi F, Watanabe Y, Yoshimoto S, Kanda H, Arai Y, et al. Gut Microbiota Promotes Obesity-Associated Liver Cancer through PGE2-Mediated Suppression of Antitumor Immunity. *Cancer Discov.* 2017;7(5):522-38.

269. Toso A, Revandkar A, Di Mitri D, Guccini I, Proietti M, Sarti M, et al. Enhancing chemotherapy efficacy in Pten-deficient prostate tumors by activating the senescence-associated antitumor immunity. *Cell Rep.* 2014;9(1):75-89.

270. Di Mitri D, Toso A, Chen JJ, Sarti M, Pinton S, Jost TR, et al. Tumour-infiltrating Gr-1+ myeloid cells antagonize senescence in cancer. *Nature.* 2014;515(7525):134-7.

271. Ruhland MK, Loza AJ, Capietto AH, Luo X, Knolhoff BL, Flanagan KC, et al. Stromal senescence establishes an immunosuppressive microenvironment that drives tumorigenesis. *Nat Commun.* 2016;7:11762.

272. Choi YW, Kim YH, Oh SY, Suh KW, Kim YS, Lee GY, et al. Senescent Tumor Cells Build a Cytokine Shield in Colorectal Cancer. *Adv Sci (Weinh).* 2021;8(4):2002497.

273. Pereira BI, Devine OP, Vukmanovic-Stejic M, Chambers ES, Subramanian P, Patel N, et al. Senescent cells evade immune clearance via HLA-E-mediated NK and CD8(+) T cell inhibition. *Nat Commun.* 2019;10(1):2387.

274. Sanwald JL, Poschmann G, Stuhler K, Behrends C, Hoffmann S, and Willbold D. The GABARAP Co-Secretome Identified by APEX2-GABARAP Proximity Labelling of Extracellular Vesicles. *Cells.* 2020;9(6).

275. Kim KE, Park I, Kim J, Kang MG, Choi WG, Shin H, et al. Dynamic tracking and identification of tissue-specific secretory proteins in the circulation of live mice. *Nat Commun.* 2021;12(1):5204.

276. Basisty N, Kale A, Jeon OH, Kuehnemann C, Payne T, Rao C, et al. A proteomic atlas of senescence-associated secretomes for aging biomarker development. *PLoS Biol.* 2020;18(1):e3000599.

277. Uyar B, Palmer D, Kowald A, Murua Escobar H, Barrantes I, Moller S, et al. Single-cell analyses of aging, inflammation and senescence. *Ageing Res Rev.* 2020;64:101156.

278. Chen W, Wang X, Wei G, Huang Y, Shi Y, Li D, et al. Single-Cell Transcriptome Analysis Reveals Six Subpopulations Reflecting Distinct Cellular Fates in Senescent Mouse Embryonic Fibroblasts. *Front Genet.* 2020;11:867.

279. Tabula Muris C. A single-cell transcriptomic atlas characterizes ageing tissues in the mouse. *Nature.* 2020;583(7817):590-5.

CHAPTER 2

REPAIR-INDEPENDENT FUNCTIONS OF DNA-PKCS PROTECT IRRADIATED CELLS FROM MITOTIC SLIPPAGE AND ACCELERATED SENESCENCE

This chapter consists of the following published manuscript in its entirety:

Y Liu, E V Efimova, A Ramamurthy, S J Kron. Repair-independent functions of DNA-PKcs protect irradiated cells from mitotic slippage and accelerated senescence. *Journal of cell science*. 2019, 132(13), jcs229385. PMID: 31189537; PMCID: PMC6633392; DOI: 10.1242/jcs.229385. 2.1

I was responsible for conducting most of the experiments and writing the manuscript. Coauthors Efimova and Ramamurthy contributed intellectually and were responsible for establishing knock-down cell lines. All of the authors contributed to manuscript editing.

2.1 Introduction

When cancer cells are subjected to genotoxic stress, failure to detect or repair DNA double strand breaks (DSBs) may result in mitotic catastrophe or lethal aneuploidy, leading to the presumed benefits of radiation and chemotherapy (1). A common rationale for targeting the DNA damage response (DDR) in cancer is to potentiate genotoxic therapy by blocking checkpoint arrest and repair (2). Of the 500-some proteins that mediate the DDR (3), the DNA-dependent protein kinase catalytic subunit (DNA-PKcs, PRKDC, XRCC7) is considered a central player in DNA damage signaling and DSB repair. An early event at many DSBs is the binding of the Ku70 and Ku80 proteins which can recruit DNA-PKcs and initiate repair via the conventional Ligase 4-dependent non-homologous end joining (NHEJ) pathway (4) . The logic that targeting NHEJ may confer or restore sensitivity to therapy has led to substantial efforts to develop DNA-PKcs inhibitors as cancer drugs (5, 6). Though several clinical candidates remain under study, others have been abandoned during development and none have reached the clinic.

DNA-PKcs and ataxia-telangiectasia mutated kinase (ATM) (7) are closely related members of the phosphatidylinositol 3-kinase-related kinase (PIKK) superfamily with shared functions in the DDR, including phosphorylating Ser139 in the carboxyl terminal tail of histone H2AX in nucleosomes adjacent to DSBs, forming γH2AX foci (8). DNA-PKcs and ATM also phosphorylate each other (9), with DNA-PKcs serving as a negative regulator of ATM (10, 11). This negative feedback may explain the seemingly inconsistent observations that while ATM inhibitors block γH2AX foci formation (12) and suppress checkpoint arrest and cellular senescence (13), DNA-PK inhibitors delay γH2AX foci resolution and promote checkpoint arrest and cellular senescence (14-17).

A complementary concern is that cell lines deficient for DNA-PKcs often display reduced

ATM expression (18). Though mechanisms have yet to be fully defined, the effect can be recapitulated by siRNA knockdown of DNA-PKcs (19) and has been linked to overexpression of microRNA miR-100 in DNA-PKcs$^{-/-}$ cells (20). Nonetheless, while the most parsimonious explanation for the DNA repair defects and radiation sensitivity in DNA-PKcs deficient cells is their lack of DNA-PKcs activity, this fails to account for the confounding effects of ATM downregulation, which may suppress all aspects of the DNA damage response including DSB repair.

Using MCF7 breast cancer as a model, we observed that specifically inhibiting DNA-PKcs conferred the expected increase in sensitivity to radiation, but this was not linked to a DSB repair defect. As with chemical inhibition, partial knockdown of DNA-PKcs allowed DSBs to be repaired without delay. Despite apparently having completed repair, the γH2AX foci formed at chromosomal breaks failed to resolve, indicating a persistent DDR. When these cells progressed to mitosis, they displayed high rates of cytokinesis failure. The surviving binucleate cells adopted the characteristic senescent phenotype of flattened cell shape and expression of senescence-associated β-galactosidase (SA-βGal). By contrast, knockdown of the Ku proteins or other core NHEJ factors was able to block DSB repair but γH2AX foci resolved on schedule, followed promptly by cell division resulting in mitotic catastrophe.

Prior studies have linked DNA-PKcs inhibition to defects in mitosis, potentially mediated by loss of interactions with polo-like kinase 1 (PLK1) and/or phosphatase 6 (PP6) (21). However, we find that the persistent γH2AX, mitotic slippage and accelerated senescence after irradiation of cells with decreased DNA-PKcs activity could all be suppressed by subsequent inhibition of ATM. Thus, while DNA-PKcs clearly plays a key role in regulating DNA damage response, our data unlink DNA-PKcs from NHEJ repair and instead define a new role in

protecting cells from persistent ATM-dependent DNA damage signaling. Although blocking DNA-PKcs can inhibit proliferation after irradiation, cells remain viable after undergoing therapy-induced senescence. Given recent studies suggesting reversibility of senescence (22, 23) and implicating senescent tumor cells in cancer recurrence after therapy (24), our results suggest reevaluating the rationale for clinical development of DNA-PKcs inhibitors.

2.2 Results

Inhibition of DNA-PKcs induces persistent γH2AX, enhances radiosensitivity and accelerates cellular senescence

Toward reexamining DNA-PKcs functions in the DNA damage response (DDR) following exposure to ionizing radiation (IR), we inhibited DNA-PKcs in MCF7 cells and then irradiated the cells to induce double strand breaks (DSBs). DNA-PKcs was targeted by transducing MCF7 cells with lentivirus expressing short hairpin RNA (shRNA) to target DNA-PKcs transcripts (shDNA-PKcs, Figure 2.2A) or treating cells expressing a scrambled shRNA control (shScr) with Nu7026 (2-(morpholin-4-yl)-benzo-[h]chomen-4-one (25)), a potent DNA-PKcs kinase inhibitor with >100 fold selectivity over ATM. We monitored the dynamics of IR-induced chromatin foci (IRIF) by immunofluorescence (IF) to detect the phosphorylation of histone H2AX to form γH2AX foci and localization of 53BP1, an adapter protein that binds at DSBs to promote DNA damage signaling and promote end-joining over homologous recombination (26). As expected for irradiated controls (27, 28), IF analysis of shScr at 0.5 h after irradiation revealed γH2AX and 53BP1 colocalized at multiple nuclear foci that decreased in number by 2 h and largely resolved within 24 h (Figure 2.1A, C), presumably reflecting the kinetics of normal DSB detection and repair. Consistent with prior studies (29), the few foci

remaining at 24 h were larger and brighter, indicating spreading of γH2AX across chromatin near unrepaired single or clustered DSBs. Further, as expected, shDNA-PKcs or shScr treated with Nu7026 each formed γH2AX and 53BP1 foci by 0.5 h, but they failed to resolve by 24 h, suggesting persistent DSBs (Figure 2.1B, C). In agreement with IF results, Western blotting revealed similar γH2AX immunoreactivity at 0.5 and 2 h after radiation with or without Nu7026, but persistent γH2AX at 24 h with Nu7026 (Figure 2.1D, Figure 2.2B and C). The rapid activation of DNA-PKcs in control cells detected by Thr2609 phosphorylation and Ser2056 phosphorylation (p-DNA-PKcs) was suppressed by Nu7026 (Figure 2.1D, Figure 2.2 and C).

Consistent with the high γH2AX levels that remained in shDNA-PKcs or Nu7026-treated shScr after irradiation, clonogenic assays revealed a decreased surviving fraction in shDNA-PKcs cells or shScr treated with Nu7026 (Figure 2.1E). Live-cell time-lapse imaging and automated cell proliferation analysis of shScr cells responding to 6 Gy in the presence or absence of Nu7026 showed that while control cells recovered within 1 day, Nu7026 suppressed cell division for up to 7 days (Figure 2.1F). Given that inhibiting DNA-PKcs promotes cellular senescence (17), we examined the shScr cells after five days, finding that DNA-PKcs inhibition increased the fraction of enlarged cells with flattened morphology expressing SA-βGal (Figure 2.1G).

Persistent γH2AX is independent of DSB repair

Reflecting the critical role attributed to DNA-PKcs in conventional NHEJ throughout the cell cycle (30) (Figure 2.3A), γH2AX foci persistence after DNA-PKcs inhibition is typically ascribed to unrepaired DSBs. To evaluate DSB repair after blocking conventional NHEJ, we constructed shXRCC6 and shXRCC5 lines to knock down the Ku70/Ku80 heterodimer and DNA-PKcs recruitment as well as shXLF, shXRCC4, shPAXX, and shLig4 to target NHEJ

factors downstream of DNA-PKcs (Figure 2.2A). Neutral comet assays confirmed that shRNA targeting conventional NHEJ factors (shNHEJ) significantly increased levels of unrepaired DSBs at 24 h (Figure 2.3B). Irrespective of the different repair defects in each shNHEJ cell line, Nu7026 failed to increase residual damage. Like shScr, each of the shNHEJ cell lines formed γH2AX foci by 2 h (Figure 2.4) that resolved by 24 h (Figure 2.3C, E). In turn, treating shScr or shNHEJ cells with Nu7026 induced foci persistence (Figure 2.3D, E).

Taken together, these data indicate that γH2AX foci formation may depend on DNA damage but not DNA-PKcs, while foci resolution depends on DNA-PKcs but not DNA repair. To directly examine DSB repair in the absence of DNA-PKcs, shScr and shDNA-PKcs, with or without Nu7026, were irradiated and neutral comet assays performed after 24 h, revealing similar levels of residual DBSs (Figure 2.3F). A time course in shScr cells showed *less* damage at 2 h after treatment with Nu7026 and a similar return to baseline by 24 h (Figure 2.3G). A second potent and selective DNA-PKcs inhibitor, Nu7441 (8-dibenzothiophen-4-yl-2-morpholin-4-yl-chromen-4-one (31)), recapitulated Nu7026's effects on MCF7 cells (Figure 2.5A, B and C). As with MCF7, Nu7026 similarly blocked foci resolution without inhibiting DSB repair in multiple cell lines including MDA-MB-435, MDA-MB-231, B16-F10, and CT26 (Figure 2.5G - K).

When conventional NHEJ fails, alternative end joining (altEJ) (32, 33) can complete DSB repair, a potential mechanism to compensate for DNA-PKcs inhibition. Thus, MCF7 cells were developed expressing shRNAs to knock down the altEJ factors XRCC1 or Lig3 (32) (Figure 2.2A). Much like in shScr or shNHEJ, foci formed and resolved in the altEJ shRNA cells on schedule but persisted upon treatment with Nu7026 (Figure 2.6A-D). In turn, the minor DSB repair defect in shXRCC1 and shLig3 was not enhanced by Nu7026 (Figure 2.6E), arguing

against activation of altEJ upon DNA-PKcs inhibition.

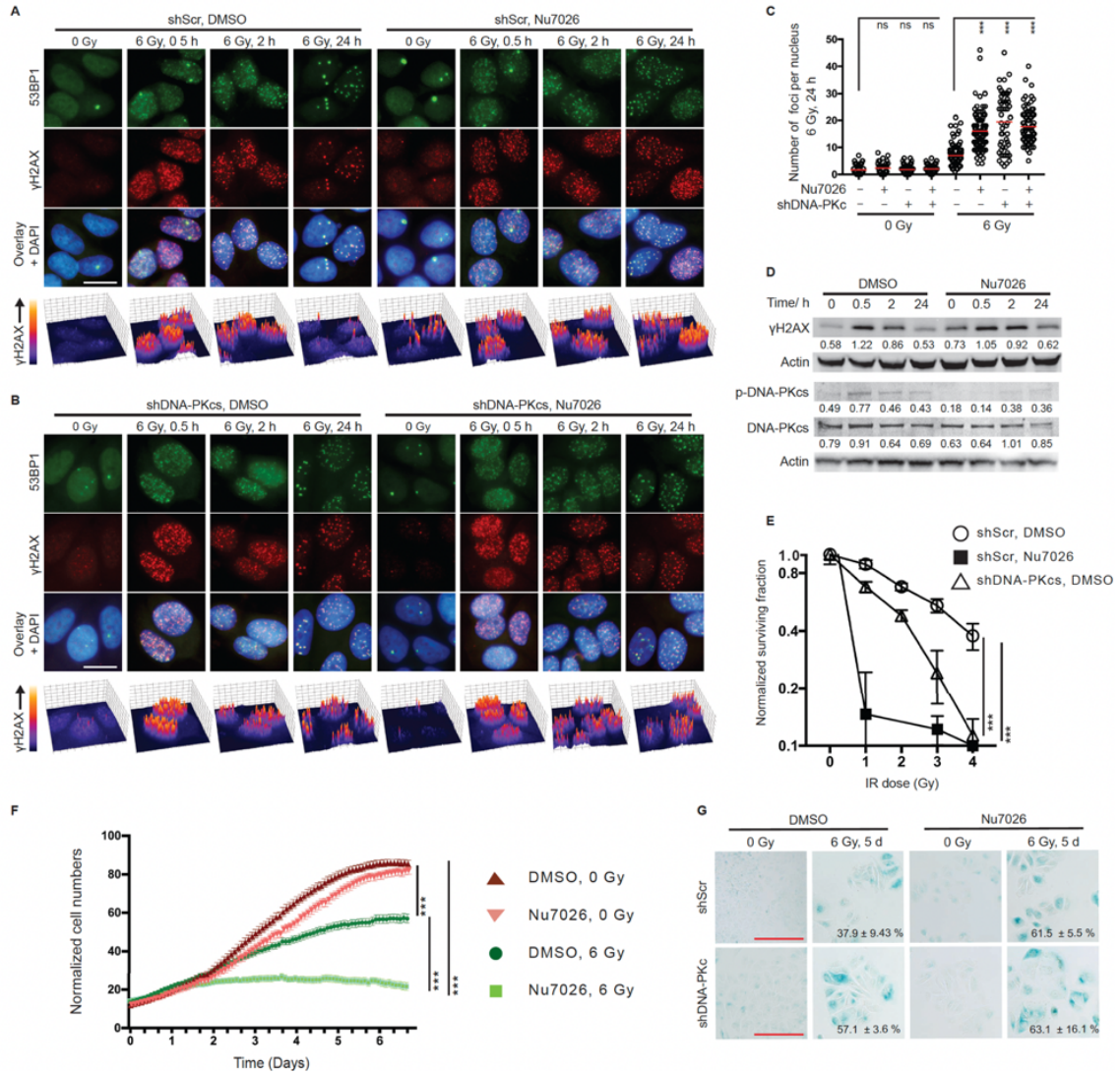

Figrue 2.1: Inhibition of DNA-PKcs induces persistent γH2AX foci, enhanced radiosensitivity and accelerated cellular senescence.

A, B. Immunofluorescence staining of γH2AX and 53BP1 foci in MCF7 cells after irradiation. shScr control (**A**) and shDNA-PKcs (**B**) cells were treated with DMSO or DNA-PKcs inhibitor Nu7026 (10 μM) 1 h before 6 Gy ionizing radiation (IR) and cells were fixed at indicated times after IR. Shown are false-colored images of anti-53BP1 (green), anti-γH2AX (red), three color overlay with DAPI (blue), and perspective plots of γH2AX staining intensity for representative examples from each condition. Images were colored and analyzed by ImageJ. Scale bar = 20 μm. **C.** Quantitation of γH2AX foci per nucleus in shScr or shDNA-PKcs treated with DMSO or Nu7026 at 24 h after 0 or 6 Gy IR. Data obtained from >100 cells (open circles) are shown as mean ± s.d. (red bar). **D.** Western analysis of time course of DNA damage response in shScr cells treated with 6 Gy in the presence of DMSO or Nu7026. Upper strips: γH2AX (phospho-Ser139) levels and ß-actin loading control. Lower strips: p-DNA-PKcs (phospho-Thr2609), total DNA-PKcs, and actin control. Normalized intensity indicated below each γH2AX and DNA-PKcs band.

Figrue 2.1: Inhibition of DNA-PKcs induces persistent γH2AX foci, enhanced radiosensitivity and accelerated cellular senescence (continued).
E. Clonogenic radiosensitivity assay comparing shScr treated with DMSO or Nu7026 (3 μM) and shDNA-PKcs. N=3, mean ± s.d. **F.** Automated proliferation analysis from time-lapse imaging over 7 d comparing shScr cells treated with DMSO or Nu7026 (3 μM) and then 0 or 6 Gy at time 0. **G.** Senescence-associated beta-galactosidase (SA-βGal) staining of shScr or shDNA-PKcs cells treated with DMSO or Nu7026 (3 μM) before 0 or 6 Gy and fixed after 5 d. Mean percentage ± s.d. of SA-βGal$^+$ cells from five 20X fields indicated. Scale bar = 200 μm. For statistical analysis, data compared to shScr DMSO control by unpaired t-test, ***, $p < 0.001$; ns, $p > 0.05$.

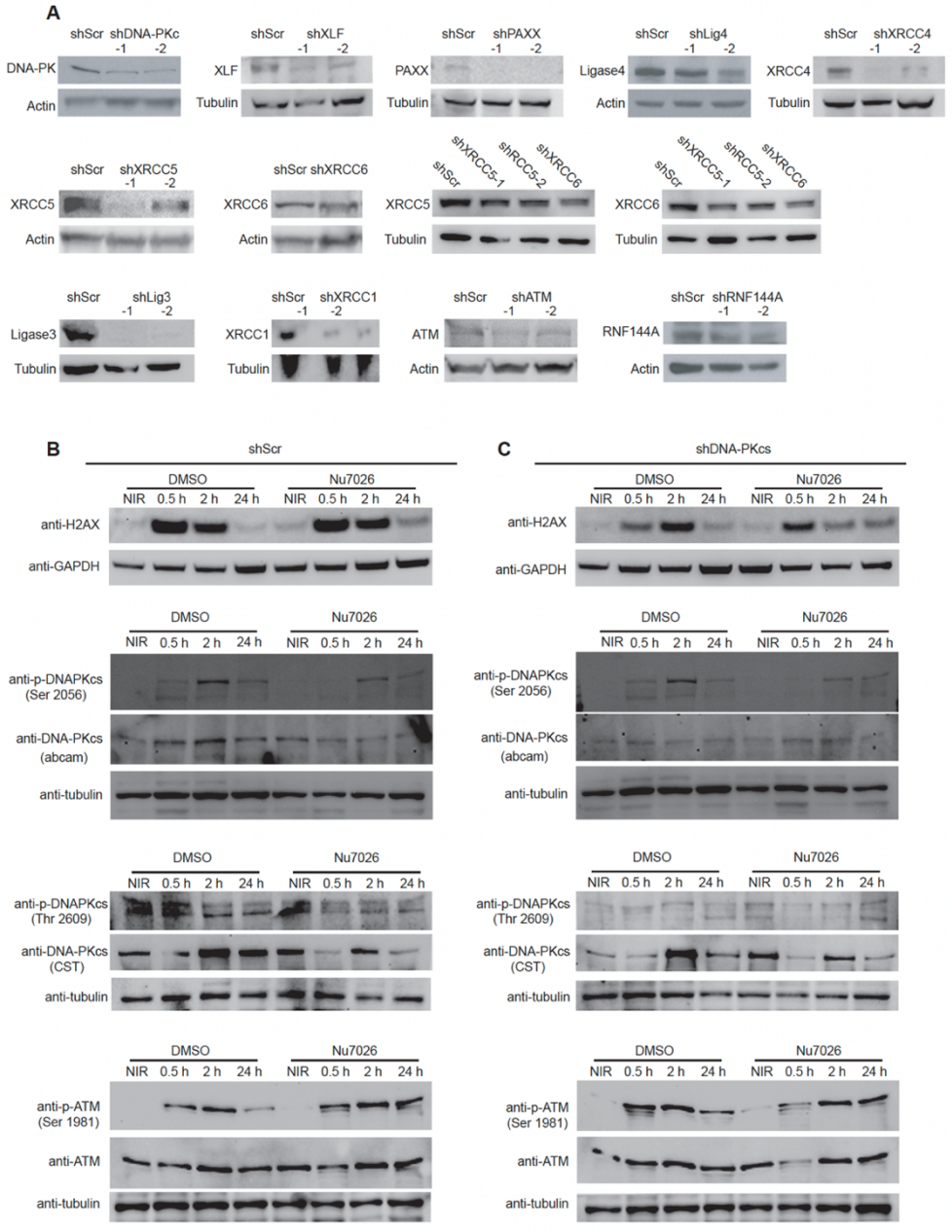

Figure 2.2: Western blot analysis of protein expression.

Figure 2.2: Western blot analysis of protein expression (continued).
A. Verification of the efficiency of corresponding shRNAs by Western blot. Cells were collected from passage 2 or 3 after selection with puromycin and whole cell lysates were extracted. **B, C.** Western blot for corresponding proteins in the presence or absence of Nu7026 (10 µM) in response to irradiation. shScr (**B**) and shDNA-PKcs (**C**) were treated with DMSO or Nu7026 (10 µM) 1 h before 6 Gy. Cell lysate was collected at the indicated time points. Approximately 70 µg total protein was loaded into each lane.

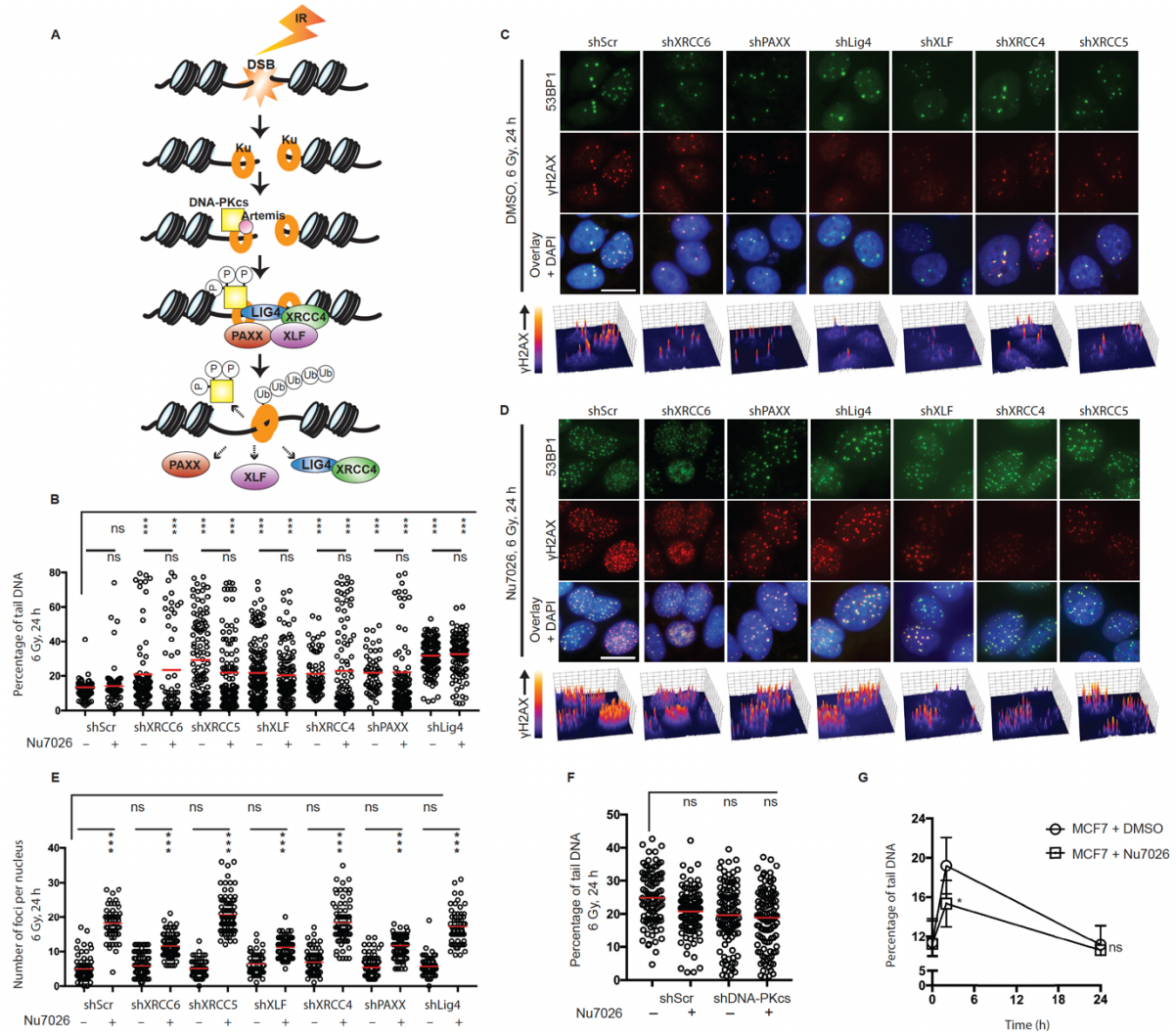

Figure 2.3: Unrepaired DSBs are not sufficient to maintain persistent γH2AX foci.
A. Schematic representation of current model for DSB repair by conventional non-homologous end joining (NHEJ). Upon DSB formation, the Ku70/80 heterodimer binds and recruits DNA-PKcs and Artemis, leading to assembly of factors which perform NHEJ and then disperse. Phosphorylated DNA-PKcs is released and Ku is degraded by Ub-mediated proteolysis, leaving behind a religated chromosome. **B.** Quantitative analysis of DSBs in shScr and shNHEJ lines. Cells were treated with DMSO or Nu7206 (10 µM) 1 h before 6 Gy, collected after 24 h and examined by neutral comet assay (single cell electrophoresis). Percent tail DNA was determined using OpenComet.

Figure 2.3: Unrepaired DSBs are not sufficient to maintain persistent γH2AX foci (continued).
C. D. Immunofluorescence analysis of γH2AX (red) and 53BP1 (green). shScr and shNHEJ were treated with DMSO (**C**) or Nu7026 (10 μM, **D**) 1 h before IR and stained 24 h after IR with anti-53BP1 (green) or anti-γH2AX (red). Three color overlay with DAPI (blue) and perspective plots of γH2AX shown for representative examples. Scale bar = 20 μm. **E.** Quantitation of γH2AX foci per nucleus at 24 h after IR for samples in **C** and **D**. **F.** Quantitative analysis of DSBs in shScr and shDNA-PKcs cells treated and analyzed as in **B**. **G.** Time course comet assay results in shScr cells treated as in **B** and collected before IR (0 h), and at 2 h and 24 h after 6 Gy. In each case, data obtained from >100 cells (open circles) are shown as mean ± s.d. (red bar). Unpaired t-tests were performed, ***, $p < 0.001$; *, $p < 0.05$; ns, $p > 0.05$.

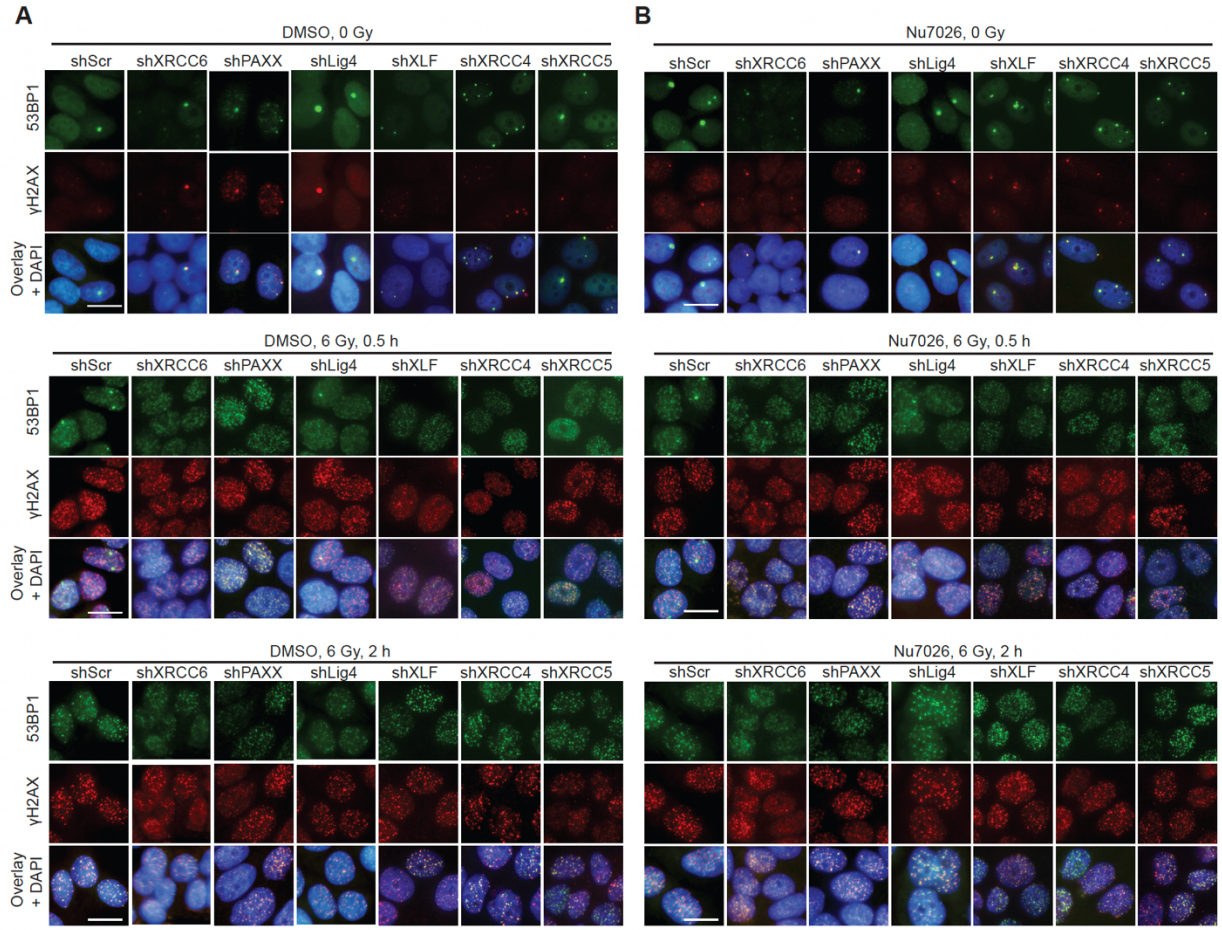

Figure 2.4: DNA-PKcs inhibitor Nu7026 does not alter foci formation in cells expressing shRNAs targeting NHEJ repair factors.
A, B. Immunofluorescence analysis of γH2AX and 53BP1. shScr and shNHEJ were treated with DMSO (**A**) or Nu7026 (10 μM) (**B**)1 h before 6 Gy. Cells were stained at indicated time points after radiation with anti-53BP1 (green) or anti-γH2AX (red). Three color overlay with DAPI (blue) shown for representative examples. Scale bar = 20 μm.

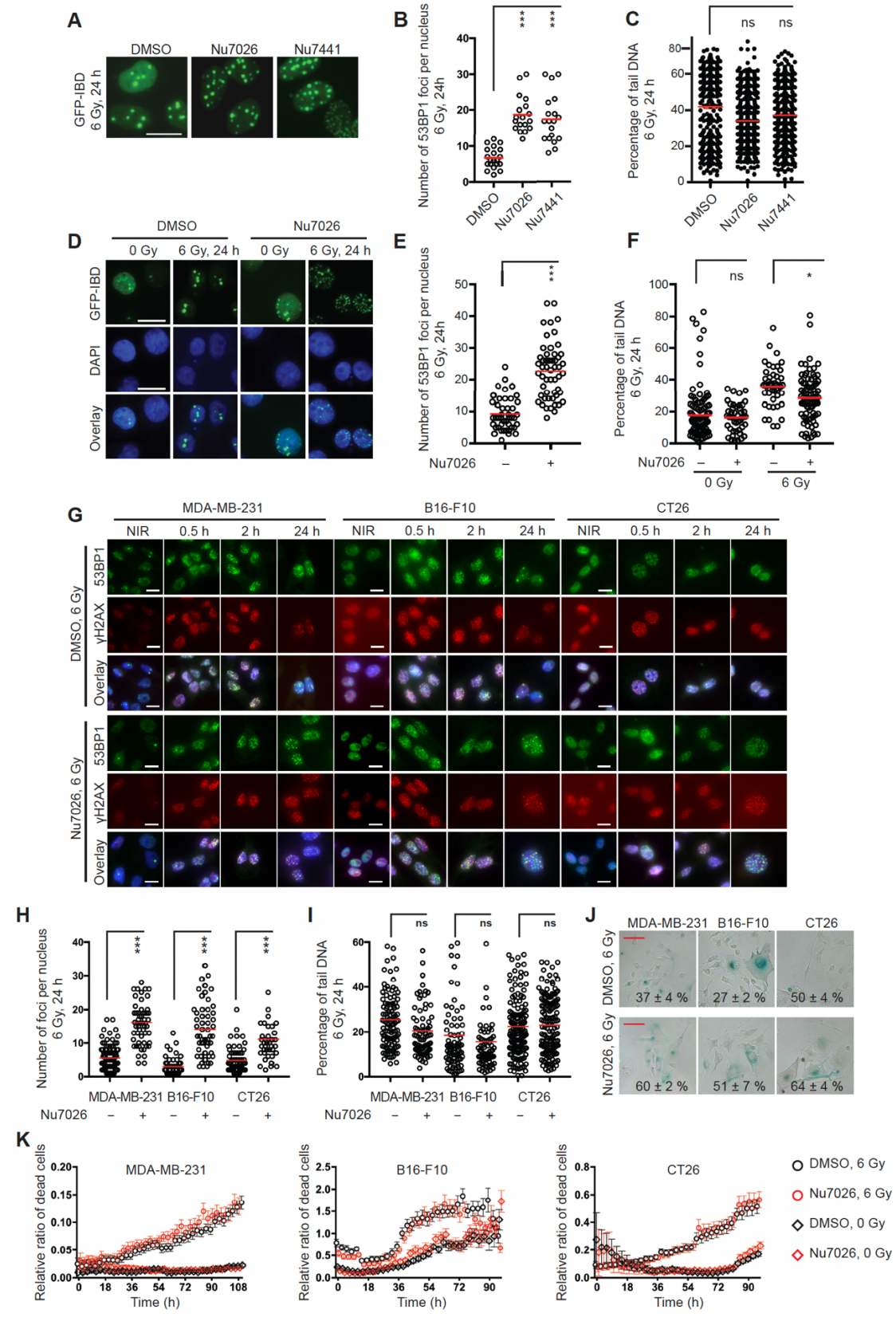

Figure 2.5: The effect of DNA-PKcs deficiency on foci resolution is not a cell-type- or inhibitor-specific phenotype.

Figure 2.5: The effect of DNA-PKcs deficiency on foci resolution is not a cell-type- or inhibitor-specific phenotype (continued).
A. Fluorescence imaging of GFP-IBD foci in MCF7 cells. MCF7 cells were treated with DMSO, Nu7026 (10 μM) or Nu7441 (1 μM) 1 h before 6 Gy. Representative images are shown at 24 h after irradiation. Scale bar = 20 μm. **B.** Quantification of GFP-IBD foci as in **A**. N > 20 cells, mean ± s.d. (red bar). **C.** Quantitative analysis of DSBs in MCF7 cells detected by neutral comet assay after treatment as in **A.** Cells were collected 24 h after 6 Gy. N > 100. **D**. Live-cell fluorescence imaging of GFP-IBD reporter for 53BP1 in MDA-MB-435 cells. MDA-MB-$435^{GFP\text{-}IBD}$ cells were treated with DNA-PKcs inhibitor Nu7026 (10 μM) 1 h before IR and images captured 24 h after 0 or 6 Gy. Representative images are shown. Scale bar = 20 μm. **E.** Quantification of GFP-IBD foci as in **D** at 24 h. N > 50 cells, mean ± s.d. (red bar). **F.** Quantitative analysis of DSBs in MDA-MB-435 cells by neutral comet assay after treatment with DMSO or Nu7026 (10 μM)1 h before 0 or 6 Gy. Cells were collected 24 h after 6 Gy. **G.** Immunofluorescence analysis of γH2AX and 53BP1. MDA-MB-231, B16-F10, and CT26 cells were treated with DMSO or Nu7026 (10 μM) 1 h before 6 Gy. Cells were stained at the indicated time points after radiation with anti-53BP1 (green) or anti-γH2AX (red). Three color overlay with DAPI (blue) shown for representative examples. Scale bar = 20 μm. **H.** Quantification of 53BP1 foci as in **G** at 24 h. N > 100 cells, mean ± s.d. (red bar). **I**. Quantitative analysis of DSBs in MDA-MB-231, B16-F10, and CT26 cells by neutral comet assay after treatment with DMSO or Nu7026 (10 μM)1 h before 6 Gy. Cells were collected 24 h after 6 Gy. N > 100 cells, mean ± s.d. (red bar). **J.** SA-βGal staining in indicated cells. Cells were treated as in **I** and stained 5 d after 6 Gy. At least 5 images were captured with randomly selected, non-overlapping fields. Representative images are shown. Mean percentage of SA-βGal^{+} cells ± s.d. from five 20X fields indicated. Scale bar = 200 μm. **K.** Growth curve of indicated cells. Cell were treated as in **I**. Cell growth was recorded by IncuCyte S3 immediately after 6 Gy for 4 d. Unpaired t-test compared to DMSO controls, ***, $p < 0.001$; *, $p < 0.05$; ns, $p > 0.05$.

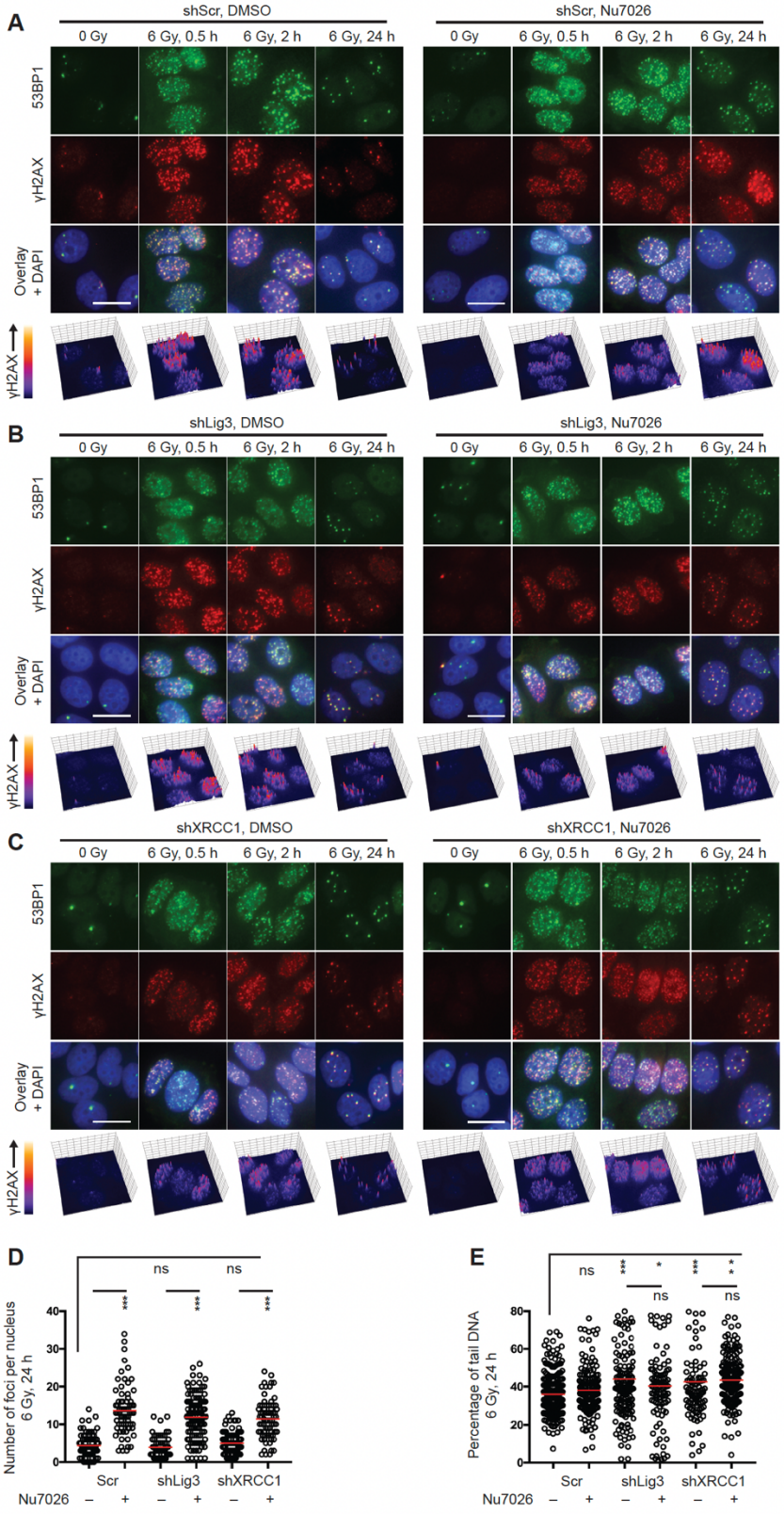

Figure 2.6: Inhibition of DNA-PKcs induces persistent foci without further delaying DSB repair in cells with alt-EJ defects.
A, B and **C**, Immunofluorescence analysis of γH2AX and 53BP1. shScr (**A**) control and shLig3 (**B**) and shXRCC1 (**C**) targeting alt-EJ were treated with Nu7026 (10 μM) 1 h before 6 Gy. At indicated time points after irradiation, cells were analyzed for foci with anti-53BP1 (green) or anti-γH2AX (red), shown as three color overlay with DAPI (blue) and perspective plots of γH2AX staining intensity for representative examples from each condition. Scale bar = 20 μm. **D.** Quantification of γH2AX foci as in **A, B** and **C** at 24 h after 6 Gy. N > 100 cells, mean ± s.d. (red bar). Unpaired t-tests compared to non-Nu7026 controls, ***, $p < 0.001$. **E.** Quantitative analysis of DSBs in MCF7 cells by neutral comet assay after treatment as in **A.** Cells were collected 24 h after 6 Gy. N > 100 cells, mean ± s.d. (red bar). Unpaired t-tests compared to DMSO controls, ***, $p < 0.001$; **, $p < 0.01$.

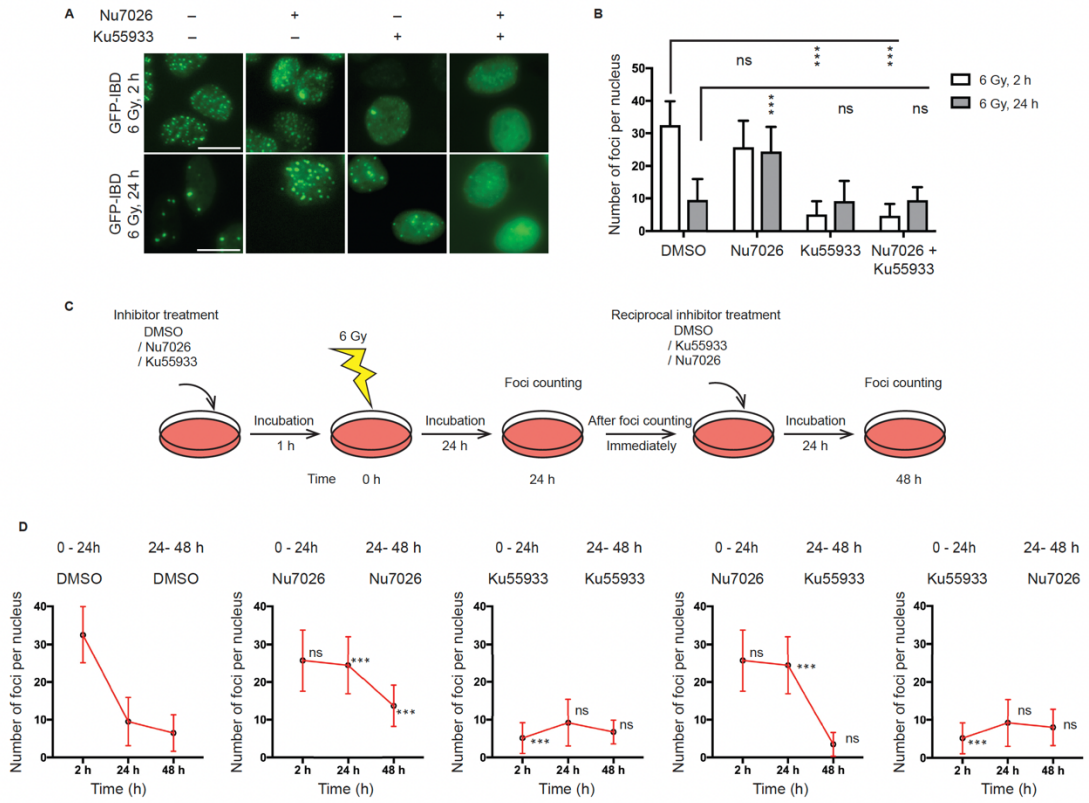

Figure 2.7: ATM activity is required for both the initiation and maintenance of γH2AX foci.

A. Live-cell fluorescence imaging of GFP-IBD reporter for 53BP1 in MCF7 cells. MCF7$^{GFP\text{-}IBD}$ cells were treated with DNA-PKcs inhibitor Nu7026 (10 μM), ATM inhibitor Ku55933 (1 μM), or both 1 h before irradiation and images captured 2 h and 24 h after 6 Gy. Representative images are shown. Scale bar = 20 μm. **B.** Quantification of GFP-IBD foci as in **A** at 2 h and 24 h. **C.** Schematic of the sequential incubation experiment. shScr cells were treated with either Ku55933 or Nu7026 1 h before 6 Gy and imaged 24 h after irradiation. Then, reciprocal inhibitors were added for another 24 h incubation period. **D.** Quantification of GFP-IBD foci per nucleus in the sequential incubation experiment. N > 50 cells, mean± s.d. Unpaired t-tests at each time point compared to DMSO controls, ***, $p < 0.001$.

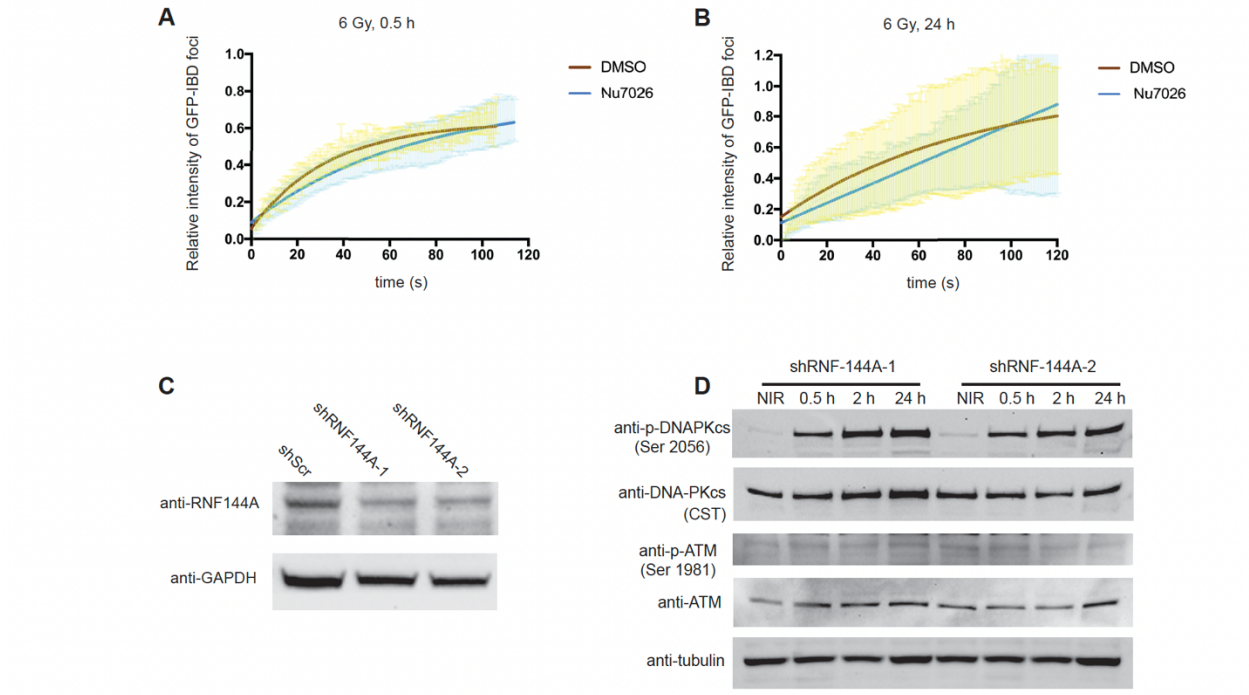

Figure 2.8: Fluorescence recovery after photobleach (FRAP) analysis of molecular exchange in GFP-IBD foci and the effect of shRNF-144A on DNA-PKcs and ATM in response to irradiation.

A, B. Fluorescence recovery after photobleach (FRAP) analysis of molecular exchange of the GFP-IBD reporter in foci formed in MCF7$^{GFP\text{-}IBD}$ cells treated with Nu7026 (10 μM) or DMSO 1 h before 6 Gy and examined at 0.5 h (**A**) and 24 h (**B**) after irradiation, representing newly formed and persistent foci respectively. Data were fitted with easyFRAP. N > 10 foci, mean (solid line) ± s.d. **C.** Western blot validation of shRNF-144A. Two shRNA-144A constructs were used. **D.** Western blot analysis of the indicated proteins in shRNF-144A cells after 6 Gy. Cell lysate was collected at the indicated time points. Approximately 70 μg total protein was loaded for each sample.

ATM activity maintains γH2AX persistence

ATM has long been considered to serve a unique role in the DDR (7). Upon activation by DSBs (34, 35), ATM mediates phosphorylation of H2AX in proximal nucleosomes (12), leading to 53BP1 accumulation and foci formation. ATM also recruits NHEJ factors to stimulate repair (36). Recent reports (10, 11) of negative regulation of ATM by DNA-PKcs raise the question whether DNA-PKcs inhibition phenotypes can be explained mechanistically by ATM deregulation. Thus, we used MCF7$^{GFP\text{-}IBD}$ cells expressing GFP fused to the 53BP1-IRIF binding domain (IBD) (37) as a live-cell reporter to examine the relative contributions of DNA-PKcs and ATM to foci formation and persistence (Figure 2.7A). Consistent with the IF analysis, Nu7026 did not appreciably alter GFP-IBD foci numbers at 2 h but blocked foci resolution at 24 h (Figure 2.7B). The selective ATM inhibitor Ku55933 (2-(4-morpholinyl)-6-(1-thianthrenyl)-4*H*-pyran-4-one (38)), alone or combined with Nu7026, blocked foci formation. To examine a role for ATM in foci persistence, we applied the inhibitors in sequence (Figure 2.7C). MCF7$^{GFP\text{-}IBD}$ was treated with either Nu7026 or Ku55933 starting 1 h before irradiation and until 24 h after IR. Cells were then washed and incubated with either Nu7026 or Ku55933 for an additional 24 h and foci were compared to DMSO control (Figure 2.7D). Cells treated with only Nu7026 or Ku55933 displayed foci persistence and lack of foci formation, respectively. However, persistent foci induced by Nu7026 resolved upon transfer to Ku55933. To distinguish among potential mechanisms, we examined the dynamics of GFP-IBD in single foci by fluorescence recovery after photobleach (FRAP) analysis (Figure 2.8A and B). GFP-IBD remained nearly as dynamic at 24 h as 30 min, whether cells were treated with DMSO or Nu7026. Taken together, these data suggest that foci persist as long at ATM remains active, perhaps reflecting a requirement for ATM to maintain γH2AX.

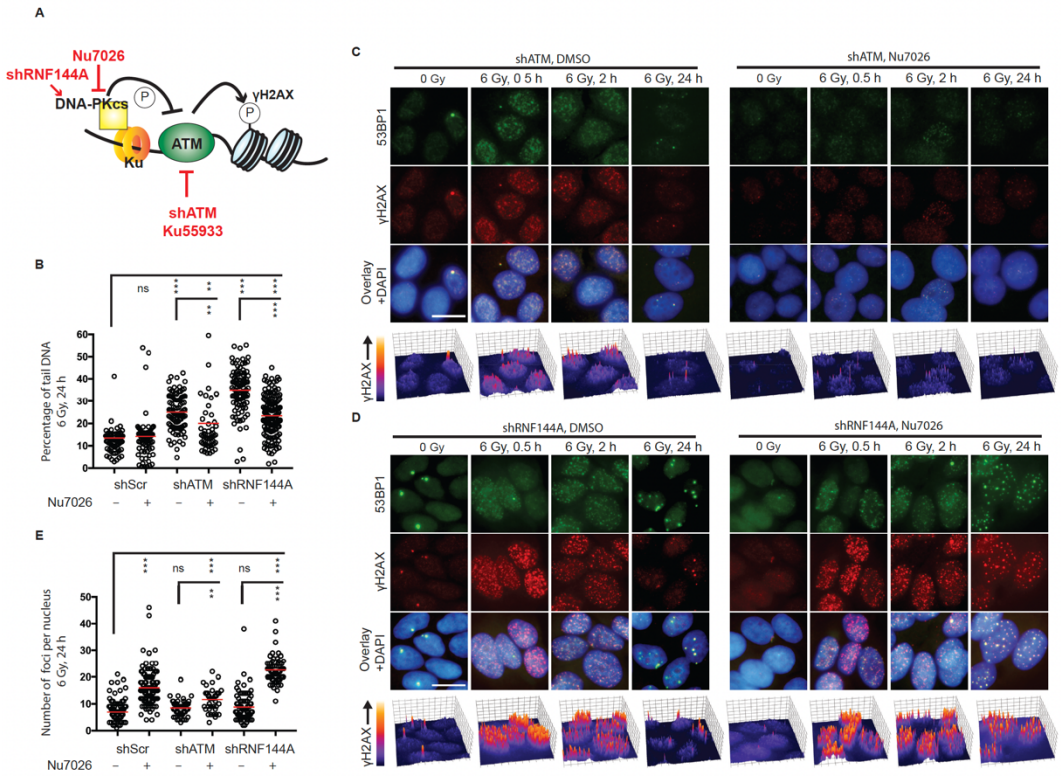

Figure 2.9: DNA-PKcs regulates γH2AX foci resolution by attenuating ATM activity. **A.** Schematic representation of the interaction between DNA-PKcs and ATM at DSBs. In DNA damage response, ATM dominantly regulates H2AX phosphorylation and thus yields γH2AX; while DNA-PKcs mediated phosphorylation of ATM impairs ATM activity. ATM can be inhibited by shATM or Ku55933 and DNA-PKcs by Nu7026. shRNF-144A prevents degradation of DNA-PKcs. **B.** Quantitative analysis of DSBs in shScr, shATM, and shRNF-144A lines by neutral comet assay after treatment with DMSO or Nu7026 1 h before IR. Cells were collected 24 h after 6 Gy. **C. D**. Immunofluorescence analysis of γH2AX and 53BP1 in shATM (**C**) and shRNF-144A (**D**) treated with DMSO or Nu7026 (10 μM)1 h before IR and fixed at the indicated time points. Cells were stained 24 h after IR with anti-53BP1 (green) or anti-γH2AX (red). Three color overlay with DAPI (blue) and perspective plots of γH2AX shown for representative examples. Scale bar = 20 μm. **E.** Quantitation of γH2AX foci per nucleus at 24 h after IR for samples in **C** and **D**. Data obtained from >100 cells (open circles) are shown as mean ± s.d. (red bar). Unpaired t-tests were performed, ***, $p < 0.001$.

DNA-PKcs downregulates ATM activity to suppress the DDR

To further examine order of function between DNA-PKcs and ATM, we established MCF7 cells expressing shRNA targeting ATM (Figure 2.2A). Additionally, we stabilized activated DNA-PKcs in MCF7 cells via shRNA targeting RNF144A, an E3 ubiquitin ligase purported to promote DNA-PKcs degradation (39) (Figure 2.8C, D and Figure 2.9A). shRNF144A induced persistent p-DNA-PKcs (S2056) at 24 h after IR and induced the loss of p-ATM (S1981) across the time course but had only minor if any impact on the total amounts of DNA-PKcs or ATM (Figure 2.8D). Neutral comet assays revealed similar DSB repair defects in shRNF-144A and shATM cells (Figure 2.9B). Strikingly, inhibition of DNA-PKcs with Nu7026 suppressed the DSB repair defect not only in shRNA-144A cells but in shATM cells. The latter effect may reflect reactivation of the remaining ATM protein expressed by shATM cells.

These results raised the question of how shATM and shRNA-144A might affect foci formation and resolution. Compared to shScr, irradiation of shATM generated fewer γH2AX and 53BP1 foci at 0.5 or 2 h (Figure 2.4C). These residual foci were lost upon treatment with Nu7026, consistent with previous observations that DNA-PKcs can initiate γH2AX foci formation in ATM-deficient cells (8). By 24 h, the foci in shATM cells resolved (Figure 2.9C, E). shRNF-144A, with or without Nu7026, displayed similar foci kinetics to shScr (Figure 2.9D, E). Together, these results support an on-off mechanism whereby ATM, activated upon sensing damage, feeds forward to stimulate DNA-PKcs and enhance detection of DSBs but then once repair is complete, the active DNA-PKcs feeds back to downregulate ATM.

Several prior studies have observed γH2AX and/or 53BP1 foci in the absence of DSBs. Persistent foci, whether associated with damage or not, are associated with cellular senescence (40, 41). However, shNHEJ cells, though lacking persistent foci, displayed enhanced senescence

compared to shScr (Figure 2.10A, B), supporting a direct role for persistent DSBs in senescence. That treating shNHEJ cells with Nu7026 further increased the percentage of senescent cells (Figure 2.10A, B) suggests independent contributions of DSBs and foci to signaling, though each may require ATM to have its effects.

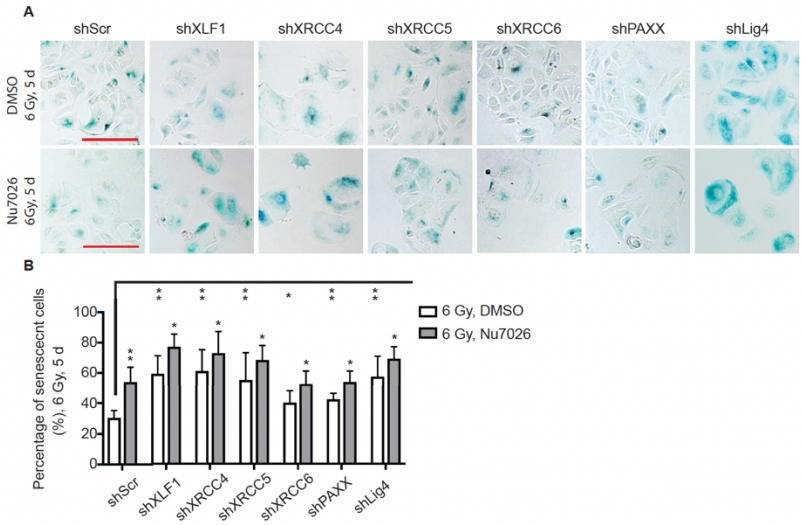

Figure 2.10: DNA-PKcs inhibition augments cellular senescence in cells with NHEJ defects. **A.** Detection of accelerated senescence by SA-βGal staining. shScr and shNHEJ cell lines were treated with DMSO or Nu7026 (3 μM) 1 h before 6 Gy irradiation, incubated for 5 d and then fixed and stained. Representative images are displayed. Scale bar = 200 μm. **B.** Mean percentage of SA-βGal$^+$ ± s.d. for each condition determined from five 20X fields. Unpaired t-test, *, $p < 0.05$; **, $p<0.01$.

DNA-PKcs protects against accelerated senescence by promoting cytokinesis

Along with DSB repair defects, DNA-PKcs inhibition has been associated with prolonged checkpoint arrest as well as mitotic defects leading to failed cytokinesis (Shang et al., 2010), resulting in mononucleated or binucleate tetraploid cells that progress into senescence (42, 43)To examine mitotic progression after irradiation, MCF7 cells were treated with 0 or 6 Gy, with or without Nu7026, incubated 24 h, immunostained for γH2AX, counterstained with DAPI and analyzed by flow cytometry. In unirradiated cells, Nu7026 appeared to suppress S phase, increasing the proportions of 2N (presumptive G1) and 4N (presumptive G2/M) cells (Figure 2.12A). After irradiation, control cells displayed increased γH2AX, accumulation in G1 and decreased S and G2/M fractions (Figure 2.11A). Nu7026 led to a further increase in γH2AX and an apparent shift toward 4N DNA content, consistent with a prolonged G2/M DNA damage checkpoint arrest or mitotic slippage. Thus, we applied live-cell time-lapse imaging to track cell cycle progression in MCF7 cells expressing FUCCI (44) fluorescent cell cycle reporters, where G1 cells express mCherry-hCdt1 (red) and S/G2 cells express mVenus-hGeminin (green). Early in S phase, cells express both reporters and between M and G1, they express neither (Figure 2.11B). Nu7026 had no appreciable effects on mitosis or cytokinesis in unirradiated cells (Figure 2.12B). However, Nu7026-treated irradiated cells displayed mitotic slippage, appearing to enter mitosis (green), round up, and initiate cytokinesis but due to a cytoplasmic bridge, nascent daughter cells (red) collapsed together to generate binucleate cells that adopted a flattened morphology characteristic of senescence (Figure 2.12B). Blocking ATM with Ku55944 partially rescued cells from cytokinesis defects and cellular senescence driven by DNA-PKcs deficiency (Figure 2.12C).

While shDNA-PKcs and shLig4 each promoted senescence after irradiation, they

displayed distinct patterns of DSB repair and foci persistence. To examine if they follow distinct pathways to senescence, we used live-cell time-lapse imaging to record shScr, shDNA-PKcs and shLig4 cells after irradiation in the presence or absence of Nu7026. For each condition, we tracked the trajectories of twenty cells through one or more rounds of cell division to determine if they yielded independent daughter cells (Figure 2.11C) and assembled their trajectories over time (Figure 2.11D and 2.12C). Here, to indicate abortive cytokinesis, nascent daughter cells were counted as two cells even if they remained connected by a cytoplasmic bridge. While shDNA-PKcs cells displayed cytokinesis failure and accumulated as binucleated cells, shLig4 returned to cell division within a day, presumably undergoing mitotic catastrophe. When shScr, shLig4 and shDNA-PKcs cells were treated with Nu7026 and then irradiated, all three displayed cytokinetic failure. We also examined the accumulation of flat, SA-βGal positive senescent cells at 4 days after irradiation, noting the fraction that appeared mononucleate or binucleate (Figure 2.11E). Although shLig4 displayed increased SA-βGal positive cells after 6 Gy, the majority of these senescent cells were mononucleated. Together with the flow cytometry analysis, this suggests senescence in shLig4 may reflect an irreversible cell cycle arrest prior to onset of S phase rather than after mitotic slippage.

While shDNA-PKcs and shLig4 each promoted senescence after irradiation, they displayed distinct patterns of DSB repair and foci persistence. To examine if they follow distinct pathways to senescence, we used live-cell time-lapse imaging to record shScr, shDNA-PKcs and shLig4 cells after irradiation in the presence or absence of Nu7026. For each condition, we tracked the trajectories of twenty cells through one or more rounds of cell division to determine if they yielded independent daughter cells (Figure 2.11C) and assembled their trajectories over time (Figure 2.11D and 2.12C). Here, to indicate abortive cytokinesis, nascent daughter cells

were counted as two cells even if they remained connected by a cytoplasmic bridge. While shDNA-PKcs cells displayed cytokinesis failure and accumulated as binucleated cells, shLig4 returned to cell division within a day, presumably undergoing mitotic catastrophe. When shScr, shLig4 and shDNA-PKcs cells were treated with Nu7026 and then irradiated, all three displayed cytokinetic failure. We also examined the accumulation of flat, SA-βGal positive senescent cells at 4 days after irradiation, noting the fraction that appeared mononucleate or binucleate (Figure 2.11E). Although shLig4 displayed increased SA-βGal positive cells after 6 Gy, the majority of these senescent cells were mononucleated. Together with the flow cytometry analysis, this suggests senescence in shLig4 may reflect an irreversible cell cycle arrest prior to onset of S phase rather than after mitotic slippage.

To confirm a mechanism linking mitotic slippage to senescence via formation of binucleated cells, even without prior DNA damage (45), we treated MCF7 FUCCI cells with the small molecule kinase inhibitors AZD1152-HQPA (barasertib) and GSK461364 to target Aurora B or PLK1 respectively and thereby disrupt mitosis and/or cytokinesis (46). Time-lapse imaging confirmed each inhibitor conferred a cytokinesis defect in unirradiated cells much like that observed with DNA-PKcs inhibition in irradiated cells, leading to binucleate cells that flattened out to adopt a senescent cell phenotype (Figure 2.12E). In turn, staining analysis after 4 days treatment with the kinase inhibitors revealed increased SA-βGal, with a high proportion of binucleate senescent cells (Figure 2.12E - G). A caveat is that most binucleate cells formed after Aurora B and PLK1 inhibition died rather than entering senescence (Figure 2.12H). The ATM/p53 target $p21^{CIP1}$ promotes cell cycle arrest, blocks apoptosis and can induce senescence on its own (47). When combined with the Aurora B or PLK1 inhibitors, $p21^{CIP1}$ overexpression rescued the binucleate cells from death (48), yielding nearly homogeneous senescence (Figure

2.12E and H).

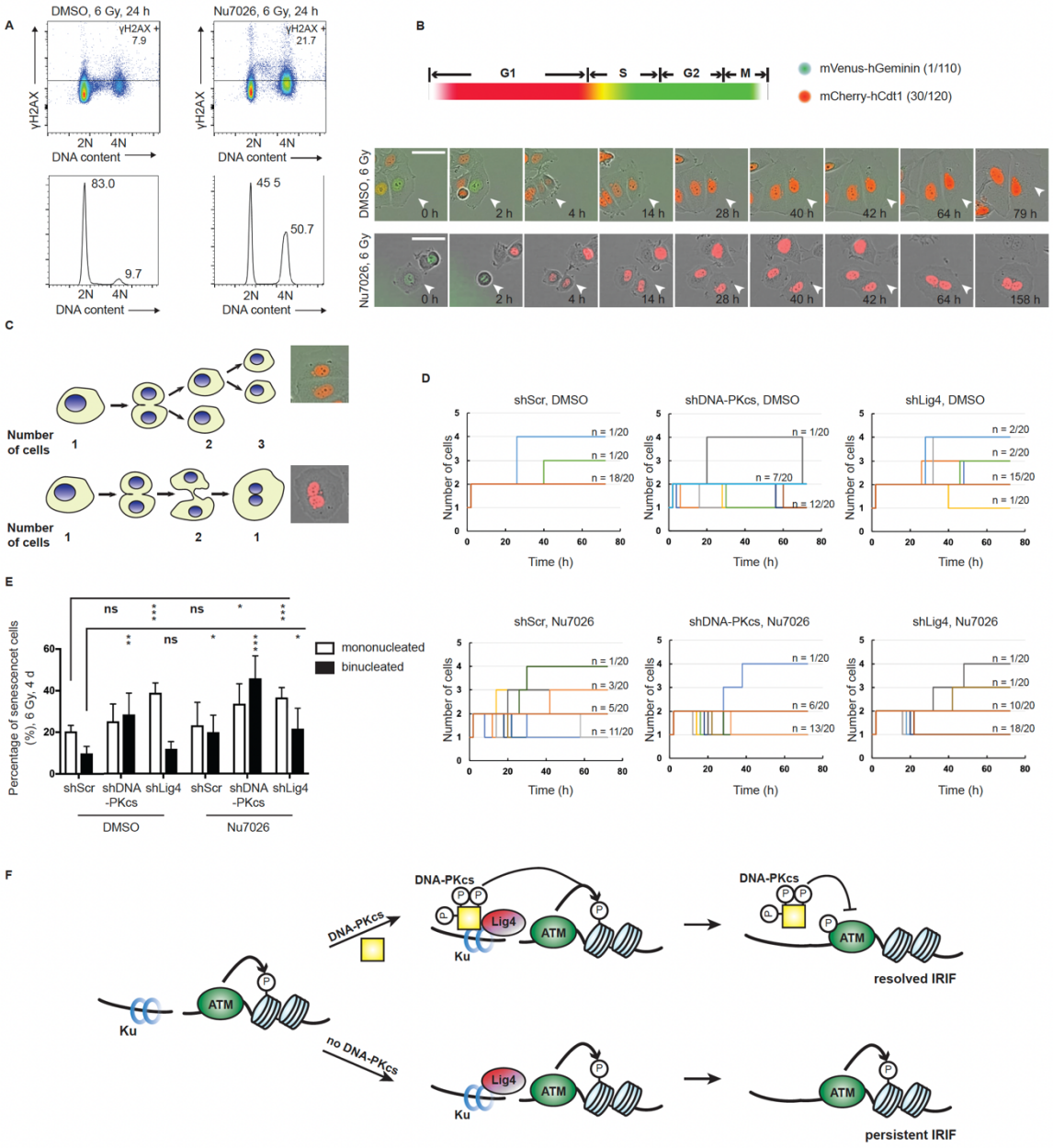

Figure 2.11: Inhibition of DNA-PKcs causes cytokinesis defects and prolonged cell cycle arrest.

A. Flow cytometry analysis of DNA content (DAPI) and γH2AX in cells treated with DMSO or Nu7026 (10 μM) 1 h before 6 Gy and then collected after 24 h. The 2D dot plots (upper) show γH2AX staining across the cell cycle. Total % γH2AX$^+$ was gated based on unirradiated cell sample. The histograms (lower) show relative abundance at each DNA content. Data acquired from 50,000 cells per sample.

Figure 2.11: Inhibition of DNA-PKcs causes cytokinesis defects and prolonged cell cycle arrest (continued).
B. Time-lapse analysis of MCF7-FUCCI cells treated the same as in **A**. (Upper) Diagram represents fluorescent FUCCI reporter expression through the cell cycle. (Lower) Representative cells shown at indicated times. Carets indicate cells that perform mitosis and cytokinesis during time course. Scale bar = 50 μm. **C.** Schematic diagrams of normal mitosis and mitotic slippage after irradiation. In normal mitosis (upper), the mother cell divides completely into two daughter cells. Each daughter can perform another cell division or become senescent. In mitotic slippage (lower), persistent cytoplasmic bridges between daughter cells precede collapse to reform a single cell that contains two nuclei, leading to cell death or senescence. **D.** Tracking cell division of single cells after irradiation. shScr, shDNA-PKcs and shLig4 cells were treated with DMSO or Nu7026 (3 μM) 1 h before 6 Gy. The time after IR at which rounding up for mitosis was first observed was set as 0 h. Then, 20 cells were tracked for each condition, revealing distinct trajectories of completed cell division and/or mitotic slippage. **E.** Analysis of senescent morphology in shScr, shDNA-PKcs and shLig4 cells treated as in **D** and tracked until 4 d after irradiation. Cells with senescent morphology were classified as mono- or bi-nucleated. Histogram shows mean ± s.d. $N > 50$. Unpaired t-test, *, $p < 0.05$; **, $p<0.01$. **F.** Schematic representation of the proposed functions of DNA-PKcs at DSBs. Initially, the Ku70/80 heterodimer and ATM are recruited to DSBs, initiating the DNA damage response, which includes phosphorylation of H2AX at Ser139 in adjacent nucleosomes leading to γH2AX foci. DNA-PKcs is recruited by Ku and activated by ATM. Thereby, in concert with ATM, DNA-PKcs can promote γH2AX foci formation and activation of the DNA damage response to induce checkpoint arrest. Once NHEJ completes DSB repair, active DNA-PK is released to down-regulate ATM, allowing γH2AX foci resolution and terminating the DNA damage response to promote cell division. Absence of DNA-PKcs does not prevent NHEJ but allows ATM to remain active, causing γH2AX foci persistence, mitotic slippage and accelerated senescence.

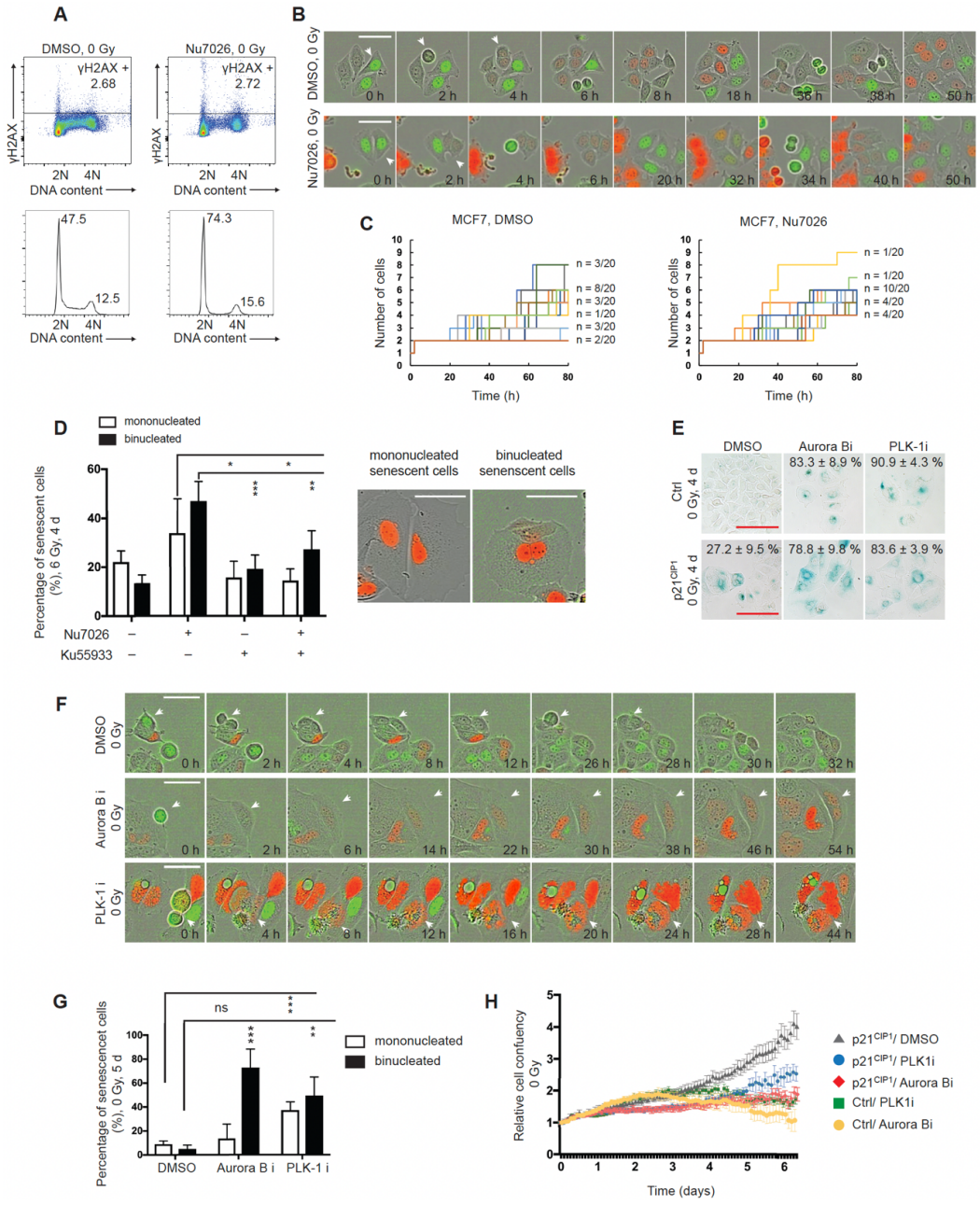

Figure 2.12: Tracking of cell behaviors after treatments.
A. Flow cytometry analysis of DNA content (DAPI) and γH2AX in cells treated with DMSO or Nu7026 (10 μM) and then collected after 24 h. The 2D dot plots (upper) show γH2AX staining across the cell cycle. The gate for γH2AX^{+} was set based these unirradiated cell sample. The histograms (lower) show relative abundance at each DNA content. Data acquired from 50,000 cells per sample. **B.** Time-lapse analysis of MCF7-FUCCI cells treated with DMSO or Nu7026 (3 μM) for 24 h before imaging. Representative cells shown at indicated times. Carets indicate cells that perform mitosis and cytokinesis during time course. Scale bar = 50 μm. **C.** Tracking cell division of single cells. MCF7 cells were treated as in **B**. The time at which rounding up for mitosis was first observed was set as 0 h. Then, 20 cells were tracked for each condition, revealing distinct trajectories of completed cell division and/or mitotic slippage.

Figure 2.12: Tracking of cell behaviors after treatments (continued).
D. ATM inhibitor Ku55933 partially rescues mitotic slippage caused by Nu7026 after 6 Gy. (Left) Analysis of senescent morphology in MFC7 cells treated with DMSO, Nu7026 (3 μM), Ku55933 (0.3 μM) or the combination for 1 h before 6 Gy and tracked by time-lapse recording. More than 50 cells from 10 randomly captured, non-overlapping images, were tracked for 4 d after irradiation. Cells with senescent morphology were classified as mono- or binucleated. Histogram shows mean ± s.d. **E.** SA-βGal staining in MCF7 cells. MCF7 control (Ctrl) or $p21^{CIPI}$ overexpression (p21) cells were treated with DMSO, Aurora B inhibitor or PLK-1 inhibitor and stained after 4 d. At least 5 images were captured from randomly selected, non-overlapping fields. Representative images are shown. Mean percentage of SA-βGal^+ cells ± s.d. from five 20x fields indicated. Scale bar = 200 μm. **F.** Time-lapse analysis of MCF7-FUCCI cells treated with DMSO, Aurora B inhibitor (Aurora B i) or PLK-1 inhibitor (PLK-1 i). Representative cells shown at indicated times. Carets indicate cells that performed mitosis and cytokinesis during the time course. Scale bar = 50 μm. **G.** Analysis of senescent morphology in MCF7 cells treated as in **F**. More than 50 cells from 10 randomly captured, non-overlapping images, were tracked to 5 d after irradiation. Cells with senescent morphology were classified as mono- or binucleated. Histogram shows mean ± s.d. for each condition. **H**, Automated proliferation analysis from time-lapse imaging over 6 d comparing control (Ctrl) or $p21^{CIPI}$ overexpression (p21) cells treated with DMSO, Aurora B inhibitor or PLK-1 inhibitor. For statistical analysis, unpaired t-test, **, $p < 0.01$; ***, $p < 0.001$. (Right) Diagram represents mononucleated or binucleated senescent cells. Scale bar = 50 μm.

2.3 Discussion

DNA-PKcs is a phosphatidylinositol 3-kinase-related kinase (PIKK) activated by binding of its Ku70 and Ku80 partners to DNA ends (49). The search for endogenous substrates initially led to transcription factors such as p53, Sp1, c-Myc, and c-Jun but eventually yielded a wide range of other proteins (50). Mutant cells display DNA repair defects, a prolonged proliferative arrest and decreased survival after exposure to radiation or other genotoxic agents (51). While attention initially focused on p53 activation, DNA-PKcs was also found to phosphorylate the Ku proteins along with other NHEJ factors including XRCC4, Lig4 and XLF, implicating DNA-PKcs in non-homologous end joining (NHEJ), the primary mode of DSB repair throughout the cell cycle (30). Remarkably, our current understanding that DNA-PKcs serves an essential role in NHEJ repair appears to rely almost exclusively on studies in a small number of DNA-PKcs deficient cell lines (e.g. DNA-PKcs$^{-/-}$ MO59J human glioma (51)) and complementation with constructs derived from a reassembled DNA-PKcs cDNA (52). A common feature of DNA-PKcs$^{-/-}$ models is the coinciding downregulation of ATM (18). Strikingly, Peng et al. (19) found that even a transient knockdown of DNA-PKcs with siRNA recapitulated this effect, resulting in loss of both ATM transcript and protein within days. Then, as the siRNA effects were lost, transcript and protein levels were restored not only for DNA-PKcs but also ATM. Perhaps, lacking negative regulation by DNA-PKcs (10, 11), constitutively active ATM may induce autoregulatory factors (e.g. microRNA miR-100 (20, 53)) that mediate its downregulation. Thus, a caveat in assigning DNA-PKcs an essential role in DSB repair is that this ignores our long-standing knowledge of coregulation with ATM, which itself plays multiple roles in DNA damage response. In sum, while a direct role for DNA-PKcs in NHEJ is well accepted, it remains to be

rigorously established. Nonetheless, only limited evidence has been published to date (e.g. (15)) that appears to challenge the prevailing model.

Here, we showed that MCF7 human breast cancer cells either treated with the specific DNA-PKcs inhibitor Nu7026 and/or expressing an shRNA targeting DNA-PKcs displayed unperturbed DSB repair in neutral comet assays. By contrast, shRNA knockdown of Ku70, Ku80, Lig4 and other NHEJ factors (shNHEJ) conferred a dramatic repair defect after irradiation, whether DNA-PKcs was active or not. Arguing against alternative end joining compensating for the NHEJ defect (32), shRNA knockdowns of Lig3 and XRCC1 failed to block DNA-PKcs-independent DSB repair.

While we obtained no evidence for a role in NHEJ, DNA-PKcs activity was critical in mediating recovery from DNA damage response. Cells lacking DNA-PKcs displayed persistent γH2AX foci and cell proliferation arrest even after apparently completing DSB repair. In turn, despite a significant DSB repair defect in shNHEJ cells, γH2AX foci resolved on schedule and cells returned to proliferation. Moreover, inhibiting DNA-PKcs in shNHEJ cells led to γH2AX foci persistence and cell cycle arrest, confirming uncoupling between DNA damage and the DDR. Inhibiting ATM both blocked DSB repair and overcame the phenotypes of DNA-PKcs inhibition. A mechanism consistent with our data is for ATM to serve as the key driver that initiates and maintains the DDR and activates DSB repair while DNA-PKcs functions downstream, initially working in concert with ATM but then opposing ATM signaling to terminate the DDR. Remarkably, even when DSBs persist, the negative feedback from DNA-PKcs can still terminate the DDR. Indeed, inhibiting DNA-PKcs partly *suppressed* the DSB repair defect in shATM and several shNHEJ lines. Here, DNA-PKcs appears to antagonize DSB repair and promote aneuploidy rather than preserve genomic integrity.

Toward resolving the apparent paradox, our results are most consistent with recent studies establishing DNA-PKcs as a negative regulator of ATM after DNA damage (11). A conservative model is that Ku70/80 heterodimer and ATM are recruited to DSBs, initiating the DNA damage response. Recruited by Ku, DNA-PKcs initially functions in concert with ATM to activate the DNA damage response. Together, they phosphorylate substrates in chromatin surrounding the DSB. Phosphorylation of H2AX at Ser139 in adjacent nucleosomes leads to γH2AX foci that promote DNA repair and induce cell cycle arrest (Figure 2.11F). While ATM makes the major contribution to DDR activation, DNA-PKcs activity is critical for normal recovery, mediated by downregulating ATM as DNA repair progresses. A model compatible with much of the literature is that Ku proteins bound at DSBs indeed recruit and activate DNA-PKcs kinase activity but also tether it in place. Our study suggests that subsequent release of active DNA-PKcs might serve as a mechanism to signal successful NHEJ repair, permitting downregulation of ATM and local foci resolution. Thus, in the absence of DNA-PKcs, while NHEJ can proceed, ATM remains active, resulting in γH2AX foci persistence, mitotic slippage and accelerated senescence. One inference is that the repair defects classically observed in DNA-PKcs deficient cell lines could reflect compensatory changes to accommodate ATM deregulation rather than loss of DNA-PKcs activity *per se*.

Nonetheless, our results do not rule out a specific role for DNA-PKcs in promoting DSB repair. One recent report found DNA-PKcs dispensable for rapid rejoining of compatible ends (54) but suggested a role in Lig4-mediated repair of complex damage (55). Complex DSBs may require end processing such as by the DNA-PKcs substrate Artemis, an endonuclease that accelerates NHEJ by clipping 5' overhangs (56). Nonetheless, the ^{60}Co gamma radiation (1.25 MeV) used here to induce DSBs produces more clustered damage than simple, ligatable breaks

(57), suggesting that DNA-PKcs-independent repair can also rejoin complex DSBs (58). Further, despite lacking DNA-PKcs, yeast can perform rapid and efficient NHEJ of a wide range of lesions (59), though other PIKKs may provide the critical functions. Even then, insofar as diverse prokaryotes (60) can perform end-joining repair and express homologs of Ku proteins and Lig4 (61) but appear to lack PIKKs altogether, DNA-PKcs was apparently not required for NHEJ for the first few billion years of evolution (62).

Along with persistent γH2AX, we observed a profound cytokinesis defect, consistent with known roles for DNA-PKcs in cell division after DNA damage. Cells lacking DNA-PKcs performed mitosis and initiated cell division but displayed persistent cytoplasmic bridges that caused nascent daughter cells to collapse together, resulting in binucleate tetraploid cells that progressed to senescence. Consistent with prior work linking mitotic slippage to senescence (45), we confirmed that inhibition of Aurora B or PLK1 was sufficient to produce cytokinetic failure and enhanced senescence in MCF7 cells, even without prior irradiation. Taken together, the senescent phenotype after irradiation of cells lacking DNA-PKcs activity may be linked primarily to mitotic defects rather than any impacts on DNA repair.

The underlying rationale for development of DNA-PKcs inhibitors has long been to target NHEJ repair and thereby augment genotoxic cancer therapy. However, preclinical studies have begun to implicate alternative mechanisms of action. While Nu7441 induces chemo- and radio-sensitization in xenograft models (14, 16), these effects may not depend on DSB repair (15). The activity of the orally available DNA-PKcs inhibitor M3814 (nedisertib), an effective radiosensitizer in xenograft tumors (63) currently under investigation in clinical trials, has recently been ascribed to deregulation of ATM and p53 (64). Our data add to the emerging picture that the major role of DNA-PKcs in radiation tolerance may be in recovery after repair.

In conclusion, our study assigns DNA-PKcs a new primary role in the radiation response as the critical factor protecting cells against the deleterious effects of constitutive ATM activity. In the absence of DNA-PKcs, despite substantially completing DSB repair, unopposed ATM signaling leads to mitotic slippage and senescent arrest. Given concerns that therapy-induced senescence may be reversible (22, 23) and recent studies implicating inflammatory mediators released by senescent cells not only in tissue aging and carcinogenesis (65) but also in driving adverse effects and resistance to therapy (24), these findings suggest a reevaluation of DNA-PKcs as a cancer target.

2.4 Material and methods

Cell lines and cell culture

Human mammary carcinoma cell line MCF7$^{Tet\text{-}On}$ and Lenti-XTM293T cell line were obtained from Takara. Cell lines MDA-MB-435 (human melanoma), MDA-MB-231 (human breast cancer), B16-F10 (mouse melanoma), and CT26 (mouse colon cancer) were obtained from ATCC. The MCF7$^{GFP\text{-}IBD}$ cell line with GFP fused to the 53BP1 IRIF binding domain (IBD) under tetracycline-inducible control has been reported previously (37). A previously described MCF7 cell line with FUCCI cell cycle reporter constructs (44) was reconstructed here by transduction with lentivirus expressing mVenus-hGeminin (1/110)/pCSII-EF-MCS and mCherry-hCdt1 (30/120)/pCSII-EF-MCS. Cells with positive expression were selected by fluorescence-activated cell sorting (FACS).

Human cells were maintained in DMEM medium containing 4.5 g/L glucose (Thermo) supplemented with 10% Tet-approved FBS (Atlanta Biologicals) and 1% penicillin/streptomycin (Thermo). Mouse cells were maintained in RPMI 1640 medium (Thermo) supplemented with 10% Tet-approved FBS (Atlanta Biologicals) and 1% penicillin/streptomycin (Thermo). The cells were tested for mycoplasma and authenticated by short tandem repeat profile (IDEXX BioResearch) prior to performing experiments. All experiments were performed within 3 to 10 passages after thawing cells. Cells were treated with small molecules or DMSO vehicle 1 h before irradiation. All chemical probes used in this study are listed in Table 1.

shRNA knockdowns

Pairs of Sigma MISSION shRNAs targeting expression of PRKDC (DNA-PKcs), ATM, RNF144A, XRCC6 (Ku70), XRCC5 (Ku80), Lig4, 53BP1, PAXX, XRCC4, XLF, Lig3, XRCC1, and a non-targeting scrambled (Scr) negative control were obtained as pLKO.1-puro

vectors and used according to manufacturer's instructions. Lentivirus-containing supernatant was produced by transfection of the 293T Lenti-X cell line with corresponding plasmids and packaged plasmid mix and applied to MCF7^{Tet-On} (Takara) cells. Following selection in the presence of puromycin, pairs of stable MCF7^{Tet-On} cell lines with silencing of PRKDC, ATM, RNF144A, XRCC6, XRCC5, Lig4, 53BP1, PAXX, XRCC4, XLF, Lig3 and XRCC1 protein expression were established. Cells from the third passage post-selection were frozen in liquid N_2 as a stock and most experiments were performed within 4-10 passages. At least 2 shRNA constructs targeting different sequences of the corresponding mRNA were evaluated for each gene. Cells were collected from passage 2 or passage 3 after selection with puromycin and whole cell lysates were extracted. Silencing of targeted genes was validated by Western blot (Fig. S1A) and the shRNA with greatest apparent knock-down based on protein expression was used for experiments. Phenotypes were validated by shRNAs conferring consistent effects on formation and resolution of foci compared to scrambled control. shRNAs and antibodies used in this study are described in Table 2 and 3.

Clonogenic assays

Cells were plated at 100 cells per well in 6 well plates in triplicate and irradiated with doses of 1, 2, 3 and 4 Gy using a GammaCell ^{60}Co source (MDS Nordion) with dose rate ranging from 10.5 to 9.4 cGy/sec depending on the date of the experiment. Cells remained in culture for 3 weeks before staining with crystal violet (0.5%) and colonies of at least 50 cells were counted.

Neutral comet assays

For neutral comet assays, cells were seeded at 1 x 10^5 per well in 6-well plates prior to irradiation. After 24 h, cells were mixed with Comet LM agarose and single cell electrophoresis was performed on CometSlides (Trevigen). Slides were fixed, dried, stained with SYBR green

(Thermo) and imaged on a Zeiss Axiovert 40CFL with a 10X Plan-NeoFluar objective and AxioCam digital camera controlled by AxioVision 4.8 software. Two or more replicates were performed. Images were analyzed using an ImageJ comet assay macro (http://www.med.unc.edu/microscopy/resources/imagejplugins-and-macros/comet-assay) and plugin OpenComet (66) (http://www.cometbio.org/index.html).

Ionizing radiation-induced foci imaging

To image ionizing radiation-induced foci (IRIF), $MCF7^{GFP\text{-}IBD}$ cells were seeded on cover glass at 2.5 x 10^4 per well in 24 well plates. Expression of the GFP-IBD reporter was induced with 1 μg/mL doxycycline treatment for 48 h. After treatment with DNA-PKcs and/or ATM inhibitors, cells were fixed with 4% PFA at the indicated time point, stained with 5 μg/mL Hoechst 33342 (Sigma-Aldrich), and mounted using ProLong Gold (Invitrogen). For immunofluorescence staining, cells were fixed with 4% PFA and permeabilized with 10% Triton-X 100 for 10 min. After blocking with 5% BSA, primary antibodies for γH2AX (Millipore, 05-636, 1:1000) or 53BP1 (Novus, NB100-304, 1:1000) were then incubated on cell slides overnight at 4° C. Following PBS washes, fluorescent secondary antibodies (Jackson ImmunoResearch) were applied for 1 h at room temperature. Cell slides were mounted with ProLong Gold after PBS washes. Foci images were captured on an Zeiss Axiovert 40CFL with a 40X Plan-NeoFluar objective and pseudo-colored using ImageJ. Two or more replicates were performed.

SA-βGal assay

Cells were seeded at 3 x 10^4 per well in 6-well plates and treated with inhibitors for 1 h prior to irradiation. Cells were fixed after 4 or 5 days and assayed for SA-βGal activity as described (37). Images were captured on a Zeiss Axiovert 200M microscope with 20X Plan-

NeoFluar objective and Axiocam digital camera controlled by OpenLab software. SA-βGal positive and negative cells were counted in multiple fields, yielding an average percentage indicated on each SA-βGal image as mean ± SEM. Two or more replicates were performed.

Western blotting

5 x 10^5 cells were plated in P-100 Petri dishes and cells were harvested after 48 h. Whole cell lysates were prepared using M-PER lysis reagent (Thermo) in the presence of protease and phosphatase inhibitors (Thermo). 20 μg of protein was loaded per well, separated on a NuPage 3-8% Tris-Acetate precast gels (Invitrogen), and transferred onto PVDF membrane (EMB Millipore). After dividing blots into strips by apparent MW, immunoblotting was performed using primary antibodies including anti-DNA-PKcs, anti-phospho-DNA-PKcs, anti-γH2AX and anti-actin and detected with peroxidase-conjugated secondary antibodies (Thermo, NA934vs or NA931). This was followed by detection with ECL peroxidase substrate (Thermo).

Flow cytometry

For sample preparation, MCF7 cells were collected 24 h after irradiation, then fixed with 2% PFA for 10 min on ice and permeabilized with 90% ice-cold methanol. Following blocking with 1% BSA, cells were incubated with an Alexa Flour 647 conjugated anti-γH2AX (anti-H2AX phosphoserine 139, Cell Signaling Technology, CST9720, 1:50) for 2 h and then washed using 1% BSA. 3 μg/ml DAPI was added to samples for DNA staining 15 min before flow cytometry. Flow cytometric data were acquired using a BD Fortessa X20 using FACSDiva software. 50,000 viable cells were acquired per sample. Flow cytometric data were analyzed using FlowJo software.

Time-lapse live cell analysis

ShScr, shDNA-PKcs or MCF7-FUCCI cells were seeded in a 6-well plate with 30,000

cells per well. After 24 h in culture, cells were treated with DMSO or Nu7026 and/or irradiated with 6 Gy. The plates were then analyzed by time-lapse in an IncuCyteS3 live cell imaging system. Phase contrast, green and red channel images were acquired at 20X magnification with scanning every 2 h for 7 d. More than 25 non-overlapping fields were captured for each well. Quantitative analysis of cell confluency was performed using IncuCyteS3 2018 software.

Fluorescence recovery after photobleaching (FRAP) analysis

Photobleaching was carried out on MCF7$^{GFP\text{-}IBD}$ cells after doxycycline induction. A 40X oil immersion objective of Leica SP8 laser scanning confocal microscope was used for all FRAP experiments. Photobleaching was achieved with 405 nm laser excitation for 10 s at full intensity. Data acquisition was performed with an excitation at 488 nm with 40% intensity for image scanning. At least 10 independent experiments were performed for each condition. Cells were imaged every second. ROI of the bleached area was acquired by ImageJ and normalized with easyFRAP (67). Fluorescence recovery plots were fitted to a one-phase association exponential curve.

Statistical analysis

Statistical significance for anti-γH2AX, anti-53BP1 and GFP-IBD foci counting and comet assays was determined using the non-paired Student's t test. Calculations were performed using Prism software (GraphPad) or Excel. P values ≤ 0.05 were considered statistically significant.

Table 2.1 List of chemical probes and their working concentrations.

Chemical probe	**Targeted protein**	**Company**	**Catalog #**	**Working concentration**
Nu7026	DNA-PKcs	Selleckchem	S2893	10 μM
Ku55933	ATM	Selleckchem	S1092	5 μM
CHIR124	Chk1	Cayman	16553	0.5 μM
Chk2 inhibitor	Chk2	Cayman	17552	5 μM
MK-8745	Aurora A	MedChem Express	HY-13819	1 μM
AZD1152-HQPA	Aurora B	MedChem Express	10126	0.5 μM
GSK461364	PLK-1	MedChem Express	50877	0.5 μM

Table 2.2 List of shRNAs.

Targeted protein	Sigma MISSION shRNA Catalog #	shRNA sequence
DNA-PKcs (PRKDC)(a)	TRCN0000195491	CCGGCCTCCAGGTTAGGATTAATTGCTCGAGCAATTAATCCTAACC TGGAGGTTTTTTG
DNA-PKcs (PRKDC)(b)	TRCN0000194719	CCGGCCTGAAGTCTTTACAACATATCTCGAGATATGTTGTAAAGAC TTCAGGTTTTTTG
ATM(a)	TRCN0000039948	CCGGCCTTTCATTCAGCCTTTAGAACTCGAGTTCTAAAGGCTGAAT GAAAGGTTTTTG
ATM (b)	TRCN0000039951	CCGGGCCTCCAATTCTTCACAGTAACTCGAGTTACTGGAAGAATTG GAGGTTTTTG
XRCC4 (a)	TRCN0000040117	CCGGCCTCAGGAGAATCAGCTTCAACTCGAGTTGAAGCTGATTCTC CTGAGGTTTTTG
XRCC4 (b)	TRCN0000009875	CCGGTGTGTGAGTGCTAAGGAAGCTCTCGAGAGCTTCCTTAGCACT CACACATTTTTG
XRCC5(a)	TRCN0000295856	CCGGAGAGGAAGCCTCTGGAAGTTCCTCGAGGAACTTCCAGAGGC TTCCTCTTTTTTG
XRCC5(b)	TRCN0000307986	CCGGAATCTAAGAGAGCTGCCATCGCTCGAGCGATGGCAGCTCTC TTAGATTTTTTTG
XRCC6 (a)	TRCN0000039608	CCGGCGACATAAGTCGAGGGACTTTCTCGAGAAAGTCCCTCGACT TATGTCGTTTTTG
XLF (a)	TRCN0000275632	CCGGTACCATGGACTTTAGGTATATCTCGAGATATACCTAAAGTCC ATGGTATTTTTG
XLF (b)	TRCN0000275628	CCGGGCTAGCAACGTTACTTCATATCTCGAGATATGAAGTAACGTT GCTAGCTTTTTG
PAXX(C9orf142)(a)	TRCN0000263653	CCGGCTCTTCTTACCAGACCCAGATCTCGAGATCTGGGTCTGGTAA GAAGAGTTTTTG
PAXX(C9orf142)(b)	TRCN0000263654	CCGGACAGAGCATCCCTGACGCTTTCTCGAGAAAGCGTCAGGGAT GCTCTGTTTTTTG
Ligase4(a)	TRCN0000040004	CCGGGCCCGTGAATATGATTGCTATCTCGAGATAGCAATCATATTC ACGGGCTTTTTG
Ligase4(b)	TRCN0000040005	CCGGGCTCGCATCTAAACACCTTTACTCGAGTAAAGGTGTTTAGAT GCGAGCTTTTTG
RNF144A(a)	TRCN0000004413	CCGGGAACGAGATTGAGTGCATGGTCTCGAGACCATGCACTCAAT CTCGTTCTTTTT
RNF144A(b)	TRCN0000421486	CCGGATGTTGAGCTCTTGATCAAAGCTCGAGCTTTGATCAAGAGCT CAACATTTTTTTG
XRCC1(a)	TRCN0000007912	CCGGCCTTCTGGTCACCTCATCTTTCTCGAGAAAGATGAGGTGACCA GAAGGTTTTT
XRCC1(b)	TRCN0000007913	CCGGCCAGTGCTCCAGGAAGATATACTCGAGTATATCTTCCTGGAGC ACTGGTTTTT
Ligase3(a)	TRCN0000048499	CCGGCCGGATCATGTTCTCAGAAATCTCGAGATTTCTGAGAACATGA TCCGGTTTTTG
Ligase3(b)	TRCN0000048500	CCGGGCTGAGTAACTCCAACAGCAACTCGAGTTGCTGTTGGAGTTA CTCAGCTTTTTG

Table 2.3 List of antibodies.

Antibody/protein	**Company**	**Catalog #**	**Dilution**
γ-H2AX, clone JBW301	EMD Millipore	05-636	1:1000
γ-H2AX(Alexa 647 conjugate)	Cell Signaling Technology	9720	1:50
γ-H2AX	Cell Signaling Technology	9718	1:1000
53BP1	Novus	NB100-304	1:1000
DNA-PKcs	Abcam	ab32566	1:500
DNA-PKcs	Cell Signaling Technology	12311	1:1000
DNA-PKcs (Phospho T2609)	Abcam	ab97611	1:500
DNA-PKcs (Phospho S2056)	Abcam	ab124918	1:1000
ATM	Abcam	ab78	1:200
ATM	Cell Signaling Technology	2873	1:1000
ATM (Phospho S1981)	Cell Signaling Technology	4526	1:1000
XRCC5	Abcam	ab80592	1:1000
Ku80	Cell Signaling Technology	2180	1:1000
XRCC6	Abcam	ab202022	1:1000
XRCC4	Abcam	ab97351	1:1000
PAXX	Abcam	ab126353	1:1000
XLF	Abcam	ab33499	1:1000
Ligase4	Abcam	ab26039	1:800
RNF144A	Abcam	ab89260	1:100
Actin (HRP conjugate)	Proteintech	HRP-60008	1:10000
Tubulin (HRP conjugate)	Proteintech	HRP-66031	1:10000

2.5 References

1. Ciccia A, and Elledge SJ. The DNA damage response: making it safe to play with knives. *Molecular cell.* 2010;40(2):179-204.

2. O'Connor MJ. Targeting the DNA damage response in cancer. *Molecular cell.* 2015;60(4):547-60.

3. Pearl LH, Schierz AC, Ward SE, Al-Lazikani B, and Pearl FM. Therapeutic opportunities within the DNA damage response. *Nature Reviews Cancer.* 2015;15(3):166.

4. Jette N, and Lees-Miller SP. The DNA-dependent protein kinase: A multifunctional protein kinase with roles in DNA double strand break repair and mitosis. *Progress in biophysics and molecular biology.* 2015;117(2-3):194-205.

5. Salles B, Calsou P, Frit P, and Muller C. The DNA repair complex DNA-PK, a pharmacological target in cancer chemotherapy and radiotherapy. *Pathologie Biologie.* 2006;54(4):185-93.

6. Davidson D, Amrein L, Panasci L, and Aloyz R. Small molecules, inhibitors of DNA-PK, targeting DNA repair, and beyond. *Frontiers in pharmacology.* 2013;4:5.

7. Yang J, Yu Y, Hamrick HE, and Duerksen-Hughes PJ. ATM, ATR and DNA-PK: initiators of the cellular genotoxic stress responses. *Carcinogenesis.* 2003;24(10):1571-80.

8. Stiff T, O'Driscoll M, Rief N, Iwabuchi K, Löbrich M, and Jeggo PA. ATM and DNA-PK function redundantly to phosphorylate H2AX after exposure to ionizing radiation. *Cancer research.* 2004;64(7):2390-6.

9. Chen BP, Uematsu N, Kobayashi J, Lerenthal Y, Krempler A, Yajima H, et al. Ataxia telangiectasia mutated (ATM) is essential for DNA-PKcs phosphorylations at the Thr-2609 cluster upon DNA double strand break. *Journal of Biological Chemistry.* 2007;282(9):6582-7.

10. Finzel A, Grybowski A, Strasen J, Cristiano E, and Loewer A. Hyperactivation of ATM upon DNA-PKcs inhibition modulates p53 dynamics and cell fate in response to DNA damage. *Molecular Biology of the Cell.* 2016;27(15):2360-7.

11. Zhou Y, Lee J-H, Jiang W, Crowe JL, Zha S, and Paull TT. Regulation of the DNA damage response by DNA-PKcs inhibitory phosphorylation of ATM. *Molecular cell.* 2017;65(1):91-104.

12. Burma S, Chen BP, Murphy M, Kurimasa A, and Chen DJ. ATM phosphorylates histone H2AX in response to DNA double-strand breaks. *Journal of Biological Chemistry.* 2001;276(45):42462-7.

13. Kang HT, Park JT, Choi K, Kim Y, Choi HJC, Jung CW, et al. Chemical screening identifies ATM as a target for alleviating senescence. *Nature chemical biology.* 2017;13(6):616.

14. Ciszewski WM, Tavecchio M, Dastych J, and Curtin NJ. DNA-PK inhibition by NU7441 sensitizes breast cancer cells to ionizing radiation and doxorubicin. *Breast cancer research and treatment.* 2014;143(1):47-55.

15. Sunada S, Kanai H, Lee Y, Yasuda T, Hirakawa H, Liu C, et al. Nontoxic concentration of DNA‐PK inhibitor NU7441 radio‐sensitizes lung tumor cells with little effect on double strand break repair. *Cancer science.* 2016;107(9):1250-5.

16. Zhao Y, Thomas HD, Batey MA, Cowell IG, Richardson CJ, Griffin RJ, et al. Preclinical evaluation of a potent novel DNA-dependent protein kinase inhibitor NU7441. *Cancer research.* 2006;66(10):5354-62.

17. Azad A, Jackson S, Cullinane C, Natoli A, Neilsen PM, Callen DF, et al. Inhibition of DNA-Dependent Protein Kinase Induces Accelerated Senescence in Irradiated Human Cancer Cells. *Molecular Cancer Research.* 2011;9:1696-707.

18. Neal JA, and Meek K. Deciphering phenotypic variance in different models of DNA-PKcs deficiency. *DNA repair.* 2019;73:7-16.

19. Peng Y, Woods RG, Beamish H, Ye R, Lees-Miller SP, Lavin MF, et al. Deficiency in the catalytic subunit of DNA-dependent protein kinase causes down-regulation of ATM. *Cancer research.* 2005;65(5):1670-7.

20. Ng WL, Yan D, Zhang X, Mo Y-Y, and Wang Y. Over-expression of miR-100 is responsible for the low-expression of ATM in the human glioma cell line: M059J. *DNA repair.* 2010;9(11):1170-5.

21. Douglas P, Ye R, Trinkle-Mulcahy L, Neal JA, De Wever V, Morrice NA, et al. Polo-like kinase 1 (PLK1) and protein phosphatase 6 (PP6) regulate DNA-dependent protein kinase catalytic subunit (DNA-PKcs) phosphorylation in mitosis. *Bioscience reports.* 2014;34(3):e00113.

22. Wang Q, Wu PC, Dong DZ, Ivanova I, Chu E, Zeliadt S, et al. Polyploidy road to therapy‐induced cellular senescence and escape. *International journal of cancer.* 2013;132(7):1505-15.

23. Chakradeo S, W Elmore L, and A Gewirtz D. Is senescence reversible? *Current drug targets.* 2016;17(4):460-6.

24. Demaria M, O'Leary MN, Chang J, Shao L, Liu S, Alimirah F, et al. Cellular senescence promotes adverse effects of chemotherapy and cancer relapse. *Cancer discovery.* 2016:165-76.

25. Nutley B, Smith N, Hayes A, Kelland L, Brunton L, Golding B, et al. Preclinical pharmacokinetics and metabolism of a novel prototype DNA-PK inhibitor NU7026. *British journal of cancer.* 2005;93(9):1011.

26. Panier S, and Boulton SJ. Double-strand break repair: 53BP1 comes into focus. *Nature reviews Molecular cell biology.* 2014;15(1):7.

27. Rogakou EP, Pilch DR, Orr AH, Ivanova VS, and Bonner WM. DNA double-stranded breaks induce histone H2AX phosphorylation on serine 139. *Journal of biological chemistry.* 1998;273(10):5858-68.

28. Schultz LB, Chehab NH, Malikzay A, and Halazonetis TD. p53 binding protein 1 (53BP1) is an early participant in the cellular response to DNA double-strand breaks. *The Journal of cell biology.* 2000;151(7):1381-90.

29. Bouquet F, Muller C, and Salles B. The loss of γH2AX signal is a marker of DNA double strand breaks repair only at low levels of DNA damage. *Cell cycle.* 2006;5(10):1116-22.

30. Chang HH, Pannunzio NR, Adachi N, and Lieber MR. Non-homologous DNA end joining and alternative pathways to double-strand break repair. *Nature reviews Molecular cell biology.* 2017;18(8):495.

31. Leahy JJ, Golding BT, Griffin RJ, Hardcastle IR, Richardson C, Rigoreau L, et al. Identification of a highly potent and selective DNA-dependent protein kinase (DNA-PK) inhibitor (NU7441) by screening of chromenone libraries. *Bioorganic & medicinal chemistry letters.* 2004;14(24):6083-7.

32. Iliakis G. Backup pathways of NHEJ in cells of higher eukaryotes: cell cycle dependence. *Radiotherapy and Oncology.* 2009;92(3):310-5.

33. Lieber MR. NHEJ and its backup pathways in chromosomal translocations. *Nature Structural and Molecular Biology.* 2010;17(4):393.

34. You Z, Bailis JM, Johnson SA, Dilworth SM, and Hunter T. Rapid activation of ATM on DNA flanking double-strand breaks. *Nature cell biology.* 2007;9(11):1311.

35. Hartlerode AJ, Morgan MJ, Wu Y, Buis J, and Ferguson DO. Recruitment and activation of the ATM kinase in the absence of DNA-damage sensors. *Nature structural and molecular biology.* 2015;22(9):736.

36. Blackford AN, and Jackson SP. ATM, ATR, and DNA-PK: the trinity at the heart of the DNA damage response. *Molecular cell.* 2017;66(6):801-17.

37. Efimova EV, Mauceri HJ, Golden DW, Labay E, Bindokas VP, Darga TE, et al. Poly (ADP-ribose) polymerase inhibitor induces accelerated senescence in irradiated breast cancer cells and tumors. *Cancer research.* 2010:0008-5472. CAN-09-4224.

38. Hickson I, Zhao Y, Richardson CJ, Green SJ, Martin NM, Orr AI, et al. Identification and characterization of a novel and specific inhibitor of the ataxia-telangiectasia mutated kinase ATM. *Cancer research.* 2004;64(24):9152-9.

39. Ho S-R, Mahanic CS, Lee Y-J, and Lin W-C. RNF144A, an E3 ubiquitin ligase for DNA-PKcs, promotes apoptosis during DNA damage. *Proceedings of the National Academy of Sciences.* 2014;111(26):E2646-E55.

40. Fumagalli M, Rossiello F, Mondello C, and di Fagagna FdA. Stable cellular senescence is associated with persistent DDR activation. *PloS one.* 2014;9(10):e110969.

41. Rodier F, Coppé J-P, Patil CK, Hoeijmakers WA, Muñoz DP, Raza SR, et al. Persistent DNA damage signalling triggers senescence-associated inflammatory cytokine secretion. *Nature cell biology.* 2009;11(8):973.

42. Shang Z-F, Huang B, Xu Q-Z, Zhang S-M, Fan R, Liu X-D, et al. Inactivation of DNA-dependent protein kinase leads to spindle disruption and mitotic catastrophe with attenuated checkpoint protein 2 Phosphorylation in response to DNA damage. *Cancer research.* 2010;70(9):3657-66.

43. De Santis Puzzonia M, Gonzalez L, Ascenzi S, Cundari E, and Degrassi F. Tetraploid cells produced by absence of substrate adhesion during cytokinesis are limited in their proliferation and enter senescence after DNA replication. *Cell cycle.* 2016;15(2):274-82.

44. Sakaue-Sawano A, Kurokawa H, Morimura T, Hanyu A, Hama H, Osawa H, et al. Visualizing spatiotemporal dynamics of multicellular cell-cycle progression. *Cell.* 2008;132(3):487-98.

45. Panopoulos A, Pacios-Bras C, Choi J, Yenjerla M, Sussman MA, Fotedar R, et al. Failure of cell cleavage induces senescence in tetraploid primary cells. *Molecular biology of the cell.* 2014;25(20):3105-18.

46. Fededa JP, and Gerlich DW. Molecular control of animal cell cytokinesis. *Nature cell biology.* 2012;14(5):440.

47. Kagawa S, Fujiwara T, Kadowaki Y, Fukazawa T, Sok-Joo R, Roth JA, et al. Overexpression of the p21 p21 sdi1 gene induces senescence-like state in human cancer cells: implication for senescence-directed molecular therapy for cancer. *Cell death and differentiation.* 1999;6(8):765.

48. Castedo M, Perfettini J-L, Roumier T, Andreau K, Medema R, and Kroemer G. Cell death by mitotic catastrophe: a molecular definition. *Oncogene.* 2004;23(16):2825.

49. Suwa A, Hirakata M, Takeda Y, Jesch SA, Mimori T, and Hardin JA. DNA-dependent protein kinase (Ku protein-p350 complex) assembles on double-stranded DNA. *Proceedings of the National Academy of Sciences.* 1994;91(15):6904-8.

50. Goodwin JF, and Knudsen KE. Beyond DNA repair: DNA-PK function in cancer. *Cancer discovery.* 2014;4(10):1126-39.

51. Lees-Miller SP, Godbout R, Chan DW, Weinfeld M, Day RS, Barron GM, et al. Absence of p350 subunit of DNA-activated protein kinase from a radiosensitive human cell line. *Science.* 1995;267(5201):1183-5.

52. Kurimasa A, Kumano S, Boubnov NV, Story MD, Tung C-S, Peterson SR, et al. Requirement for the kinase activity of human DNA-dependent protein kinase catalytic subunit in DNA strand break rejoining. *Molecular and cellular biology.* 1999;19(5):3877-84.

53. Zhang X, Wan G, Berger FG, He X, and Lu X. The ATM kinase induces microRNA biogenesis in the DNA damage response. *Molecular cell.* 2011;41(4):371-83.

54. Cary RB, Peterson SR, Wang J, Bear DG, Bradbury EM, and Chen DJ. DNA looping by Ku and the DNA-dependent protein kinase. *Proceedings of the National Academy of Sciences.* 1997;94(9):4267-72.

55. Reynolds P, Anderson JA, Harper JV, Hill MA, Botchway SW, Parker AW, et al. The dynamics of Ku70/80 and DNA-PKcs at DSBs induced by ionizing radiation is dependent on the complexity of damage. *Nucleic acids research.* 2012;40(21):10821-31.

56. Ma Y, Pannicke U, Schwarz K, and Lieber MR. Hairpin opening and overhang processing by an Artemis/DNA-dependent protein kinase complex in nonhomologous end joining and V (D) J recombination. *Cell.* 2002;108(6):781-94.

57. Gulston M, Fulford J, Jenner T, de Lara C, and O'neill P. Clustered DNA damage induced by γ radiation in human fibroblasts (HF19), hamster (V79‐4) cells and plasmid DNA is revealed as Fpg and Nth sensitive sites. *Nucleic acids research.* 2002;30(15):3464-72.

58. Magnander K, and Elmroth K. Biological consequences of formation and repair of complex DNA damage. *Cancer letters.* 2012;327(1-2):90-6.

59. Aylon Y, and Kupiec M. DSB repair: the yeast paradigm. *DNA repair.* 2004;3(8):797-815.

60. Weller GR, Brandt VL, and Roth DB. Doing more with less in bacterial DNA repair. *Nature Structural and Molecular Biology.* 2004;11(12):1158.

61. Weller GR, Kysela B, Roy R, Tonkin LM, Scanlan E, Della M, et al. Identification of a DNA nonhomologous end-joining complex in bacteria. *Science.* 2002;297(5587):1686-9.

62. Gu J, and Lieber MR. Mechanistic flexibility as a conserved theme across 3 billion years of nonhomologous DNA end-joining. *Genes & development.* 2008;22(4):411-5.

63. Damstrup L, Zimmerman A, Sirrenberg C, Zenke F, and Vassilev L. M3814, a DNA-dependent protein Kinase inhibitor (DNA-PKi), potentiates the effect of ionizing radiation (IR) in Xenotransplanted Tumors in nude mice. *International Journal of Radiation Oncology• Biology• Physics.* 2016;94(4):940-1.

64. Guo Y, Sun Q, Liu X, Puc J, Czauderna F, Zenke F, et al. Pharmacological DNA-PK inhibition induces ATM/p53 dependent premature senescence with immunomodulatory phenotype in irradiated cancer cells. *AACR Annual Meeting.* 2018:982.

65. Hoare M, and Narita M. The Power Behind the Throne: Senescence and the Hallmarks of Cancer. *Annual Review of Cancer Biology.* 2018;2:175-94.

66. Gyori BM, Venkatachalam G, Thiagarajan P, Hsu D, and Clement M-V. OpenComet: an automated tool for comet assay image analysis. *Redox biology.* 2014;2:457-65.

67. Rapsomaniki MA, Kotsantis P, Symeonidou I-E, Giakoumakis N-N, Taraviras S, and Lygerou Z. easyFRAP: an interactive, easy-to-use tool for qualitative and quantitative analysis of FRAP data. *Bioinformatics.* 2012;28(13):1800-1.

CHAPTER 3

TARGETING TELOMERASE REVERSE TRANSCRIPTASE WITH THE COVALENT INHIBITOR NU-1 CONFERS IMMUNOGENIC RADIATION SENSITIZATION

This chapter consists of the unpublished manuscript:

Y Liu, R C Betori, J Pagacz, E V Efimova, G B Frost, D J Wolfgeher, D Wu, S B Cohen, K A Scheidt, S J Kron. A novel telomerase reverse transcriptase inhibitor NU-1 disrupts DNA repair and potentiates radiation and chemotherapy.

I was responsible for conducting biological assays and writing the manuscript. Coauthors Betori and Frost are members of the Scheidt Lab at Northwestern University. The Scheidt Lab contributed to the synthesis of chemical compounds and chemosensitization studies. Pagacz is a member of the Kron Lab and was responsible for animal studies. Efimova, Wu, and Wolfgeher are members of the Kron Lab and contributed to in vitro studies and data analysis. Cohen is an extraordinary collaborator at the University of Sydney, Australia. All of the authors contributed to manuscript editing.

3.1 Introduction

Human telomeres consist of 5-15 kb of double stranded 5'-$(TTAGGG)_n$-3' repeats terminating in a 3' G-strand overhang at the end of each chromosome that binds the shelterin complex to protect against end-to-end fusions or detection as damaged DNA (1-3). TTAGGG repeats lost from the ends during replication are restored by telomerase, an RNA-directed DNA polymerase complex where the telomerase RNA component TERC serves as a template for the telomerase reverse transcriptase TERT (4). TERT expression can be detected in adult stem cells and percursors but is silenced during somatic cell differentiation. Thus, telomeres can shorten as tissue precursors proliferate, reaching a critical length at the Hayflick limit. Eventually, telomere erosion displaces the shelterin complex, inducing a DNA damage response (DDR). Most cells die or enter replicative senescence, driving inflammation and tissue aging (5), but some may become genomically unstable and reactivate TERT (6). Thereby, the premalignant cells gain immortality, maintaining telomere integrity in the face of unlimited cell division.

The rationale that blocking telomerase might limit the proliferation of cancer cells has led to extensive efforts to target TERT for therapeutic intervention (7), yielding a wide range of synthetic agents (8, 9). Prominent examples that have advanced to preclinical and/or clinical studies include oligonucleotide drugs such as Imetelstat (GRN163L) (10), G-quadruplex stabilizers such as TMPyP4 (11), and allosteric inhibitors such as BIBR 1532 (12). Diverse natural products have also been reported to inhibit telomerase (9, 13). Though few appear promising for clinical development, chemical simplification of the catechin EGCG led to the drug-like competitive inhibitor MST-312 (14).

Maintaining telomerase suppression for long enough to achieve critical erosion has been a challenge *in vivo*, reflected in the hematopoietic toxicity and resistance that have impacted

clinical trials with Imetelstat (15). The complementary strategy of selectively damaging telomeres in TERT-expressing cells via providing altered TERC templates (16) or toxic substrates such as 6-thio-dG (17) or other dNTPs (18) is promising but may similarly be limited by toxicity. Beyond repeat synthesis, TERT has long been linked to non-canonical, extra-telomeric activities that enhance stress responses, support stemness and promote cell growth and survival (19-23). Multiple studies published over the past two decades confirm early reports (24-26) that TERT expression and/or activity significantly impact cancer cell sensitivity to radiation and/or chemotherapy, both *in vitro* and *in vivo* (19, 21, 27). Early on, this effect was ascribed to a direct role for TERT in repairing double strand breaks (DSBs) (28-30), though mechanisms have remained poorly defined. A confounding factor is that telomere dysfunction itself affects sensitivity to therapy, perhaps reflecting a feedback loop where telomeres may serve as oxidative stress sensors (31, 32) and that short or damaged telomeres radiosensitize both normal and cancer cells (33, 34). Nonetheless, many of TERT's roles in stress response appear to be independent of telomere length and the sensitizing effects of TERT inhibitors do not require prolonged treatment or telomere attrition.

The *Streptomyces* macrolide antibiotic chrolactomycin was previously identified as a micromolar telomerase inhibitor *in vitro* and proposed to act by covalent binding via a reactive exocyclic methylene group to a nucleophile in the TERT catalytic site (35). Total synthesis has prevented conventional structure-activity analysis to date, inspiring the alternative approach of developing simplified chrolactomycin analogs. This effort yielded NU-1 (36) (Figure 3.1A), a novel small-molecule inhibitor bearing an exocyclic methylene that conjugates to a conserved active site cysteine to inhibit TERT in telomerase-positive cancer cell lines. Confirming the mechanism of action, NU-1 has no effects on telomerase-negative cells while the non-reactive

des-exomethylene analog NU-2 fails to inhibit TERT or otherwise impact telomerase-positive cells.

Here, we used NU-1 to examine the potential for covalent TERT inhibitors to enhance conventional cancer therapy. Consistent with prior *in vitro* studies, NU-1 and other TERT inhibitors sensitized human cancer cells to radiation and genotoxic chemotherapy. Treating telomerase-positive cancer cells with NU-1 prior to radiation delayed DSB repair, prolonged γH2AX foci persistence, extended G1 cell cycle arrest, and promoted cell senescence, suggesting a direct mechanism of radiosensitization. These effects of NU-1 were not observed in a cancer cell line lacking TERT expression. NU-1 also displayed radiosensitization in CT26 mouse colon carcinoma cells both *in vitro* and *in vivo*. When CT26 tumors were treated with an otherwise ineffective radiation dose, most were eliminated when the BALB/c mice were concomitantly treated with NU-1, perhaps reflecting greater persistent DNA damage and/or increased $CD8^+$ T cell infiltrate. Supporting an immune mechanism, CT26 cells treated with NU-1 and radiation form senescent cells that stimulate dendritic cell (DC) maturation/activation and, thereby, $CD8^+$ T cell proliferation. Considering the potential advantages of targeted covalent inhibitors as probes and drugs (37-39), irreversible inhibition of TERT, as with NU-1, may offer a direct path to tumor-specific sensitizers to improve the efficacy of radiation and other cancer therapies.

3.2 Results

NU-1 treatment impacts DNA damage pathway gene expression

Our previous studies (36) demonstrated that at concentrations > 1 μM, NU-1 decreases cell viability in telomerase-positive human cancer cell lines, including MCF7 ER^+ breast cancer (IC_{50} 27 μM), MDA-MB-231 triple-negative breast cancer, A549 lung adenocarcinoma, HeLa cervical cancer, and ACHN renal cell carcinoma. However, two telomerase-negative, ALT cell lines (40), Saos-2 osteosarcoma and VA-13 SV40 immortalized fetal lung fibroblast, were unaffected. The toxic effects of NU-1 appeared within 24 to 48 h, far too rapidly to depend on telomere erosion, given the expected loss of only a few telomeric repeats per population doubling. Towards examining mechanisms of the apparent TERT addiction exposed by NU-1, the mRNA expression profiles of MCF7 cells treated with 0.5 μM NU-1 or DMSO vehicle for 48 h were compared by sequencing polyA-RNA, revealing 2,117 upregulated and 2,069 downregulated genes (Figure 3.1B and C). Consistent with previous studies (41), Reactome Gene Ontology (GO) term pathway analysis of the differentially expressed genes identified the pathways *Cell Cycle* and *DNA Repair* as the two most downregulated in NU-1 treated cells, based on both number of genes and significance (-logP 35.9 and 11.7, respectively, Figure 3.1C). Consistent with targeting TERT, NU-1 also induced down-regulation of the pathways *Telomere Maintenance* (-logP 3.09). Upregulated GO terms included metabolic, secretion, and membrane-related pathways (Figure 3.1B). GO analysis with other databases revealed complementary patterns, including downregulation of DNA repair (Figure 3.2A-E).

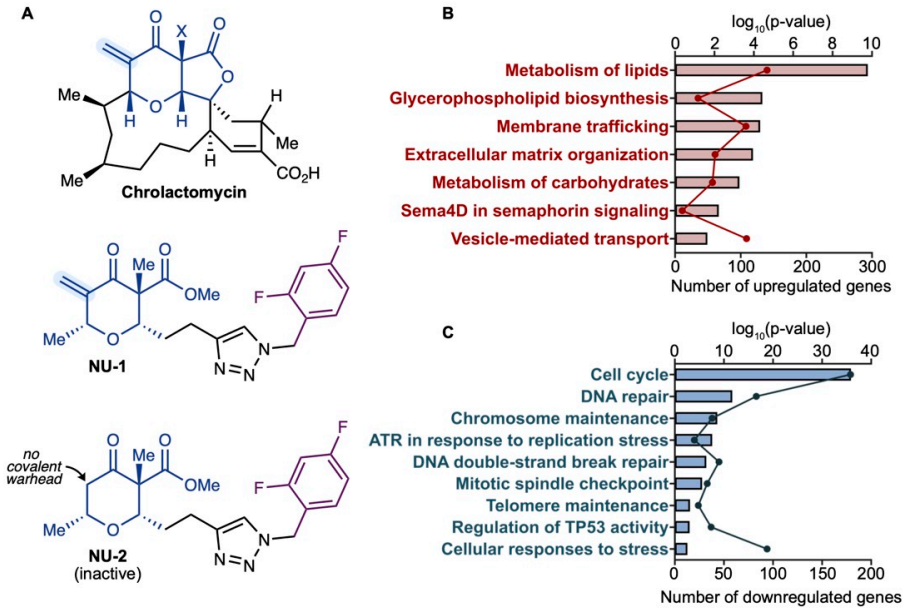

Figure 3.1: TERT inhibitor NU-1 modulates cancer cell gene expression.
A, Chemical structure of TERT inhibitor chrolactomycin, NU-1 and its inactive des-exomethylene analog NU-2. **B**, **C**, Reactome Gene Ontology (GO) analysis of differentially expressed genes (DEGs). Shown are enrichment of upregulated (**B**) and downregulated (**C**) genes in NU-1 treated MCF7 human breast carcinoma cells. Dots indicate the number of DEGs and bars indicate the -Log_{10}(p-value) for each enriched pathway.

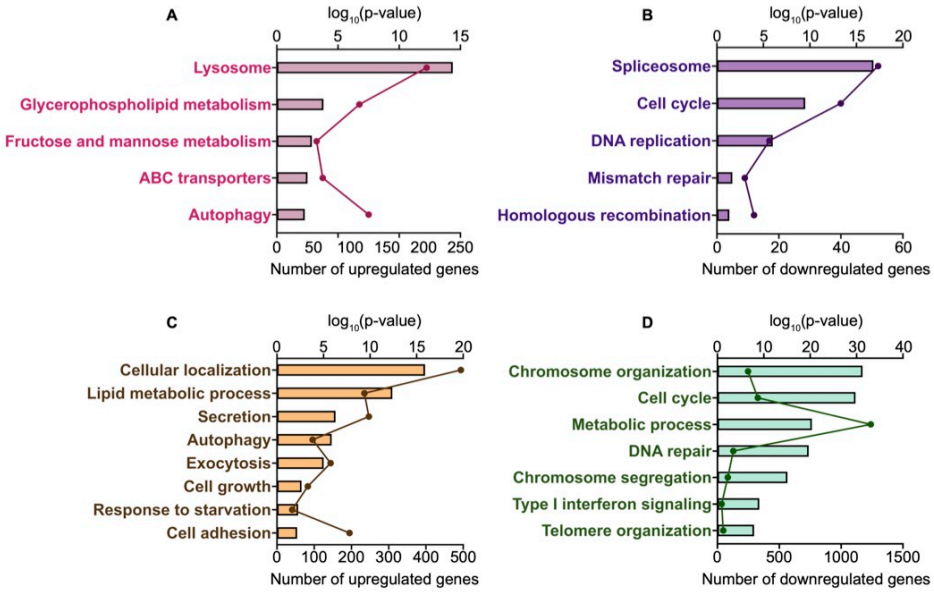

E

Ingenuity Canonical Pathways	-log(p-value)	Up/Down
Interferon Signaling	5.07	↓
NER Pathway	4.46	↓
NRF2-mediated Oxidative Stress Response	4.24	↑
Cell Cycle: G2/M DNA Damage Checkpoint Regulation	3.95	↑
Triacylglycerol Biosynthesis	3.49	↑
Role of BRCA1 in DNA Damage Response	3.45	↓
Pyrimidine Ribonucleotides De Novo Biosynthesis	3.12	↑
Sirtuin Signaling Pathway	3.08	↑

Figure 3.2: NU-1 treatment alters signaling pathways in MCF7 cells.
A-D, GO term enrichment analysis using DAVID bioinformatics resources confirms Reactome enriched pathways. **A, B,** Kyoto Encyclopedia of Genes and Genomes (KEGG) enrichment of upregulated (**A**) and downregulated (**B**) differentially expressed genes in NU-1 treated cells. **C, D,** Biological Process (BG) gene ontology analysis of upregulated (**C**) and downregulated (**D**) differentially expressed genes in NU-1 treated MCF7 cells. Dots indicate the number of DEGs and bars indicate the -Log_{10}(p-value) for each enriched pathway. **E**, Ingenuity canonical pathway (IPA) analysis differentially expressed genes after NU-1 treatment.

NU-1 enhances the chemo-sensitivity of telomerase-positive cancer cells

Toward confirming prior studies and the gene expression analysis, we examined whether NU-1 confers sensitivity to genotoxic stress. Thus, MCF7 cells were incubated for 4 h with NU-1 (0.5 μM), the inactive des-exomethylene analog NU-2 (0.5 μM), the non-competitive inhibitor BIBR 1532 (10 μM), the reversible competitive inhibitor MST-312 (1 μM), or the vehicle DMSO, and then 24 h with the topoisomerase I poison irinotecan (1 nM to 100 μM) and analyzed for cell viability. Each of the TERT inhibitors significantly sensitized MCF7 cells to irinotecan, with NU-1 displaying the strongest effects (Figure 3.3A). NU-1 also sensitized MCF7 cells to topoisomerase II poisons doxorubicin and etoposide and the spindle poison paclitaxel (Figure 3.3A). By contrast, no appreciable sensitizing effects of NU-1 or other TERT inhibitors were observed in the ALT cell line Saos-2 (Figure 3.3B). Another telomerase-positive cell line, A549, displayed a similar pattern to MCF7 (Figure 3.3C). Calculating a combination index (CI (42)) confirmed synergy between NU-1 and chemotherapy agents (Table 1). Interestingly, the TERT inhibitors lost their sensitizing effects on MCF7 cells when added at the same time as, or 4 h after, irinotecan (Figure 3.3D and E), suggesting that TERT's critical protective activity mediates its effects early in the response. These results support NU-1 as a potential sensitizer for genotoxic cancer therapies.

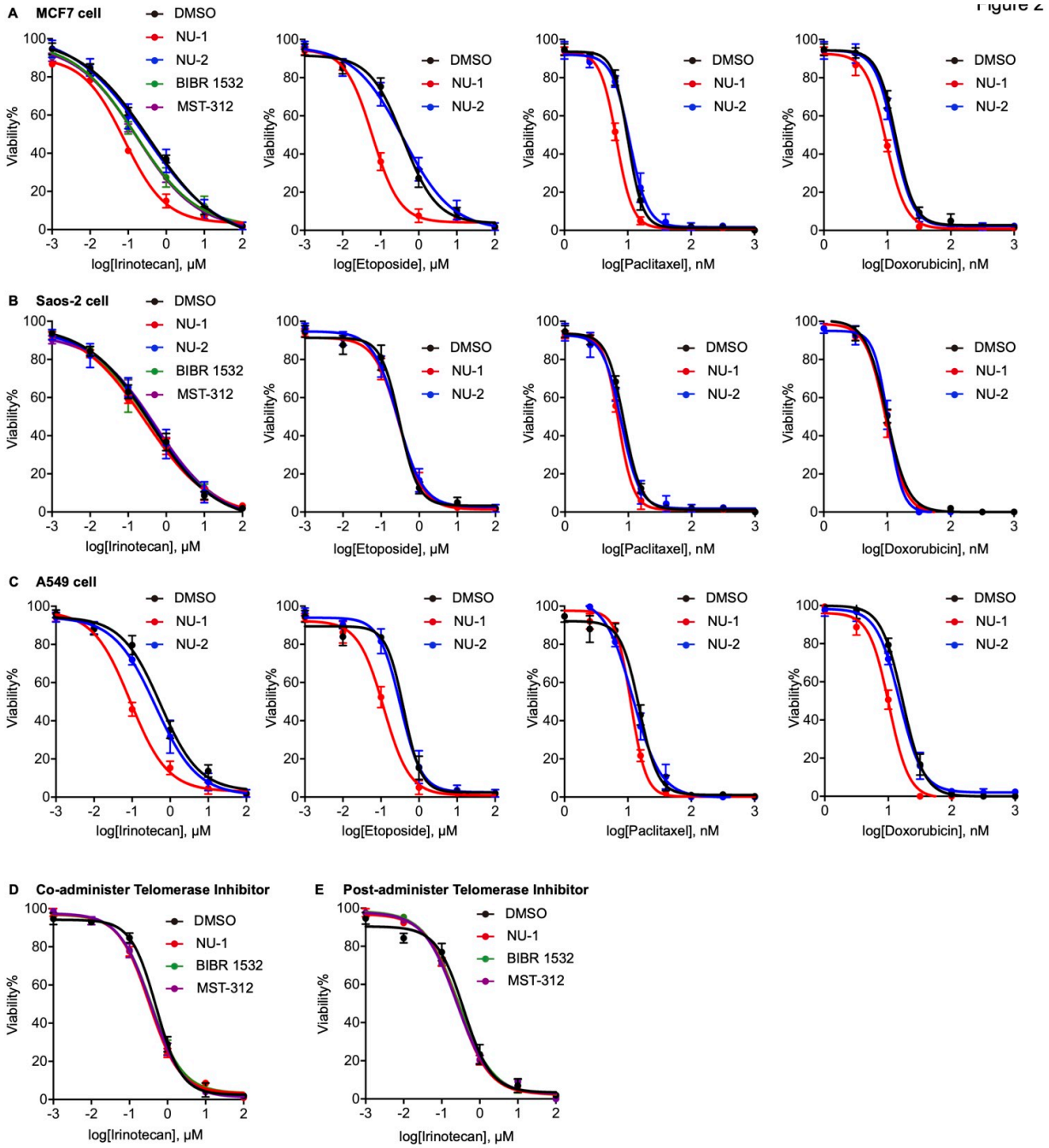

Figure 3.3: TERT inhibition sensitizes telomerase-positive cells to chemotherapy.
A-E, Dose-response curves indicating the viability of MCF7 (**A**), Saos-2 (**B**), and A549 cells (**C**) treated for 4 h with DMSO, NU-1 (0.5 μM), or NU-2 (0.5 μM), BIBR 1532 (10 μM), MST-312 (1 μM) and then 24 h with indicated concentration of irinotecan, etoposide, paclitaxel, or doxorubicin. Cell viability was determined by ATP bioluminescence assay. **D**, **E**, Dose-response curve of the viability of MCF7 cells treated with DMSO control, NU-1 (0.5 μM), BIBR 1532 (10 μM), or MST-312 (1 μM) along with irinotecan. For co-administration (**D**), DMSO or telomerase inhibitors and irinotecan were added together. For post-administration (**E**), cells were incubated with irinotecan for 4 h before adding DMSO or telomerase inhibitors. Cell viability was determined at 24 h after treatment. Data from three replicates, mean ± s.e.m.

NU-1 enhances radiosensitivity in vitro

The non-covalent TERT inhibitors BIBR 1532 and MST-312 have been reported as radiosensitizers in human cancer cell lines (e.g. (43, 44)). To examine whether NU-1 has comparable effects, MCF7 cells were treated with DMSO control, NU-1 (0.5 μM), BIBR-1532 (10 μM), or MST-312 (1 μM), at concentrations below those that impacted clonogenicity on their own (Figure 3.3A), followed by increasing doses of ionizing radiation (IR, 0-5 Gy). A clonogenic survival assay demonstrated that each of the TERT inhibitors conferred radiosensitization, with NU-1 displaying the strongest effects (Figure 3.4B and C, Table 2). Toward further examining the effects of TERT inhibition on cell proliferation, apoptosis and senescence, we treated MCF7 cells with chrolactomycin (0.5 μM), NU-1 (0.5 μM), NU-2 (0.5 μM), BIBR-1532 (10 μM), MST-312 (1 μM), or DMSO, followed by 0 or 6 Gy IR and then incubated for 7 days in the continued presence of drugs for time-lapse live-cell imaging in an Incucyte S3. The TERT inhibitors did not limit cell proliferation of unirradiated cells but significantly slowed recovery and/or proliferation following irradiation (Figure 3.4D). This could not be ascribed to increased cell death as staining cells with the cell membrane integrity probe YO-PRO-1 indicated no increased effects of the TERT inhibitors over radiation alone (Figure 3.4E). However, examining the time-lapse results revealed that many of the surviving cells treated with both TERT inhibitors and radiation displayed an enlarged and flattened morphology characteristic of cellular senescence. Thus, we examined senescence-associated β-galactosidase (SA-βGal) and cell morphology at 6 days after irradiation. Senescent cells were not observed without radiation. After 6 Gy alone, we detected 34 ± 4% enlarged, SA-βGal$^+$ cells. The inactive analog NU-2 displayed a similar level of cellular senescence to the vehicle, 34 ± 8%. Addition of NU-1, chrolactomycin, BIBR 1532 or MST-312 increased the proportion of enlarged, SA-βGal$^+$

cells after irradiation to 54 ± 4%, 55 ± 5%, 53 ± 8% and 55 ± 6% respectively (Figure 3.4F and G). As shown in the images, even among the cells not judged as senescent, few displayed the characteristic size and shape of proliferating MCF7 cells. Notably, even 50 nM NU-1 or chrolactomycin was sufficient to enhance senescence after 6 Gy, though with less potency (Figure 3.4H).

Cellular senescence is defined as a state of stable cell cycle arrest. To explore how TERT inhibition might promote senescence, we examined the distribution of cell cycle stages of MCF7 cells based on their DNA content after irradiation in the presence or absence of NU-1, BIBR 1532, or MST-312. Proliferating MCF7 cells were distributed as ~45% 2N (G1), 35% between 2 and 4N (S), and 20% 4N (G2/M). After 24 h treatment, TERT inhibitors had no appreciable effects on their own. Cells treated with 6 Gy IR and then allowed to recover for 24 h displayed an increase in G1 cells to 62% and decrease in S phase to 22%, consistent with unrepaired DNA damage. Addition of TERT inhibitors 1 h prior to 6 Gy further expanded the G1 population (~71%) and reduced S (~15%) (Figure 3.3I and Figure 3.5A). To visualize senescent cell cycle arrest and/or mitotic catastrophe, we performed time-lapse live-cell imaging of MCF7-FUCCI cells, which stably express fluorescent ubiquitination-based cell cycle indicators (FUCCI (45)) that allow individual cells to be tracked through G1 (mCherry-hCdt1$_{30\text{-}120}$), S/G2 (mVenus-hGeminin$_{1\text{-}110}$), and M phase. MCF7-FUCCI cells were treated with chrolactomycin, NU-1, or NU-2 and then 6 Gy, and incubated in the Incucyte S3, imaging at 2 h intervals for 6 days. After irradiation, most of the surviving NU-2 treated cells eventually resumed proliferation but ~40% remained arrested, displaying persistent expression of the G1 phase marker mCherry-hCdt1 (red) and developing a senescent morphology (Figure 3.4J). This pattern was enhanced by treating cells with chrolactomycin or NU-1 (Figure 3.4J), where ~80% of the surviving cells displayed

mCherry-hCdt1 expression and a senescent morphology at 6 days. These results confirm that even short-term TERT inhibition can potentiate radiation in promoting accelerated senescence, apparently independent of telomere erosion.

Similar experiments were conducted in telomerase negative Saos-2 cells. Cells were assayed for clonogenic survival in the presence of NU-1 (1 μM), BIBR 1532 (20 μM), or DMSO control (Figure 3.6A). Neither NU-1 nor BIBR 1532 displayed radiosensitization in Saos-2 cells (Figure 3.6B and C, Table 2). Treating Saos-2 cells with TERT inhibitors for 1 h before 0 or 6 Gy did not change recovery and/or proliferation compared to DMSO or NU-2 control (Figure 3.6D). Further, at 6 days after 6 Gy, 33 ± 5% of Saos-2 cells accumulated as SA-βGal$^+$ cells with senescent morphology, irrespective of treatment with DMSO, NU-2, NU-1, chrolactomycin, BIBR 1532, or MST-312 (Figure 3.6E and F).

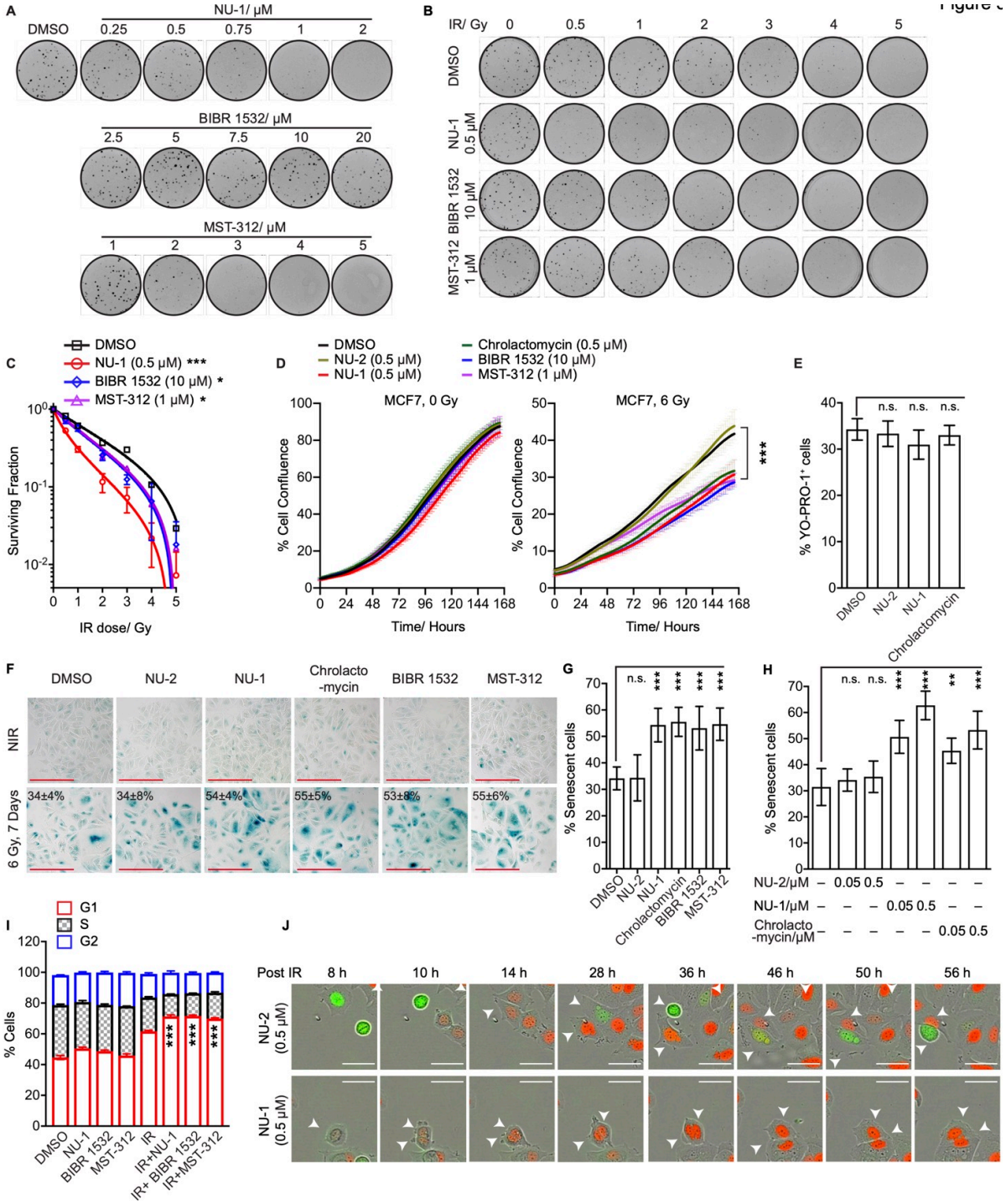

Figure 3.4: TERT inhibition induces radiosensitivity and cellular senescence.
A, Clonogenic assay of cells after telomerase inhibition. MCF7 cells were treated with DMSO control, NU-1, BIBR 1532, or MST-312 at the indicated concentration. **B**, Clonogenic survival of cells after irradiation in the presence or absence of telomerase inhibitors. MCF7 cells were treated with DMSO vehicle, NU-1 (0.5 μM), BIBR 1532 (10 μM) or MST-312 (1 μM) and irradiated at 0, 0.25, 0.5, 1, 2, 3, 4, 5 Gy as indicated. Experiments in **A** and **B** were done in triplicate. Shown are representative images.

Figure 3.4: TERT inhibition induces radiosensitivity and cellular senescence (continued). **C**, Normalized surviving fractions of MCF7 cells in **B**. Colonies with more than 50 cells were counted. Data from three replicates, mean ± s.d. **D**, Automated proliferation analysis from time-lapse imaging over 6 days comparing MCF7 cells treated with DMSO, NU-2 (0.5 μM), NU-1 (0.5 μM), chrolactomycin (0.5 μM), BIBR 1532 (10 μM), and MST-312 (1 μM) for 1 h before 0 (left) or 6 Gy (right) at time 0. Results are shown as mean ± s.d. Images of 25 non-overlapping fields were captured for analysis of each sample. **E**, Quantification of YO-PRO-1 positive cells. MCF7 cells were treated with DMSO control, NU-2 (0.5 μM), NU-1 (0.5 μM) or chrolactomycin (0.5 μM) 1 h before 6 Gy. Cells were stained with YO-PRO-1 6 days after IR. Data from 16 non-overlapping images, mean ± s.d. **F**, SA-βGal staining of MCF7 cells treated as in **D**, after 6 days. Representative 20X images. Scale bars: 200 μm. **G**, Quantification of SA-βGal-positive MCF7 cells. Cells were treated and irradiated as in **F**. Data from 5 non-overlapping images, mean ± s.d. **H**, Quantification of the percentage of SA-βGal-positive cells after MCF7 cells treated with DMSO, chrolactomycin, NU-1, or NU-2 at indicated doses for 1 h and followed by 6 Gy. Then cells were incubated for 6 days, fixed, and stained for SA-βGal. Data obtained from 5 non-overlapping images are shown as mean ± s.d. **I**, The proportion of MCF7 cells at different cell cycle stages. Cells were treated with indicated compounds for 1 h before 0 Gy or 6 Gy irradiation. 24 h after IR, cells were stained with DAPI and analyzed for DNA content using flow cytometry. Data from flow cytometry histogram analysis, three replicates, mean ± s.d. **J**, Live imaging of MCF7 FUCCI cells after 6 Gy irradiation. Cells were treated with NU-1 or NU-2 for 1 h before 6 Gy at time 0 h. MCF7 FUCCI cells display red fluorescence in G1 phase and green fluorescence in S/G2. Successive representative 20X images are shown. Arrows indicate the mother and daughter cells that were tracked. Scale bars: 50 μm. For statistical analysis, *** $P < 0.001$; ** $0.001 < P < 0.01$, n.s. $P > 0.05$ compared to DMSO vehicle (unpaired t-test).

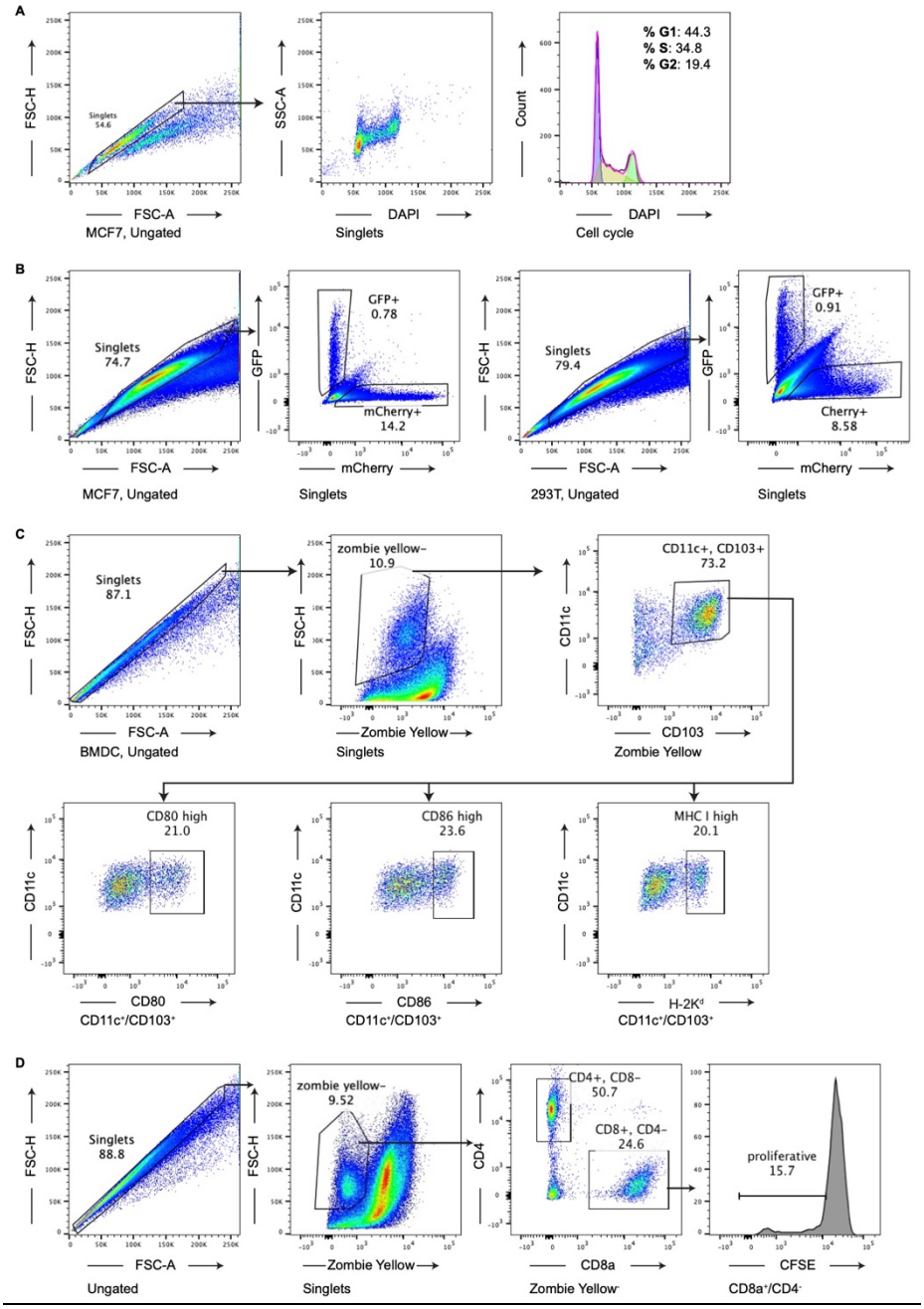

Figure 3.5: Gating strategy of flow cytometric analysis.
A, MCF7 single-cell population was selected based on forward and side scatter (FSC and SSC). The DNA content was analyzed by the intensity of DAPI staining. **B**, MCF7 (right) or 293T (left) cells were first gated singularity as in **A**. Then the gated single-cell population was analyzed for mCherry and GFP expression. **C**, Bone marrow-derived dendric cells were first gated singularity as in **A**. Then live cells were identified by the size and Zombie yellow exclusion. Live cells were gated on co-expression of CD11c and CD103 to identify dendritic cells. Dendritic cell population was gated for expression of activation/maturation markers CD80, CD86, and H-2K^d. **D**, Cells were first gated singularity, size, and viability as in **A**. Live cells were further grouped into CD8$^+$ and CD4$^+$ T cell populations. CFSE dilution was measured in both CD8$^+$ and CD4$^+$ T cells.

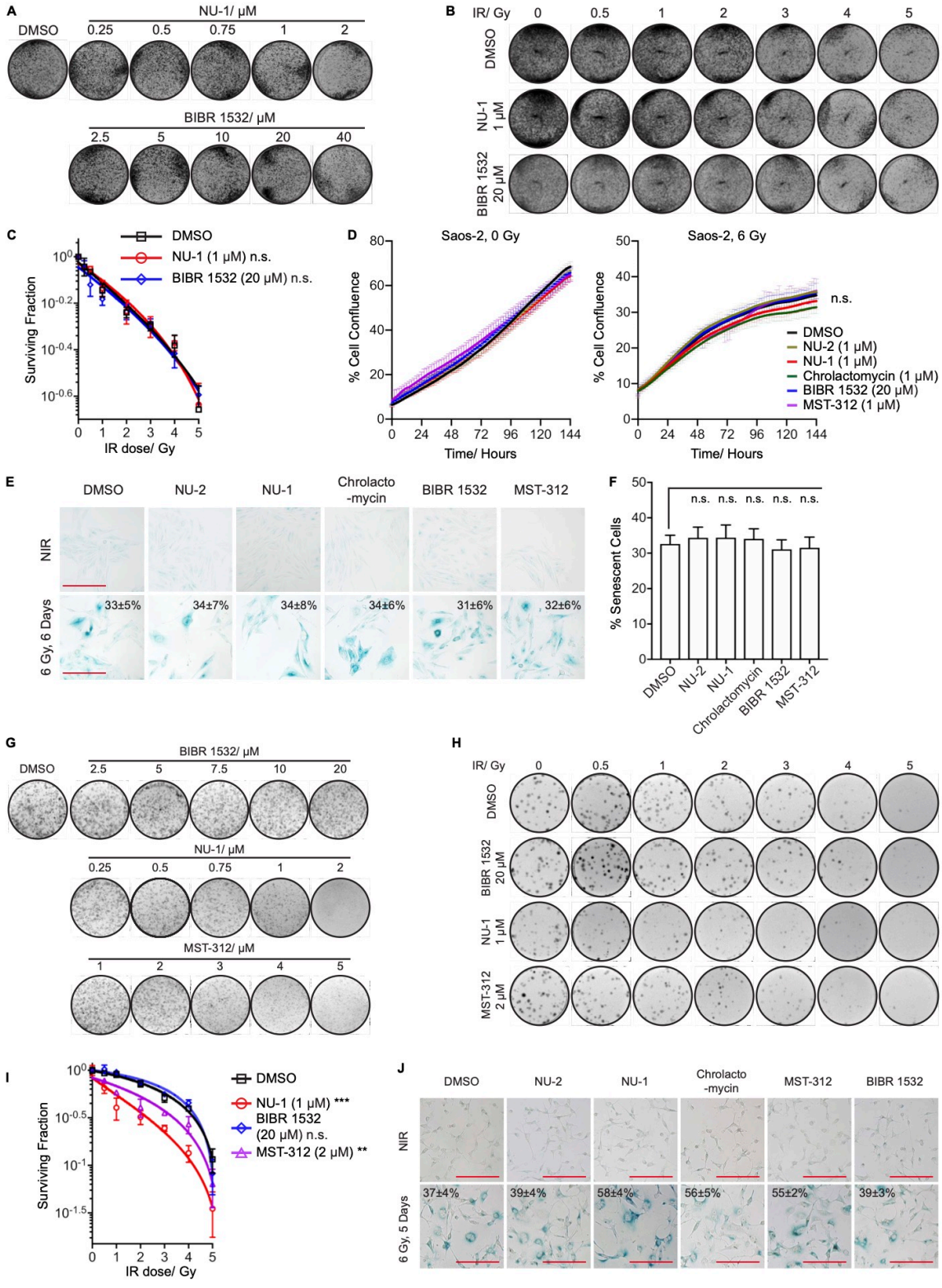

Figure 3.6: TERT inhibition sensitizes telomerase positive cells to radiation.
A, Clonogenic survival of Saos-2 cells after telomerase inhibition. Saos-2 cells were treated with DMSO control, NU-1, or BIBR 1532 at the indicated concentrations.

Figure 3.6: TERT inhibition sensitizes telomerase positive cells to radiation (continued). **B**, Clonogenic survival of Saos-2 cells after irradiation in the presence or absence of telomerase inhibitors. Saos-2 cells were treated with DMSO control, NU-1 (1 μM), or BIBR 1532 (20 μM) and irradiated at the indicated dose. Experiments in **A** and **B** were done in triplicate. Represented images are shown. **C**, Quantitative analysis of **B**. Data from three replicates, mean ± s.d. **D**, Automated proliferation analysis from time-lapse imaging over 6 days comparing Saos-2 cells treated the same as in **B**, followed by 0 (left) or 6 Gy (right) at time 0. Results are shown as mean ± s.d. Images of 25 non-overlapping fields were captured for analysis of each sample. **E**, SA-βGal staining of Saos-2 cells. Saos-2 cells were treated as in **D**, then fixed and stained after 6 days. Shown are represented images. Scale bars: 200 μm. **F**, Quantification of SA-βGal-positive Saos-2 cells after IR. Data from 5 non-overlapping images, mean ± s.d. **G,** Clonogenic assay of CT26 cells after telomerase inhibition. CT26 cells were treated with DMSO control, NU-1, BIBR 1532, or MST-312 at the indicated concentrations. **H**, Clonogenic survival of CT26 cells after irradiation in the presence or absence of inhibitors. CT26 cells were treated with DMSO, BIBR 1532 (20 μM), NU-1 (1 μM), or MST-312 (2 μM) for 1 h, followed by irradiation at the indicated doses. All experiments in **G** and **H** were done in triplicate. Representative images are shown. **I**, Quantitative analysis of **H**. Normalized surviving fractions indicating the average of three replicates are shown. **J**, SA-βGal staining of CT26 cells. CT26 cells were treated the same as in **H**, followed by irradiation at 0 or 10 Gy. Cells were fixed and stained 5 days after radiation. Representative 20X images are shown. Scale bars: 200 μm. For statistical analysis, *** $P < 0.001$; ** $0.001 < P < 0.01$; n.s. $P > 0.05$ compared to DMSO (unrepaired t-test).

TERT inhibition delays chromosomal double strand break repair after irradiation

Prior studies have demonstrated persistent DNA damage in cells treated with telomerase inhibitors along with genotoxic stress, suggesting a direct mechanism of radiosensitization. MCF7 cells were treated with NU-2 (0.5 μM), NU-1 (0.5 μM), chrolactomycin (0.5 μM), BIBR 1532 (10 μM), or MST-312 (1 μM) for 1 h and then irradiated with 0 or 6 Gy, incubated 24 h (roughly one cell cycle for unperturbed MCF7 cells (46)), and examined by immunofluorescence for 53BP1 and γH2AX foci as markers for persistent chromosomal double strand breaks (DSBs). Unirradiated cells, treated with TERT inhibitors or not, yielded a similar average of ~5 53BP1 and γH2AX foci per nucleus (Figure 3.7A and C). However, at 24 h after 6 Gy, persistent 53BP1 and γH2AX foci were increased after treatment with TERT inhibitors compared to controls (Figure 3.7B and C). Cells treated with as low as 100 nM or as high as 1 μM chrolactomycin or NU-1 displayed a similar pattern (Figure 3.8A and B). To distinguish whether the presumptive DSBs might instead be telomere dysfunction induced foci (TIFs), we co-stained telomeres with a PNA probe along with γH2AX. A similar apparent colocalization of ~2% was observed whether cells were treated with 0 or 6 Gy and TERT inhibitors or controls (Figure 3.7D and E).

Although the formation and resolution of 53BP1 and γH2AX foci after irradiation serve as a useful proxy for DSB formation and repair, multiple conditions can uncouple foci persistence from DSB repair (e.g. (47)). Thus, we used single-cell electrophoresis, the so-called neutral comet assay, to directly evaluate DNA damage in MCF7 cells, where chromosomal fragments form a "comet tail" whose length and intensity correspond to the number of DSBs (48). Consistent with the 53BP1 and γH2AX foci staining, TERT inhibitors did not increase % tail DNA above background in unirradiated cells. However, in cells examined 24 h after 6 Gy, TERT inhibition significantly enhanced % tail DNA, indicating a defect in DSB repair (Figure

3.7F and G). In turn, increased % tail DNA could not be explained by damage to telomeres. To examine the cell cycle distribution of damage, the data were plotted against nuclear DNA content, using DAPI for γH2AX foci and total DNA for comet assay. The radiation-treated cells displayed a high apparent G1 DNA content, as predicted by flow cytometry, but no clear bias in the distribution of persistent foci or unrepaired DSBs (Figure 3.8C-E).

To examine TERT dependence, we similarly examined effects of NU-1 on DSB persistence in telomerase-negative Saos-2 cells. After treating Saos-2 cells with DMSO or 1 μM NU-1 and 0 or 6 Gy, NU-1 appeared not to impact 53BP1 or γH2AX foci on its own or combined with IR (Figure 3.7H and I). In turn, neutral comet assays revealed similar levels of unrepaired DSBs at 24 h after irradiation, with or without NU-1 (Figure 3.7J and K). These data suggest that the radiosensitizing effects of NU-1 that delay DSB repair are mediated by TERT inhibition.

TERT inhibition targets non-homologous end-joining repair

Radiation-induced DSBs are heterogeneous, occur throughout the cell cycle, and can be repaired by multiple mechanisms, with the majority rejoined by conventional non-homologous end joining (NHEJ) or homologous recombination (HR) (49-52). NHEJ predominates throughout the cell cycle (53, 54) and NHEJ must be partly suppressed to allow HR repair during S and G2 phases, when sister chromatids are available as repair templates (55). Given this, while the pattern of G1 cell cycle arrest and DSB persistence induced by NU-1 are most consistent with DSB repair defects throughout the cell cycle, multiple pathways may be affected. In prior work, radiosensitization by TERT inhibition has been ascribed to impaired DNA damage signaling (44), a specific defect in HR (43) and other mechanisms. To directly examine impacts on DSB repair pathway choice, we utilized the Traffic Light Repair Reporter system (Figure 3.9A),

which is based on analysis of fluorescent protein expression after I-Sce cleavage of a non-fluorescent artificial substrate that reports repair via NHEJ by expressing mCherry versus template-directed HR by expressing eGFP (Figure 3.9A) (56). MCF7 cells were infected with lentivirus carrying reporter constructs, treated with NU-1, chrolactomycin, BIBR 1532, or DMSO control for 72 h and then analyzed by flow cytometry (Figure 3.5B). The apparent NHEJ/HR ratio was significantly decreased by TERT inhibition (Figure 3.9B), reflecting decreased NHEJ repair without significant change to HR (Figure 3.9B). An even greater decrease in NHEJ/HR ratio was observed upon TERT inhibition in telomerase-positive (57) HEK 293T human embryonic kidney cells (Figure 3.9C), though here the loss of NHEJ appeared to also impact repair pathway choice, leading to increased repair by HR, thereby confirming the specificity of the effect (Figure 3.9C). Taken together, our results suggest that targeting TERT leads to slower chromosomal DSB rejoining after radiation due to reduced NHEJ repair.

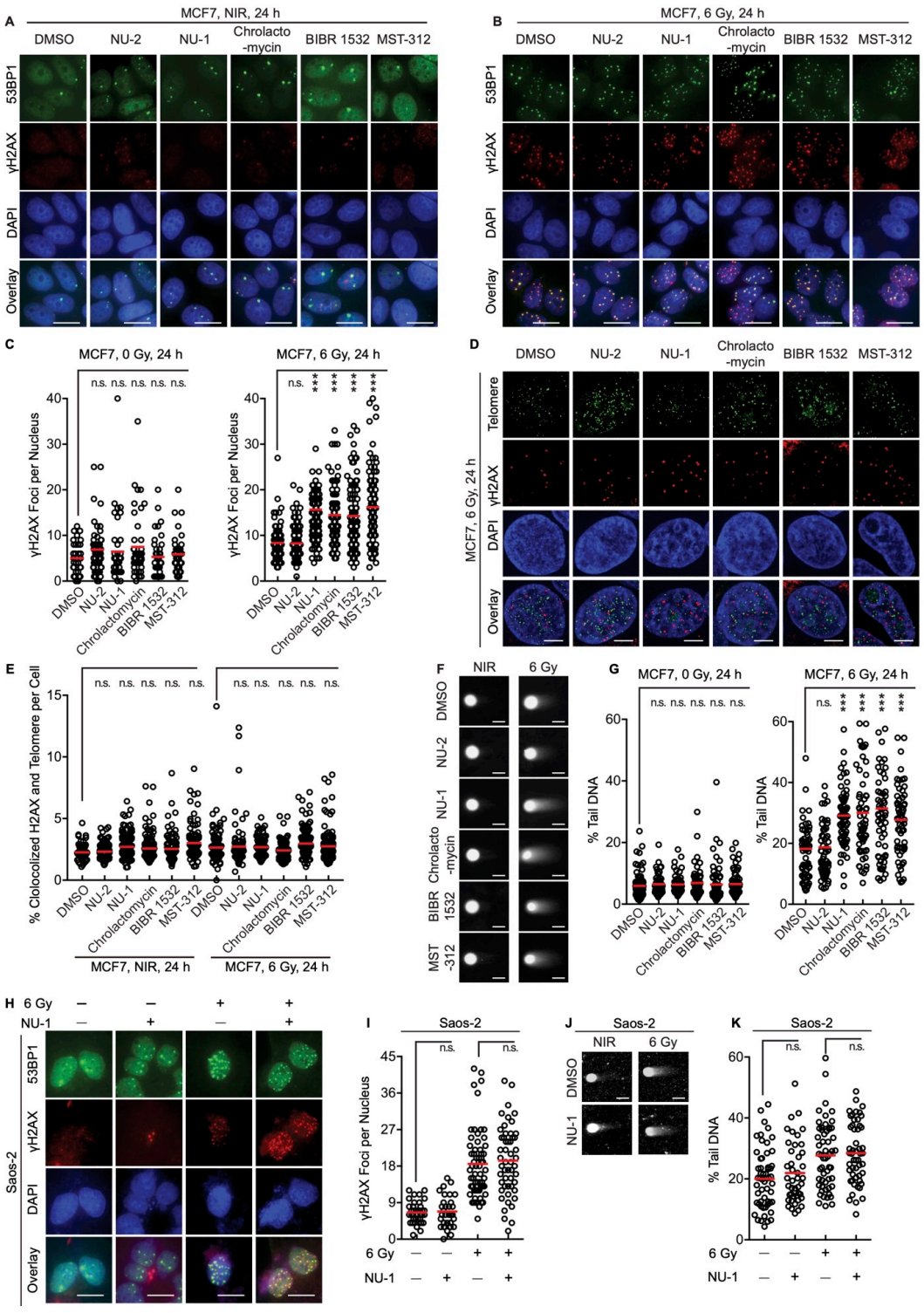

Figure 3.7: TERT inhibition induces persistent DNA damage foci and delays DNA double-strand break repair after irradiation in telomerase positive cells.

A, **B**, Immunofluorescence staining of DNA damage foci in MFC7 cells after 0 Gy (**A**) or 6 Gy (**B**) in the presence or absence of TERT inhibitors.

Figure 3.7: TERT inhibition induces persistent DNA damage foci and delays DNA double-strand break repair after irradiation in telomerase positive cells (continued).
MCF7 cells were treated with DMSO vehicle, NU-2 (0.5 μM), NU-1 (0.5 μM), chrolactomycin (0.5 μM), BIBR 1532 (10 μM), or MST-312 (1 μM) for 1 h, followed by 6 Gy irradiation, then fixed and stained after 24 h. Shown are representative pseudo-colored images of immunofluorescence with anti-53BP1 (green) or anti-γH2AX (red), DAPI (blue), and a three-color overlay. Scale bars, 20 μm. **C**, Quantification of γH2AX foci in cells 24 h after 0 or 6 Gy. **D**, Localization of γH2AX foci and telomeres in MCF7 cells after 6 Gy in the presence or absence of TERT inhibitors. Cells were treated as in **A**, then fixed and stained after 24 h. Shown are representative pseudo-colored images of immunofluorescence with anti-γH2AX (red), telomere peptide nucleic acid (PNA) probe (green), DAPI (blue), and a three-color overlay. Scale bars: 20 μm. **E**, Quantification analysis of colocalized telomere and γH2AX signal in **D**. **F**, MCF7 cells were treated as in **A**, **B**, followed by 0 or 6 Gy irradiation, then collected after 24 h and examined by neutral single cell electrophoresis (comet) assay. Shown are representative images at 10X demonstrating "comet tails" due to unrepaired chromosomal DSBs. Scale bars, 20 μm. **G,** Quantification analysis of comet assay in **F**. The fraction of DNA staining in the comet tail is proportional to unrepaired DSBs. **H**, Saos2 cells were treated with DMSO or NU-1 (1 μM) for 1 h, then 0 or 6 Gy, fixed after 24 h and stained with anti-53BP1 (green), anti-γH2AX (red) and DAPI (blue). The three-color overlay is shown for representative examples. Scale bars, 20 μm. **I**, Quantification of γH2AX foci for samples in **H**. **J**, Saos2 cells treated as in **H** were examined by neutral comet assay after 24 h. Representative 10X images are shown. Scale bar: 20 μm. **K**, Quantification of comet assay results in **J**. For quantification analysis, > 50 cells were analyzed. Shown are individual cells (open circles) and mean (red bar). *** $P < 0.001$; ** $0.001 < P < 0.01$; n.s. $P > 0.05$ compared to DMSO treatment (unpaired t-test).

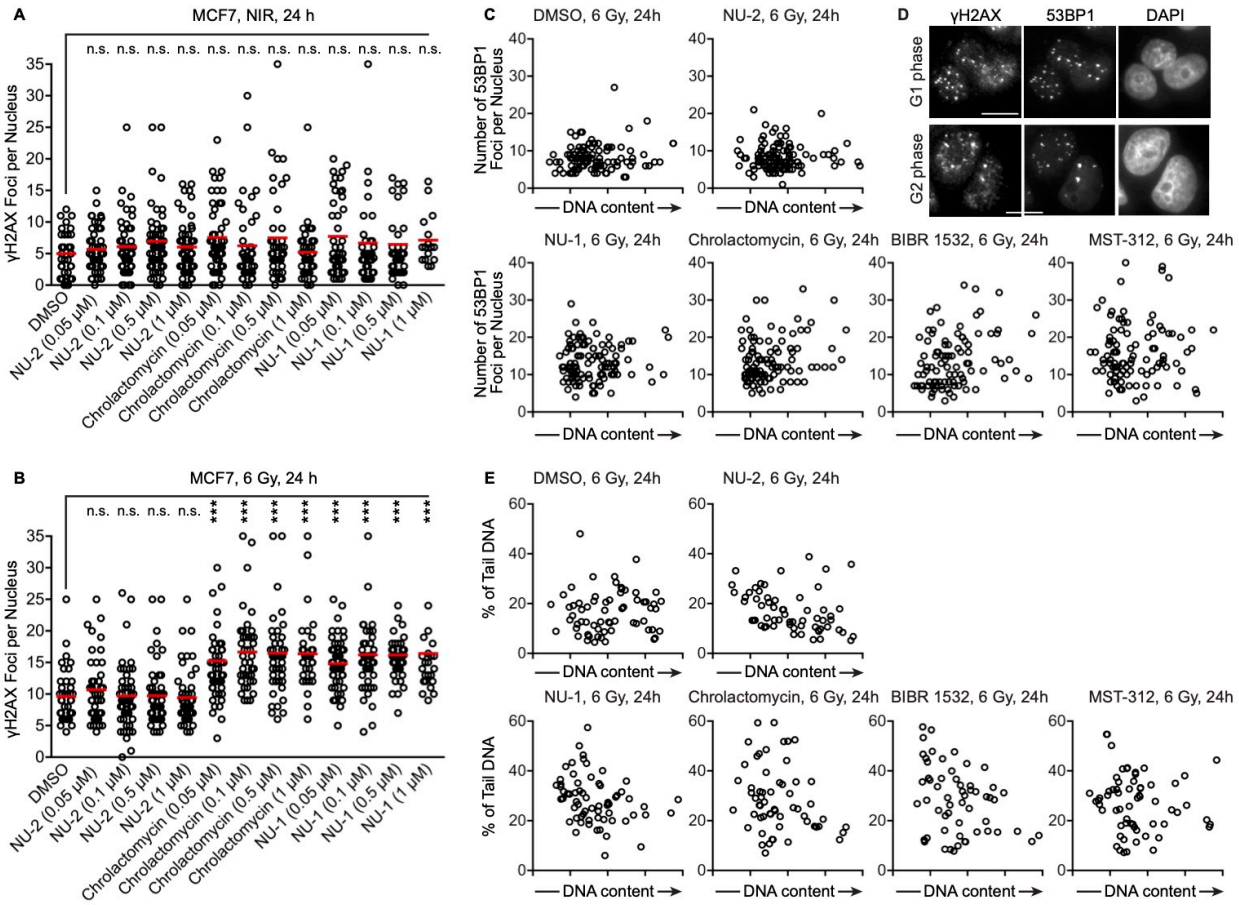

Figure 3.8: TERT inhibition promotes DNA damage foci persistence in MCF7 cells.
A, **B**, Quantification of γH2AX foci in MCF7 cells. Cells were treated with DMSO, chrolactomycin, NU-1, or NU-2 at indicated doses for 1 h, followed by 0 (**A**) or 6 Gy (**B**), fixed after 24 h and stained for γH2AX. > 30 cells were analyzed. Shown are individual cells (open circles) and mean (red bar). *** $P < 0.001$; n.s. $P > 0.05$ compared to DMSO (unpaired t-test). **C**, MCF7 cells were treated and processed the same as in **Figure 3.3B**. The number of 53BP1 foci and DNA content were measured for individual cells. DNA content was measured using imageJ based on DAPI intensity. Shown are individual cells (open circles). **D**, Representative images of MCF7 cells with G1 and G2 DNA content. MCF7 cells were treated with NU-1 (0.5 μM) for 1 h, followed 6 Gy irradiation, then fixed and stained after 24 h. Scale bars, 20 μm. **E**, Neutral comet assays with MCF7 cells were performed the same as in **Figure 3.3F** and **G**. The % tail DNA and total DNA content were measured for the same comet using imageJ.

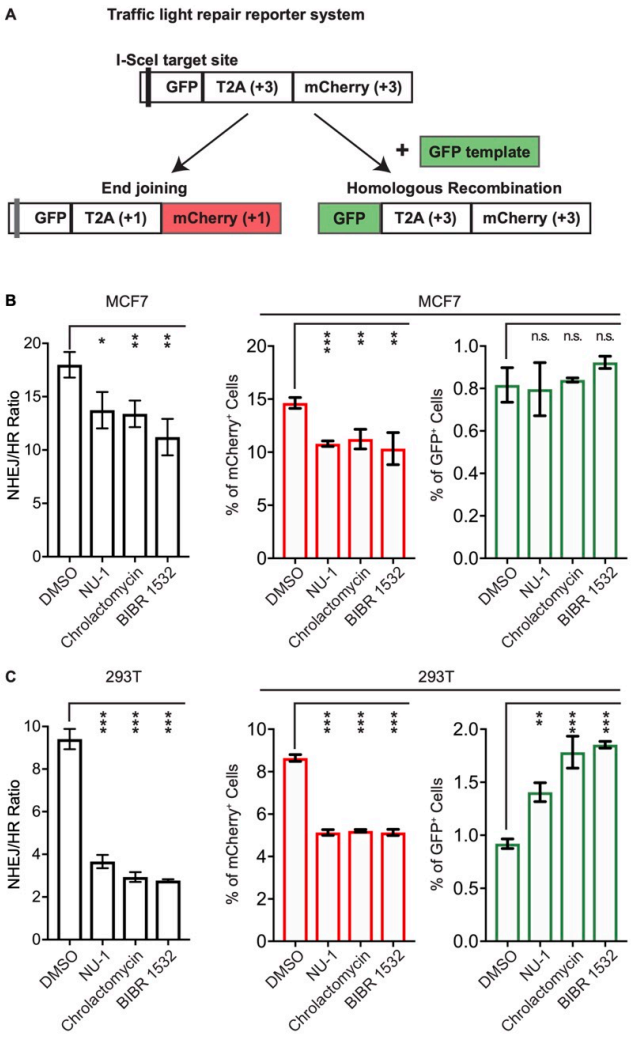

Figure 3.9: TERT inhibition targets the non-homologous end-joining DSB repair pathway. **A**, Diagram of the Traffic Light repair (TLR) reporter system. Repair of an I-Sce-induced DSB in individual cells by NHEJ versus HR results in expression of mCherry or GFP, detected by flow cytometry. **B**, **C**, The ratio of end-joining to homologous recombination (left) and the quantification of mCherry$^+$ or GFP$^+$ cells (right) among whole single cell population in MCF7 (**B**) and 293T cells (**C**). Data from three replicates, mean ± s.d. *** $P < 0.001$; ** $0.001 < P < 0.01$; * $0.01 < P < 0.05$ compared to DMSO treatment (unpaired t-test).

NU-1 sensitizes CT26 tumors to radiation and enhances anti-tumor immunity

Genetic or pharmaceutical inhibition of TERT has been shown to radiosensitize human tumor xenografts in athymic nude mice (27). Toward enabling *in vivo* studies in an immunocompetent host, we assessed NU-1 effects on the BALB/c-derived colon carcinoma cell line CT26. Examining TERT inhibitors in this cell line demonstrated that 1 μM NU-1 and 2 μM MST-312 were tolerated in a clonogenic assay while BIBR 1532 was non-toxic even at 20 μM, consistent with its lack of activity on murine TERT (12) (Figure 3.6G). Non-toxic doses of NU-1 (1 μM) and MST-312 (2 μM) sensitized CT26 cells to radiation doses up to 5 Gy and enhanced senescence induction by 6 Gy while BIBR 1532 (20 μM) had no similar effects (Figure 3.6H-J, Table 2). After confirming that NU-1 was well-tolerated by BALB/c mice, we then evaluated the growth of subcutaneous CT26 tumors treated with daily intraperitoneal injections of 10 mg/kg NU-1 on Days 9 to 13 after tumor inoculation, with or without a single 10 Gy X-ray dose on Day 11 (Figure 3.6A). NU-1 had no appreciable effect on its own while 10 Gy irradiation produced a moderate growth delay (Figure 3.10B and C, Figure 3.11A and B). Tumors treated with both NU-1 and 10 Gy displayed a marked growth delay with most of the tumors (7/8) were eliminated within two weeks after treatment. To examine recurrence, we continued to monitor three tumors each from the 10 Gy alone (tumor size 121, 27 and 0 mm^3 at day 28) and the NU-1 + 10 Gy combination treatment (tumor size 5, 0 and 0 mm^3 at day 28) groups until Day 54. Each of the tumors that had not disappeared by Day 28 resumed growth but tumors that had been eliminated did not recur (Figure 3.11C). Histology analysis of tumors removed on Day 18 revealed marked tissue destruction and loss of cellularity after NU-1 + 10 Gy combination treatment while immunofluorescence revealed lower expression of proliferation marker Ki-67 and persistent γH2AX compared to 10 Gy alone (Figure 3.10D and E).

The elimination of tumors by combined NU-1 and radiation treatment suggested the potentiation of anti-tumor immune response. Therefore, we probed sections of the tumors obtained 5 days after treatment to detect $CD45^+$ immune infiltrate, $CD11c^+$ dendritic cells (DCs), $CD8^+$ cytotoxic T cells and activation markers granzyme B and perforin. NU-1 + 10 Gy treated tumors displayed markedly higher tumor immune infiltration ($CD45^+$), including increased dendritic cells ($CD11c^+$) (Figure 3.10F) along with higher levels of cytotoxic T cells, many of which appeared activated ($CD8^+$/granzyme B^+, Figure 3.10G). This pattern is consistent with immunogenic radiosensitization by NU-1, enabling an effective anti-tumor immune response. To examine the role of adaptive immunity further, CT26 tumors were formed in immunodeficent NSG mice lacking mature B, T or NK cells and treated with 10 Gy alone or combined with NU-1, again following the schema in Figure 3.6A. Compared to CT26 tumors in wildtype BALB/c mice, 10 Gy alone induced less growth delay in NSG mice (Figure 3.10H and Figure 3.11D). While concomitant treatment with NU-1 was still able to enhance the radiation growth delay in immunodeficient mice, the effect was no longer sufficient to eliminate tumors.

Senescent CT26 cells formed by TERT inhibition and radiation activate DCs to prime T cells

A prerequisite for priming of a cytotoxic T cell-mediated immune response is for DCs to present tumor antigens in the context of the major histocompatibility complex (MHC) (58). To model the process *in vitro*, we treated CT26 cells with DMSO, NU-1, or MST-312 for 5 days and with 0 or 10 Gy and co-cultured them overnight with bone marrow-derived $CD11c^+$/$CD103^+$ dendritic cells (BMDCs) (Figure 3.12A). BMDC activation and maturation was examined by flow cytometric analysis of costimulatory molecules CD86 and CD80, as well as MHC I molecule $H\text{-}2K^d$ (Figure 3.5C). Overall, the irradiated CT26 cells produced higher surface

expression of CD86, CD80, and H-2K^{d} Class I MHC (Figure 3.12B). The TERT inhibitors further increased the level of H-2K^{d}, which may be limiting for CD8^{+} T cell stimulation (58). To examine DC APC function, we combined BMDCs that had been cocultured with CT26 cells with splenocytes that were obtained from mice immunized with irradiated CT26 cells and labeled with carboxyfluorescein succinimidyl ester (CFSE) (Figure 3.12A). CFSE dilution was examined after 5 days by flow cytometry (Figure 3.5D). DCs co-cultured with unirradiated CT26 cells, treated with TERT inhibitors or not, drove proliferation of 10-16% of CD8^{+} T cells. DCs co-cultured with irradiated CT26 cells increased proliferating CD8^{+} cells to 26.4% while NU-1 or MST-312 treated and irradiated CT26 cells yielded 33.5% and 30.4% proliferating CD8^{+} T cells (Fig.12C). BMDCs cocultured with irradiated CT26 cells also induced more CD4^{+} T cell proliferation, but with no appreciable impact from TERT inhibitors (Figure 3.12D). Overall, the pattern confirms the potential for combining NU-1 and radiation to promote a cytotoxic T cell-mediated anti-tumor immune response.

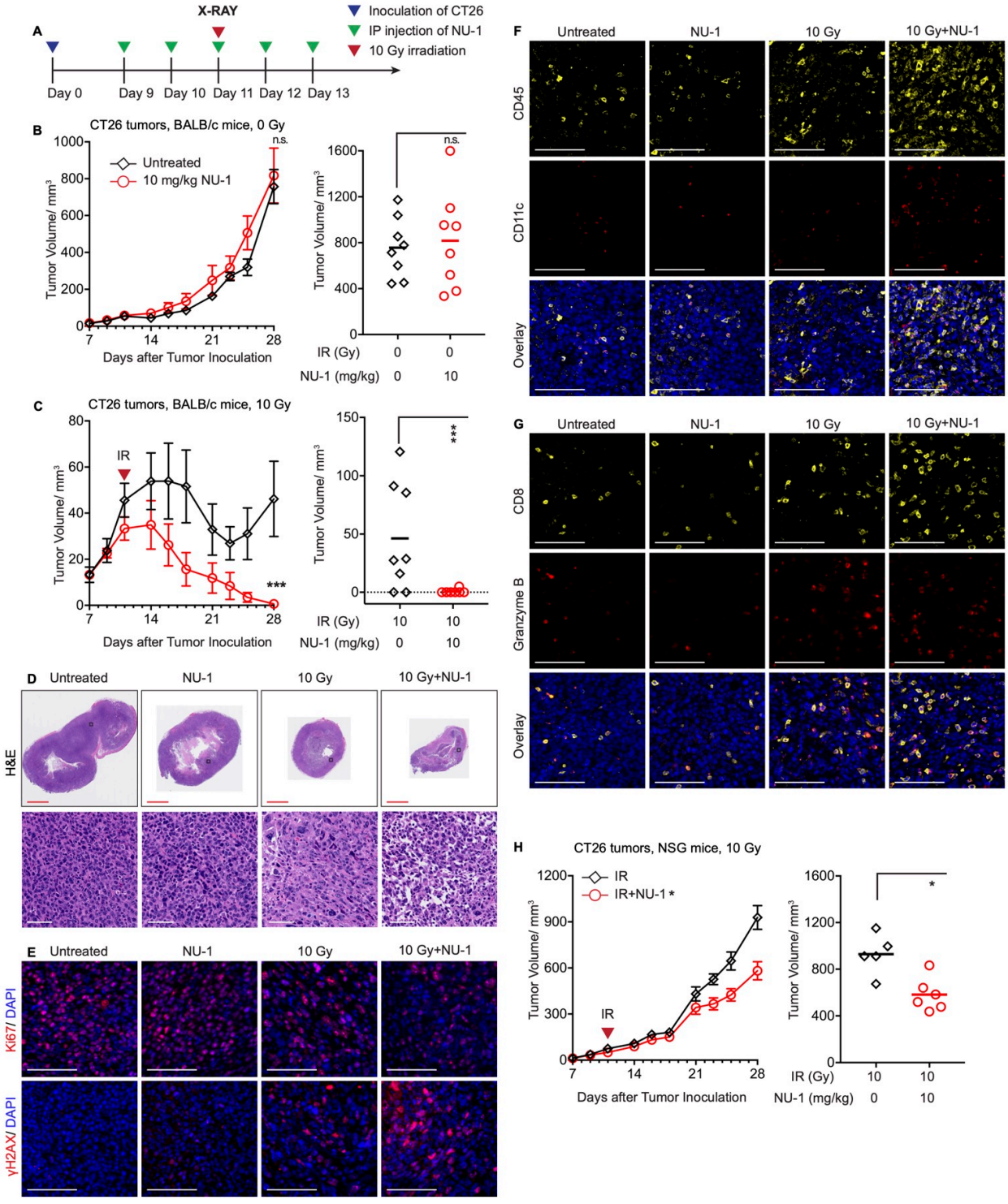

Figure 3.10: NU-1 confers immunogenic radiation sensitization that leads to tumor elimination.

A, Experimental schema for treating mice bearing CT26 subcutaneous tumors with NU-1 intraperitoneal injection and/or external beam irradiation. **B**, **C**, Growth of CT26 tumors in BALB/c mice treated with 10 mg/kg NU-1 alone (**B**) or in combination with 10 Gy irradiation (**C**).

Figure 3.10: NU-1 confers immunogenic radiation sensitization that leads to tumor elimination (continued).
Left, tumors were measured with calipers every 2-3 days with 8 mice per treatment group, mean ± s.e.m. Right, tumor volumes at day 28 after inoculation, showing individual tumors (open square or circle) and mean (bar). **D**, Hematoxylin and eosin (H&E) staining of CT26 tumor sections. CT26 tumors were collected 5 days after treatment, fixed, embedded and sectioned. Serial sections to those shown were used. Shown are representative H&E whole section scanning (scale bar: 2.5 mm) and selected enlarged regions (scale bar: 60 μm). **E-G**, Immunofluorescence staining of immune infiltrate in treated tumors. Serial sections of the tumors in **D** were used. Shown are representative pseudo-colored images of staining for proliferation marker Ki67 (red) or DNA damage marker γH2AX (red), overlaid with DAPI (blue) (**E**), or total immune cell marker CD45 (yellow) and dendritic cell CD11c (red) (**F**), or cytotoxic T cell CD8 (yellow) and Granzyme B (red), DAPI (blue), and a three-color overlay (**G**). Scale bars: 20 μm. **H**, Growth of CT26 tumors in NSG mice. CT26 tumor-bearing NSG mice were treated with radiation, with or without NU-1, as in **C**. Left, tumors were measured every 2-3 days with 5-6 mice per treatment group, mean ± s.e.m. Right, tumor volumes at day 28 after inoculation, showing individual tumors (open square or circle) and mean (bar). *** $P < 0.001$, * $P < 0.05$, n.s. $P > 0.05$ (unpaired t-test).

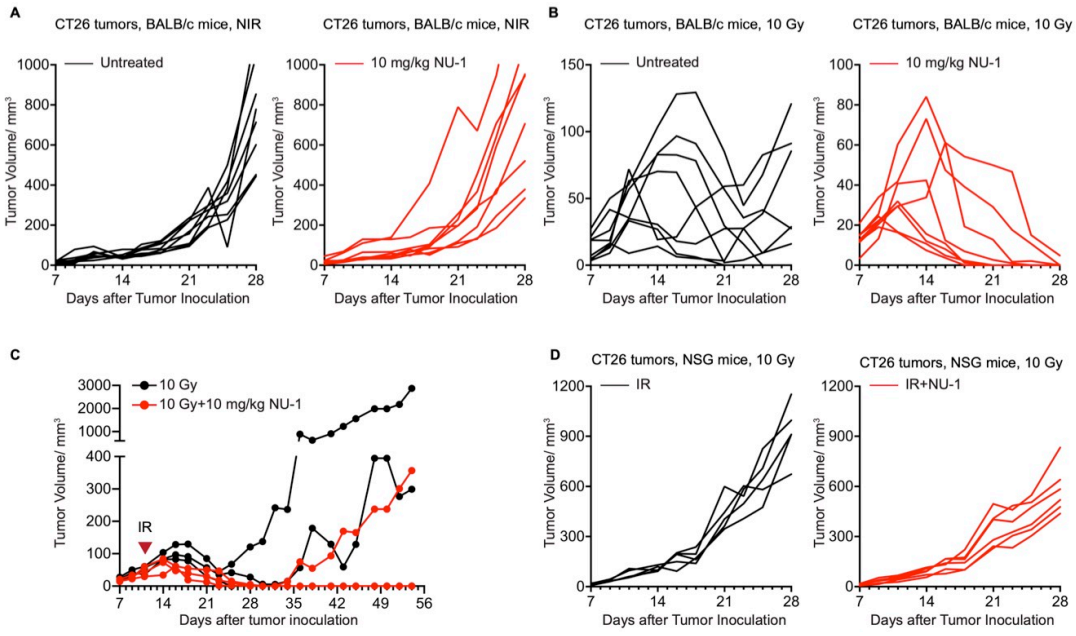

Figure 3.11: TERT inhibition sensitizes CT26 tumors to radiation
A-D, Growth curve of individual CT26 tumors. **A**, **B**, Tumor growth of individual BALB/c mice in **Figure 3.5B-C**. **C**, 3 BALB/c mice after radiation alone or combined with NU-1 were measured for 54 days after tumor inoculation. Tumors were irradiated on Day 11. **D**, Tumor growth of individual NSG mice in **Figure 3.5F.**

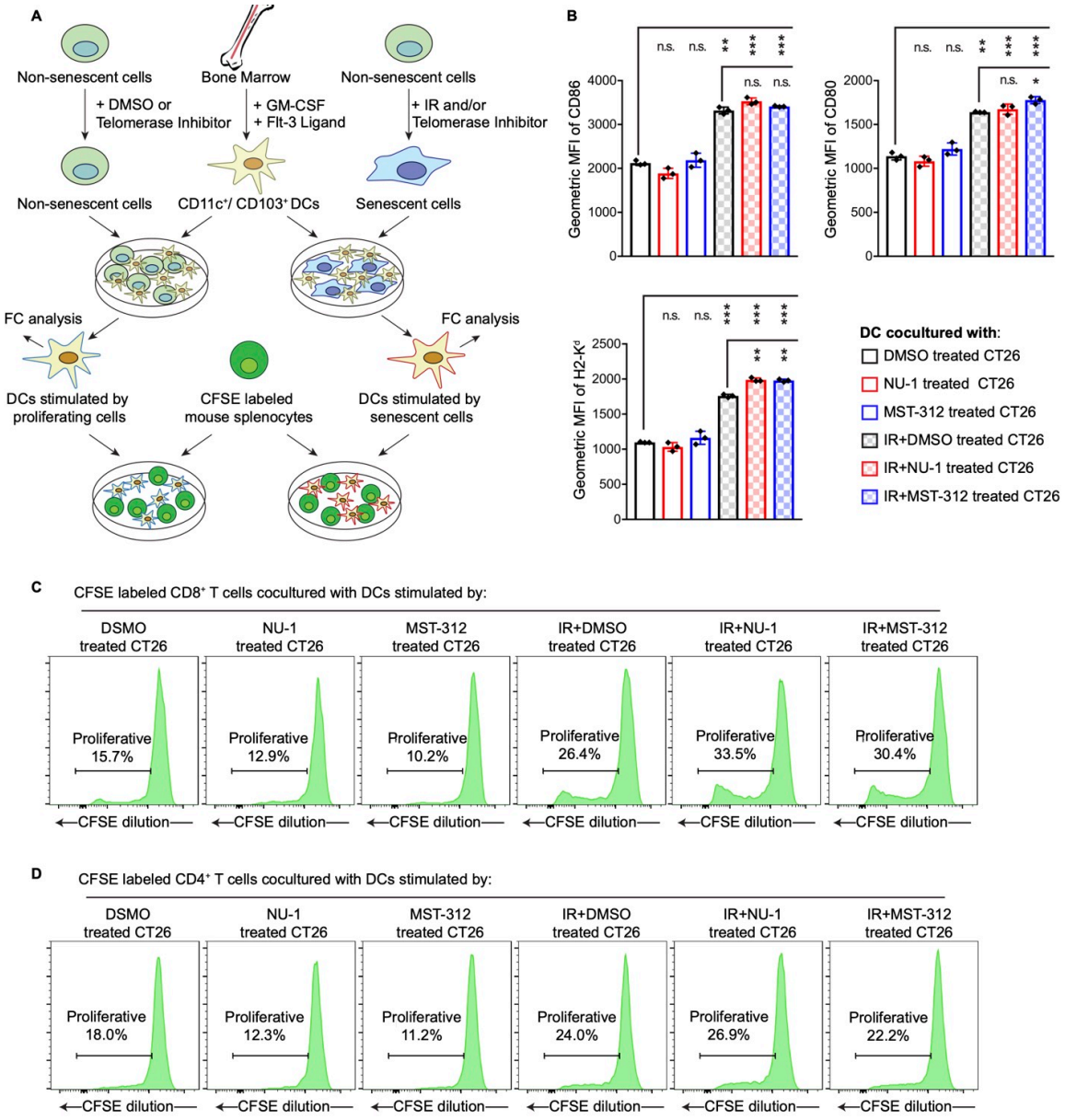

Figure 3.12: TERT inhibition with radiation forms immunogenic senescent CT26 cells capable of stimulating DC function.

A, Experimental schema for stimulating BMDCs with CT26 cells. **B**, Quantitative analysis of DC activation/maturation. CT26 cells treated with DMSO, NU-1, or MST-312 ±10 Gy radiation, incubated 5 days in culture, and combined with BMDCs overnight. The Zombie yellow$^-$ /CD11c$^+$/CD103$^+$ DC population was analyzed by flow cytometry for maturation markers. Shown are data from three experiments, mean ± s.d. *** $P < 0.001$, ** $0.001 < P < 0.01$, n.s. $P > 0.05$ (unpaired t-test). MFI, mean fluorescence intensity. **C**, **D**, Assays of DCs stimulated by CT26 cells for activation of CD8$^+$ (**C**) or CD4$^+$ (**D**) T cell proliferation. Carboxyfluorescein succinimidyl ester (CFSE) labeled murine splenocytes were cocultured for 5 days with DCs pre-stimulated by CT26 cells treated with DMSO, NU-1, MST-312 alone or combined with 10 Gy. Shown are Zombie yellow$^-$/CD8$^+$/CD4$^-$ T cell population (**C**) and Zombie yellow$^-$/CD8$^-$/CD4$^+$ T cell population (**D**).

3.3 Discussion

The expression of telomerase reverse transcriptase (TERT) in adult humans is generally limited to stem and progenitor cells in continuously proliferative tissues (2), including lymphoid tissue and bone marrow along with epithelial tissue (59). A majority of human cancers constitutively express TERT, often resulting from promoter mutations and/or epigenetic changes (2), and many at comparatively high levels, with a negative impact on overall survival (60). A long-standing assumption has been that TERT serves a primary role in maintaining telomere length to support unlimited cell division during tumor growth. Hopes to exploit this potential Achilles heel have long driven development and translation of telomerase inhibitors, with most efforts focused on TERT (1). Limiting proliferative potential remains attractive as a strategy to deplete cancer stem cells and limit recurrence or metastasis but the need for continuous telomerase suppression may incur dose-limiting toxicities such as cytopenias. Of the few agents that remain under clinical development, Imetelstat displays activity in myelofibrosis and myelodysplastic syndrome in Phase II studies (61, 62), though the mechanism of action may not require telomere erosion (63). Along these lines, leveraging TERT to acutely damage telomeres by incorporating toxic substrates such as 6-thio-dG (17) or other analogs (18) can target proliferating tumor cells but may not spare normal stem cells.

As an alternative, multiple TERT inhibitors have been shown to potentiate the effects of radiation or chemotherapy agents (21, 27), apparently independently of telomere length. Indeed, TERT performs multiple non-canonical functions beyond telomere maintenance that contribute to cancer cell survival, proliferation, and immortality (19-23). While cancer cell lines may lose viability upon TERT inhibition *in vitro*, short-term telomerase inhibition is not therapeutic on its own *in vivo*. However, TERT may serve multiple roles in mediating resistance to genotoxic

cancer therapy. In response to cell stress, TERT can translocate to mitochondria, where its activity protects mitochondrial integrity and reduces ROS and resulting DNA damage (64, 65). A recent report identifies this mitochondrial role as critical to TERT addiction in NRAS-mutant melanoma (66). Of particular relevance here, TERT has long been implicated in chromosomal DNA repair (28-30), though whether this reflects catalytic activity at sites of DNA damage and/or enhanced DNA repair gene expression remains poorly defined.

In recent work (36), we reported NU-1 as a novel, irreversible TERT inhibitor developed via chemical simplification of the natural product chrolactomycin. While NU-1's covalent mechanism of action might facilitate continuous suppression of TERT, we would not expect tumor specificity and thus similar dose-limiting toxicities to those observed with Imetelstat. Thus, we have explored using NU-1 for short intervals to expose TERT addiction and/or sensitize tumors to ionizing radiation, which has the advantage of allowing tumors to be targeted while sparing other proliferative tissues.

NU-1 significantly enhances the effects of radiation *in vitro*. Cells display persistent DNA damage signaling and delayed DNA double-strand break (DSB) repair, leading to prolonged cell cycle arrest and accelerated senescence. The slower DSB repair appears to reflect a specific defect in non-homologous end-joining (NHEJ) without a similar impact on homologous recombination (HR). A direct role in NHEJ is consistent with early studies that implicated TERT in end-joining and rapid chromosomal DSB repair (28-30), though divergent from TERT's canonical role in telomere maintenance and resulting protection against NHEJ-mediated end-to-end fusions and chromosome instability. Taken together, our results reinforce earlier work (28, 29, 67) that raised concerns about hTERT-immortalized cell lines as "normal cell" controls for studies of radiation response.

Our most striking results came from examining radiosensitization *in vivo*. Using an immunogenic tumor model (68), CT26 colon carcinoma flank tumors in syngeneic BALB/c mice, short-term treatment with NU-1 was neither toxic nor effective on its own but markedly enhanced the effects of radiation. Radiation induced a growth delay, but the combination led to tumor elimination. NU-1 decreased tumor cell proliferation and increased persistent DNA damage versus radiation alone. Notably, there was a greater accumulation of dendritic cells and activated cytotoxic T cells in combination-treated tumors. A key role for adaptive immunity was consistent with the decreased impact of NU-1 on radiation response of CT26 tumors formed in NOD scid gamma (NSG) immunodeficient mice. Modeling this *in vitro*, when tumor cells treated with TERT inhibitors and radiation to induce senescence were cocultured with immature DCs, this resulted in DC activation and maturation and increased cytotoxic T cell priming, indicating competence as antigen-presenting cells. A favorable interpretation is that targeting TERT with NU-1 potentiates an effective anti-tumor immune response by promoting immunogenic senescence (69) in irradiated tumors and thereby boosting radiation-induced *in situ* vaccination (70).

Overall, NU-1 may provide a valuable probe to explore DNA repair and/or other non-canonical functions of TERT toward overcoming resistance to conventional therapies in telomerase-positive cancers. A caveat is that catalytic inhibition with NU-1 may have little or no impact on enzyme-independent roles of TERT (19, 71) that may contribute to therapy resistance. For example, catalytically inactive TERT maintains protein-protein interactions that mediate telomere protective functions (72). Similarly, TERT contains a BH3-like motif that interacts with Bcl-2 family proteins to play an anti-apoptotic role (73). Other enzyme-independent roles are in transcription where TERT binds p65 to activate NF-κB (74), stabilizes and activates MYC (75),

binds SP1 to induce VEGF (76), and associates with Pol III to drive tRNA expression (77). Nonetheless, NU-1 appeared to impact expression of cell cycle and DNA damage response pathway genes even in undamaged cells, suggesting that TERT catalytic activity might also influence transcription, even if indirectly.

A prolonged DNA damage response (DDR) was observed both *in vitro* and *in vivo* when cells were treated with combined radiation and NU-1, providing a potential link to anti-tumor immunity via cytoplasmic DNA sensing, immunogenic cell death and/or other mechanisms (78). Considering ongoing efforts to leverage the DDR to enhance immunotherapy, TERT is a promising target, not only given its extra-telomeric roles in DNA repair as studied here but also via activity at telomeres that may impact cGAS-STING-mediated inflammatory signaling (79, 80). This latter pathway was recently leveraged to target a cytotoxic T cell response to telomerase-positive tumors in mice using 6-thio-dG to damage telomeres (81). Whether localized to chromosome arms or telomeres, unrepairable DNA damage will promote tumor cells to display DAMPs and release inflammatory mediators. This is enhanced when cells enter senescence and express a senescence-associated secretory phenotype (SASP) or undergo immunogenic cell death (78, 82). In particular, dendritic cells exposed to injured cancer cells with DNA damage increase surface expression of MHC and costimulatory molecules, enhancing T cell priming capacity (83). Indeed, we observed a pattern of persistent DNA damage and infiltration of DCs and activated cytotoxic T cells in sections of tumors treated with NU-1 and radiation. However, TERT's role in protecting tumors from radiation and anti-tumor immune response may go beyond DNA repair to involve other non-canonical functions that modulate cell stress response and promote survival. Looking forward, NU-1 and other chrolactomycin analogs can provide useful tools to dissect mechanisms linking telomerase reactivation to tumor immune

evasion and to validate TERT as a tumor-specific target to potentiate conventional, targeted or immune therapies.

3.4 Material and Methods

Cell lines and tissue culture

MCF7, Saos-2, HEK-293 and CT26 cell lines were obtained from ATCC. MCF7 stably expressing the tetracycline-regulated transactivator Tet-On Advanced was obtained from Takara (Cat No. 632108). An MCF7 cell line with FUCCI cell cycle reporter constructs was reconstructed here by transduction with lentivirus expressing mVenus-hGeminin (1/110)/pCSII-EF-MCS and mCherry-hCdt1 (30/120)/pCSII-EF-MCS (a kind gift of Atsushi Miyawaki, RIKEN Center for Brain Science, Japan) (45). Cells with positive expression were selected by fluorescence-activated cell sorting (FACS).

Human and mouse tumor cells were maintained in DMEM containing 4.5 g/l glucose (Thermo Fisher Scientific) supplemented with 10% Tet-approved FBS (Atlanta Biologicals) and 1% penicillin/streptomycin (Thermo Fisher Scientific). The cells were tested for mycoplasma contamination and authenticated by a short tandem repeat profile (IDEXX BioResearch) prior to performing experiments. All experiments were performed within 3 to 10 passages after thawing cells.

The basic murine immune cell culture medium was RPMI medium (Thermo Fisher Scientific) supplemented with 10% heat-inactivated FBS (Thermo Fisher Scientific), 1% penicillin/streptomycin (Thermo Fisher Scientific), and 50 μM β-mercaptoethanol.

Chemical probes

Chrolactomycin was isolated from *Actinospica* (a kind gift of M. Iorio at NAICONS Scrl, Milan, Italy) and NU-1 and the des-exomethylene analog NU-2 were synthesized and purified as

described (36). BIBR 1532 and MST-312 were obtained from Cayman Chemical. Irinotecan, doxorubicin, etoposide and paclitaxel were obtained from Selleck Chemicals.

RNA sequencing analysis

3×10^4 MCF-7 cells were seeded in a T25 flask, cultured overnight, and treated with 0.5 μM NU-1 or DMSO for 48 h. Media was removed, cells were washed 2 times with PBS, followed by chemical disassociation with TrypLe (Thermo Fisher). Media was added to quench the TrypLe, the cell suspension was centrifuged at 300 × g for 5 min and pellets were shipped to Applied Biological Materials for RNA isolation and total RNA sequencing. RNA was isolated using Trizol (Thermo Fisher). The quality of the RNA extraction was assessed by gel electrophoresis. All the samples passed internal QC for library preparation. Sequencing libraries were prepared using Illumina TruSeq Stranded mRNA Library Preparation kit following the manufacturer's recommendations. The quality of the libraries was assessed using Qubit DNA assay, Agilent Bioanalyzer, and qPCR. All libraries passed internal QC. Sequencing was performed with an Illumina NextSeq system.

To carry out the transcriptomic study, paired-end reads were aligned with the hg38 human reference genome by Hisat2. The abundance of genes was quantified by Htseq-count. Analysis of differentially expressed genes (DEGs) between NU-1 treated and control cells was performed with EdgeR in R studio, with dispersion value estimated as 0.01. Genes were considered significantly upregulated if they displayed fold change > 1.5 and P value < 0.1 and significantly downregulated if fold change < -1.5 and P value < 0.1, comparing NU-1 treated and control cells. The DEG lists were subjected to GO analysis by Reactome (84), DAVID (85), and Ingenuity Pathway Analysis (IPA) (86) to detect enriched pathways.

Chemosensitization studies

MCF-7, A549, and Saos-2 cells were seeded in 96 well plates. After cell attachment, the old medium was replaced by fresh medium containing 0.5 μM NU-1, 0.5 μM NU-2, 10 μM BIBR 1532, 0.5 μM MST-312 or DMSO vehicle. After incubation for 4 h, DMSO stock solutions of irinotecan, etoposide, paclitaxel, or doxorubicin were added at indicated concentrations and incubated for 24 h. Plates were removed from the incubator and allowed to equilibrate to room temperature for 30 min. 50 μL of freshly prepared CellTiter-Glo (Promega) reagent was added to each well, mixed on an orbital shaker for 10 min and luminescence was recorded on a PerkinElmer Enspire multimode plate reader.

For co-administration chemosensitization studies, MCF7 cells were incubated with the medium containing either 0.5 μM NU-1 or DMSO and irinotecan at indicated concentrations. The plates were incubated for 24 h and collected for CellTiter-Glo assay. For post-administration chemosensitization studies, MCF7 cells were incubated with irinotecan for 4 h, followed by addition of either 0.5 μM NU-1 or DMSO. Then the plates were incubated for another 24 h before CellTiter-Glo assay.

Combination Index analysis

Towards quantitatively measuring the extent of drug interaction, a combination index (CI) was calculated using the following formula:

$$CI = \frac{C_{A,x}}{IC_{x,A}} + \frac{C_{B,x}}{IC_{x,B}}$$

where a CI less than, equal to, and more than 1 indicates synergy, additivity, and antagonism, respectively (42). The cell viability IC_{50} of NU-1 in MCF7 and A549 cells is 21 μM and 35 μM respectively (36).

Clonogenicity assays

MCF7, Saos-2, and CT26 cells were plated at 100 cells per well in 6-well plates in triplicate. For measuring radiosensitivity, cells were treated with TERT inhibitors 1 h prior to irradiation with a GammaCell ^{60}Co γ-ray source (Nordion) with a dose rate of 7.09 cGy/sec. MCF7 and Saos-2 cells were cultured for 3 weeks and CT26 for 2 weeks before crystal violet staining. Colonies of at least 50 cells were counted. The surviving fraction (SF) was calculated using the following formula:

$$SF\ (x\ Gy) = \frac{\text{No. of colonies at x Gy}}{\text{No. of colonies at 0 Gy}}$$

Time-lapse live-cell analysis

Cells were seeded in a six-well plate with 3×10^4 cells per well, treated with DMSO vehicle, chrolactomycin, NU-1, or NU-2 for 1 h and irradiated with 0 or 6 Gy using the ^{60}Co γ-ray source at 7.09 cGy/sec. The plates were then analyzed by time-lapse imaging in an IncuCyteS3 (Sartorius) live-cell imaging system. Phase contrast, green and red channel images were acquired at 20X magnification with scanning every 2 h for 6-7 days. More than 16 non-overlapping fields were captured for each well. Quantitative analysis of cell confluency was performed using IncuCyteS3 2019 software.

SA-βGal senescence assay

Cells were seeded at 3×10^4 per well in six-well plates and treated with inhibitors for 1 h prior to irradiation. 5 or 6 days after irradiation, cells were fixed in 2% PFA and stained for 16 h at 37° C. Staining buffer contains 1 mg/ml X-Gal (X4281C, Golden Bio), 40 mM Citric acid/sodium phosphate, 150 mM NaCl, 2 mM MgCl2, 3.3 mM $K_3[Fe(CN)_6]$, 3.3 mM

$K_4[Fe(CN)_6]$, pH 6. After staining, images were captured on a Zeiss Axiovert 200M microscope with a 20X Plan-NeoFluar objective and Axiocam digital camera. SA-β-Gal-positive and -negative cells were counted in more than 5 fields, yielding an average percentage indicated on each SA-βGal image as mean ± S.D. Two or more replicates were performed.

Apoptosis analysis

MCF7 cells were seeded in a six-well plate with 3×10^4 cells per well, treated with DMSO, chrolactomycin, NU-1 or NU-2, and irradiated with 0 or 6 Gy. 6 days after irradiation, cells were incubated with 1 μM YO-PRO-1 iodide (Thermo Fisher) for 30 min at 37° C and imaged in the IncuCyteS3. Phase contrast and green channel images were acquired at 20X magnification with scanning. 25 non-overlapping fields were captured for each well. Quantitative analysis of cell confluency was performed using IncuCyteS3 2019 software.

Cell cycle analysis

MCF7 cells were seeded at 3×10^4 per well in 6-well plates overnight, and then treated with DMSO, NU-1, BIBR 1532, or MST-312 for 1 h before irradiation with 0 or 6 Gy. 24 h after IR, cells were trypsinized, fixed with 70% cold ethanol and stained with 1 μg/mL DAPI. Cells were analyzed using a BD Fortessa 4-15 HTS Flow cytometer. DAPI signal was measured using a 405-nm laser for excitation and a 450/50 filter for detection. Data were analyzed by FlowJo univariate cell cycle analysis.

Irradiation and DNA damage foci imaging

MCF7 or Saos-2 cells were seeded on cover glass at 2.5×10^4 per well in 24-well plates. Cells were treated with DMSO, NU-2, chrolactomycin, NU-1, BIBR 1532, or MST-312 at the indicated concentration for 1 h and irradiated with 0 or 6 Gy. 24 h after irradiation, cells were fixed with 4% PFA and permeabilized with 0.2% Triton-X 100 for 10 min. After blocking with 5% BSA, primary antibodies for γH2AX (Millipore, 05-636, 1:1000) or 53BP1 (Novus, NB100-304, 1:1000) were then incubated on cell slides overnight at 4°C. Following PBS washes, fluorescent secondary antibodies (Jackson ImmunoResearch) were applied for 1 h at room temperature. Cell slides were mounted with ProLong Gold after PBS washes. Foci images were captured on a Zeiss Axiovert 40CFL with a 40X Plan-NeoFluar objective and pseudo-colored using ImageJ. Two or more replicates were performed.

Telomere PNA and γH2AX double staining

3×10^4 MCF7 cells were grown on sterile coverslips and treated with indicated TERT inhibitors 1 h before irradiation. 24 h after IR, cells were fixed with 2% paraformaldehyde, permeabilized with 0.2% Triton-X100, blocked with 5% BSA, and incubate with anti-γH2AX (Millipore, JBW301) antibodies overnight at 4° C as mentioned above. After application of the secondary antibody (Jackson ImmunoResearch), cells were washed with PBS three times and fixed in 2% paraformaldehyde 15 min at room temperature. Then peptide nucleic acid fluorescence *in situ* hybridization (PNA FISH) with Alexa488-TelG probe (PNA Bio, F1008) was performed according to the manufacturer's protocol. Briefly, cells were incubated with 100 μg/ml RNase A solution and then dehydrated in 70%, 85% and 100% cold ethanol. 0.5 μM PNA probe in 20 μl hybridization buffer (20 mM Tris, pH 7.4, 60% formamide, 0.5% of blocking

reagent (Roche 11096176001)) was heated at 85° C for 5 min. The preheated staining solution was applied to cells at 85 °C for 10 min for denaturation followed by overnight hybridization at room temperature in the dark. Cells were then washed twice in washing solution (2XSSC/0.1% Tween-20) at 55° C for 10 min, incubated with DAPI, and mounted with ProLong Gold Antifade Mountant (Thermo Fisher). Images were taken using a 3i Marianas Spinning Disk Confocal with 100X oil objective.

Neutral comet assay

For neutral comet assays, cells were seeded at 5×10^4 cells per well in six-well plates prior to small molecule treatment and/or irradiation. 24 h after irradiation, single cell suspension (2×10^5 cells/ ml) was mixed with Comet LM agarose and single cell electrophoresis was performed on CometSlides (Trevigen) according to the manufacture's protocol. Slides were fixed, dried, stained with SYBR green (Thermo Fisher Scientific), and imaged on a Zeiss Axiovert 40CFL with a 10× Plan-NeoFluar objective. Two or more replicates were performed. Images were analyzed using an ImageJ comet assay macro (https://www.med.unc.edu/microscopy/resources/imagej-plugins-and-macros/comet-assay/).

Traffic Light Repair Reporter assay

The experiments were performed as described (56). Three constructs for traffic light repair reporter (TLR) system: pCVL SFFV-EF1s HA.NLS.Sce, pCVL Traffic Light Reporter 1.1 (Sce target) Ef1a Puro and pCVL SFFV d14GFP Donor were obtained from Addgene. Lentivirus-containing supernatant was produced by transfection of the 293T Lenti-X cell line with corresponding plasmids and packaged plasmid mix. Then lentivirus-containing supernatant was applied to MCF7 Tet-On (Takara) cell or HEK 293T cell line. MCF7 Tet-On cells or HEK

293T cells were treated with DMSO control, NU-1 (0.5 μM), chrolactomycin (0.5 μM) or BIBR 1532 (10 μM). 3 days later, cells were collected and analyzed using BD Fortessa 4-15 HTS Flow cytometer. eGFP fluorescence was measured using a 488-nm laser for excitation and a 530/30 filter for detection, while mCherry fluorescence was measured by using a 561-nm laser for excitation and a 610/20 filter for detection. Data were analyzed using FloJo software.

In vivo studies of radiation response

BALB/c wildtype and NOD scid gamma (NSG) mice were maintained according to the guidelines of the Institutional Animal Care and Use Committee and radiated using a RadSource RS-2000 X-Ray generator operating at 160 kV and 25 mA with 10 Gy, calibrated by NIST traceable dosimetry. 0.5 million CT26 cells in 100 μL PBS were subcutaneously injected into the flank of 7-9 week BALB/c mice or NSG mice. On day 9 after tumor inoculation (tumors with an average volume of 30 mm^3), the tumor bearing BALB/c mice were randomly divided into 4 groups of 8, while the NSG mice were randomly divided into 2 groups of 5-6. For NU-1 treatment, 10 mg/kg of NU-1 was intraperitoneally injected to mice 2 days before, the day of and 2 days after irradiation. Tumor volume was measured using calipers every 2-3 days from day 7 after tumor inoculation. Considering attrition, no animals that formed tumors after injection with CT26 cells were excluded from any studies reported here. No animals died before the final days shown for each experiment except for those sacrificed due to their tumors reaching a humane endpoint. All animal experiments were performed according to the guidelines established and approved by the IACUC of the University of Chicago.

Histology and immunofluorescence

CT26 tumors were collected 5 days after treatment and fixed in 10% neutral formalin. Formaldehyde-fixed paraffin-embedded (FFPE) tumors were sectioned and stained with hematoxylin and eosin (H&E) by the Human Tissue Resource Center. The immunohistochemistry on the tumor section was done as previously described (87). Simply, the tumor section was deparaffinized with xylene, rehydrated, and immersed in 10 mM sodium citrate buffer (pH 6.0) for 30 min at 90° C for antigen retrieval. After that, the tumor section was blocked in 5% BSA, stained with anti-Ki67, anti-γH2AX, anti-CD45, anti-CD11c, anti-CD8, anti-granzyme B and/or anti-perforin primary antibodies at 4° C overnight. Followed by washing, tumor sections were stained with fluorophore-conjugated secondary antibodies (Vector Labs) and DAPI. The H&E stained tissue sections were scanned using an Olympus VS200 SlideView Whole Slide Scanner. The fluorescent tumor sections were imaged using a 3i Marianas Spinning Disk Confocal with a 20X objective. The detailed primary antibody information is provided in Supplementary Table 1.

In vitro immune cell assays

Bone marrow dendritic cells (BMDCs) were differentiated as previously described (88). Briefly, bone marrow was isolated from 7-8 week BALB/c mice, maintained in immune cell culture medium supplemented with 1 ng/mL mouse recombinant GM-CSF (PeproTech) and 200 ng/mL mouse recombinant Flt-3 ligand (PeproTech) for 14 days to form immature BMDCs. CT26 cells were treated for 5 days with DMSO, NU-1 (1 μM), or MST-312 (1 μM) alone or combined with 10 Gy irradiation. Then CT26 cells were washed twice with PBS and maintained in immune cell culture medium overnight, and then cocultured with BMDCs for 12-16 h in a 2:1

ratio. After coculture, suspension BMDCs were collected and stained with Zombie yellow (BioLegend) for 10 min at room temperature, followed by staining with CD11c, CD103, CD86, CD80, H-2K^d antibodies for 45 min at 4° C. Cells were analyzed using a BD Fortessa 4-15 HTS Flow cytometer and FlowJo software.

To prepare CT26 immunized mice, 7-9 week BALB/c mice were injected subcutaneously twice at 10 day intervals with 0.5 x 10^6 irradiated (20 Gy) CT26 cells. Splenocytes were isolated from immunized mice and stained with 0.5 μM carboxyfluorescein succinimidyl ester (CFSE) for 10 min at room temperature (89). After washing, CFSE labeled splenocytes were co-cultured for 5 days in a 20:1 ratio with BMDCs pre-stimulated with CT26 cells as described above. After coculturing, cells were collected and incubated with Zombie yellow for 10 min at room temperature, followed by staining with CD4 and CD8 antibodies for 30 min at 4° C. Cells were analyzed using a BD Fortessa 4-15 HTS Flow cytometer and FlowJo software. Detailed antibody information is provided in Table 3.

Statistical analysis

Statistical significance was determined using the non-paired Student's *t*-test. Calculations were performed using Prism software (GraphPad) or Excel. $P \leq 0.05$ was considered statistically significant. Power analysis for animal experiments was performed using G*Power software, power $(1-\beta) > 0.85$ for all animal experiments.

Data availability

Data supporting the findings of this study are available within the article and from the corresponding author upon reasonable request. The RNA sequencing data are available on

Sequence Read Archive (SRA): PRJNA663346.

Table 3.1 Combination index (CI)* values of combination treatment

Compounds	MCF7	A549	Saos-2
Irinotecan + NU-1	0.29	0.33	ND
Doxorubicin + NU-1	0.45	0.36	ND
Etoposide + NU-1	0.16	0.22	ND
Paclitaxel + NU-1	0.41	0.66	ND

*CI<1, synergistic; CI=1, additive; CI>1, antagonistic.

Table 3.2 Surviving fraction at 2 Gy (SF_2)

MCF7 cells			
Treatment	Mean SF_2	s.d.	P value (compared to DMSO)
DMSO	0.369	0.038	N/A
NU-1	0.116	0.045	0.0018
BIBR 1532	0.256	0.030	0.0153
MST-312	0.245	0.035	0.0138
Saos-2 cells			
Treatment	Mean SF_2	s.d.	P value (compared to DMSO)
DMSO	0.576	0.024	N/A
NU-1	0.583	0.057	0.44
BIBR 1532	0.580	0.036	0.44
CT26 cells			
Treatment	Mean SF_2	s.d.	P value (compared to DMSO)
DMSO	0.721	0.045	N/A
NU-1	0.322	0.044	0.0004
BIBR 1532	0.727	0.020	0.44
MST-312	0.407	0.071	0.0032

Table 3.3 List of antibodies/probes

Antibody/Probe	Company	Catalog #	Application	Dilution
γ-H2AX, clone JBW301	EMD Millipore	05-636	ICC/FISH	1:1000
53BP1	Novus	NB100-304	ICC	1:1000
Alexa488-TelG probe	PNA Bio	F1008	FISH	1:20
Brilliant Violet 421™ anti-mouse CD11c Antibody	BioLegend	117329	FC	1:200
Brilliant Violet 711™ anti-mouse CD103 Antibody	BioLegend	121435	FC	1:200
APC anti-mouse CD80 Antibody	BioLegend	104713	FC	1:200
PE/Cyanine7 anti-mouse CD86 Antibody	BioLegend	105013	FC	1:200
Alexa Fluor® 488 anti-mouse H-2Kd Antibody	BioLegend	116609	FC	1:200
Purified Rat Anti-Mouse CD45	BD Biosciences	550539	IHC	1:750
CD11c (D1V9Y) Rabbit mAb	Cell Signaling Technology	97585	IHC	1:500
Granzyme B (E5V2L) Rabbit mAb (Mouse Specific)	Cell Signaling Technology	44153	IHC	1:500
CD8a Monoclonal Antibody (4SM15)	eBioscience	14-0808-82	IHC	1:500
Perforin Antibody (Mouse Specific)	Cell Signaling Technology	3693	IHC	1:500

ICC, Immunocytochemistry; FISH, Fluorescence In Situ Hybridization; FC, Flow Cytometry; IHC, Immunohistochemistry

3.5 References

1. Shay JW, and Wright WE. Telomeres and telomerase: three decades of progress. *Nat Rev Genet.* 2019;20(5):299-309.

2. Roake CM, and Artandi SE. Regulation of human telomerase in homeostasis and disease. *Nat Rev Mol Cell Biol.* 2020;21(7):384-97.

3. de Lange T. Shelterin-Mediated Telomere Protection. *Annu Rev Genet.* 2018;52:223-47.

4. Greider CW, and Blackburn EH. Identification of a specific telomere terminal transferase activity in Tetrahymena extracts. *Cell.* 1985;43(2 Pt 1):405-13.

5. Herranz N, and Gil J. Mechanisms and functions of cellular senescence. *J Clin Invest.* 2018;128(4):1238-46.

6. Begus-Nahrmann Y, Hartmann D, Kraus J, Eshraghi P, Scheffold A, Grieb M, et al. Transient telomere dysfunction induces chromosomal instability and promotes carcinogenesis. *J Clin Invest.* 2012;122(6):2283-8.

7. Guterres AN, and Villanueva J. Targeting telomerase for cancer therapy. *Oncogene.* 2020;39(36):5811-24.

8. Chen X, Tang WJ, Shi JB, Liu MM, and Liu XH. Therapeutic strategies for targeting telomerase in cancer. *Med Res Rev.* 2020;40(2):532-85.

9. Bajaj S, Kumar MS, Peters GJ, and Mayur YC. Targeting telomerase for its advent in cancer therapeutics. *Med Res Rev.* 2020;40(5):1871-919.

10. Herbert BS, Gellert GC, Hochreiter A, Pongracz K, Wright WE, Zielinska D, et al. Lipid modification of GRN163, an N3'-->P5' thio-phosphoramidate oligonucleotide, enhances the potency of telomerase inhibition. *Oncogene.* 2005;24(33):5262-8.

11. Wheelhouse RT, Sun D, Han H, Han FX, and Hurley LH. Cationic porphyrins as telomerase inhibitors: the interaction of tetra-(N-methyl-4-pyridyl) porphine with quadruplex DNA. *Journal of the American Chemical Society.* 1998;120(13):3261-2.

12. Pascolo E, Wenz C, Lingner J, Hauel N, Priepke H, Kauffmann I, et al. Mechanism of human telomerase inhibition by BIBR1532, a synthetic, non-nucleosidic drug candidate. *J Biol Chem.* 2002;277(18):15566-72.

13. Ganesan K, and Xu B. Telomerase Inhibitors from Natural Products and Their Anticancer Potential. *Int J Mol Sci.* 2017;19(1).

14. Seimiya H, Oh-hara T, Suzuki T, Naasani I, Shimazaki T, Tsuchiya K, et al. Telomere shortening and growth inhibition of human cancer cells by novel synthetic telomerase inhibitors MST-312, MST-295, and MST-1991. *Mol Cancer Ther.* 2002;1(9):657-65.

15. Shay JW. Role of telomeres and telomerase in aging and cancer. *Cancer discovery.* 2016;6(6):584-93.

16. Kim MM, Rivera MA, Botchkina IL, Shalaby R, Thor AD, and Blackburn EH. A low threshold level of expression of mutant-template telomerase RNA inhibits human tumor cell proliferation. *Proc Natl Acad Sci U S A.* 2001;98(14):7982-7.

17. Mender I, Gryaznov S, Dikmen ZG, Wright WE, and Shay JW. Induction of telomere dysfunction mediated by the telomerase substrate precursor 6-thio-2'-deoxyguanosine. *Cancer Discov.* 2015;5(1):82-95.

18. Sanford SL, Welfer GA, Freudenthal BD, and Opresko PL. Mechanisms of telomerase inhibition by oxidized and therapeutic dNTPs. *Nat Commun.* 2020;11(1):5288.

19. Lamy E, Goetz V, Erlacher M, Herz C, and Mersch-Sundermann V. hTERT: another brick in the wall of cancer cells. *Mutat Res.* 2013;752(2):119-28.

20. Low KC, and Tergaonkar V. Telomerase: central regulator of all of the hallmarks of cancer. *Trends in biochemical sciences.* 2013;38(9):426-34.

21. Arndt GM, and MacKenzie KL. New prospects for targeting telomerase beyond the telomere. *Nat Rev Cancer.* 2016;16(8):508-24.

22. Ségal-Bendirdjian E, and Geli V. Non-canonical Roles of Telomerase: Unraveling the Imbroglio. *Front Cell Dev Biol.* 2019;7:332.

23. Thompson CAH, and Wong JMY. Non-canonical Functions of Telomerase Reverse Transcriptase: Emerging Roles and Biological Relevance. *Curr Top Med Chem.* 2020;20(6):498-507.

24. Kondo Y, Kondo S, Tanaka Y, Haqqi T, Barna BP, and Cowell JK. Inhibition of telomerase increases the susceptibility of human malignant glioblastoma cells to cisplatin-induced apoptosis. *Oncogene.* 1998;16(17):2243-8.

25. Lu C, Fu W, and Mattson MP. Telomerase protects developing neurons against DNA damage-induced cell death. *Brain Res Dev Brain Res.* 2001;131(1-2):167-71.

26. Akiyama M, Yamada O, Kanda N, Akita S, Kawano T, Ohno T, et al. Telomerase overexpression in K562 leukemia cells protects against apoptosis by serum deprivation and double-stranded DNA break inducing agents, but not against DNA synthesis inhibitors. *Cancer Lett.* 2002;178(2):187-97.

27. Berardinelli F, Coluzzi E, Sgura A, and Antoccia A. Targeting telomerase and telomeres to enhance ionizing radiation effects in in vitro and in vivo cancer models. *Mutat Res Rev Mutat Res.* 2017;773:204-19.

28. Sharma GG, Gupta A, Wang H, Scherthan H, Dhar S, Gandhi V, et al. hTERT associates with human telomeres and enhances genomic stability and DNA repair. *Oncogene.* 2003;22(1):131-46.

29. Shin KH, Kang MK, Dicterow E, Kameta A, Baluda MA, and Park NH. Introduction of human telomerase reverse transcriptase to normal human fibroblasts enhances DNA repair capacity. *Clin Cancer Res.* 2004;10(7):2551-60.

30. Masutomi K, Possemato R, Wong JM, Currier JL, Tothova Z, Manola JB, et al. The telomerase reverse transcriptase regulates chromatin state and DNA damage responses. *Proc Natl Acad Sci U S A.* 2005;102(23):8222-7.

31. Oikawa S, and Kawanishi S. Site-specific DNA damage at GGG sequence by oxidative stress may accelerate telomere shortening. *FEBS Lett.* 1999;453(3):365-8.

32. von Zglinicki T, Pilger R, and Sitte N. Accumulation of single-strand breaks is the major cause of telomere shortening in human fibroblasts. *Free Radic Biol Med.* 2000;28(1):64-74.

33. Wong KK, Chang S, Weiler SR, Ganesan S, Chaudhuri J, Zhu C, et al. Telomere dysfunction impairs DNA repair and enhances sensitivity to ionizing radiation. *Nat Genet.* 2000;26(1):85-8.

34. Goytisolo FA, Samper E, Martín-Caballero J, Finnon P, Herrera E, Flores JM, et al. Short telomeres result in organismal hypersensitivity to ionizing radiation in mammals. *J Exp Med.* 2000;192(11):1625-36.

35. Nakai R, Ishida H, Asai A, Ogawa H, Yamamoto Y, Kawasaki H, et al. Telomerase inhibitors identified by a forward chemical genetics approach using a yeast strain with shortened telomere length. *Chem Biol.* 2006;13(2):183-90.

36. Betori RC, Liu Y, Mishra RK, Cohen SB, Kron SJ, and Scheidt KA. Targeted Covalent Inhibition of Telomerase. *ACS Chem Biol.* 2020;15(3):706-17.

37. Singh J, Petter RC, Baillie TA, and Whitty A. The resurgence of covalent drugs. *Nat Rev Drug Discov.* 2011;10(4):307-17.

38. Sutanto F, Konstantinidou M, and Dömling A. Covalent inhibitors: a rational approach to drug discovery. *RSC Med Chem.* 2020;11(8):876-84.

39. De Vita E. 10 years into the resurgence of covalent drugs. *Future Med Chem.* 2021;13(2):193-210.

40. Bryan TM, Englezou A, Dalla-Pozza L, Dunham MA, and Reddel RR. Evidence for an alternative mechanism for maintaining telomere length in human tumors and tumor-derived cell lines. *Nat Med.* 1997;3(11):1271-4.

41. Li S, Crothers J, Haqq CM, and Blackburn EH. Cellular and gene expression responses involved in the rapid growth inhibition of human cancer cells by RNA interference-mediated depletion of telomerase RNA. *J Biol Chem.* 2005;280(25):23709-17.

42. Zhao L, Au JL, and Wientjes MG. Comparison of methods for evaluating drug-drug interaction. *Front Biosci (Elite Ed).* 2010;2:241-9.

43. Wang Y, Sun C, Mao A, Zhang X, Zhou X, Wang Z, et al. Radiosensitization to X-ray radiation by telomerase inhibitor MST-312 in human hepatoma HepG2 cells. *Life Sci.* 2015;123:43-50.

44. Ding X, Cheng J, Pang Q, Wei X, Zhang X, Wang P, et al. BIBR1532, a Selective Telomerase Inhibitor, Enhances Radiosensitivity of Non-Small Cell Lung Cancer Through Increasing Telomere Dysfunction and ATM/CHK1 Inhibition. *Int J Radiat Oncol Biol Phys.* 2019;105(4):861-74.

45. Sakaue-Sawano A, Kurokawa H, Morimura T, Hanyu A, Hama H, Osawa H, et al. Visualizing spatiotemporal dynamics of multicellular cell-cycle progression. *Cell.* 2008;132(3):487-98.

46. Sutherland RL, Hall RE, and Taylor IW. Cell proliferation kinetics of MCF-7 human mammary carcinoma cells in culture and effects of tamoxifen on exponentially growing and plateau-phase cells. *Cancer Res.* 1983;43(9):3998-4006.

47. Liu Y, Efimova EV, Ramamurthy A, and Kron SJ. Repair-independent functions of DNA-PKcs protect irradiated cells from mitotic slippage and accelerated senescence. *J Cell Sci.* 2019;132(13).

48. Olive PL, and Banáth JP. The comet assay: a method to measure DNA damage in individual cells. *Nat Protoc.* 2006;1(1):23-9.

49. Hustedt N, and Durocher D. The control of DNA repair by the cell cycle. *Nat Cell Biol.* 2016;19(1):1-9.

50. Chang HHY, Pannunzio NR, Adachi N, and Lieber MR. Non-homologous DNA end joining and alternative pathways to double-strand break repair. *Nat Rev Mol Cell Biol.* 2017;18(8):495-506.

51. Pannunzio NR, Watanabe G, and Lieber MR. Nonhomologous DNA end-joining for repair of DNA double-strand breaks. *J Biol Chem.* 2018;293(27):10512-23.

52. Scully R, Panday A, Elango R, and Willis NA. DNA double-strand break repair-pathway choice in somatic mammalian cells. *Nature reviews Molecular cell biology.* 2019;20(11):698-714.

53. Mao Z, Bozzella M, Seluanov A, and Gorbunova V. DNA repair by nonhomologous end joining and homologous recombination during cell cycle in human cells. *Cell Cycle.* 2008;7(18):2902-6.

54. Beucher A, Birraux J, Tchouandong L, Barton O, Shibata A, Conrad S, et al. ATM and Artemis promote homologous recombination of radiation-induced DNA double-strand breaks in G2. *Embo j.* 2009;28(21):3413-27.

55. Arnoult N, Correia A, Ma J, Merlo A, Garcia-Gomez S, Maric M, et al. Regulation of DNA repair pathway choice in S and G2 phases by the NHEJ inhibitor CYREN. *Nature.* 2017;549(7673):548-52.

56. Certo MT, Ryu BY, Annis JE, Garibov M, Jarjour J, Rawlings DJ, et al. Tracking genome engineering outcome at individual DNA breakpoints. *Nature methods.* 2011;8(8):671-6.

57. Akıncılar SC, Low KC, Liu CY, Yan TD, Oji A, Ikawa M, et al. Quantitative assessment of telomerase components in cancer cell lines. *FEBS letters.* 2015;589(9):974-84.

58. Sánchez-Paulete A, Teijeira A, Cueto FJ, Garasa S, Pérez-Gracia JL, Sánchez-Arráez A, et al. Antigen cross-presentation and T-cell cross-priming in cancer immunology and immunotherapy. *Annals of Oncology.* 2017;28:xii44-xii55.

59. Uhlén M, Fagerberg L, Hallström BM, Lindskog C, Oksvold P, Mardinoglu A, et al. Proteomics. Tissue-based map of the human proteome. *Science.* 2015;347(6220):1260419.

60. Wang K, Wang RL, Liu JJ, Zhou J, Li X, Hu WW, et al. The prognostic significance of hTERT overexpression in cancers: A systematic review and meta-analysis. *Medicine (Baltimore).* 2018;97(35):e11794.

61. Mascarenhas J, Komrokji RS, Palandri F, Martino B, Niederwieser D, Reiter A, et al. Randomized, Single-Blind, Multicenter Phase II Study of Two Doses of Imetelstat in Relapsed or Refractory Myelofibrosis. *J Clin Oncol.* 2021;39(26):2881-92.

62. Steensma DP, Fenaux P, Van Eygen K, Raza A, Santini V, Germing U, et al. Imetelstat Achieves Meaningful and Durable Transfusion Independence in High Transfusion-Burden Patients With Lower-Risk Myelodysplastic Syndromes in a Phase II Study. *J Clin Oncol.* 2021;39(1):48-56.

63. Armanios M, and Greider CW. Treating Myeloproliferation--On Target or Off? *N Engl J Med.* 2015;373(10):965-6.

64. Ahmed S, Passos JF, Birket MJ, Beckmann T, Brings S, Peters H, et al. Telomerase does not counteract telomere shortening but protects mitochondrial function under oxidative stress. *Journal of cell science.* 2008;121(7):1046-53.

65. Singhapol C, Pal D, Czapiewski R, Porika M, Nelson G, and Saretzki GC. Mitochondrial telomerase protects cancer cells from nuclear DNA damage and apoptosis. *PLoS One.* 2013;8(1):e52989.

66. Reyes-Uribe P, Adrianzen-Ruesta MP, Deng Z, Echevarria-Vargas I, Mender I, Saheb S, et al. Exploiting TERT dependency as a therapeutic strategy for NRAS-mutant melanoma. *Oncogene.* 2018;37(30):4058-72.

67. Pirzio LM, Freulet-Marrière MA, Bai Y, Fouladi B, Murnane JP, Sabatier L, et al. Human fibroblasts expressing hTERT show remarkable karyotype stability even after exposure to ionizing radiation. *Cytogenet Genome Res.* 2004;104(1-4):87-94.

68. Lechner MG, Karimi SS, Barry-Holson K, Angell TE, Murphy KA, Church CH, et al. Immunogenicity of murine solid tumor models as a defining feature of in vivo behavior and response to immunotherapy. *J Immunother.* 2013;36(9):477-89.

69. Meng Y, Efimova EV, Hamzeh KW, Darga TE, Mauceri HJ, Fu YX, et al. Radiation-inducible immunotherapy for cancer: senescent tumor cells as a cancer vaccine. *Mol Ther.* 2012;20(5):1046-55.

70. Wennerberg E, Lhuillier C, Vanpouille-Box C, Pilones KA, García-Martínez E, Rudqvist NP, et al. Barriers to Radiation-Induced In Situ Tumor Vaccination. *Front Immunol.* 2017;8:229.

71. Maida Y, and Masutomi K. Telomerase reverse transcriptase moonlights: Therapeutic targets beyond telomerase. *Cancer Sci.* 2015;106(11):1486-92.

72. Perera ON, Sobinoff AP, Teber ET, Harman A, Maritz MF, Yang SF, et al. Telomerase promotes formation of a telomere protective complex in cancer cells. *Sci Adv.* 2019;5(10):eaav4409.

73. Jin Y, You L, Kim HJ, and Lee H-W. Telomerase reverse transcriptase contains a BH3-like motif and interacts with BCL-2 family members. *Molecules and cells.* 2018;41(7):684.

74. Ghosh A, Saginc G, Leow SC, Khattar E, Shin EM, Yan TD, et al. Telomerase directly regulates NF-kappaB-dependent transcription. *Nat Cell Biol.* 2012;14(12):1270-81.

75. Koh CM, Khattar E, Leow SC, Liu CY, Muller J, Ang WX, et al. Telomerase regulates MYC-driven oncogenesis independent of its reverse transcriptase activity. *J Clin Invest.* 2015;125(5):2109-22.

76. Liu N, Ding D, Hao W, Yang F, Wu X, Wang M, et al. hTERT promotes tumor angiogenesis by activating VEGF via interactions with the Sp1 transcription factor. *Nucleic Acids Res.* 2016;44(18):8693-703.

77. Khattar E, Kumar P, Liu CY, Akıncılar SC, Raju A, Lakshmanan M, et al. Telomerase reverse transcriptase promotes cancer cell proliferation by augmenting tRNA expression. *J Clin Invest.* 2016;126(10):4045-60.

78. Chabanon RM, Rouanne M, Lord CJ, Soria JC, Pasero P, and Postel-Vinay S. Targeting the DNA damage response in immuno-oncology: developments and opportunities. *Nat Rev Cancer.* 2021;21(11):701-17.

79. Chen YA, Shen YL, Hsia HY, Tiang YP, Sung TL, and Chen LY. Extrachromosomal telomere repeat DNA is linked to ALT development via cGAS-STING DNA sensing pathway. *Nat Struct Mol Biol.* 2017;24(12):1124-31.

80. Li X, Li X, Xie C, Cai S, Li M, Jin H, et al. cGAS guards against chromosome end-to-end fusions during mitosis and facilitates replicative senescence. *Protein Cell.* 2021.

81. Mender I, Zhang A, Ren Z, Han C, Deng Y, Siteni S, et al. Telomere Stress Potentiates STING-Dependent Anti-tumor Immunity. *Cancer Cell.* 2020;38(3):400-11.e6.

82. Li T, and Chen ZJ. The cGAS-cGAMP-STING pathway connects DNA damage to inflammation, senescence, and cancer. *J Exp Med.* 2018;215(5):1287-99.

83. Rad AN, Pollara G, Sohaib SA, Chiang C, Chain BM, and Katz DR. The differential influence of allogeneic tumor cell death via DNA damage on dendritic cell maturation and antigen presentation. *Cancer research.* 2003;63(16):5143-50.

84. Fabregat A, Jupe S, Matthews L, Sidiropoulos K, Gillespie M, Garapati P, et al. The Reactome Pathway Knowledgebase. *Nucleic Acids Res.* 2018;46(D1):D649-D55.

85. Huang da W, Sherman BT, and Lempicki RA. Systematic and integrative analysis of large gene lists using DAVID bioinformatics resources. *Nat Protoc.* 2009;4(1):44-57.

86. Krämer A, Green J, Pollard Jr J, and Tugendreich S. Causal analysis approaches in ingenuity pathway analysis. *Bioinformatics.* 2014;30(4):523-30.

87. Efimova EV, Ricco N, Labay E, Mauceri HJ, Flor AC, Ramamurthy A, et al. HMG-CoA Reductase Inhibition Delays DNA Repair and Promotes Senescence After Tumor Irradiation. *Mol Cancer Ther.* 2018;17(2):407-18.

88. Mayer CT, Ghorbani P, Nandan A, Dudek M, Arnold-Schrauf C, Hesse C, et al. Selective and efficient generation of functional Batf3-dependent CD103+ dendritic cells from mouse bone marrow. *Blood, The Journal of the American Society of Hematology.* 2014;124(20):3081-91.

89. Quah BJ, Warren HS, and Parish CR. Monitoring lymphocyte proliferation in vitro and in vivo with the intracellular fluorescent dye carboxyfluorescein diacetate succinimidyl ester. *Nature protocols.* 2007;2(9):2049-56.

CHAPTER 4

VACCINATION WITH SENESCENT CANCER CELLS ENHANCES CANCER THERAPIES AND SUPPRESSES METASTASIS

This chapter consists of a draft manuscript:

Y Liu, J Pagacz, S J Kron. Senescent cancer cell vaccine enhances antitumor immunity and potentiates radiation and immunotherapy.

I am responsible for *in vitro* experiments and data analysis. Pagacz and I are both responsible for animal studies and planning to share the first authorship.

4.1 Introduction

The emergence of cancer immunotherapies is changing the clinic land scope previously occupied by radiation and chemotherapies (1). Prominent examples that have reached the clinic include immune checkpoint inhibitors such as PD-L1 inhibitors, engineered immune cells such as Chimeric antigen receptor (CAR) T-cell therapy, and cancer vaccines such as Sipuleucel-T. Cancer immunotherapies rely on activating and/or reactivating anti-tumor immunity, whereas the discovery of immunogenic cell death (ICD) presents an opportunity to improve its effectiveness by boosting tumor-specific immunity (2). Traditional cancer therapies such as radiation and chemotherapies serve as ICD-inducing agents and elicit activation of a danger pathway involving the emission of ICD mediators known as damage-associated molecular patterns (DAMPs), which act as danger signals adjuvant molecules to activate the innate and adaptive immune response. DAMPs constitute a wide range of endogenous molecules exposed to the outer cell membranes or released in the extracellular matrix, including proinflammatory cytokines (Type I IFN) and HMGB1, which play critical roles in ICD mediated immune response (3). The immunogenic potentials of ICDs das led to the development of cancer vaccines that use cell lysates or whole cells taken from cancer cells undergoing ICD or antigen-presenting cells loaded with ICDs, which has elicited robust immune responses and protective immunological memory in mice and patients. Although CD was initially described for cancer cells undergoing apoptosis, it has now been extended to include alternative cell death pathways, such as necroptotic cells (4), dying cells such as feropototic cells (5), and even live tumor cells such as etoposide-damaged cancer cells (6).

Cellular senescence, typically defined as stable cell cycle arrest, plays critical roles in diverse physiological and pathological processes, including aging and cancer (7). Senescence has

been considered a hallmark of cancer and is frequently observed in premalignant tumors and cancers due to oncogene stress and cancer therapy (8, 9). As senescent cells remain metabolically active, they secrete a wide range of bioactive factors, termed the senescence-associated secretory phenotype (SASP), which closely resembles the DAMP composition (10, 11). Like DAMPs are not always immunostimulatory, cellular senescence has been considered a double-edged sword in modulating immune responses (12-14). Though SASP, senescent cells drive increases in immune suppressive myeloid cells and inhibit anti-tumor T-cell and NK cells responses, contributing to tumor development and resistance to therapy (15-18). However, senescent cells are also known to promote the immune surveillance of cancers, which has long been considered a critical mechanism in limiting carcinogenesis. Senescence induced by oncogenic stresses facilitates the recruitment and activation of innate and adaptive immune cells, including monocytes, macrophages, neutrophils, NK cells, and T cells, which contribute to the surveillance of premalignant cells and thus control cancers (19-24). Senescence triggered by serval therapies also was reported to enhance anti-tumor immunity and treatment outcomes. For instance, genotoxic chemotherapy-induced senescence upregulated Gr-1^{+} myeloid cells to inhibit cancer (25); aneuploid senescent cells promoted NK cell-mediated tumor clearance (26); senescence generated by CDK4/6 inhibition led to T cell-dependent anti-tumor immunity (27). Although SASP might be primarily responsible for the senescence-associated immune response, the altered expression of major histocompatibility complex (MHC) molecules and altered antigen presentation in senescent cells also play critical roles (18, 27).

In a previous study, we have reported that senescent mouse cells induced by ionizing radiation (IR) and poly(ADP-ribose) polymerase (PARP) inhibitor veliparib produce immunostimulatory cytokines and activate cytotoxic T cell-mediated anti-tumor immunity

against specific tumor antigens such as SIY and rat Her2 antigen (28). Here, we have confirmed the capability of senescent cells to activate T cell response against a specific endogenous tumor antigen in vivo. The single-cell RNA sequencing (scRNA-seq) analysis on splenocytes cocultured with senescent cells revealed DCs as directly involved in the senescence-associated immune response. Using *in vitro* coculture experiments, we verified that senescent cells could promote DC activation/maturation via STING-dependent mechanisms as well as T-cell priming. The latter process can be further improved with the additional PD-L1 antibody. We examined the potential of using senescent cancer cells as prophylactic and therapeutic vaccines. Immunization of senescent cells in naive immune-competent hosts induced a remarkable rejection of tumor cell challenge. Treatment of senescent cell vaccines repressed tumor growth in tumor-bearing mice, while increased therapy effectiveness was observed when combining senescence vaccine with radiation or immune checkpoint inhibitors. Flow cytometric analysis on tumors validated that senescent cell vaccine significantly increased tumor immune infiltrate. Surprisingly, senescent cell vaccines could also suppress tumor metastasis. Furthermore, we demonstrated that the DCs activated by senescent cancer cells could also repress local tumors, especially when combined with radiotherapy, and limit metastasis. Our studies suggested that senescent tumor cells, or DCs stimulated by senescent cells, may offer significant translational implications in enhancing anti-tumor immunity to benefit the treatment of both local and metastatic cancer.

4.2 Results

Senescent cells induce anti-tumor immunogenicity with the cross-priming CD8+ T cells *in vivo*

As a model for testing the effect of senescent cells on immunity against endogenous tumor antigen, we utilized the mouse colon carcinoma CT26 cell line expressing a known

epitope AH1 (SPSYVYHQF), derived from the envelope glycoprotein 70 (gp70) of murine leukemia retroviral virus (MuLV) (29). As shown in Figure 4.1A, > 95% CT26 cells treated with 12 Gy ionizing radiation (IR) and 20 μM veliparib developed SA-βGal$^+$ senescence phenotype within 5 days. In order to determine the effects of senescent cells in vivo, we injected 0.5 million senescent cells or PBS controls under the back skin of naïve BALB/c mice. 2 days after injection, swelling of draining lymph nodes was observed from mice challenged with senescent cells compared to the controls (Figure 4.1B). Furthermore, these enlarged inguinal lymph nodes also displayed a significantly increased percentage of AH1 specific CD8$^+$ T cells (Figure 4.1C and D), indicating the potential of senescent cells in stimulating the expansion of antigen-specific cytotoxic T lymphocytes (CTLs). Upon the fact that AH1 specific CTLs are effective at eliminating CT26 tumors (29), we reasoned that injection of senescent cells might protect animals against tumorigenesis. To test this, BALB/c mice were injected with senescent cells on Day -5, followed by challenging with proliferating CT26 cells at the same site on Day 0 (Figure 4.1E). Although all the control mice developed tumors, no tumor development was observed on immunized animals (Figure 4.1F). However, senescence treatment lost its protective effects against tumor growth in NOD SCID gamma (NSG) mice (Figure 4.1G). These results indicated that senescent cells as cancer vaccines provide sufficient protection against tumorigenesis in an immune response-dependent manner. To examine whether the anti-tumor immunity induced by senescent cells is antigen-dependent, we challenged BALB/c mice with breast cancer 4T1 cells, which express the same AH1 antigen as CT26, after the senescent CT26 cell vaccination (Figure 4.1H). Senescent CT26 vaccine displayed modest protective effects against 4T1 tumors, resulting in a 25% tumor-free rate and delayed tumor development. A single dose of α-PD-L1 antibody appeared not to affect tumor-taken rate on its own, whereas 75% of mice treated with the

combined senescence vaccine and PD-L1 antibody were free from tumorigenesis (Figure 4.1I). Using these experiments, we demonstrated that senescent cells could trigger cross-protective immunity in response to specific tumor antigens, which could be further elevated by blocking immune checkpoints.

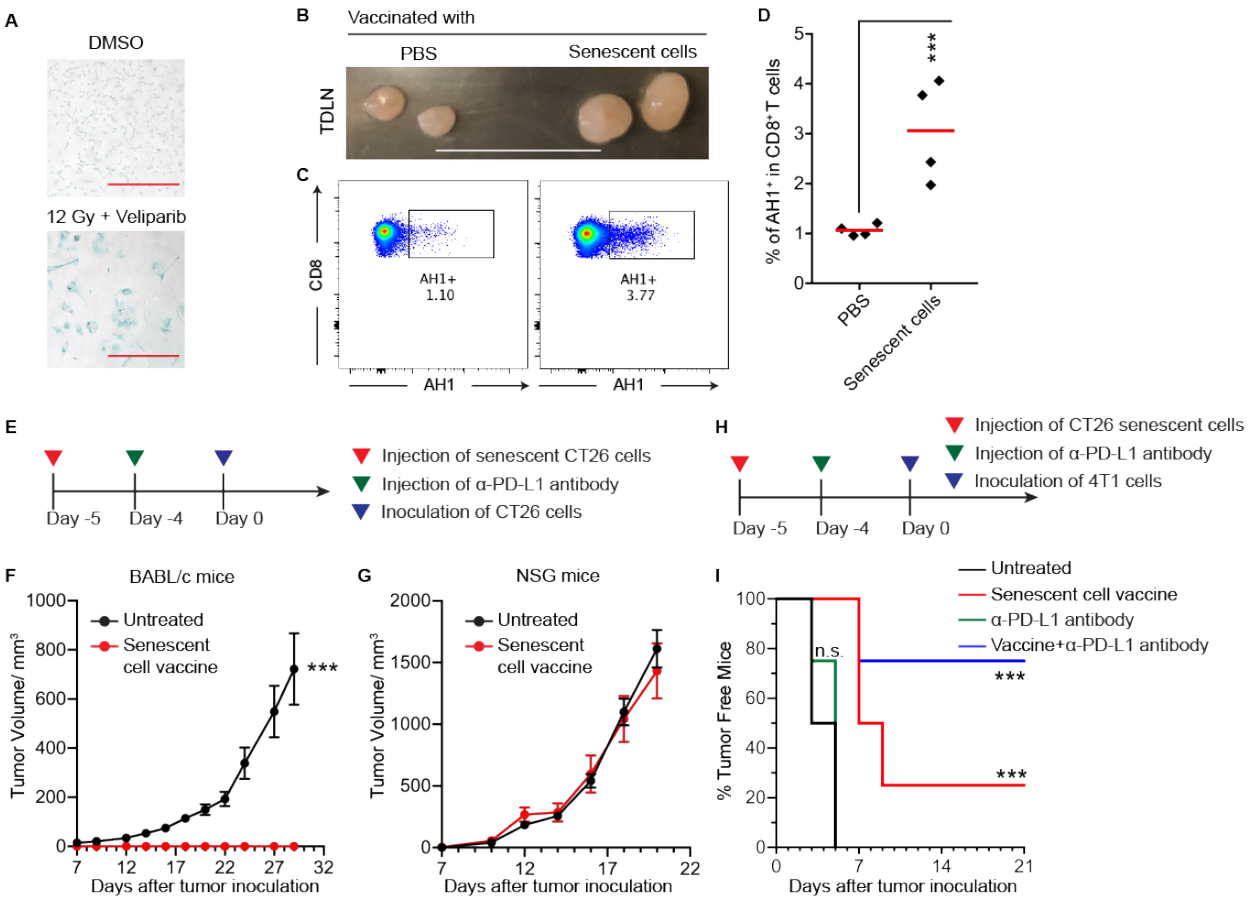

Figure 4.1: Senescent cells induce anti-tumor immunogenicity with cross-priming CD8+ T cells in immune-competent hosts.

A, SA-βGal staining of CT26 cells. CT26 were treated with DMSO control or 12 Gy IR+veliparib (20 μM), then fixed and stained after 5 days. Representative 20X images. Scale bars: 200 μm. B, Representative image of mouse draining lymph nodes after injection of senescent cells. BALB/c mice were subcutaneously injected with 0.5 m senescent CT26 cells or PBS control on their back. 2 days later, the draining inguinal lymph nodes were collected. Scale bars: 1 cm. C, Representative dot plots showing $AH1^+CD8^+$ T cell population in mouse draining lymph node. The lymph nodes were collected as described in B, then dissociated and stained for flow cytometric analysis. $CD8^+$ single cell population was analyzed. D, Quantification of the percentage of AH1+ T cells. Shown are individual mouse (square) and mean (bar). *** $P < 0.001$. E, Experimental schema for senescent cell vaccination and viable CT26 cell challenging in BALB/c or NSG mice. Naïve or vaccinated mice were challenged with 0.25 million CT26 cells on Day 0. F and G, The growth of CT26 tumors in BALB/c (F) or NSG mice (G). The tumor development was measured using a caliper every 2-3 days. n=5, the total number of mice per group. H, Experimental schema for senescent CT26 vaccination and viable 4T1 cell challenging in the presence or absence of α-PD-L1. BALB/c mice were vaccinated with senescent CT26 cells, α-PD-L1 antibody, or the combination treatment. Then the naïve or vaccinated mice were subcutaneously inoculated with 0.5 million 4T1 cells on Day 0. G, Kaplan-Meier curve of 4T1 tumor development over time. The tumor development was monitored every 2-3 days.

Single-cell RNA sequencing reveals that senescent cells mediate immune responses primarily through dendritic cells

To dissect the immune cell response induced by senescent cells, we cocultured splenocytes from CT26 tumor-bearing mice with proliferating or senescent CT26 cells in vitro, then collected the suspension cells for single-cell RNA sequencing (scRNA-seq) (Figure 4.2A). After 3-day coculturing, examination of the cell mixtures revealed 11 cell clusters, including both immune and non-immune cells (Figure 4.2B-E). In order to further investigate the exact type of immune cells affected by senescent cells that could provoke anti-tumor effects, we excluded the population of B cells, tumor cells, endothelial cells, hematopoietic stem cells (HSCs). Analysis of the rest of the immune cells generated 8 cells clusters based on their signature genes (Figure 4.2F and G). Comparing splenocytes cocultured with senescent cell populations to those cocultured with proliferating cell populations, conventional dendritic cells (cDC1) displayed the most differences. Reactome Gene Ontology (GO) term pathway analysis of the differentially expressed genes indicated that coculture with senescent cells induces upregulation of the pathways Defense response, Cytokine response, T cell activation, and Antigen processing (Figure 4.2J). Downregulated GO terms include Protein metabolism and Carbohydrate metabolism (Figure 4.2K). Consistently, a higher T cell population, especially $CD8^+$ T cells, was observed in cocultures of splenocytes with senescent cells than with proliferating cells (Figure 4.2F and G). These results demonstrated the possibility that senescent cells modulate T cell response by activating DCs as a primary target.

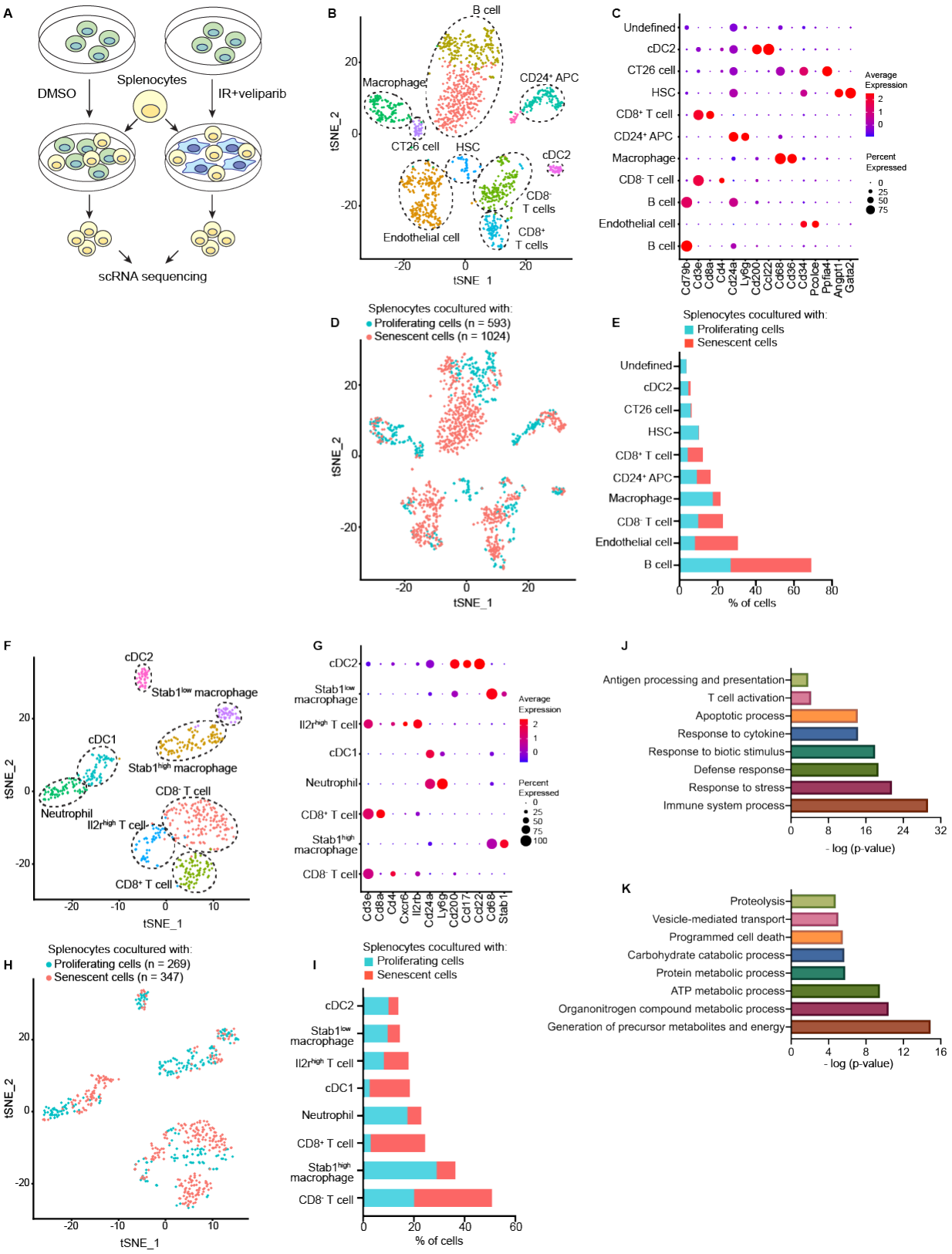

Figure 4.2: Single-cell RNA sequencing (scRNA-seq) reveals that dendritic cells are one of the main targets of senescent cells.

Figure 4.2: Single-cell RNA sequencing (scRNA-seq) reveals that dendritic cells are one of the main targets of senescent cells (continued).
A, Experimental schema for collecting splenocytes for scRNA-seq after coculturing with senescent CT26 cells. Senescence was induced by IR+veliparib (20 μM) as indicated in Figure 5.1A. Splenocytes were isolated from BALB/c mice bearing CT26 tumors and cocultured with senescent or proliferating CT26 cells for 3 days. The suspended cells were then analyzed through scRNA-seq. B-E, Integration analysis on splenocytes cocultured with senescent or proliferating CT26 cells. B, tSNE plot demonstrating 11 cell clusters from 1,618 cells identified by single-cell RNA-seq. C, Dot plot demonstrating the expression of marker genes in each cell cluster. D and E, tSNE (D) and bar graph (E) reveal the composition of cell clusters. APC, antigen-presenting cells. DC, dendritic cell. HSC, a hematopoietic stem cell. F-I, Integration analysis on splenocytes after excluding the clusters of B cells, HSCs, endothelial cells, CT26 cells, and undefined cells. F, tSNE plot demonstrating 8 cell clusters from 616 cells. G, Dot plot demonstrating the expression of marker genes in each cell cluster. H and I, tSNE (H) and bar graph (I) demonstrating the composition of cell clusters. J and K, Reactome Gene Ontology (GO) analysis of differential expressed genes among DCs. Shown are enrichment of upregulated (J) and downregulated signaling pathways (K) in splenocytes cocultured with senescent cells compared to those cocultured with proliferating cells.

Senescent cells phagocytized by bone-marrow derived dendritic cells (BMDCs) promote T cell proliferation *in vitro*

Toward confirming prior studies and the gene expression analysis, we examined the effects of senescent cells on bone marrow-derived dendritic cells (BMDCs). Considering that a broad spectrum of stimuli can induce cancer cell senescence, we also investigated whether different inducers affect the immunogenicity of senescent cells. Therefore, CT26 cells were treated with 12 Gy radiation (IR), IR+veliparib, topoisomerase II poison etoposide, and PLK-1 inhibitor GSK461364, which induced 86%, 95%, 96%, and 94% SA-gal$^+$ senescent cells respectively in 5 days (Figure 4.3A). Cells treated with DMSO or veliparib for 5 days were used as non-senescent controls. To access phagocytosis, the BMDCs were cocultured overnight with senescent cells or control cells labeled with lipophilic membrane dye PHK26 or pH-sensitive fluorescent probe pHrodo Red, followed by staining and flow cytometric analysis (Figure 4.3B). BMDCs appeared to engulf senescent cells more effectively than proliferating cells in general, while inequivalent efficiency was observed in senescent cells induced by different treatments (Figure 4.3C and D). BMDC activation and maturation were further examined by flow cytometric analysis of costimulatory molecules CD86 and CD80, as well as MHC I molecule H-2Kd (Figure 3.5C). Overall, senescent CT26 cells produced a higher surface expression of CD86, CD80, and H-2Kd Class I MHC. Interestingly, senescent cells also upregulated PDL1 expression on BMDCs, whereas IR+veliparib-mediated senescence was shown to produce minimal PDL1 upregulation, which may be limiting for CD8+ T cell stimulation (Figure 4.3E). Senescent 4T1 cells elicited similar activation effects on BMDCs (Figure 4.4).

To examine APC function, we combined BMDCs that had been cocultured with CT26 cells with splenocytes that were obtained from mice immunized with irradiated CT26 cells and

labeled with carboxyfluorescein succinimidyl ester (CFSE). CFSE dilution was examined after 5 days by flow cytometry (Figure 4.3B). BMDCs cocultured with non-senescent CT26 cells, treated with veliparib or not, triggered the proliferation of 20-27% of $CD8^+$ T cells. DCs cocultured with senescent cells induced by IR, IR+veliparib, etoposide, or GSK461364 induced senescent cells yielded 32.1%, 42.9%, 37.5%, and 15% proliferating $CD8^+$ T cells, respectively (Figure 4.5A). Similarly, BMDCs cocultured with senescent CT26 cells, except those induced by GSK461364, also induced more $CD4^+$ T cell proliferation (Figure 4.5C). Considering PD-L1 level on DCs was upregulated after coculturing with senescent cells, we also examined the effects of PD-L1 antibody on T cell proliferation. Overall, T cells incubated in the presence of α-PD-L1 displayed a higher proliferation rate (Figure 4.5B and D). Similar results were observed when using 4T1 cells (Figure 4.6A-D). These patterns confirmed the potential of senescent cells, especially those induced by IR+veliparib, in promoting T cell response and associated anti-tumor effects.

Stimulator of interferon genes (STING), an endoplasmic reticulum-associated membrane protein, has been reported to play critical roles in anti-tumor immunity. STING is activated by cGMP-AMP (cGAMP), produced by cGMP-AMP synthase (cGAS) once it senses cytosolic double-strand DNA. Then the activated STING triggers the production of inflammatory cytokines and other immune mediators through regulating multiple transcriptional factors, including IFR3 and NF- κB (30). The prior studies demonstrated cGAS-STING signaling pathway is essential for cellular senescence (31, 32). Although STING deficiency appeared not to affect oncogene RAS-induced senescence in mice, it led to impaired immunosurveillance of oncogenic RAS, suggesting the importance of STING in the anti-tumor immune response (33). Indeed, STING and IRF3 are required for prime CD8+ T cells in response to tumor antigens

(34). Therefore, we hypothesized that STING in therapy-induced senescent cells might play critical roles in DC activation and associated immune response. To test that, we utilized covalent STING inhibitor C178 (35) at a concentration that does not affect cell growth or senescence development on its own (Figure 4.7A and B). Consistent with a covalent mechanism, washing the treated cells to remove free C178 and then incubating in fresh culture media did not restore STING signals even after 24 h. We cocultured BMDCs with either senescent or non-senescent CT26 cells pretreated with or without C178, then assessed for maturation/activation, and found that senescent CT26 cells with inhibited STING showed diminished ability to activate DCs (Figure 4.7C). Similar results were observed when using the 4T1 cell line (Figure 4.7D-F). These results indicated that STING activation in senescent cells is required for mediating DC activation.

Additionally, we compared senescent cells with apoptotic cells and DNA damage-injured cells in terms of their ability to stimulate DCs. Senescent cells were incubated with Bcl-2 inhibitor ABT263 overnight, resulting in ~78% Annexin V^+/PI^+ apoptotic cells. Damaged cells were CT26 cells treated with IR or IR+veliparib and used for BMDC culture experiment on the following day. After coculturing with senescent, apoptotic, damaged, or proliferating control cells, BMDCs were analyzed through flow cytometry on CD80, CD86, and another MHC I molecule H2-Ld, indicating that senescent cells contributed more to DC maturation/activation than apoptotic or damaged cells.

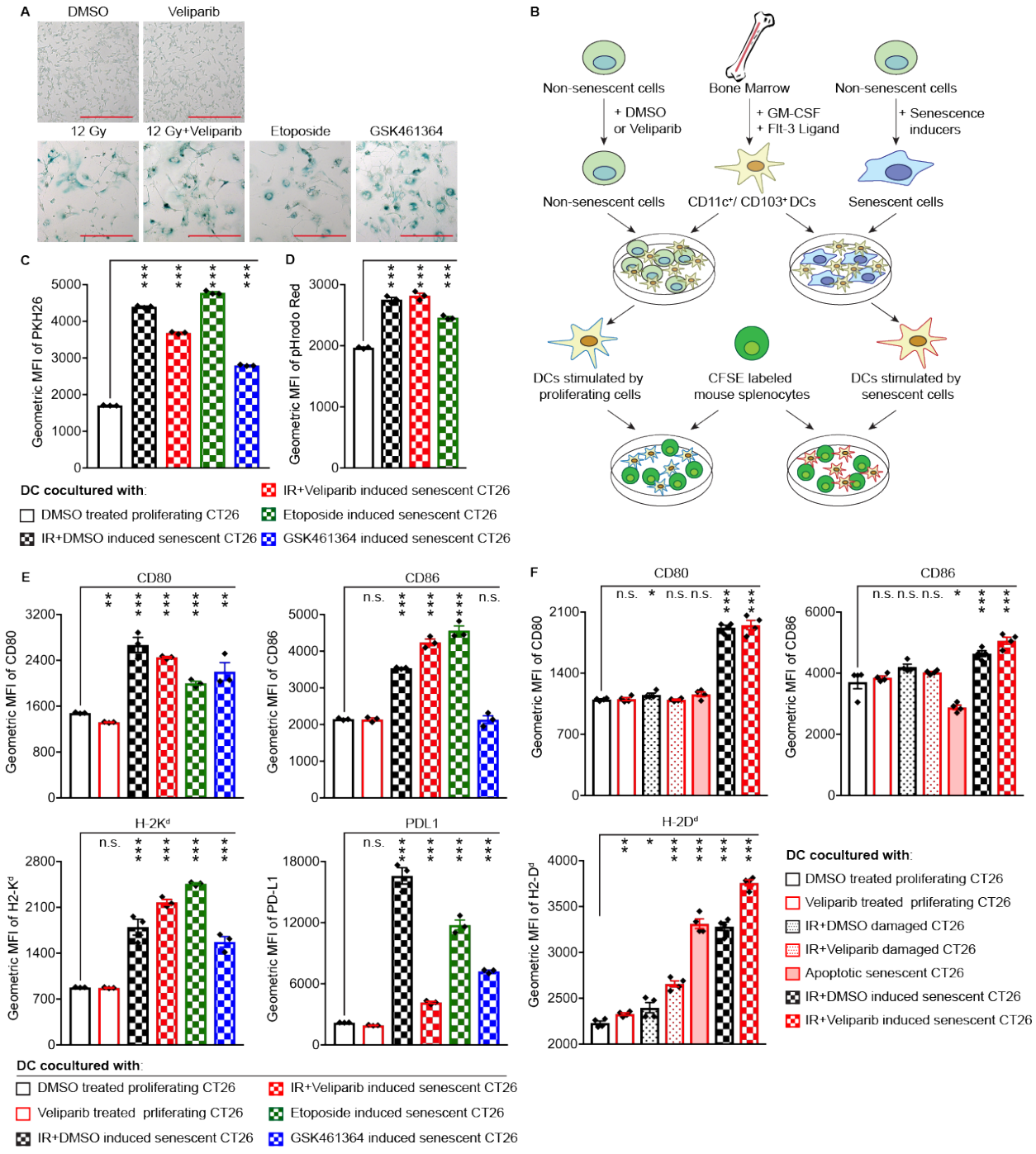

Figure 4.3: Senescent CT26 cells promote DC maturation/activation *in vitro*.
A, SA-βGal staining of CT26 cells. CT26 cells treated with DMSO vehicle or veliparib (20 μM) were used as controls. Cellular senescence was induced by 12 Gy IR, IR+veliparib (20 μM), etoposide (2 μM), or GSK461364 (5 μM). Scale bars: 200 μm. B, Experimental schema for coculture experiments *in vitro*. Proliferating or senescent CT26 cells were prepared as in A. Bone marrow-derived dendritic cells (BMDCs) were cocultured with senescent or proliferating CT26 for 12-14 hours, then used for flow cytometric analysis or T cell-priming assays. C and D, Phagocytosis assays indicating effective uptake of senescent cells by BMDCs.

Figure 4.3: Senescent CT26 cells promote DC maturation/activation *in vitro* (continued). BMDCs were cocultured with PHK26 (C) or pHrodo Red (D) labeled CT26 cells overnight as indicated in B, followed by staining and analysis through flow cytometry. The geometric mean fluorescence intensity (MFI) of PHK26 (C) or pHrodo Red (D) on BMDCs were calculated using FlowJo. Zombie yellow$^-$/CD11c$^+$/CD103$^+$ single cell population was analyzed. Shown from three experiments, mean ± s.d. *** $P < 0.001$. (unpaired t-test). E, Quantitative analysis of DC activation/maturation. BMDCs were cocultured with CT26 cells as in B, then stained and analyzed through flow cytometry. Zombie yellow$^-$/CD11c$^+$/CD103$^+$ DC population were analyzed. Shown from three experiments, mean ± s.d. *** $P < 0.001$, ** $0.001 < P < 0.01$, n.s. $P > 0.05$ (unpaired t-test). MFI, mean fluorescence intensity. F, Comparison of the BMDC stimulation capability between proliferating cells, damaged cells, apoptotic cells, and senescent cells. Proliferating or senescent CT26 cells were prepared as in A. CT26 cells were damaged by 12 Gy IR alone or IR+veliparib (20 μM), and used for coculture experiments 1 day later. Apoptotic senescent cells were prepared by incubating IR+veliparib driven senescent cells with ABT263 (5 μM) overnight. BMDCs were cocultured with tumor cells overnight, followed by staining and flow cytometric analysis. Shown from three experiments, mean ± s.d. *** $P < 0.001$, ** $0.001 < P < 0.01$, n.s. $P > 0.05$ (unpaired t-test). MFI, mean fluorescence intensity.

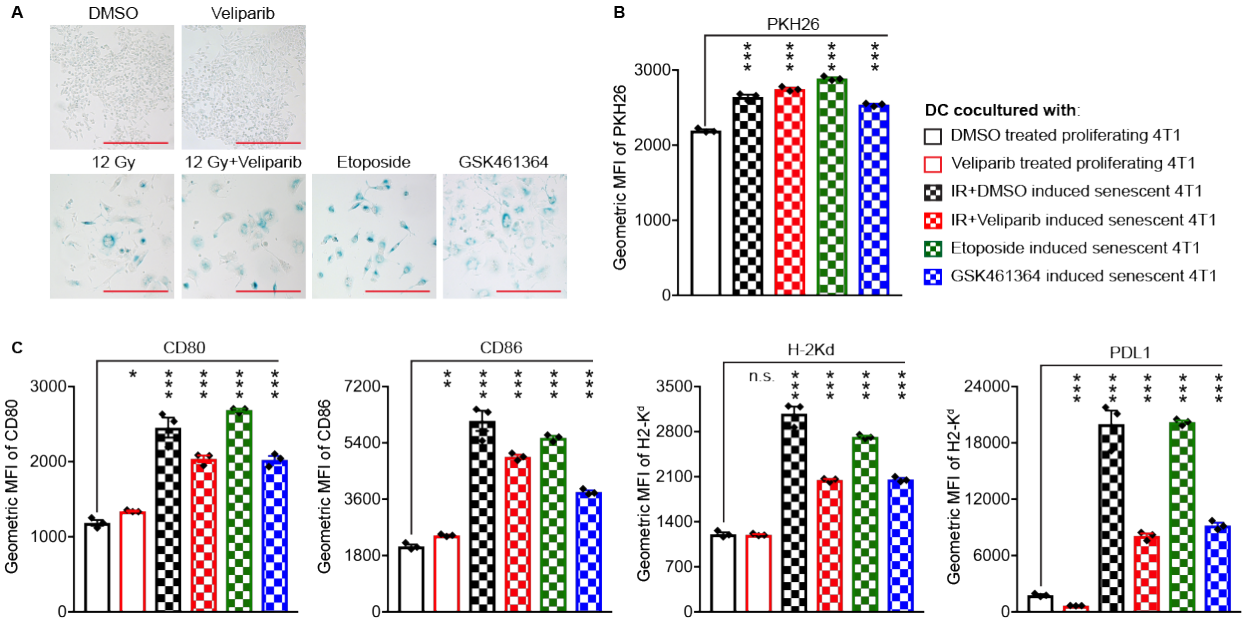

Figure 4.4: Senescent 4T1 cells promote DC maturation/activation *in vitro*. A, SA-βGal staining of 4T1 cells. 4T1 cells treated with DMSO vehicle or veliparib (20 μM) were used as controls. Cellular senescence was induced by 12 Gy IR, IR+veliparib (20 μM), etoposide (2 μM), or GSK461364 (5 μM). Scale bars: 200 μm. B, Quantification of PHK26 intensity on BMDCs demonstrating effective uptake of senescent cells by BMDCs. Proliferating or senescent 4T1 cells were prepared as in A. BMDCs were cocultured with PHK26 labeled 4T1 cells overnight, followed by staining and analysis through flow cytometry. CD11c$^+$ single cell population was analyzed. Shown from three experiments, mean ± s.d. *** $P < 0.001$. (unpaired t-test). E, Quantitative analysis of DC activation/maturation. BMDCs were cocultured with unlabeled 4T1 cells as in B, then stained and analyzed through flow cytometry. Zombie yellow$^-$/CD11c$^+$/CD103$^+$ DC population were analyzed. Shown from three experiments, mean ± s.d. *** $P < 0.001$, ** $0.001 < P < 0.01$, n.s. $P > 0.05$ (unpaired t-test). MFI, mean fluorescence intensity.

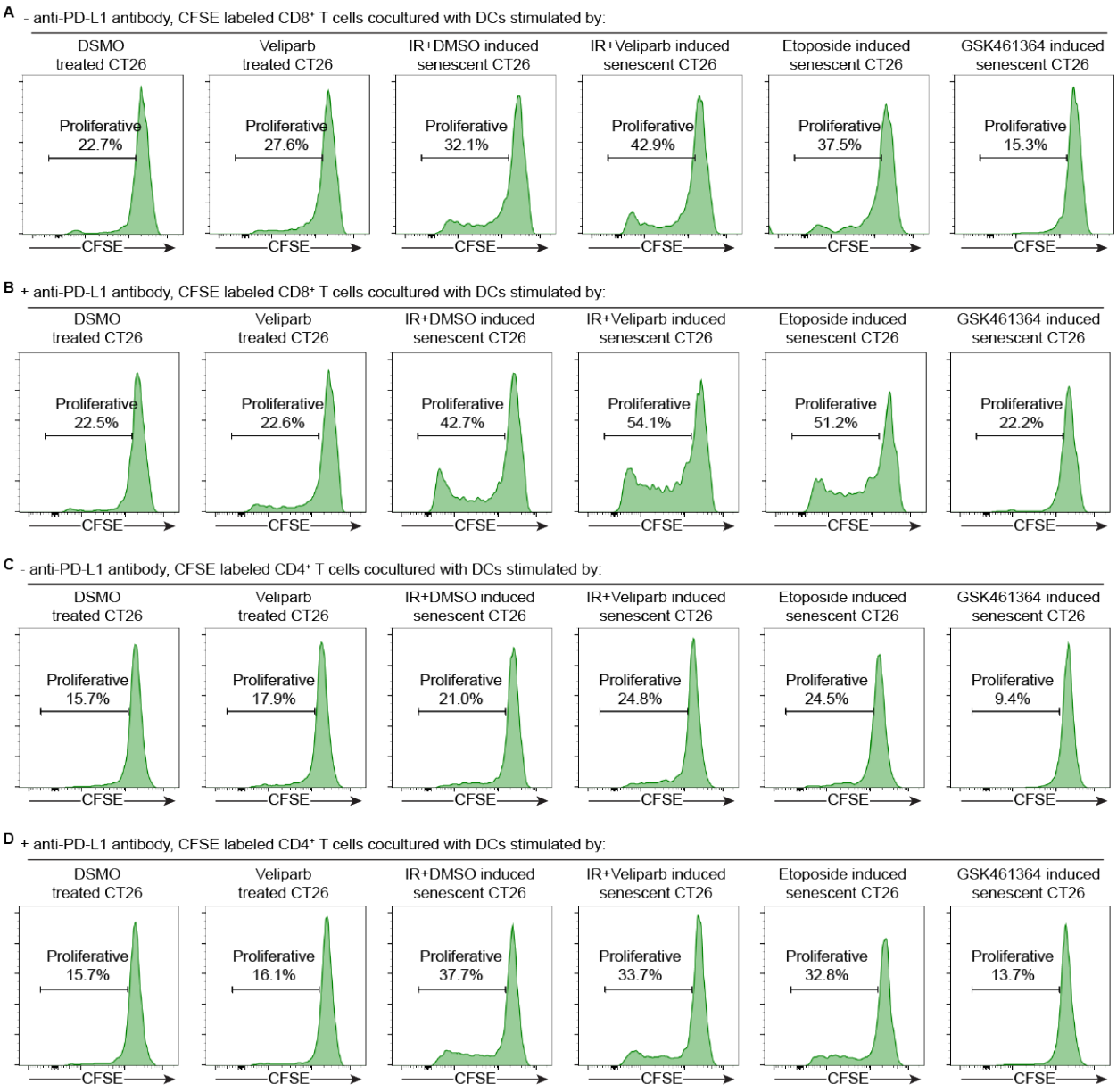

Figure 4.5: Senescent CT26 cells promote the capability of BMDCs in priming T cells. A-D Assays of DCs stimulated by CT26 cells for stimulating the proliferation of $CD8^+$ (A and B) or $CD4^+$ (C and D) T cell. As indicated in Figure 5.3B, carboxyfluorescein succinimidyl ester (CFSE) labeled murine splenocytes were cocultured for 5 days with DCs pre-stimulated by proliferating or senescent CT26 cells in the presence (B and D) or absence (A and C) of α-PD-L1 antibody. The proliferating CT26 cells were treated with DMSO vehicle or veliparib (20 μM) as controls, while senescent cells were induced by IR, IR+veliparib, etoposide, or GSK461364. Shown are Zombie $yellow^-/CD8^+/CD4^-$ T cell population (A and B) and Zombie $yellow^-/CD8^-/CD4^+$ T cell population (C and D).

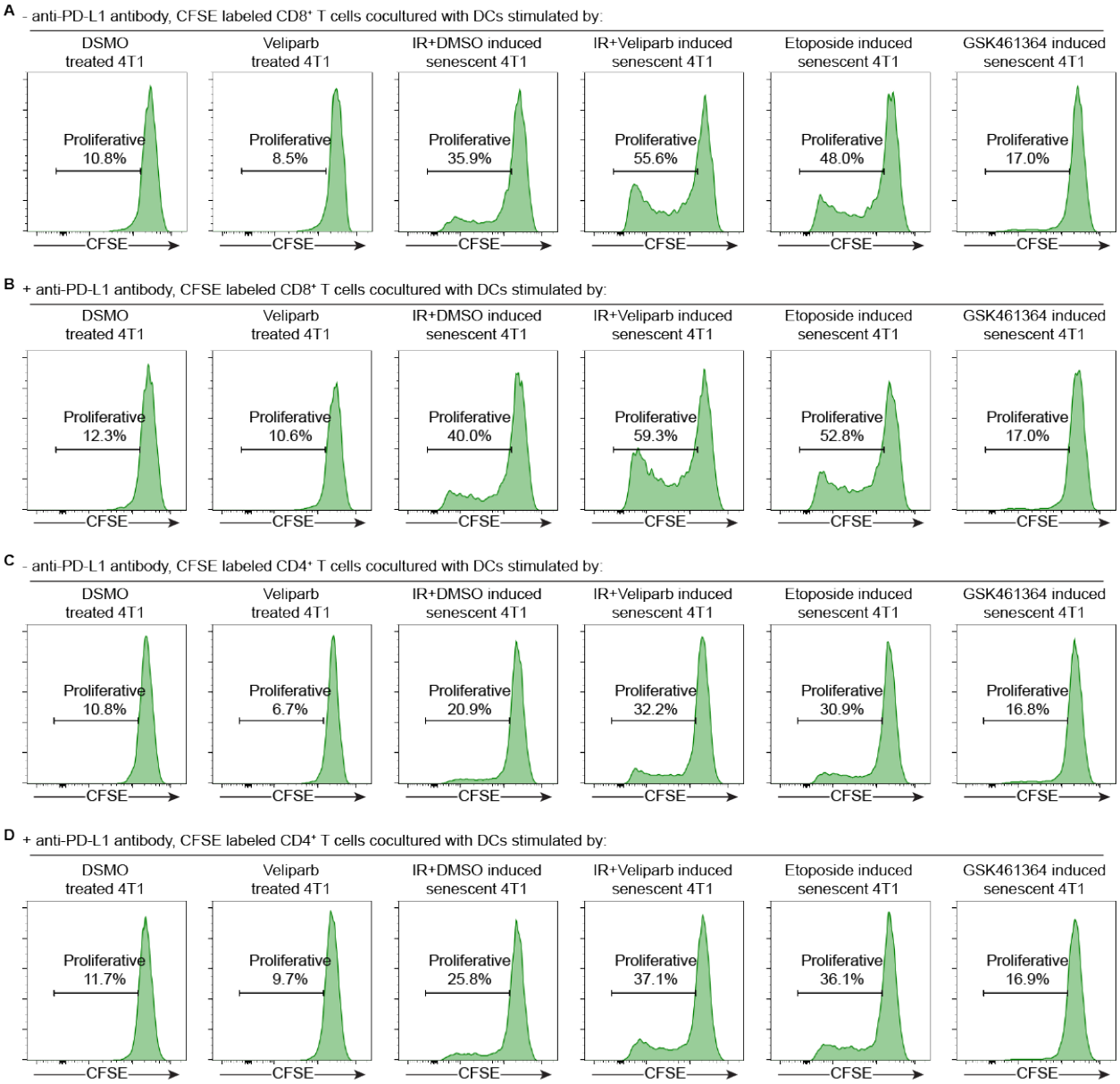

Figure 4.6: Senescent 4T1 cells promote the capability of BMDCs in priming T cells.
A-D Assays of BMDCs stimulated by 4T1 cells for stimulating the proliferation of $CD8^+$ (A and B) or $CD4^+$ (C and D) T cell. As indicated in Figure 5.5, carboxyfluorescein succinimidyl ester (CFSE) labeled murine splenocytes were cocultured for 5 days with DCs pre-stimulated by proliferating or senescent 4T1 cells in the presence (B and D) or absence (A and C) of α-PD-L1 antibody. The proliferating 4T1 cells were treated with DMSO vehicle or veliparib (20 μM) as controls, while senescent cells were induced by IR, IR+veliparib, etoposide, or GSK461364. Shown are Zombie $yellow^-/CD8^+/CD4^-$ T cell population (A and B) and Zombie $yellow^-/CD8^-/CD4^+$ T cell population (C and D).

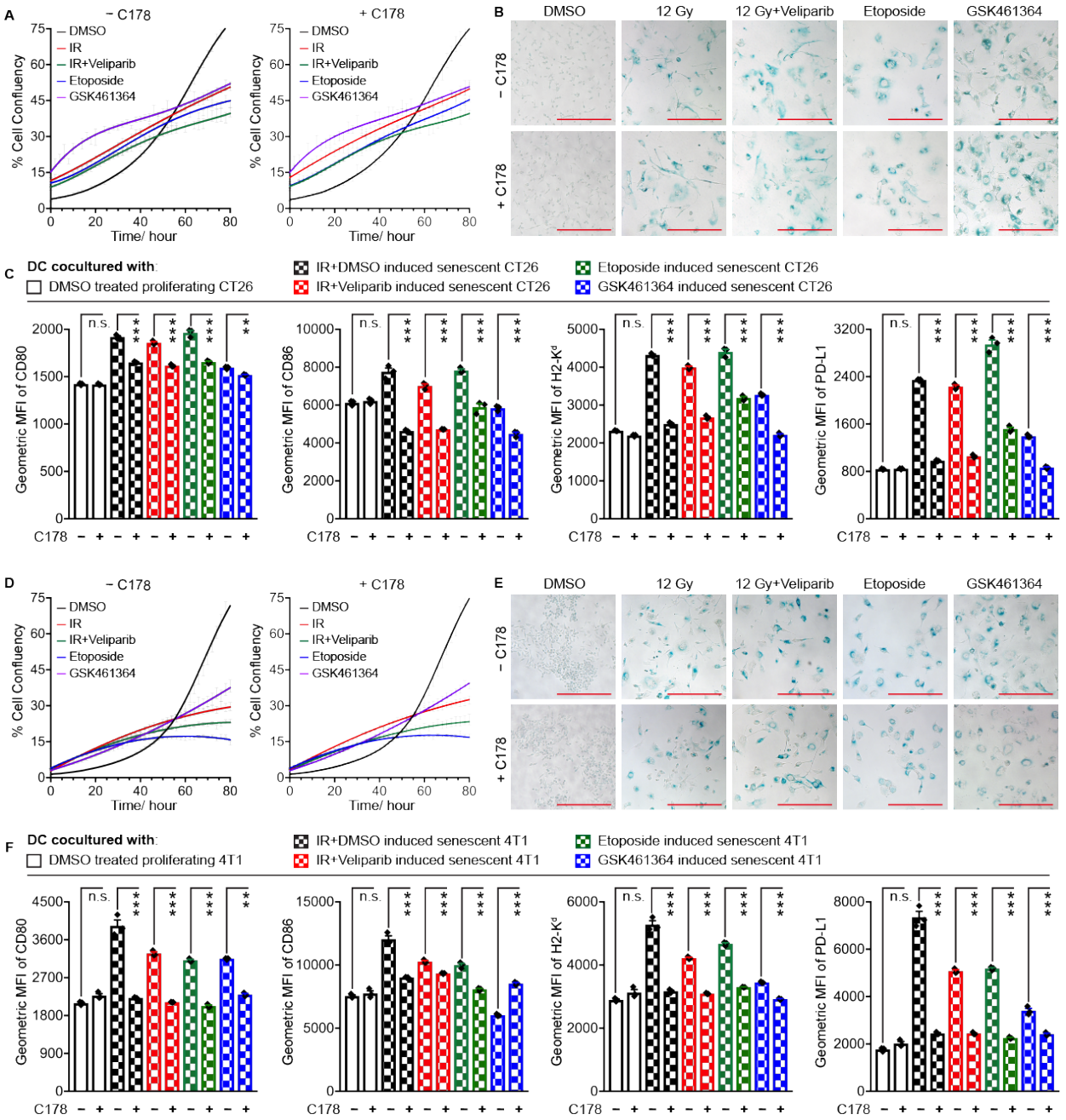

Figure 4.7: STING signals in senescent cells are required for BMDC activation.
A and D, Automated cell growth analysis from time-lapse imaging over 3 days. CT26 (A) or 4T1 cells (D) treated with DMSO, IR, IR+veliparib, etoposide, and GSK461364 in the presence or absence of C178 at time 0. Results are shown as mean ± s.e.m. Images of 16 non-overlapping fields were captured for analysis of each sample. B and E, SA-βGal staining of CT26 (B) or 4T1 cells (E). Cells were treated the same as A and D, followed by fixation and staining after 5 days. Scale bars: 200 μm. C and F, E, Quantitative analysis of DC activation/maturation. BMDCs were cocultured with CT26 (C) or 4T1 cells (F) overnight, then stained and analyzed through flow cytometry. Zombie yellow$^-$/CD11c$^+$/CD103$^+$ DC population were analyzed. Shown from three experiments, mean ± s.d. *** $P < 0.001$, ** $0.001 < P < 0.01$, n.s. $P > 0.05$ (unpaired t-test). MFI, mean fluorescence intensity.

Vaccination of senescent cells suppresses tumor growth and promotes anti-tumor immune response

According to our *in vitro* experiments, DCs stimulated by IR+veliparib induced senescent cells are most effective in priming T cells. Our prior studies have reported IR+veliparib induced senescent B16.SIY cells as a radiosensitizing cancer vaccine in syngeneic mice (28). In order to investigate the possibility of using senescent cells against endogenous tumor antigen for treating cancer, we evaluated the growth of subcutaneous CT26 tumors treated with twice injecting 0.5 million senescent CT26 cells peritumorally in a 5-day interval with or without a single X-ray dose of 10 Gy in the middle of the treatment. Considering that tumor immunity varies according to tumor sizes (36), we started the treatment either on Day 9 (average tumor volume ~ 60 mm^3) or Day 12 (average tumor volume ~ 150 mm^3) after tumor inoculation. Senescent cell vaccines alone demonstrated modest suppression of tumor growth, although their effects are more potent when treating smaller tumors. 10 Gy IR provided a moderate growth delay while most of the tumors started regrowth 10 days later. Tumors treated with both senescent vaccine and 10 Gy displayed a remarked growth delay, with all of the tumors disappearing within 2 weeks after treatment. In brief, senescent cancer vaccine monotherapy delays tumor growth specifically when it is administered early, and it significantly enhances the effectiveness of radiotherapy.

Our in vitro studies have demonstrated that the immune checkpoint blockade PD-L1 antibody can further enhance the T cell response mediated by senescent cells, so we examined whether the combination therapy involving senescence vaccine and PD-L1 antibody could be synergetic in cancer treatment. Accordingly, CT26 tumor-bearing BALB/c mice received the peritumoral injection of senescent cells twice in a 5-day interval and/or a single intravenous injection of α-PD-L1 antibody. When senescent cells were administered in mice with tumors <

60 mm^3, a comparable tumor suppression effect was observed as well as α-PD-L1 treatment, while the combination therapy displayed strong synergistic effects leading to 3/6 tumors eventually disappearing (Figure 4.8A-C). Similar effects of the senescent cell vaccine and/or PD-L1 antibody on tumor regression were detected in 4T1 tumors as well. For tumors > 150 mm^3, PD-L1 antibody had no appreciable effect on tumor growth, senescence vaccine displayed modest effects, and the combination treatment provided superior tumor control (Figure 4.8D-F).

The elimination of tumors by combined senescent cells and radiation/ immunotherapy suggested the potentiation of an anti-tumor immune response. Therefore, we obtained tumors 5 days after treatment to detect $CD45^+$ immune infiltrate, $CD11c^+/CD103^+$ DCs, $CD3^+/CD4^+$ helper T cells, $CD3^+/CD8^+$ cytotoxic T cells, and $CD3^-/CD49b^+$ natural killer (NK) cells. Treatment of senescent cells significantly increased the percentage of immune cells, including DCs and cytotoxic T cells, and when combined with radiation/ immune checkpoint blockade therapy, this treatment further enhanced all evaluated immune cells compared to monotherapy (Figure 4.9A-E). This pattern indicated that the senescent cell vaccine enables an effective anti-tumor immune response, synergizing with radio- and immuno-therapy.

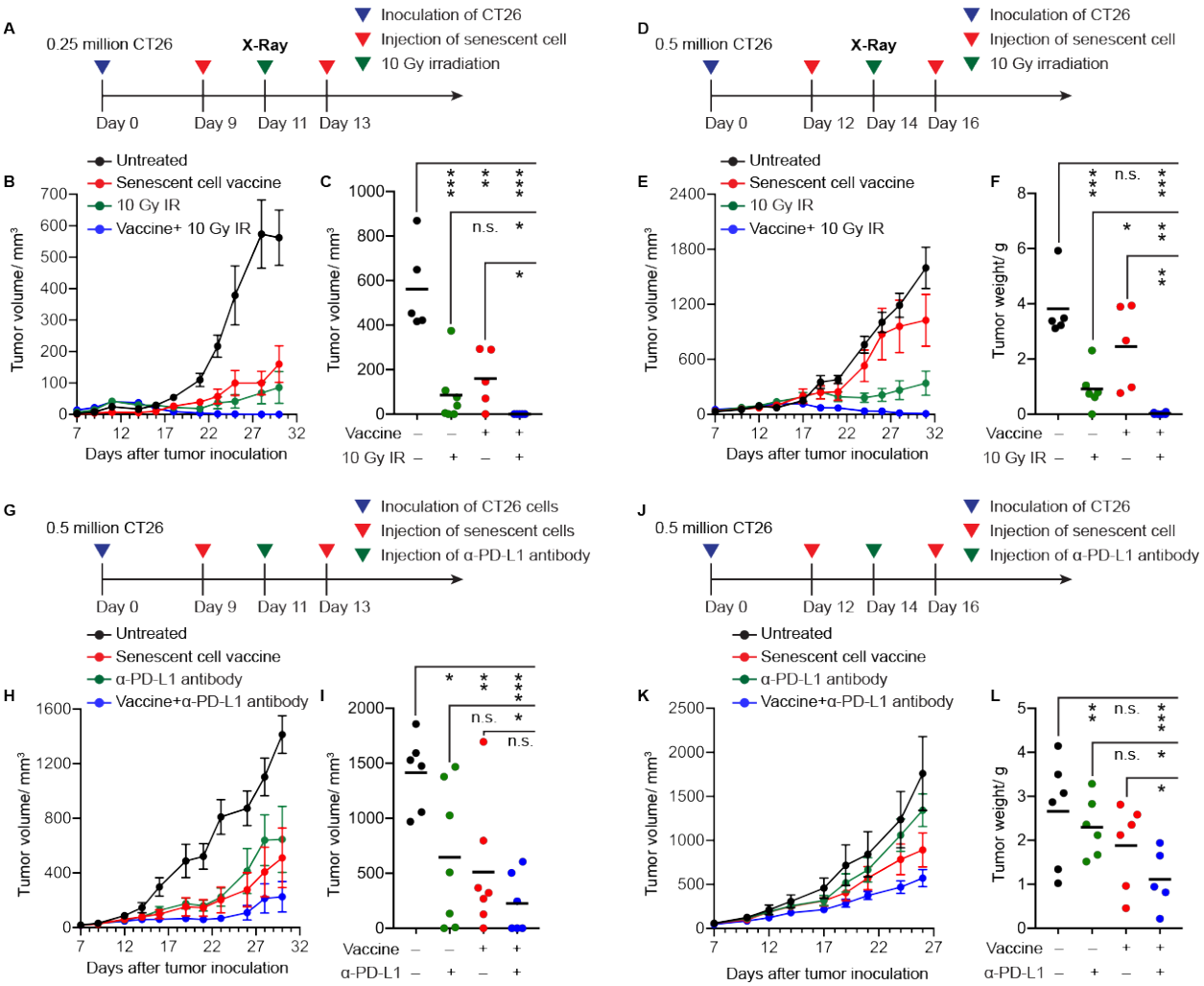

Figure 4.8: Senescent cell vaccine suppresses tumor growth and potentiates cancer therapies *in vivo*.

A-F, Senescent cell vaccine potentiates radiotherapy. A and D, Experimental schema for treating mice bearing CT26 subcutaneous tumors with peritumoral injection of senescent cell vaccine and/or external beam irradiation. B and E, Growth of CT26 tumors in mice were treated with senescent cell vaccine alone or in combination with IR. Tumors were measured with calipers every 2-3 days with 5-7 mice per treatment group, mean ± s.e.m. C, The volume of CT26 tumors at day 30 after inoculation. F, The weight of CT26 tumors at day 31 after inoculation. Shown are individual tumors (circle) and mean (bar). *** $P < 0.001$, ** $0.001 < P < 0.01$, * $0.01 < P < 0.05$, n.s. $P > 0.05$ (unpaired t-test). G - L, Senescent cell vaccine potentiates immunotherapy. G and J, Experimental schema for treating mice bearing CT26 subcutaneous tumors with peritumoral injection of senescent cell vaccine and/or systemic treatment of α-PD-L1 antibody. H and K, Growth of CT26 tumors in mice were treated with senescent cell vaccine alone or in combination with PD-L1 antibody. Tumors were measured with calipers every 2-3 days with 5-7 mice per treatment group, mean ± s.e.m. I, The volume of CT26 tumors at day 30 after inoculation. L, The weight of CT26 tumors at day 26 after inoculation. Shown are individual tumors (circle) and mean (bar). *** $P < 0.001$, ** $0.001 < P < 0.01$, * $0.01 < P < 0.05$, n.s. $P > 0.05$ (unpaired t-test).

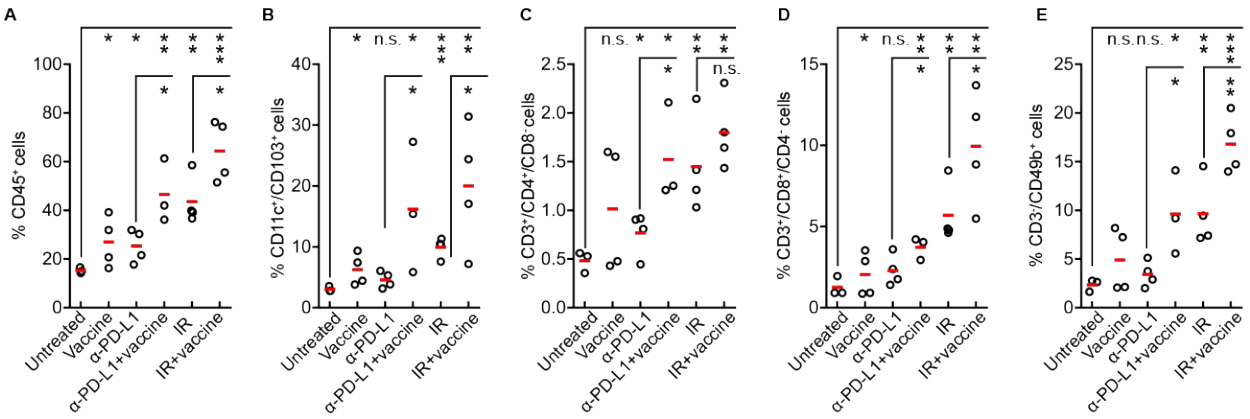

Figure 4.9: Senescent cell vaccine promotes tumor immune infiltrate.
A-E, Quantification of immune infiltrate in CT26 tumors. The mice bearing CT26 subcutaneous tumors were treated as in Figure 5.8. Then the tumors were collected 5 days after treatments, dissociated and stained for flow cytometric analysis. Zombie yellow$^-$ single cell population were analyzed. The total immune cell CD45$^+$ (A), dendritic cell CD11c$^+$/CD103$^+$ (B), helper T cell CD3$^+$/CD4$^+$/CD8$^-$ (C), cytotoxic T cell CD3$^+$/CD8$^+$/CD4$^-$ (D), and NK cell CD3$^-$/CD49b$^+$ (E) were quantified. Shown individual mouse (open circle) and mean (bar). *** $P < 0.001$, ** $0.001 < P < 0.01$, ** $P < 0.05$, n.s. $P > 0.05$ (unpaired t-test).

Senescent cell vaccine suppresses lung metastasis

Metastasis has been reported as the primary cause of cancer-related deaths due to a lack of effective treatment (37). According to many preclinical and clinical studies, tumor cell vaccines have long been considered a promising treatment for metastatic cancer (38-40). As a simplified model, we injected 4T1 cells through the tail vein of BALB/c mice on Day 0 to establish lung metastasis. For examining whether senescent cells could prevent or treat lung metastasis, 0.5 million senescent 4T1 cells were injected subcutaneously into mice respectively on Day -6 and -1 or Day 1. Then the lungs were collected on Day 21 for microscopic and histological examination (Figure 4.10A). Mice pre-immunized with senescent cells showed a significant reduction in lung metastases, with 3/5 of mice not developing metastatic foci (Figure 4.10B-E). Senescence vaccination after tumor cell inoculation also effectively suppressed pulmonary metastases, even though the metastases were not completely eliminated (Figure 4.10B-E). In Mice intravenously receiving as high as 0.25 million 4T1 cells, treatment with the same amount of senescent cells displayed similar patterns.

Dendritic cell vaccine recapitulates the effects of senescent cell vaccine and results in immunological anti-tumor memory in treated mice

Our in vitro data indicated that senescent cells were capable of mediating the response of T cells through DCs, so we examined whether ex vivo activated DCs by senescent cells would have similar anti-tumor effects as a senescence vaccine in BALB/c mice. After pre-stimulating for ~12 h with IR + veliparib-induced CT26 senescent cells, the BMDCs were injected adjacent to CT26 tumors according to the same schedule as the senescent cell vaccine, with or without a single X-ray dose of 10 Gy (Figure 4.11A). The 10 Gy radiation consistently provided moderate

but non-curative suppression on tumor growth. Activated DCs by senescent cells alone demonstrated some slowdowns, which were further enhanced by radiation, leading to the elimination of most tumors (Figure 4.11B and C). As a test of immunological memory, mice with tumors that had collapsed completely after the DC+IR treatment were re-challenged with 0.5 million CT26 cells, which caused no tumor growth, compared with the 100% tumor take rate of similarly injected naive mice (Figure 4.11D and E).

Furthermore, we investigated whether senescent cell-activated DCs are capable of suppressing 4T1 lung metastasis. For this, BALB/c were intravenously injected with 60,000 4T1 cells on Day 0, followed by DC vaccination on Days 1 and 5, with or without systemic α-PD-L1 antibody treatment on Day 3 (Figure 4.11F). The lungs were removed and examined on Day 21. The number of metastatic lung lesions was comparable when mice were untreated or given anti-PD-L1 antibody, while this number was significantly smaller when mice were treated with DC vaccine (Figure 4.11G and H). The mice who received combination therapy of the DC vaccine and PD-L1 antibody developed the least frequent lung metastases, suggesting synergetic effects (Figure 4.11G and H). Histology analysis of lung sections displayed a similar pattern (Figure 4.11I). These studies suggest the potential senescence-stimulated DCs as an anti-cancer vaccine for treating local and metastatic tumors.

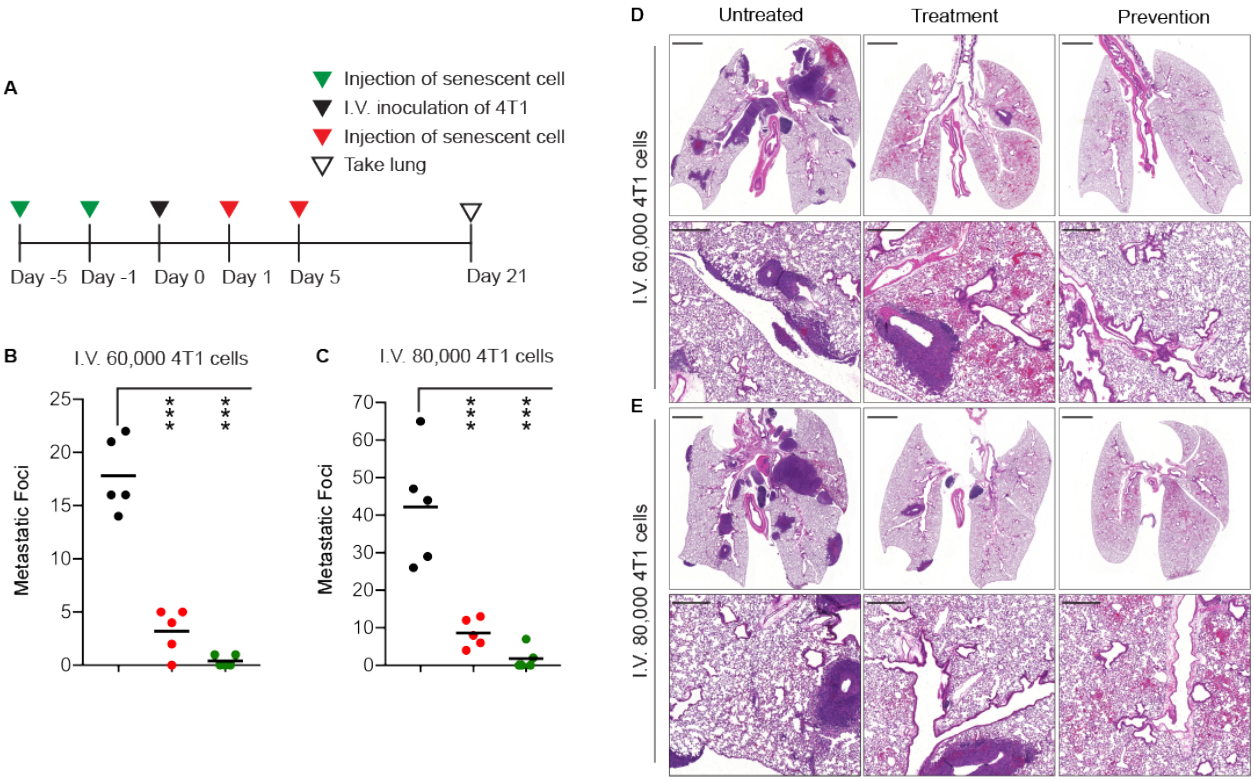

Figure 4.10: Senescent cell vaccine limits 4T1 lung metastasis.
A, Experimental schema for creating 4T1 lung metastasis and senescent cell treatment. For preventing lung metastasis, senescent cells were subcutaneous injected into BALB/c mice twice in a 4-day interval, followed by intravenous inoculation of 4T1 cells one day after. For treating lung metastasis, BALB/c mice were intravenously injected with 4T1 cells, followed by the treatment with senescent cell vaccine. B and C, The quantification of metastatic foci on the lung surface. BALB/c mice were inoculated with 60,000 (B) or 80,000 4T1 cells (C), while the lungs were collected 21 days after tumor cell inoculation. Shown individual mouse (dot) and mean (bar). *** $P < 0.001$, ** $0.001 < P < 0.01$, n.s. $P > 0.05$ (unpaired t-test). D and E, Represented hematoxylin and eosin (H&E) staining of mouse lung sections. BALB/c mice were inoculated with 60,000 (D) or 80,000 4T1 cells (E). The lungs were collected as in B and C, then fixed and stained. Scale bars: 2 mm (upper) and 50 μm (lower).

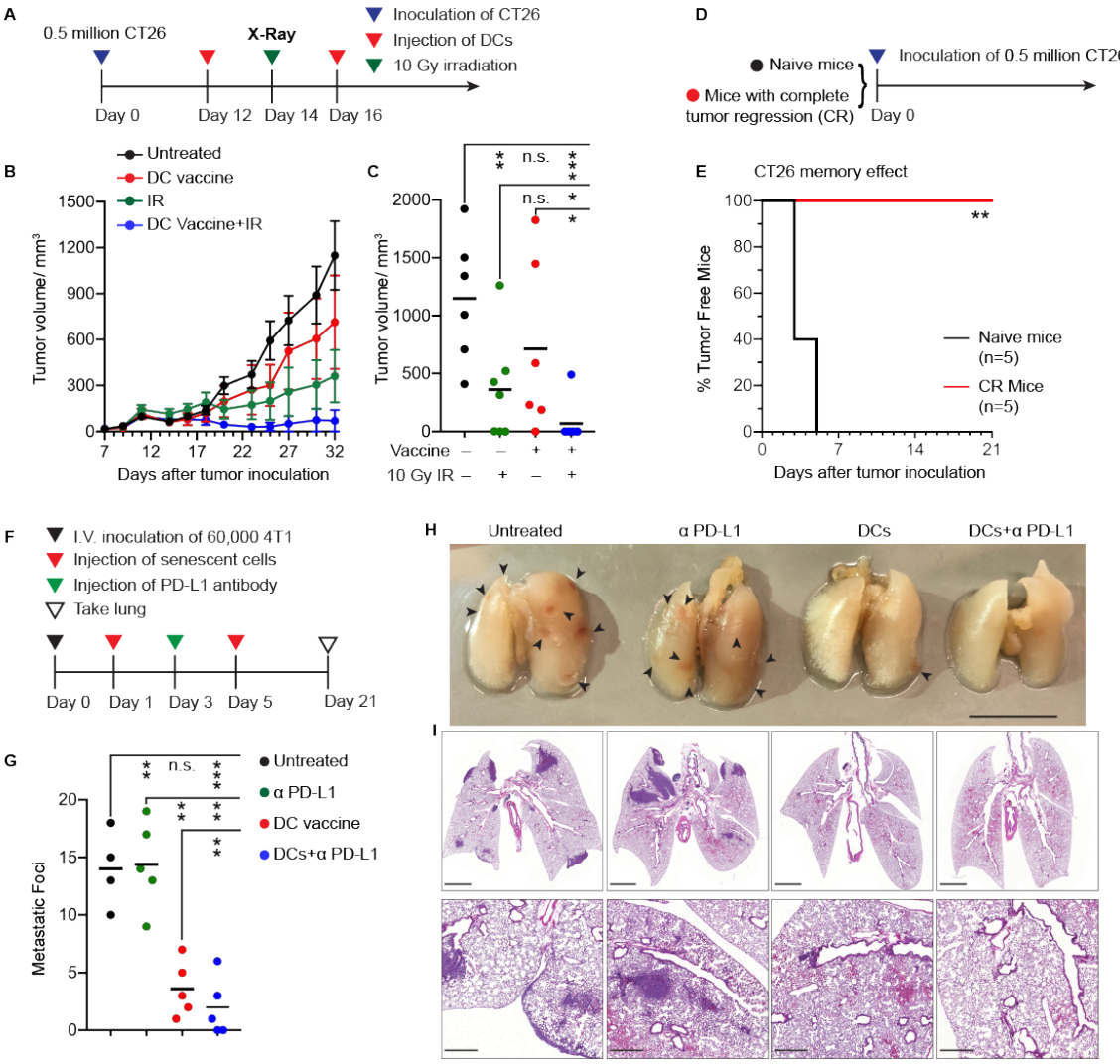

Figure 4.11: DC vaccine potentiates radiotherapy and suppresses tumor metastasis.
A, Experimental schema for treating mice bearing CT26 subcutaneous tumors with DC vaccine peritumoral injection and/or external beam irradiation. B, Growth of CT26 tumors in mice were treated with DC vaccine alone or in combination with IR. Tumors were measured with calipers every 2-3 days with 5-7 mice per treatment group, mean ± s.e.m. C, The volume of CT26 tumors at day 31 after inoculation. Shown are individual tumors (circle) and mean (bar). *** $P < 0.001$, n.s. $P > 0.05$ (unpaired t-test). D, Experimental schema for challenging naïve BALB/c mice or mice displayed complete response to IR+DC treatment. E, Kaplan-Meier curve of the progression of tumor development over time. Each mouse was challenged with 0.25 million CT26 cells. The tumor development was monitored every 2-3 days. n=5 in each experimental group. F, Experimental schema for treating mice against tumor metastasis. 60,000 4T1 cells were intravenously inoculated into BALB/c mice. Then mice were treated with subcutaneous injection of DC and/or intravenous injection of α-PD-L1 antibody as indicated. G, Quantification of the metastatic foci on lung surface. The lungs were collected 21 days after tumor cell inoculation. Shown individual mouse (dot) and mean (bar). *** $P < 0.001$, ** $0.001 < P < 0.01$, n.s. $P > 0.05$ (unpaired t-test). H, Represented photographs of lungs with metastases. Scale bars: 1 cm. I, Represented hematoxylin and eosin (H&E) staining of the lungs with metastatic tumors. Scale bars: 2 mm (upper) and 50 μm (lower).

4.3 Discussion

In many studies, cellular senescence has been shown to promote anti-tumor immunity in situ as a result of the production of immunostimulatory SASP and the presentation of tumor antigens (28). Our studies confirmed that senescent cells stimulate dendritic cell maturation/activation and T cell priming. Senescent cells displayed the highest potency as DC stimulators than apoptotic or injured cells. In comparing senescent cells triggered by various mechanisms, IR+veliparib induced senescence elicited the highest potency in priming T cells, which might be partially explained by its diminished effects on PD-L1 upregulation, as PD-L1 inhibits T cell activity when interacting with PD-1. Pro-inflammatory cytokines have been identified as major components of SASPs produced by cells undergoing stress-induced senescence. In the tumor microenvironment, these inflammatory cytokines were considered to be responsible for upregulating PD-L1 (41), while veliparib may control the expression of PDL1due to its anti-inflammatory properties. Indeed, veliparib and other PRAP inhibitors have demonstrated effects on reducing pro-inflammatory cytokines, including TNF-α, IL-1β, and IL-6, on the models of tissue injuries both in vitro and in vivo (42-44). The role of veliparib-involved senescence progression and SASP reprogramming in enhancing anti-tumor immunity is still under investigation.

STING singling is well known for inducing type I interferons (IFNs), which are crucial for DC maturation and activation (45-47). Other studies have demonstrated that the activation of STING signaling upregulated the expression of class I MHC molecules in human melanoma cells, resulting in increased antigenicity and enhanced tumor antigen recognition by immune cells (48). Activating STING in tumor cells led to an increase in $CD8^+$ T cell infiltration in the tumor microenvironment (49, 50), suggesting the critical role of STING signaling in anti-tumor

immunity. In *Sting*-knockout mice, senescence-mediated immune-surveillance has been impaired, which may be attributed to the lack of STING signals in senescent, non-senescent, and immune cells (33). In this study, we have demonstrated that activated STING signaling in senescent cells is crucial to their ability to modulate DCs, while future studies might be required to investigate how STING signals contribute to the immunogenicity of senescent cells in detail.

Cancer vaccines are exciting developments in cancer immunotherapy that trigger specific immune responses against tumor antigens, with the goal of controlling tumor growth, inducing tumor regression, eliminating minimal residuals, and establishing lasting anti-tumor memories (40, 51, 52). One cancer vaccine platform is the whole-cell vaccine developed using autologous patient-derived or allogeneic tumor cells that express immunogens representative of an individual patient's tumors (40, 52). A general principle of the whole-cell vaccination is to genetically modify tumor cells that express immunostimulatory cytokines such as granulocyte-macrophage colony-stimulating factor (GM-CSF), to attracts and antigen-presenting cells (APCs) and promote uptake of tumor cells for cross-presentation (53-56). Then these modified cells are irradiated to prevent further cell division before serving as the vaccine. Examples of whole-cell vaccines under clinical investigation include GVAX for pancreatic and prostate cancers (53, 54), and Vigil for ovarian cancer (55, 56). Other platforms for whole-cell vaccines discussed in preclinical studies include early ferroptotic cells (5), necroptotic cells (4), and etoposide-injured cells (6). Many studies have demonstrated that stress-induced senescent cells display an enhanced secretion of immune-stimulating cytokines and elevated presentation of tumor antigens (28, 57), suggesting a potential for the whole-cell vaccine. We have previously addressed senescent tumor cells induced by radiation and veliparib as promising in situ and traditional vaccines. The present study found that immunization with senescent cells significantly

enhanced anti-tumor immune responses against endogenous tumor antigens, leading to suppression of local tumor growth and metastases.

The lack of immune infiltrates and/or high level of immune checkpoints in tumors appears to compromise the efficacy of therapeutic cancer vaccines. Therefore, the combination therapy might significantly affect the therapy outcome (58). As demonstrated in multiple preclinical and clinical research, the combined use of cancer vaccines with immune checkpoint inhibitors such as anti-CTLA-4 and anti-PD-1 antibodies significantly enhances anti-tumor efficacy (51, 59, 60). Consistently, our results indicated that senescent cell vaccines synergized with anti-PD-L1 antibody systemic treatment. Additionally, an increasing number of preclinical/clinical data indicated that ionizing radiation (IR) sensitizes refractory tumors to immunotherapies by promoting the recruitment of intratumoral DCs and cytotoxic T cells (61-63). In our study, the combination therapy with senescence vaccine and radiation resulted in remarkable tumor suppression, with most tumors completely disappearing.

Despite being a controversial topic, the reversibility of senescence may be an obstacle to the clinical application of the senescent cell vaccine. In this study, we also investigated the potential of DCs activated by senescent cells *ex vivo* as cancer vaccines and confirmed the efficiency of this approach in suppressing tumor growth and metastasis. For decades, DC-based cancer vaccines have been extensively researched, and the only FDA-approved cancer therapeutic vaccine is a DC vaccines, sipuleucel-T (64). The rationale for DC vaccines is that DCs collect antigens from various tumors and transport them to secondary lymphoid organs to activate antigen-specific T cells (51). Current *ex vivo* methods for producing DC vaccine include activating DC with cytokines such as GM-CSF (e.g., sipuleucel-T (64)) and activating cocktails (e.g., ilixadencel with R848, Poly I:C and IFN-γ (65)), and/or loading DC with tumor antigens in

the form of peptides (e.g., MART-1 vaccine (66)), proteins (e.g., sipuleucel-T (64)), and tumor lysates (e.g., OC-DC (67)), while these strategies only displayed modest clinical benefit. Our study described a novel approach to preparing DC vaccines using senescent tumor cells, which effectively suppressed tumor growth, enhanced radiotherapy, and reduced metastasis. The clinical application of this strategy as neoadjuvant and/or adjuvant therapy might further improve cancer treatment.

4.4 Material and Methods

Cell line and tissue culture

The mouse colon carcinoma cell line CT26 (HTB-85) and mosue breast mammary carcinoma cell line 4T1 were obtained from ATCC. Cells were maintained in RPMI 1640 (Thermo Fisher Scientific) supplemented with 10% FBS (Atlanta Biologicals) and 1% penicillin/streptomycin (Thermo Fisher Scientific). The cells were tested for mycoplasma contamination and authenticated by a short tandem repeat profile (IDEXX BioResearch) prior to performing experiments. All experiments were performed within 3 to 10 passages after thawing cells. The basic murine immune cell culture medium is RPMI 1640 (Thermo Fisher Scientific) supplemented with 10% heat-inactivated FBS (Thermo Fisher Scientific), 1% penicillin/streptomycin (Thermo Fisher Scientific), and 50 μM β-mercaptoethanol.

Animals

BALB/c wildtype and NOD scid gamma (NSG) mice were maintained and processed according to the guidelines of the Institutional Animal Care and Use Committee.

Chemical probes

Veliparib was a kind gift from AbbVie. Etoposide, GSK46136 and C178 were obtained from Cayman Chemical.

Senescence induction and SA-βGal assay

To induce cellular senescence, cells were seeded at 2×10^4/mL in plates and treated with etoposide (Cayman Chemical, 2 μM), GSK461364 (Cayman Chemical, 5 μM), 12 Gy IR, or

IR+veliparib (AbbVie, 20 μM). Cells treated with DMSO vehicle or veliparib alone served as controls. 5 days after treatment, cells were fixed in 2% PFA and stained for 16-32 h at 37 °C. Staining buffer contains 1 mg/mL X-Gal (X4281C, Golden Bio), 40 mM Citric acid/sodium phosphate, 150 mM NaCl, 2 mM $MgCl_2$, 3.3 mM $K_3[Fe(CN)_6]$, 3.3 mM $K_4[Fe(CN)_6]$, pH 6. After staining, images were captured on a Zeiss Axiovert 200M microscope with a 10× Plan-NeoFluar objective and Axiocam digital camera. SA-β-Gal-positive and -negative cells were counted in more than 5 fields, yielding an average percentage indicated on each SA-βGal image as mean ± s.d. Two or more replicates were performed.

Single cell RNA sequencing

To get splenocytes, the spleens were isolated from BALB/c mice bearing subcutaneous CT26 tumors, mashed in a petri dish through a 40 μm cell strainer, and resuspended in basic murine immune cell culture medium. The red blood cells were lysed using Red Blood Cell Lysis Buffer (Biolegend) according to the manufacture's protocol. The senescent CT26 cells were induced using 12 Gy IR+veliparib as described above, while the proliferating CT26 cells treated with DMSO vehicle were used as control. Both senescent and proliferating cells were washed twice with PBS, replaced with fresh murine immune cell culture medium, then cocultured with splenocytes for 3 days. The suspended cells were collected into the concentration of $5x10^5$ cells/ mL. The cell samples for single cell RNA sequencing ware prepared using a 10X Genomics Chromium controller, followed by Next-Gen (Illumina) Sequencing in the Genomics Facility. The data were analyzed using Seurat packages in R (68).

Preparation of mouse BMDCs

Bone marrow derived dendritic cells (BMDCs) were differentiated as previously described (69). Briefly, bone marrow was isolated from 7-8 weeks BALB/c mice, maintained in basic immune cell culture medium supplemented with 1ng/mL mouse recombinant GM-CSF (PerproTech) and 200ng/mL mouse recombinant Flt-3 ligand (PerproTech) for 14-16 days, with refreshing the medium on Day 6, 9, and 12.

Phagocytosis assays

Senescent and proliferating cells were prepared as described above, then labeled with PKH26 (Singma) or PhordoRed (Singma) for 15 min at 37 °C respectively. The cells were washed and cocultured with BMDCs in a ratio 1:2 overnight. Then the cocultured cells were harvested, stained with fluorophore conjugated CD11c and using BD Fortessa 4-15 HTS Flow cytometer and FlowJo software.

Cells were labeled with PhordoRed (Singma) for xx min at xxx . The cells were washed and cocultured with BMDCs in a ratio 1:2 overnight. Then the cocultured cells were harvested, stained with zombie yellow (BioLegend) for 10 min at room temperature, followed by staining with CD11c and CD103 antibodies for 45 min at 4 °C. Cells were analyzed using BD Fortessa 4-15 HTS Flow cytometer and FlowJo software. True uptake by BMDCs was determined using a gating strategy that alllws analysis of only single cells and was determined CD11c+/CD103+ cells.

Analysis of BMDCs surface marker expression

Senescent and proliferating cells were prepared as described above, in the presence or absence of STING inhibitor C178. To induce damaged cells, CT26 cells were treated with 12 Gy

IR or IR+veliparib, then utilized 1 day later for BMDC coculture experiments. To prepare apoptotic senescent cells, senescent CT26 cells induced by IR+veliparib were treated with ABT-263 (Cayman Chemical, 5 μM) overnight. All the tumors cells were washed twice with PBS, then cocultured with BMDCs for 12-16 hours in a 1:2 ratio in basic immune cell culture medium. After coculture, suspended cells were collected and incubated with zombie yellow (BioLegend) for 10 min at room temperature, followed by staining with CD11c, CD103, CD86, CD80, PD-L1, H-2K^d or H-2L^d antibodies for 45 min at 4 °C. Cells were analyzed using BD Fortessa 4-15 HTS Flow cytometer and FlowJo software.

Analysis of T cell cross-priming and proliferation

To prepare CT26 immunized mice, 7-9 week BALB/c mice were subcutaneously injected with 0.5 million irradiated CT26 or 4T1 cells (20 Gy) twice with a 10-day interval. The splenocytes were isolated from immunized mice and stained with 0.5 μM carboxyfluorescein succinimidyl ester (CFSE) for 10 min at room temperature (70). After washing, CFSE labeled splenocytes were cocultured for 5 days in a 20:1 ratio with BMDCs pre-stimulated by proliferating or senescent CT26 cells. After coculturing, cells were collected and incubated with zombie yellow (BioLegend) for 10 min at room temperature, followed by staining with CD4 and CD8a antibodies for 30 min at 4 °C. Cells were analyzed using BD Fortessa 4-15 HTS Flow cytometer and FlowJo software.

Preparation of senescent cell vaccine and DC vaccine for *in vivo* treatment

1x10^6 CT26 cells or 4T1 cells were seeded into T175 flask, then treated with 20 μM veliparib and 12 Gy radiation. 5 days after radiation, cells were trypsinized and washed in PBS,

then resuspended in cold PBS to a final concentration $5x10^6$ cells/ mL. Naïve dendric cells (DCs) were prepared from mouse bone marrow as described above, followed by coculturing with senescent cells induced by IR+veliparib for 10-14 hours. The suspended DCs were collected and washed in PBS, then resuspended in cold PBS to a final concentration $5x10^6$ cells/ mL.

Flow cytometric analysis of AH-1 specific T cells

7-8 week BALB/c mice received subcutaneous injection of with 0.5 million senescent CT26 cells or PBS control. 2 days after, the draining inguinal lymph nodes were isolated, dissociated and stained with FITC AH-1 dextramer (Immudex) according to manufactures' protocol. Briefly, ~ $2x10^6$ cells in 50 μL staining buffer were incubated with AH-1 dextramer for 10 min at room temperature, then Alexa Fluor® 647 CD8 antibody (Clone KT15, BioRad) was added for another 20 min in dark. After washing, cells were analyzed using BD Fortessa 4-15 HTS Flow cytometer and FlowJo software.

***In vivo* prophylactic or therapeutic tumor vaccination**

For prophylactic vaccination, 7-8 week BALB/c or NSG mice were received subcutaneous injection of with 0.5 million senescent CT26 cells or PBS vehicle on Day -5, and/or intravenous injection of α-PD-L1 antibody (0.2 mg each, Bio X Cell) on Day -4. The naïve mice or vaccinated mice were challenged with 0.5 million CT26 cells or 4T1 cells in 100 μL PBS subcutaneously on Day 0. The tumor development was monitored every 2-3 days for 3 weeks and the tumor volume was measured using a caliper from day 7 after tumor inoculation.

For therapeutic vaccination, 7-8 week BALB/c mice were subcutaneously inoculated with 0.25 million or 0.5 million CT26 or 4T1 cells in 100 μL PBS on Day 0. The treatment

began from Day 9 or 12 days, when the tumor volume of an approximate 60 mm^3 or 150mm^3 average were detectable by caliper. 100 μL of cell vaccine was peritumorally injected into mice twice with a 5-day interval. Where indicated, groups of mice also received 10 Gy external beam irradiation or intravenous administration of anti-PD-L1 antibody (0.2 mg each, Bio X Cell) at single dose. Tumor radiation was conducted using a RadSource RS-2000 X-Ray generator operating at 160 kV and 25 mA with 10 Gy, calibrated by NIST traceable dosimetry. Tumor volume was measured using calipers every 2-3 days from day 7 after tumor inoculation.

In tumor rechallenge experiments, naïve mice controls or mice who developed complete tumor regression and remained tumor free for >10 days were subcutaneously injected with 0.25 million CT26 cells on the back. The tumor development was monitored every 2-3 days for 3 weeks.

4T1 lung metastatic assays

4T1 cells were injected into the tail veins of 7-8 week female BALB/c mice on Day 0. Mice received subcutaneous injection of cell vaccine on Day -5 and Day -1 as prophylactic vaccination, or on Day 1 and Day 5 as treatment. Where indicated, mice also received intravenous administration of anti-PD-L1 antibody (0.2 mg each, Bio X Cell) at single dose. On Day 21, mice were euthanized, lungs were collected and fixed in 10% neutral formalin.

Flow cytometric analysis of tumor infiltrated immune cells

CT26 or 4T1 tumors were collected 5 days after treatment and dissociated using Tumor Dissociation Kit (Miltenyi) according to manufacturer's protocol. Briefly, tumor tissues were transferred into the gentleMACS C Tubes containing enzyme mix. Then the C tubes were run on a gentleMACS™ Dissociator using gentleMACS program m_impTumor_02. After termination

of the program, samples were incubated for 30 min at 37 °C. After dissociation, the cell suspensions were filtered through a 70 μm strainer and pelleted by centrifugation at 300×g for 5 min. The cell pellet was resuspended in PBS, incubated with zombie yellow for 10 min at room temperature. After washing with PBS, the cells were stained with fluorophore conjugated CD45, CD3, CD4, CD8, CD49b, CD11c, and CD103 antibodies for 30 min at 4 °C, followed by analysis using BD Fortessa 4-15 HTS Flow cytometer and FlowJo software.

Histology and Immunohistochemistry

CT26 or 4T1 tumors were collected 5 days after treatment and fixed in 10% neutral formalin. Formaldehyde-fixed paraffin-embedded (FFPE) tumors were sectioned and stained with hematoxylin and eosin (H&E) by the Human Tissue Resource Center. The H&E stained tissue sections were scanned using Olympus VS200 SlideView Whole Slide Scanner.

Statistical analysis

Statistical significance was determined using the non-paired Student's t-test. Calculations were performed using Prism software (GraphPad) or Excel. $P \leq 0.05$ was considered statistically significant.

4.5 References

1. Papaioannou NE, Beniata OV, Vitsos P, Tsitsilonis O, and Samara P. Harnessing the immune system to improve cancer therapy. *Ann Transl Med.* 2016;4(14):261.

2. Galluzzi L, Buque A, Kepp O, Zitvogel L, and Kroemer G. Immunogenic cell death in cancer and infectious disease. *Nat Rev Immunol.* 2017;17(2):97-111.

3. Fucikova J, Kepp O, Kasikova L, Petroni G, Yamazaki T, Liu P, et al. Detection of immunogenic cell death and its relevance for cancer therapy. *Cell Death Dis.* 2020;11(11):1013.

4. Aaes TL, Kaczmarek A, Delvaeye T, De Craene B, De Koker S, Heyndrickx L, et al. Vaccination with Necroptotic Cancer Cells Induces Efficient Anti-tumor Immunity. *Cell Rep.* 2016;15(2):274-87.

5. Efimova I, Catanzaro E, Van der Meeren L, Turubanova VD, Hammad H, Mishchenko TA, et al. Vaccination with early ferroptotic cancer cells induces efficient antitumor immunity. *J Immunother Cancer.* 2020;8(2).

6. Sriram G, Milling LE, Chen JK, Kong YW, Joughin BA, Abraham W, et al. The injury response to DNA damage in live tumor cells promotes antitumor immunity. *Sci Signal.* 2021;14(705):eabc4764.

7. Munoz-Espin D, and Serrano M. Cellular senescence: from physiology to pathology. *Nat Rev Mol Cell Biol.* 2014;15(7):482-96.

8. Hanahan D. Hallmarks of Cancer: New Dimensions. *Cancer Discov.* 2022;12(1):31-46.

9. Lee S, and Schmitt CA. The dynamic nature of senescence in cancer. *Nat Cell Biol.* 2019;21(1):94-101.

10. Davalos AR, Kawahara M, Malhotra GK, Schaum N, Huang J, Ved U, et al. p53-dependent release of Alarmin HMGB1 is a central mediator of senescent phenotypes. *J Cell Biol.* 2013;201(4):613-29.

11. Basisty N, Kale A, Jeon OH, Kuehnemann C, Payne T, Rao C, et al. A proteomic atlas of senescence-associated secretomes for aging biomarker development. *PLoS Biol.* 2020;18(1):e3000599.

12. Prasanna PG, Citrin DE, Hildesheim J, Ahmed MM, Venkatachalam S, Riscuta G, et al. Therapy-Induced Senescence: Opportunities to Improve Anticancer Therapy. *J Natl Cancer Inst.* 2021;113(10):1285-98.

13. Faget DV, Ren QH, and Stewart SA. Unmasking senescence: context-dependent effects of SASP in cancer. *Nat Rev Cancer.* 2019;19(8):439-53.

14. Schosserer M, Grillari J, and Breitenbach M. The Dual Role of Cellular Senescence in Developing Tumors and Their Response to Cancer Therapy. *Front Oncol.* 2017;7.

15. Ruhland MK, Loza AJ, Capietto AH, Luo X, Knolhoff BL, Flanagan KC, et al. Stromal senescence establishes an immunosuppressive microenvironment that drives tumorigenesis. *Nat Commun.* 2016;7:11762.

16. Eggert T, Wolter K, Ji J, Ma C, Yevsa T, Klotz S, et al. Distinct Functions of Senescence-Associated Immune Responses in Liver Tumor Surveillance and Tumor Progression. *Cancer Cell.* 2016;30(4):533-47.

17. Loo TM, Kamachi F, Watanabe Y, Yoshimoto S, Kanda H, Arai Y, et al. Gut Microbiota Promotes Obesity-Associated Liver Cancer through PGE2-Mediated Suppression of Antitumor Immunity. *Cancer Discov.* 2017;7(5):522-38.

18. Pereira BI, Devine OP, Vukmanovic-Stejic M, Chambers ES, Subramanian P, Patel N, et al. Senescent cells evade immune clearance via HLA-E-mediated NK and CD8(+) T cell inhibition. *Nat Commun.* 2019;10(1):2387.

19. Krizhanovsky V, Yon M, Dickins RA, Hearn S, Simon J, Miething C, et al. Senescence of activated stellate cells limits liver fibrosis. *Cell.* 2008;134(4):657-67.

20. Sagiv A, Biran A, Yon M, Simon J, Lowe SW, and Krizhanovsky V. Granule exocytosis mediates immune surveillance of senescent cells. *Oncogene.* 2013;32(15):1971-7.

21. Kang TW, Yevsa T, Woller N, Hoenicke L, Wuestefeld T, Dauch D, et al. Senescence surveillance of pre-malignant hepatocytes limits liver cancer development. *Nature.* 2011;479(7374):547-51.

22. Iannello A, Thompson TW, Ardolino M, Lowe SW, and Raulet DH. p53-dependent chemokine production by senescent tumor cells supports NKG2D-dependent tumor elimination by natural killer cells. *J Exp Med.* 2013;210(10):2057-69.

23. Xue W, Zender L, Miething C, Dickins RA, Hernando E, Krizhanovsky V, et al. Senescence and tumour clearance is triggered by p53 restoration in murine liver carcinomas. *Nature.* 2007;445(7128):656-60.

24. Tasdemir N, Banito A, Roe JS, Alonso-Curbelo D, Camiolo M, Tschaharganeh DF, et al. BRD4 Connects Enhancer Remodeling to Senescence Immune Surveillance. *Cancer Discov.* 2016;6(6):612-29.

25. Di Mitri D, Toso A, Chen JJ, Sarti M, Pinton S, Jost TR, et al. Tumour-infiltrating Gr-1+ myeloid cells antagonize senescence in cancer. *Nature.* 2014;515(7525):134-7.

26. Wang RW, Vigano S, Ben-David U, Amon A, and Santaguida S. Aneuploid senescent cells activate NF-kappaB to promote their immune clearance by NK cells. *EMBO Rep.* 2021;22(8):e52032.

27. Goel S, DeCristo MJ, Watt AC, BrinJones H, Sceneay J, Li BB, et al. CDK4/6 inhibition triggers anti-tumour immunity. *Nature.* 2017;548(7668):471-5.

28. Meng Y, Efimova EV, Hamzeh KW, Darga TE, Mauceri HJ, Fu YX, et al. Radiation-inducible immunotherapy for cancer: senescent tumor cells as a cancer vaccine. *Mol Ther.* 2012;20(5):1046-55.

29. Huang AY, Gulden PH, Woods AS, Thomas MC, Tong CD, Wang W, et al. The immunodominant major histocompatibility complex class I-restricted antigen of a murine colon tumor derives from an endogenous retroviral gene product. *Proc Natl Acad Sci U S A.* 1996;93(18):9730-5.

30. Yum S, Li MH, Frankel AE, and Chen ZJJ. Roles of the cGAS-STING Pathway in Cancer Immunosurveillance and Immunotherapy. *Annu Rev Canc Biol.* 2019;3:323-44.

31. Yang H, Wang HZ, Ren JY, Chen Q, and Chen ZJJ. cGAS is essential for cellular senescence. *P Natl Acad Sci USA.* 2017;114(23):E4612-E20.

32. Li T, and Chen ZJ. The cGAS-cGAMP-STING pathway connects DNA damage to inflammation, senescence, and cancer. *J Exp Med.* 2018;215(5):1287-99.

33. Dou Z, Ghosh K, Vizioli MG, Zhu J, Sen P, Wangensteen KJ, et al. Cytoplasmic chromatin triggers inflammation in senescence and cancer. *Nature.* 2017;550(7676):402-6.

34. Woo SR, Fuertes MB, Corrales L, Spranger S, Furdyna MJ, Leung MY, et al. STING-dependent cytosolic DNA sensing mediates innate immune recognition of immunogenic tumors. *Immunity.* 2014;41(5):830-42.

35. Haag SM, Gulen MF, Reymond L, Gibelin A, Abrami L, Decout A, et al. Targeting STING with covalent small-molecule inhibitors. *Nature.* 2018;559(7713):269-73.

36. Nesseler JP, Lee MH, Nguyen C, Kalbasi A, Sayre JW, Romero T, et al. Tumor Size Matters-Understanding Concomitant Tumor Immunity in the Context of Hypofractionated Radiotherapy with Immunotherapy. *Cancers (Basel).* 2020;12(3).

37. Fares J, Fares MY, Khachfe HH, Salhab HA, and Fares Y. Molecular principles of metastasis: a hallmark of cancer revisited. *Signal Transduct Target Ther.* 2020;5(1):28.

38. Berd D, Maguire HC, Jr., McCue P, and Mastrangelo MJ. Treatment of metastatic melanoma with an autologous tumor-cell vaccine: clinical and immunologic results in 64 patients. *J Clin Oncol.* 1990;8(11):1858-67.

39. Wang T, Wang D, Yu H, Feng B, Zhou F, Zhang H, et al. A cancer vaccine-mediated postoperative immunotherapy for recurrent and metastatic tumors. *Nat Commun.* 2018;9(1):1532.

40. Jou J, Harrington KJ, Zocca MB, Ehrnrooth E, and Cohen EEW. The Changing Landscape of Therapeutic Cancer Vaccines-Novel Platforms and Neoantigen Identification. *Clin Cancer Res.* 2021;27(3):689-703.

41. Cha JH, Chan LC, Li CW, Hsu JL, and Hung MC. Mechanisms Controlling PD-L1 Expression in Cancer. *Mol Cell.* 2019;76(3):359-70.

42. Irvine KA, Bishop RK, Won SJ, Xu J, Hamel KA, Coppes V, et al. Effects of Veliparib on Microglial Activation and Functional Outcomes after Traumatic Brain Injury in the Rat and Pig. *J Neurotrauma.* 2018;35(7):918-29.

43. Ahmad A, Haas De Mello A, Szczesny B, Toro G, Marcatti M, Druzhyna N, et al. Effects of the Poly(ADP-Ribose) Polymerase Inhibitor Olaparib in Cerulein-Induced Pancreatitis. *Shock.* 2020;53(5):653-65.

44. Ahmad A, Olah G, Herndon DN, and Szabo C. The clinically used PARP inhibitor olaparib improves organ function, suppresses inflammatory responses and accelerates wound healing in a murine model of third-degree burn injury. *Br J Pharmacol.* 2018;175(2):232-45.

45. Simmons DP, Wearsch PA, Canaday DH, Meyerson HJ, Liu YC, Wang Y, et al. Type I IFN Drives a Distinctive Dendritic Cell Maturation Phenotype That Allows Continued Class II MHC Synthesis and Antigen Processing. *J Immunol.* 2012;188(7):3116-26.

46. Chen Q, Sun L, and Chen ZJ. Regulation and function of the cGAS-STING pathway of cytosolic DNA sensing. *Nat Immunol.* 2016;17(10):1142-9.

47. Kwon J, and Bakhoum SF. The Cytosolic DNA-Sensing cGAS-STING Pathway in Cancer. *Cancer Discov.* 2020;10(1):26-39.

48. Falahat R, Perez-Villarroel P, Mailloux AW, Zhu GY, Pilon-Thomas S, Barber GN, et al. STING Signaling in Melanoma Cells Shapes Antigenicity and Can Promote Antitumor T-cell Activity. *Cancer Immunol Res.* 2019;7(11):1837-48.

49. Demaria O, De Gassart A, Coso S, Gestermann N, Di Domizio J, Flatz L, et al. STING activation of tumor endothelial cells initiates spontaneous and therapeutic antitumor immunity. *Proc Natl Acad Sci U S A.* 2015;112(50):15408-13.

50. Yang H, Lee WS, Kong SJ, Kim CG, Kim JH, Chang SK, et al. STING activation reprograms tumor vasculatures and synergizes with VEGFR2 blockade. *J Clin Invest.* 2019;129(10):4350-64.

51. Saxena M, van der Burg SH, Melief CJM, and Bhardwaj N. Therapeutic cancer vaccines. *Nat Rev Cancer.* 2021;21(6):360-78.

52. Le DT, Pardoll DM, and Jaffee EM. Cellular vaccine approaches. *Cancer J.* 2010;16(4):304-10.

53. Le DT, Wang-Gillam A, Picozzi V, Greten TF, Crocenzi T, Springett G, et al. Safety and survival with GVAX pancreas prime and Listeria Monocytogenes-expressing mesothelin (CRS-207) boost vaccines for metastatic pancreatic cancer. *J Clin Oncol.* 2015;33(12):1325-33.

54. Small EJ, Sacks N, Nemunaitis J, Urba WJ, Dula E, Centeno AS, et al. Granulocyte macrophage colony-stimulating factor--secreting allogeneic cellular immunotherapy for hormone-refractory prostate cancer. *Clin Cancer Res.* 2007;13(13):3883-91.

55. Senzer N, Barve M, Kuhn J, Melnyk A, Beitsch P, Lazar M, et al. Phase I trial of "bi-shRNAi(furin)/GMCSF DNA/autologous tumor cell" vaccine (FANG) in advanced cancer. *Mol Ther.* 2012;20(3):679-86.

56. Rocconi RP, Stanbery L, Madeira da Silva L, Barrington RA, Aaron P, Manning L, et al. Long-Term Follow-Up of Gemogenovatucel-T (Vigil) Survival and Molecular Signals of Immune Response in Recurrent Ovarian Cancer. *Vaccines (Basel).* 2021;9(8).

57. Toso A, Revandkar A, Di Mitri D, Guccini I, Proietti M, Sarti M, et al. Enhancing chemotherapy efficacy in Pten-deficient prostate tumors by activating the senescence-associated antitumor immunity. *Cell Rep.* 2014;9(1):75-89.

58. Weichselbaum RR, Liang H, Deng L, and Fu YX. Radiotherapy and immunotherapy: a beneficial liaison? *Nat Rev Clin Oncol.* 2017;14(6):365-79.

59. Zhao J, Chen Y, Ding ZY, and Liu JY. Safety and Efficacy of Therapeutic Cancer Vaccines Alone or in Combination With Immune Checkpoint Inhibitors in Cancer Treatment. *Front Pharmacol.* 2019;10:1184.

60. Schlom J. Therapeutic cancer vaccines: current status and moving forward. *J Natl Cancer Inst.* 2012;104(8):599-613.

61. Arina A, Beckett M, Fernandez C, Zheng W, Pitroda S, Chmura SJ, et al. Tumor-reprogrammed resident T cells resist radiation to control tumors. *Nat Commun.* 2019;10(1):3959.

62. Lugade AA, Moran JP, Gerber SA, Rose RC, Frelinger JG, and Lord EM. Local radiation therapy of B16 melanoma tumors increases the generation of tumor antigen-specific effector cells that traffic to the tumor. *J Immunol.* 2005;174(12):7516-23.

63. Deng L, Liang H, Xu M, Yang X, Burnette B, Arina A, et al. STING-Dependent Cytosolic DNA Sensing Promotes Radiation-Induced Type I Interferon-Dependent Antitumor Immunity in Immunogenic Tumors. *Immunity.* 2014;41(5):843-52.

64. Kantoff PW, Higano CS, Shore ND, Berger ER, Small EJ, Penson DF, et al. Sipuleucel-T immunotherapy for castration-resistant prostate cancer. *N Engl J Med.* 2010;363(5):411-22.

65. Karlsson-Parra A, Kovacka J, Heimann E, Jorvid M, Zeilemaker S, Longhurst S, et al. Ilixadencel - an Allogeneic Cell-Based Anticancer Immune Primer for Intratumoral Administration. *Pharm Res-Dordr.* 2018;35(8).

66. Lawson DH, Lee S, Zhao F, Tarhini AA, Margolin KA, Ernstoff MS, et al. Randomized, Placebo-Controlled, Phase III Trial of Yeast-Derived Granulocyte-Macrophage Colony-Stimulating Factor (GM-CSF) Versus Peptide Vaccination Versus GM-CSF Plus Peptide Vaccination Versus Placebo in Patients With No Evidence of Disease After Complete Surgical Resection of Locally Advanced and/or Stage IV Melanoma: A Trial of the Eastern Cooperative Oncology Group-American College of Radiology Imaging Network Cancer Research Group (E4697). *J Clin Oncol.* 2015;33(34):4066-76.

67. Tanyi JL, Bobisse S, Ophir E, Tuyaerts S, Roberti A, Genolet R, et al. Personalized cancer vaccine effectively mobilizes antitumor T cell immunity in ovarian cancer. *Sci Transl Med.* 2018;10(436).

68. Stuart T, Butler A, Hoffman P, Hafemeister C, Papalexi E, Mauck WM, 3rd, et al. Comprehensive Integration of Single-Cell Data. *Cell.* 2019;177(7):1888-902 e21.

69. Mayer CT, Ghorbani P, Nandan A, Dudek M, Arnold-Schrauf C, Hesse C, et al. Selective and efficient generation of functional Batf3-dependent CD103+ dendritic cells from mouse bone marrow. *Blood, The Journal of the American Society of Hematology.* 2014;124(20):3081-91.

70. Quah BJ, Warren HS, and Parish CR. Monitoring lymphocyte proliferation in vitro and in vivo with the intracellular fluorescent dye carboxyfluorescein diacetate succinimidyl ester. *Nature protocols.* 2007;2(9):2049-56.

CHAPTER 5

SENESCENT CELLS DISPLAY DIFFERENT SENSITIVITY TO BCL-2 INHIBITOR ABT-263 ASSOCIATED SENOLYTIC ACTIVITY

This chapter consists of a draft manuscript:

Y Liu, D Wu, S J Kron. The senescent bystander effects enhance the sensitivity of tumor cells to Bcl-2 inhibitor.

I am responsible for preliminary experiments. Wu and I are both responsible for completing the project.

5.1 Introduction

Cellular senescence is a process in which cells undergo prolonged cell cycle arrest and develop distinctive phenotypic alterations, including enlarged morphology, dysregulated metabolism, altered epigenetic modification, increased expression of the senescence-associated beta galactosidase (SA- β-Gal), cyclin-dependent inhibitors such as $p16^{INK4a}$ (CDKN1A) and $p21^{CIP1}$ (CDKN1A), Bcl-2 family members and others (1). Senescent cells secret abundant soluble and insoluble factors, including cytokines, chemokines, growth factors, matrix metalloprotein kinase, lipids, nucleotide acids and vesicles, which are collectively termed as senescence-associated secretion phenotype (SASP) (2-4). Together with cell-cell contacts, SASP contributes to the complex crosstalk between senescent cells and the local cells, including neoplastic cells, stromal cells, and immune cells (5).

Cells become senescence after extensive replication that causes telomere shortening or from exposure to genotoxic, oncogenic, and/or oxidative stress (6). Many cancer therapies, involving ionizing radiation, alkylating agents, topoisomerase poisons, cyclin-dependent kinase 4/6 inhibitors, PARP inhibitors, BRAF inhibitors, EGFR receptors, and androgen deprivation, have been considered to induce both malignant and non-malignant cells into senescence, termed therapy induced senescence (TIS) (4, 7). TIS was purported as a beneficial outcome of cancer therapy considering their incapability of proliferation. However, it has been recognized that accumulated TIS cells play critical roles in promoting tumor relapse, metastasis, and therapy resistance through paracrine effects (8), as well as organ dysfunctions which may account for many adverse effects of cancer therapies (9). Interestingly, senescent cells can potentiate their own effects by inducing senescence in the neighboring cells (10).

To diminish TIS cells associated deleterious effects, the investigation about targeting senescent cells has rapidly expanded and led to a novel one-two punch cancer therapy approach (11). For the first punch, cancer therapies, while accomplishing tumor cell killing, also induce senescence in both tumor and normal tissues. For the second punch, senescent cells are selectively eliminated by senolytics, a class of compounds that preferentially induce cell death in senescent cells. It has been reported that genetic and pharmacological removal of TIS cells reduces side effects and inhibits tumor relapse and metastasis (12). The promising outcomes of senothrapies, which is originally identified in the studies of aging (13), has led to extensive investigation and yielded a wide range of chemical agents. Prominent examples that have advanced to preclinical and/or clinical studies include natural products such as quercetin (14) and fisetin (15), the receptor tyrosine kinase inhibitor dasatinib (14), the BH3 mimetics such as navitoclax (ABT-263) (15, 16), ABT-737 (17). Other senolytic drugs, such as HDAC inhibitor and BET inhibitor, are also under development.

Currently, navitoclax, an inhibitor targeting Bcl-2 family proteins, is one of the most promising candidates in senolysis preclinical studies for alleviating aging-related diseases and one-two punch cancer therapies. Clearance of TIS cells by navitoclax has been reported to enhance tumor regression and overall survival in multiple murine tumor models (16, 18, 19). Navitoclax has shown remarkable capacity in targeting senescent tumor cells induced by various therapeutic interventions, including radiation (16, 20), PARP inhibitor Olaparib (19), anti-tumor antibiotic doxorubicin (16), topoisomerase poison etoposide (20, 21), aurora kinase inhibitor (21), and BET inhibitor (22). However, a recent study reported that senescent prostate cancer cells induced by enzalutamide, an androgen receptor inhibitor, are not sensitive to navitoclax, indicating that senescence inducers appear to dictate senolytic sensitivity of senescent cells (20).

Here, we utilized p53 WT mouse colon carcinoma CT26 cells, induced cellular senescence dependent or independent of DNA damage, and compared their sensitivity to navitoclax. Consistent with the prior study (20), we observed a positive correlation between DNA damage response and navitoclax sensitivity in senescent cancer cells. The p53 deficient mouse breast cancer 4T1 cells and human breast cancer MDA-MB-231 cells displayed the complementary navitoclax response, indicating that the navitoclax sensitivity of senescent cells is independent of p53 status. The expression level of BH3-only proteins in senescent cells appeared not to explain their navitoclax sensitivity. We further investigated how senescent cells affect the navitoclax response of the bystander cells through direct or transwell coculture experiments. And we observed that senescent cells which are hypersensitive to navitoclax (e.g., senescence induced by etoposide or IR+veliparib) are able to promote navitoclax induced apoptosis in the neighboring non-senescent cells in a SASP-dependent manner. These experiments elucidated that senescent cells modulate the local response to navitoclax treatment both cell through both autonomous or non- autonomous mechanisms. Our studies revealed that the critical roles of senescence inducers in precepting the navitoclax sensitivity of senescent cells and the bystander non-senescent cells. These findings suggest a reevaluation of the choice of senescence inducers for navitoclax involved one-two punch cancer therapies.

5.2 Results

Therapy induced senescence (TIS) can be generated either dependent or independent of DNA damage

It has been reported that many treatments, including chemo- and radio-therapies, are able to induce senescence in a plethora of cancer cell lines (Ref). As such, we utilized mouse colon carcinoma CT26 cells and examined the senescence induction capability of various preclinical and clinical treatments: CDK4/6 inhibitor Palbociclib (10 μM), PLK1 inhibitor GSK461364 (5 μM), topoisomerase II poison Etoposide (2 μM), 12 Gy irradiation (IR) and the combination of IR with PARP inhibitor veliparib (20 μM), or DNA-PKcs inhibitor NU7026 (10 μM). DMSO treatment was used as control. 5 days after treatment, we examined senescence-associated β-galactosidase (SA-βGal) and cell morphology. Senescent cells were not observed when treated with DMSO vehicle. Palbociclib, GSK461364, and Etoposide induced xx%. ~ 70% SA-βGal+ cells were observed after a single dose of IR, while the addition of Veliparib or NU7026 increased it to xx% or xx% respectively (Figure 5.1A). As shown in the images, even among the cells not judged as senescent, few displayed the characteristic size and shape of proliferating CT26 cells. The same treatments were applied to p53 deficient mouse breast cancer 4T1 cells, and human triple negative breast cancer MDA-MB-231 cells and similar efficiencies of senescence induction were observed.

Cellular senescence can be induced dependent or independent of DNA damage signaling. To evaluate whether the senescence induced above is associated with DNA damage, CT26 cells were treated with Palbociclib, GSK461364, Etoposide, 12 Gy IR and the combination of IR with Veliparib or NU7026, incubated 24 h, and examined by immunofluorescence for γH2AX foci as markers for persistent chromosomal double strand breaks (DSBs). Compared to DMSO control,

CT26 cells treated with Palbociclib or GSK461364 displayed comparable number and pattern of γH2AX foci, which may or may not be ascribed to damaged DNA (23). Etoposide treatment induced numerous bright γH2AX foci in CT26 cells. IR alone also led to persistent γH2AX foci while the addition of Veliparib or NU7026 significantly increased the foci number. Although all the treatments are capable of inducing cellular senescence, Palbociclib or GSK461364 appeared not to create DNA damage, while Etoposide (2 μM), IR, IR+Veliparib or IR+NU7026 damaged the DNA seriously (Figure 5.2B). Notably, cells treated with IR+NU7026 may contain the similar amount unrepaired DNA damage compared to IR treatment (24), while Veliparib may have delayed DNA repair (25).

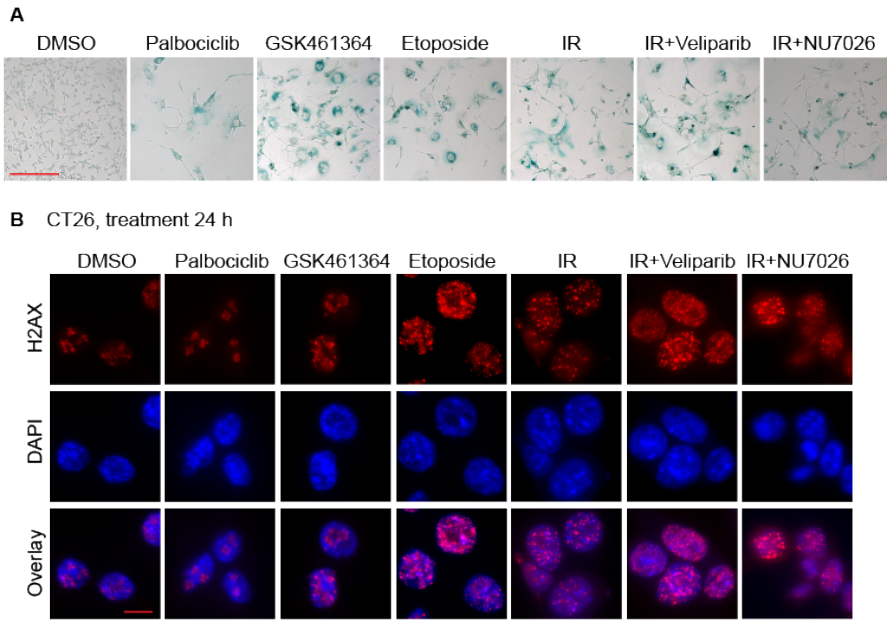

Figure 5.1 Cellular senescence can be induced through DNA damage dependent or independent manner.
A, SA-beta-gal staining of senescent cells. B, CT26 cells were treated the same as in A, then fixed and stained 24 h after treatment. Shown are represented pseudo-colored images of immunofluorescence with anti-γH2AX (red), DAPI (blue), and a two-color overlay. Scale bars, 20 μm.

Senescence inducers dictate the sensitivity of senescent cells to Navitoclax (ABT-263)

A recent study reported that navitoclax displays senolysis activity in senescent cells triggered by olaparib, a trapping PAPR inhibitor that caused DNA damage, while navitoclax loses its potency in targeting senescent cells induced with androgen receptor inhibitor enzalutamide (20). As the senescence we described above were generated through various mechanisms, we compared their sensitivity to navitoclax. CT26 cells were treated with DMSO control, Palbociclib, GSK461364, Etoposide, IR, IR+veliparib, or IR+NU7026 for 5 days, followed by incubating with increased doses of navitoclax (0-5 μM) for 24 hours. Then the cell viability was measured through the MTT assays (26) (Figure 5.2A). The control proliferating cells were not sensitive and remained > 80% viability when exposed to 2.5 μM navitoclax. With 2.5 μM navitoclax treatment, ~ 50% palbociclib or GSK461364 induced senescent cells survived, while only ~ 30% viability was observed with etoposide induced senescent cells. At lower navitoclax concentration (< 2.5 μM), etoposide induced senescent cells also displayed higher sensitivity compared to palbociclib or GSK461364. Senescent cells created by palbociclib or GSK461364 showed a similar sensitivity to low concentrations of navitoclax (< 2.5 μM) while palbociclib triggered senescence was more resistant to navitoclax at high dose (5 μM). ~50% of senescent cells induced by 12 Gy IR alone persisted after 2.5 μM navitoclax treatment, while the percentage of viability decreased to ~45% and ~25% respectively for senescence generated through the combination of IR and NU7026 or Veliparib. Notably, even 1.25 μM navitoclax is sufficient to eliminate over 50% senescent cells induced by IR+Veliparib. The similar experiments were conducted in p53 deficient 4T1 and MDA-MB-231 cells (Figure 5.2B and C). As is shown in Figure 5.2A, etoposide or IR+Veliparib induced senescence displayed the hypersensitivity to navitoclax compared to senescent cells created through other treatments.

These results indicated that the navitoclax sensitivity of senescent cells is determined by senescence inducer and associated mechanisms, which seemed to be independent of p53 status. Although our results also appeared to display a positive correlation between persistent DNA damage of senescent cells and their sensitivity to navitoclax, more studies are required to concrete and explain this observation.

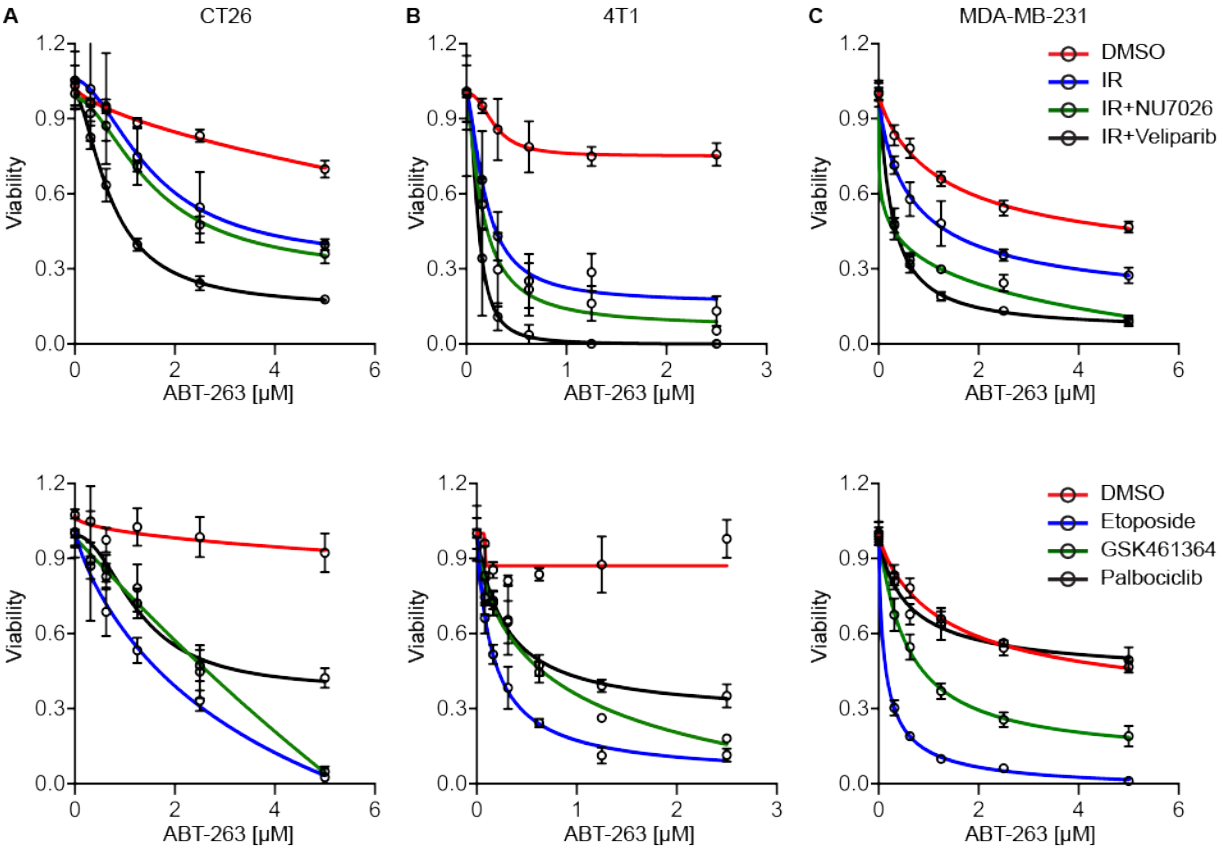

Figure 5.2 The sensitivity of senescent cells to navitoclax induced senolysis varies dependent on the senescence inducers.
A-C, Dose-response curves indicating the viability of CT26 (A), 4T1 (B), and MDA-MB-231 (C) cells. Cells were treated with with DMSO, Palbociclib (10 μM), Etoposide (2 μM), GSK461364 (5 μM), 12 Gy IR, IR+Veliparib (20 μM), or IR+NU7026 (10 μM) for 5 days, and then 24 hours with navitoclax at indicated concentrations (0-5 μM). Cell viability was determined by MTT assay. Data from three replicates, mean ± s.d.

The elevated expression of Bcl-2 family proteins has been considered a mechanism that overcomes pro-apoptotic stresses in senescent cells (1, 17). As a BH3 mimetic, navitoclax inhibits Bcl-2, Bcl-x_L and Bcl-w, though its senolysis activity is mainly ascribed to the inhibition of Bcl-w and/or Bcl-x_L (16) while the inhibition Bcl-2 appears to be dispensable (17, 27). However, not all senescent cells display apoptosis resistance dependent on Bcl-2 proteins (18, 28). The senescent cells with low level of NOXA rely on the anti-apoptotic functions of MCL1, and displays resistance to navitoclax (18). To examine whether the navitoclax sensitivity in senescent cells is associated with NOXA and/or other BH3-only proteins, we collected whole cell lysate from control proliferating CT26 cells and senescent CT26 cells induced by GSK461364, Rtoposide, IR, and IR+veliparib (10 μM). The Western blot analysis for NOXA, Bim, and Bak did not show clear differences between navitoclax sensitive and insensitive senescent cells. Similarly, no such pattern was observed in senescent 4T1 cells (Figure 5.3).

Senescent cells enhance the sensitivity of their neighboring non-senescent cells to navitoclax via bystander effects

It has been extensively studied that senescent cells affect their neighboring cell through non-autonomous mechanisms (SASP), which contribute to extracellular matrix remodeling, cell growth alteration, and immune response (29, 30). However, the cancer field has yet to provide insights about how senescent cells regulate the navitoclax response in the adjacent non-senescent cells. To study this, we created navitoclax sensitive senescence through treating CT26 cells with etoposide or 12 Gy IR+veliparib for 5 days. Then the control proliferating cells or senescent cells were cocultured with CellTrace Far Red labeled non-senescent CT26 cells overnight, followed by incubating in the presence or absence of navitoclax (5 μM) for 24 h. The cell apoptosis and/or

death were analyzed by co-staining the cells with annexin-V, a protein that binds to phosphatidylserine which flips to the outer leaflet of cell membrane during apoptosis, and propidium iodide (PI), a nucleic acid dye that is permeant to dead cells but not to live cells. The percentage of cell apoptosis and/or death in the bystander non-senescent cells were quantified using flow cytometry (Figure 5.4A). Compared to proliferating cells, senescent cells appeared to increase the overall apoptosis of the bystander cells, which is potentially due to the increasing DNA damage (10). Under 5 μM navitoclax, ~15% apoptosis (Annexin V+/ PI-) and ~5% death (Annexin V+/ PI-) of non-senescent cells were observed with treatment when cocultured with proliferating cells. However, the percentage of apoptotic and dead cells increased to 35% and 25%, or 30% and 22% respectively when cocultured with senescent cells triggered by IR+veliparib or etoposide. A similar enhancement of apoptosis in the bystander non-senescent cells was observed with 10 μM navitoclax when cocultured with senescent cells (Figure 5.4B). Such effects were also detected in 4T1 cells.

Senescent cells conduct bystander effect through both SASP (31, 32) and gap-junction mediated cell-cell contact (10). Towards investigating whether cell-cell contact is required for senescence mediated navitoclax sensitivity, we created cellular senescence in transwell by IR alone or IR+Veliparib, and seeded non-senescent CT26 cells into transwell inserts with 0.4 μm pores, which allows the permeant of SASP factors while blocks the contact between senescent and non-senescent cells. Then 0 or 5 μM navitoclax was added into the transwell inserts. After 24 h, the apoptosis and/or death of cells from the transwell inserts were analyzed through annexin V-PI double staining (Figure 5.4C). Consistent with coculture experiment results, senescent cells promoted apoptosis in the neighboring non-senescent cells even without navitoclax treatment, while IR+veliparib induced senescence displayed stronger effects. 5 μM

navitoclax triggered 16.2% apoptosis (Annexin V+/ PI-) and 3.4% cell death (Annexin V+/ PI+) in non-senescent CT26 cells. These were further increased to 18.2% and 4.3%, or 26.7% and 7.0% respectively when non-senescent cells were cocultured with IR or IR+veliparib driven senescence (Figure 5.4D). These results indicated that SASP is sufficient to reprogram the navitoclax response of the neighboring non-senescent cells.

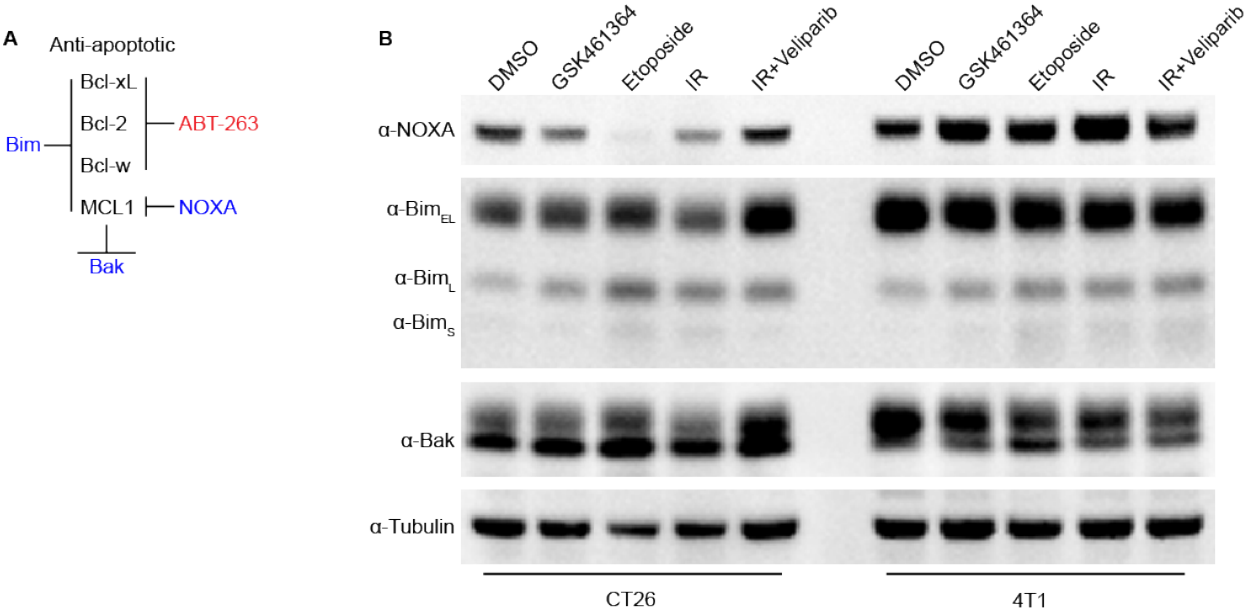

Figure 5.3 The expression of BH3-only proteins in senescent cells.
A, Simplified schematic representation of the interaction between anti-apoptotic proteins (Black) and BH3-only proteins (Blue). B, Western blot analysis of the BH3-only proteins in senescent cells. CT26 and 4T1 cells were treated for 5 days with DMSO control, GSK461364 (5 μM), Etoposide (2 μM), 12 Gy IR, or IR+verliparib (20 μM). Then the whole cell lysate was collected for Western blot analysis. Shown strips are NOXA (10 kD), Bim (Bim_S 12 kD, Bim_L 15kD, Bim_{EL} 23 kD), Bak (25 kD), and tubulin loading control (55 kD).

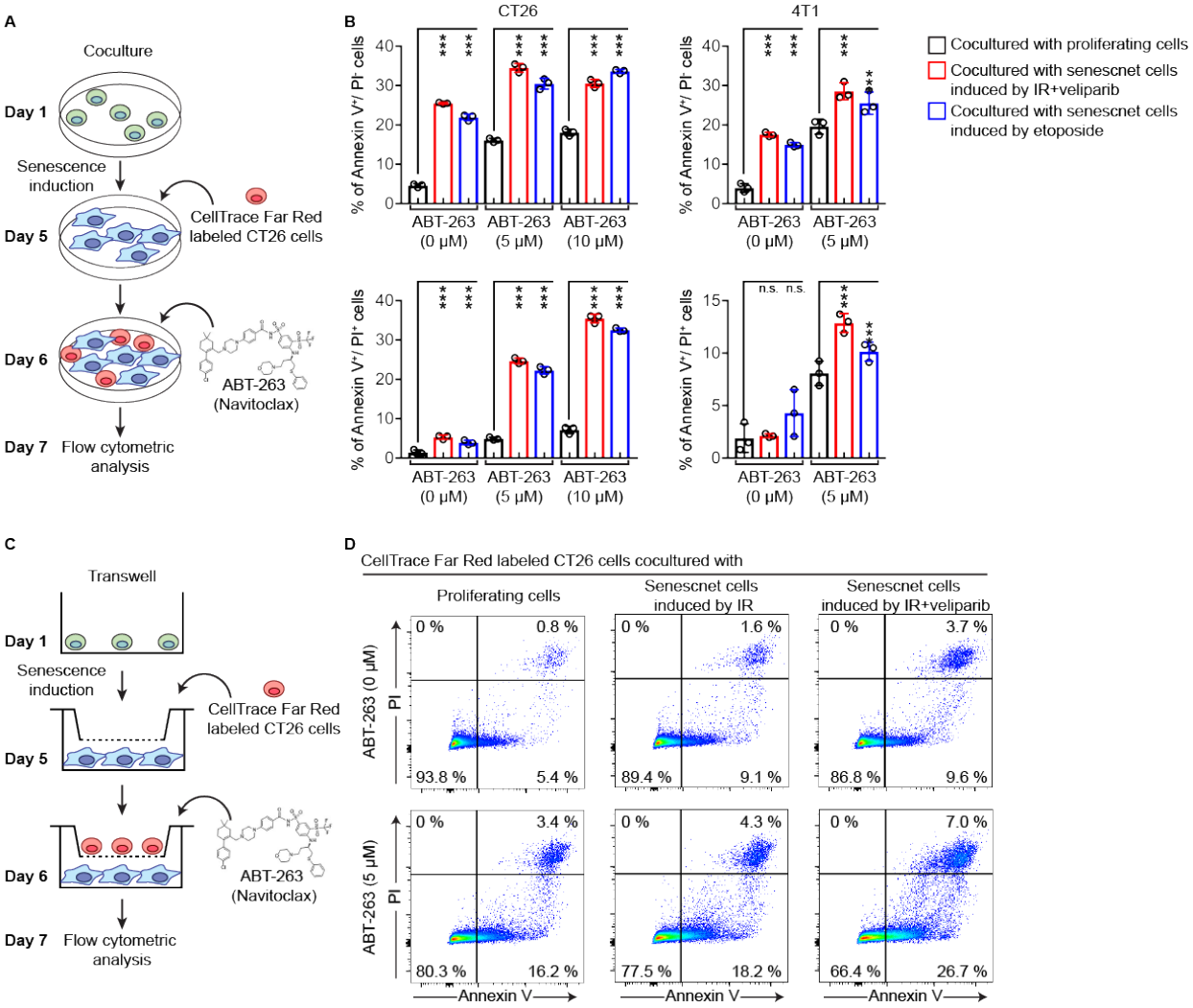

Figure 5.4 Senescent cells enhance the sensitivity of their neighboring non-senescent cells to navitoclax via bystander effects.

A, Schematic of the coculture experiment. CT26 cells were treated for 4 days with DMSO control, Etoposide (2 μM), or 12 Gy IR+veliparib (20 μM), and cocultured with CellTrace™ Far Red dye labeled proliferating CT26 cells overnight. Then the mixed cells were incubated with 0, 5, or 10 μM navitoclax for 24 h. The navitoclax induced cell death and apoptosis was analyzed through flow cytometry. B, Quantitative analysis of cell apoptosis/death. Cells were prepared as described in A, and stained with annexin V and PI for flow cytometric analysis. Far Red$^+$ single cell population were analyzed. Shown from three experiments, mean ± s.d. *** $P < 0.001$, ** $0.001 < P < 0.01$, ns $P > 0.05$ (unpaired t-test). C, Schematic of the transwell coculture experiment. CT26 cells seeded in transwell were treated for 4 days with DMSO control, 12Gy IR, or IR+veliparib (20 μM). The CellTrace™ Far Red dye labeled proliferating CT26 cells were seeded in the transwell inserts and cocultured overnight with senescent cells or proliferating cells as control. 0 or 5 μM navitoclax was added in the transwell insert for 24 h incubation. Cell death and apoptosis was analyzed through flow cytometry the same as in A. D, Represented flow cytometric dot plots of the non-senescent cells in transwell inserts. Cells were prepared as described in C, then stained with annexin V and PI for flow cytometric analysis. Shown are gated Far Red$^+$ single cell populations.

5.3 Discussion

Our studies indicated that senescent cells induced by different stimuli display various sensitivity to ABT-263 induced apoptosis. Consistent with a recent publication, DNA damage-associated senescence appeared more sensitive to ABT-263 treatment than DNA damage-independent senescence. This observation is consistent with a recent study in which senescent cells were created by DNA damage inducers radiation, olaparib, or non-DNA damage agent enzalutamide (20). However, no discernible patterns were observed in the expression of BH3 proteins in DNA damage-dependent or independent senescent cells. The molecular mechanisms that regulate the response of senescent cells to ABT-263 treatment are under investigation. Furthermore, this study revealed that senescent cells sensitize their neighboring non-senescent cells to ABT-263 induced apoptosis through paracrine effects. It has been long observed that senescent cells are able to modulate their bystander non-senescent cells, termed bystander effects (10). Several studies have demonstrated that senescent cells spread senescence toward their neighbors via gap junctions or secretion in vitro, where NF-kB signaling appears to be a critical player during this process (10, 31, 33-35). However, it remains to be determined how senescent cells increase the sensitivity of non-senescent nearby cells to ABT-263.

Since radiation therapy is widely used in cancer treatment and may induce both cell death and senescence in tumors, one strategy to improve treatment outcomes is to target senescent cells with senolytic compounds, such as ABT-263, after the onset of cellular senescence, also known as the "one-two punch" approach (11, 36). Meanwhile, veliparib has been reported as a radiosensitizer that enhances IR-associated senescence both in vitro and in vivo (37, 38). Interestingly, our studies revealed that senescence induced by IR+veliparib displays greater sensitivity to ABT-263 and stronger bystander effects on neighboring cells compared to

senescence induced by IR alone. These results suggested the potential of veliparib in sensitizing radiated tumors to senolytic involved "one-two punch" cancer therapy. The timing and dosage of veliparib treatment may need to be examined in future in vivo studies in order to improve radiotherapy in terms of the "one-two punch" strategy.

5.4 Material and Methods

Cell line and tissue culture

The mouse colon carcinoma cell line CT26 (HTB-85), mouse breast mammary carcinoma cell line 4T1, and human breast cancer cell line MDA-MB-231 were obtained from ATCC. The murine cells were maintained in RPMI 1640 (Thermo Fisher Scientific) supplemented with 10% FBS (Atlanta Biologicals) and 1% penicillin/streptomycin (Thermo Fisher Scientific). The human cells were maintained in DMEM containing 4.5 g/l glucose (Thermo Fisher Scientific) supplemented with 10% Tet-approved FBS (Atlanta Biologicals) and 1% penicillin/streptomycin (Thermo Fisher Scientific). The cells were tested for mycoplasma contamination and authenticated by a short tandem repeat profile (IDEXX BioResearch) prior to performing experiments. All experiments were performed within 3 to 10 passages after thawing cells.

DNA damage foci staining

Cells were seeded on cover glass at 30,000 per well in 24-well plates, treated with DMSO, Palbociclib (10 μM), GSK461364 (5 μM), Etoposide (2 μM), 12 Gy irradiation (IR) and the combination of IR with PARP inhibitor veliparib (20 μM) or NU7026 (10 μM). The inhibitors were added 1 h prior to irradiation. 24 h after irradiation, cells were fixed with 4% PFA and permeabilized with 0.2% Triton-X 100 for 10 min. After blocking with 5% BSA, primary antibodies for γH2AX (Millipore, 05-636, 1:1000) were then incubated on cell slides overnight at 4°C. Following PBS washes, fluorescent secondary antibodies (Jackson ImmunoResearch) were applied for 1 h at room temperature. Cell slides were mounted with ProLong Gold after PBS washes. Foci images were captured on a Zeiss Axiovert 40CFL with a

40X Plan-NeoFluar objective and pseudo-colored using ImageJ. Two or more replicates were performed.

SA-βGal assay

Cells were seeded at 40,000 per well in six-well plates, treated with Palbociclib (10 μM), GSK461364 (5 μM), Etoposide (2 μM), 12 Gy irradiation (IR) and the combination of IR with PARP inhibitor veliparib (20 μM) or NU7026 (10 μM). The inhibitors were added 1 h prior to irradiation. 5 or 6 days after treatment, cells were fixed in 2% PFA and stained for 16 h at 37 °C. Staining buffer contains 1 mg/ml X-Gal (X4281C, Golden Bio), 40 mM Citric acid/sodium phosphate, 150 mM NaCl, 2 mM MgCl2, 3.3 mM $K_3[Fe(CN)_6]$, 3.3 mM $K_4[Fe(CN)_6]$, pH 6. After staining, images were captured on a Zeiss Axiovert 200M microscope with a 20× Plan-NeoFluar objective and Axiocam digital camera. SA-β-Gal-positive and -negative cells were counted in more than 5 fields, yielding an average percentage indicated on each SA-βGal image as mean ± s.d. Two or more replicates were performed.

MTT assays

Cells were seeded at 2,000 per well in 96-well plates and treated with DMSO, Palbociclib (10 μM), Etoposide (2 μM), GSK461364 (5 μM), 12 Gy IR, IR+Veliparib (20 μM), or IR+NU7026 (10 μM) as described above. 5 or 6 days later, MTT assays were conducted as previously described (26). Briefly, MTT solution contains 6 mM MTS and 0.33 mM PMS, PH 5.2-5.4. The cell cultured medium was removed and 100 μL MTT solution was added each well immediately. The plates were incubated for 1.5 h at 37 °C and the absorbance was measured at 570 nm using a Synergy Neo HST Plate Reader.

Western blot

200,000 cells were plated in P-100 Petri dishes and treated with DMSO, Etoposide (2 μM), GSK461364 (5 μM), 10 Gy IR, or IR+veliparib (20 μM). 5 or 6 days later, cells were harvested by scraping in 1 ml lysis buffer. Whole-cell lysates were prepared using RIPA lysis reagent (Thermo Fisher Scientific) in the presence of protease and phosphatase inhibitors (Thermo Fisher Scientific). 20 μg of protein was loaded per well, separated on a NuPage 4-12% Tris-Base precast gels (Invitrogen), and transferred onto a PVDF membrane (Millipore). After dividing blots into strips by apparent molecular mass, immunoblotting was performed using NOXA, Bim, Bak, and Tubulin primary antibodies (Cell Signaling Technology) and detected with peroxidase-conjugated secondary antibodies (Thermo Fisher Scientific, NA934vs or NA931). This was followed by detection with ECL peroxidase substrate (Thermo Fisher Scientific).

Coculture assays

Cells were seeded at 40, 000 per well in six-well plates and treated with DMSO, Etoposide (2 μM), 12 Gy IR, or IR+Veliparib (20 μM) as described above. 4 or 5 days later, media was removed, cells were washed twice with PBS, followed by replacement of fresh media. To prepare cells for coculture, proliferating cells were collected at ~ 1 million cells/ mL in PBS, incubated with 1 μM CellTrace™ Far Red dye (Invitrogen) for 10 min at 37 °C, and then washed in complete medium twice. For direct coculture experiments, 20,000 labeled cells were directly added into the same well with senescent cells. For coculture experiments using transwell, 20,000 labeled cells were seeded in the transwell inserts, and the transwell inserts were put onto the

wells where senescent cells were cultured. After overnight coculture, the mixed cells were treated with 0, 5 or 10 μM ABT263 for 24 h, followed by flow cytometric analysis of cell apoptosis/death using annexin V-PI double staining assay.

Annexin V-propidium iodide (PI) double staining

The staining was performed using FITC Annexin V/Dead Cell Apoptosis Kit (Invitrogen) according to the manufacture's protocol. Briefly, attached cells were collected from plates using accutase and mixed with suspended cells. The mixed cells were washed in cold PBS and incubated in 1x annexin binding buffer containing FITC annexin V and 1 μg/mL PI for 15 min at room temperature. Cells were analyzed using BD Fortessa 4-15 HTS Flow cytometer. FITC Annexin V signal was measured using a 488-nm laser for excitation and a 525/50 filter for detection, while PI signal was measured using a 561-nm laser for excitation and a 582/15 filter for detection. Data were analyzed by FlowJo univariate cell cycle analysis.

Statistical analysis

Statistical significance was determined using the non-paired Student's *t*-test. Calculations were performed using Prism software (GraphPad) or Excel. $P \leq 0.05$ was considered statistically significant.

5.5 References

1. Hernandez-Segura A, Nehme J, and Demaria M. Hallmarks of cellular senescence. *Trends in cell biology.* 2018;28(6):436-53.

2. Basisty N, Kale A, Jeon OH, Kuehnemann C, Payne T, Rao C, et al. A proteomic atlas of senescence-associated secretomes for aging biomarker development. *PLoS biology.* 2020;18(1):e3000599.

3. Campisi J. Aging, cellular senescence, and cancer. *Annual review of physiology.* 2013;75:685-705.

4. Prasanna PG, Citrin DE, Hildesheim J, Ahmed MM, Venkatachalam S, Riscuta G, et al. Therapy-induced senescence: opportunities to improve anticancer therapy. *JNCI: Journal of the National Cancer Institute.* 2021;113(10):1285-98.

5. Lee S, and Schmitt CA. The dynamic nature of senescence in cancer. *Nature cell biology.* 2019;21(1):94-101.

6. Muñoz-Espín D, and Serrano M. Cellular senescence: from physiology to pathology. *Nature reviews Molecular cell biology.* 2014;15(7):482-96.

7. Ewald JA, Desotelle JA, Wilding G, and Jarrard DF. Therapy-induced senescence in cancer. *JNCI: Journal of the National Cancer Institute.* 2010;102(20):1536-46.

8. Saleh T, Bloukh S, Carpenter VJ, Alwohoush E, Bakeer J, Darwish S, et al. Therapy-induced senescence: An “old” friend becomes the enemy. *Cancers.* 2020;12(4):822.

9. Demaria M, O'Leary MN, Chang J, Shao L, Liu S, Alimirah F, et al. Cellular senescence promotes adverse effects of chemotherapy and cancer relapse. *Cancer discovery.* 2017;7(2):165-76.

10. Nelson G, Wordsworth J, Wang C, Jurk D, Lawless C, Martin-Ruiz C, et al. A senescent cell bystander effect: Senescence-induced senescence. *Aging cell.* 2012;11(2):345-9.

11. Sieben CJ, Sturmlechner I, van de Sluis B, and van Deursen JM. Two-step senescence-focused cancer therapies. *Trends in cell biology.* 2018;28(9):723-37.

12. Myrianthopoulos V, Evangelou K, Vasileiou PV, Cooks T, Vassilakopoulos TP, Pangalis GA, et al. Senescence and senotherapeutics: a new field in cancer therapy. *Pharmacology & Therapeutics.* 2019;193:31-49.

13. Robbins PD, Jurk D, Khosla S, Kirkland JL, LeBrasseur NK, Miller JD, et al. Senolytic drugs: reducing senescent cell viability to extend health span. *Annual review of pharmacology and toxicology.* 2021;61:779-803.

14. Zhu Y, Tchkonia T, Pirtskhalava T, Gower AC, Ding H, Giorgadze N, et al. The Achilles' heel of senescent cells: from transcriptome to senolytic drugs. *Aging cell.* 2015;14(4):644-58.

15. Zhu Y, Doornebal EJ, Pirtskhalava T, Giorgadze N, Wentworth M, Fuhrmann-Stroissnigg H, et al. New agents that target senescent cells: the flavone, fisetin, and the BCL-XL inhibitors, A1331852 and A1155463. *Aging (Albany NY).* 2017;9(3):955.

16. Saleh T, Carpenter VJ, Tyutyunyk-Massey L, Murray G, Leverson JD, Souers AJ, et al. Clearance of therapy-induced senescent tumor cells by the senolytic ABT-263 via interference with BCL-XL–BAX interaction. *Molecular oncology.* 2020;14(10):2504.

17. Yosef R, Pilpel N, Tokarsky-Amiel R, Biran A, Ovadya Y, Cohen S, et al. Directed elimination of senescent cells by inhibition of BCL-W and BCL-XL. *Nature communications.* 2016;7(1):1-11.

18. Shahbandi A, Rao SG, Anderson AY, Frey WD, Olayiwola JO, Ungerleider NA, et al. BH3 mimetics selectively eliminate chemotherapy-induced senescent cells and improve response in TP53 wild-type breast cancer. *Cell Death & Differentiation.* 2020;27(11):3097-116.

19. Fleury H, Malaquin N, Tu V, Gilbert S, Martinez A, Olivier M-A, et al. Exploiting interconnected synthetic lethal interactions between PARP inhibition and cancer cell reversible senescence. *Nature communications.* 2019;10(1):1-15.

20. Malaquin N, Vancayseele A, Gilbert S, Antenor-Habazac L, Olivier M-A, Ait Ali Brahem Z, et al. DNA damage-but not enzalutamide-induced senescence in prostate cancer promotes senolytic Bcl-xL inhibitor sensitivity. *Cells.* 2020;9(7):1593.

21. Wang L, de Oliveira RL, Wang C, Neto JMF, Mainardi S, Evers B, et al. High-throughput functional genetic and compound screens identify targets for senescence induction in cancer. *Cell reports.* 2017;21(3):773-83.

22. Gayle SS, Sahni JM, Webb BM, Weber-Bonk KL, Shively MS, Spina R, et al. Targeting BCL-xL improves the efficacy of bromodomain and extra-terminal protein inhibitors in triple-negative breast cancer by eliciting the death of senescent cells. *Journal of Biological Chemistry.* 2019;294(3):875-86.

23. McManus KJ, and Hendzel MJ. ATM-dependent DNA damage-independent mitotic phosphorylation of H2AX in normally growing mammalian cells. *Molecular biology of the cell.* 2005;16(10):5013-25.

24. Liu Y, Efimova EV, Ramamurthy A, and Kron SJ. Repair-independent functions of DNA-PKcs protect irradiated cells from mitotic slippage and accelerated senescence. *Journal of cell science.* 2019;132(13):jcs229385.

25. Efimova EV, Mauceri HJ, Golden DW, Labay E, Bindokas VP, Darga TE, et al. Poly (ADP-ribose) polymerase inhibitor induces accelerated senescence in irradiated breast cancer cells and tumors. *Cancer research.* 2010;70(15):6277-82.

26. Cory AH, Owen TC, Barltrop JA, and Cory JG. Use of an aqueous soluble tetrazolium/formazan assay for cell growth assays in culture. *Cancer communications.* 1991;3(7):207-12.

27. Zhu Y, Tchkonia T, Fuhrmann-Stroissnigg H, Dai HM, Ling YY, Stout MB, et al. Identification of a novel senolytic agent, navitoclax, targeting the Bcl-2 family of anti-apoptotic factors. *Aging cell.* 2016;15(3):428-35.

28. Sasaki M, Kumazaki T, Takano H, Nishiyama M, and Mitsui Y. Senescent cells are resistant to death despite low Bcl-2 level. *Mechanisms of ageing and development.* 2001;122(15):1695-706.

29. Coppé J-P, Desprez P-Y, Krtolica A, and Campisi J. The senescence-associated secretory phenotype: the dark side of tumor suppression. *Annual Review of Pathology: Mechanisms of Disease.* 2010;5:99-118.

30. Faget DV, Ren Q, and Stewart SA. Unmasking senescence: context-dependent effects of SASP in cancer. *Nature Reviews Cancer.* 2019;19(8):439-53.

31. Nelson G, Kucheryavenko O, Wordsworth J, and von Zglinicki T. The senescent bystander effect is caused by ROS-activated NF-κB signalling. *Mechanisms of ageing and development.* 2018;170:30-6.

32. Liao E, Hsu Y, Chuah Q, Lee Y, Hu J, Huang T, et al. Radiation induces senescence and a bystander effect through metabolic alterations. *Cell death & disease.* 2014;5(5):e1255-e.

33. da Silva PFL, Ogrodnik M, Kucheryavenko O, Glibert J, Miwa S, Cameron K, et al. The bystander effect contributes to the accumulation of senescent cells in vivo. *Aging Cell.* 2019;18(1):e12848.

34. Sapega O, Mikyskova R, Bieblova J, Mrazkova B, Hodny Z, and Reinis M. Distinct phenotypes and 'bystander' effects of senescent tumour cells induced by docetaxel or immunomodulatory cytokines. *Int J Oncol.* 2018;53(5):1997-2009.

35. Nelson G, Kucheryavenko O, Wordsworth J, and von Zglinicki T. The senescent bystander effect is caused by ROS-activated NF-kappaB signalling. *Mech Ageing Dev.* 2018;170:30-6.

36. Wang L, and Bernards R. Taking advantage of drug resistance, a new approach in the war on cancer. *Front Med.* 2018;12(4):490-5.

37. Meng Y, Efimova EV, Hamzeh KW, Darga TE, Mauceri HJ, Fu YX, et al. Radiation-inducible immunotherapy for cancer: senescent tumor cells as a cancer vaccine. *Mol Ther.* 2012;20(5):1046-55.

38. Michmerhuizen AR, Pesch AM, Moubadder L, Chandler BC, Wilder-Romans K, Cameron M, et al. PARP1 Inhibition Radiosensitizes Models of Inflammatory Breast Cancer to Ionizing Radiation. *Mol Cancer Ther.* 2019;18(11):2063-73.

CHAPTER 6

DISCUSSION

This thesis mainly focused on cancer cell senescence and discussed its induction strategies, functions in cancer therapy, and elimination using senolytics (Figure 6.1).

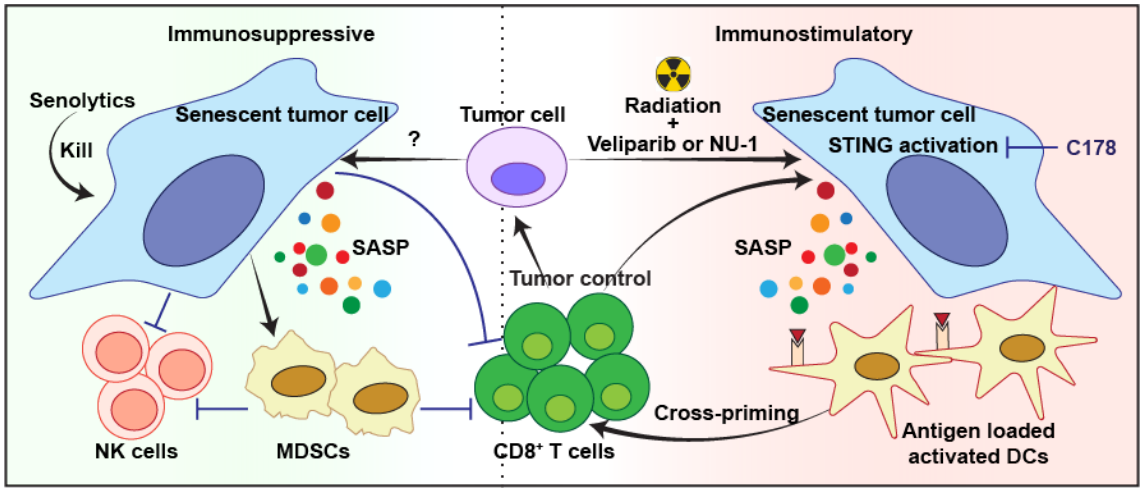

Figure 6.1: Tumor cell senescence in cancer therapy.
Treatment-induced tumor cell senescence can either be beneficial or detrimental in cancer treatment. The results of this thesis suggest that senescent cells induced by radiation and veliparib (PAPR1/2 inhibitor) or radiation and NU-1 (TERT inhibitor) are immunogenic. These senescent cells stimulate dendritic cell activity/maturing, which primes T cells and increases anti-tumor immunity. STING activation in senescent cells was found to be necessary for DC stimulation, though the precise mechanisms remain to be determined. However, we cannot ignore the fact that certain types of senescent tumor cells can serve as the immunosuppressive mechanism by promoting myeloid-derived suppressor cells (MDSCs) to suppress cytotoxic immune cells or directly inhibit them natural killer cells and T cells. One promising way to eliminate the harmful effects of senescence is to target senescent cells with senolytics.

The studies here demonstrated the DNA repair independent role of DNA-PKcs in response to radiation (1). Inhibition of DNA-PKcs led to persistent DNA damage foci after radiation through unleashing the activity of ATM, an essential enzyme that phosphorylates H2AX and thus contributes to the formation of foci complex, instead of blocking DNA repair (1). While ATM can activate DNA-PKcs (2), other studies reported that DNA-PKcs downregulates ATM through phosphorylation (3), creating a negative feedback loop. Previous Although the detailed mechanism is still unclear, it has been demonstrated that knock-down of DNA-PKcs decreases ATM expression in both mRNA and protein level (4), indicating a critical cross-regulation between DNA-PKcs and ATM to maintain the balance of DNA repair and other DNA damage associated signals. This regulation of DNA-PKcs and ATM in terms of expression and activity requires further investigation. Meanwhile, this work revealed that inhibition of DNA-PKcs led to mitotic slippage and thus promoted cellular senescence after radiation, which might be explained, at least partially, by its interaction with PLK (5-7). Furthermore, this study allowed me to examine various senescence inducers that drive DNA damage-dependent or independent senescence in both human and mouse cell lines.

In 2020, our collaborator from Northwestern University reported a novel covalent TERT inhibitor NU-1 (8). Through utilizing NU-1 and other commercially available TERT inhibitors targeting TERT enzymatic activity, this thesis demonstrated that TERT catalytic activity is required to effectively repair DNA double-strand breaks (DSBs) induced by ionizing radiation (IR). I further extended the effects of TERT to a specific DSB repair mechanism, non-homologous end joining (NHEJ). Although TERT is well-known due to its capability in extending telomeres and thus protecting the integrity of chromosomes (9-11), a growing number of studies have reported the telomere-independent functions of TERT, also called the non-

canonical function of TERT, which could be dependent or independent on TERT's enzymatic activity (12-16). According to the studies presented in this thesis, the role of TERT in DSB repair appears to be one of the non-canonical functions of TERT that requires enzymatic activity. However, these studies did not rule out the possibility that the catalytic-dead TERT also contributes to DNA repair and damage response (DDR). A TERT knock-out cell line, with or without expressing catalytic -active or -dead TERT (e.g., D868A (17)) may help investigate these questions in the future.

Accordingly, inhibition of TERT sensitized telomerase-positive cells to radiation and genotoxic chemotherapeutic agents. Strikingly, a significantly enhanced radiosensitization and anti-tumor immune response were observed when applying NU-1 with radiotherapy in immune-competent hosts. The in vitro experiments further revealed that NU-1 facilitates cancer cell senescence in response to IR, while these senescent cells can promote dendritic cell (DC) activation/maturation and cytotoxic T cell-priming. Meanwhile, the senescent cells induced by IR+TERT inhibition appeared to be more immunogenic than those induced by IR alone, which might be, at least partially, explained by increased DNA damage and downstream signaling pathway such as STING (18-21). Another possibility is that the non-canonical functions of TERT contribute to the immune escape of cancer cells, either directly or indirectly, which requires further studies to explore. As TERT is expressed in ~90% of cancers and is identified as a central regulator of cancer hallmarks (22), the studies in this thesis suggested a reconsideration of targeting telomerase, such as using NU-1 in this case, particularly in combination with genotoxic cancer treatments, as a tumor-specific therapy, which might help to improve the clinical outcomes.

Multiple TERT-derived epitopes have been identified in both humans and mice (23, 24). Interestingly, TERT peptide on the cell surface and/or in the tumor microenvironment has long been investigated as a tumor-specific vaccine to promote anti-tumor immunity, which has proven effective in pre-clinical models and is even being investigated in clinical trials (24-26). Although the exact functions of TERT-derived epitopes remain obscure, one strategy might be worth trying is to drive nuclear and/or cytoplasmic TERT as TERT-derived epitopes which are presented through MHC molecules, which might increase the immunosurveillance of tumor cells but decrease their resistance to cancer therapies. However, to address this approach, the mechanisms by which endogenous cytoplasmic and/or nuclear TERT can be loaded onto MHC molecules might need to be comprehended first.

In the meantime, this work indicated the effects of senescent cells on stimulating immunosurveillance of tumors. Therefore, the next chapter investigated the impacts of senescent cells on the immune response. I have used splenocytes as sensors of the senescence-induced immune response. After coculturing with senescent cells, the single-cell RNA sequencing analysis of splenocytes revealed that the dendric cell might be the primary type of immune cells regulated by senescent cells. The in vitro experiments further confirmed that senescent cells induced by DNA damage display potent impacts on activating DCs and cytotoxic T cell proliferation. Notably, the senescent cells induced by GSK461364 (a PLK-1 inhibitor) appeared not to be efficient stimuli for DC activation or T cell priming, indicating that the immunogenicity of senescent cells may be dependent on their inducers and corresponding signaling pathways. The studies in this thesis demonstrated that activated STING signals are required for senescence-mediated DC activation, which might be due to the critical functions of STING activity in cytokine secretion and MHC-dependent antigen presentation (27-29). The cGAS-STING

signaling pathway can be activated through cytoplasmic DNA (30), mitochondria DNA (31), micronuclei (32), and even DNA-containing exosomes (33), all of which can be produced by senescent cells. It has also been reported that STING activation can be directly modulated by other signals, such as ATM, the key player in DDR (34). In Chapter 1, we have discussed the various stress signals that are triggered in senescent cells by a variety of senescence-related factors, which are likely to cause different levels of STING activation through multiple mechanisms. Meanwhile, the downstream factors of STING signaling include IRF3, NF-kB, and various other transcriptional factors, inducing the expression of proteins that may cross-talk with each other and other signaling molecules, thereby forming complicated networks and/or feedback loops (35). Future studies should investigate the regulation of STING activity in senescent cells. Like many other signaling pathways, STING signals appear to be highly dynamic in different stages of senescent cells (36, 37). Therefore, the tools to track the dynamics of STING and its corresponded products will significantly contribute to our understanding of molecular modulation and even the heterogeneity of cellular senescence. Despite the cGAS-STING signals being initially identified as an innate immune response against virus attack, numerous studies have demonstrated the importance of STING in tumor cells and/or immune cells for anti-tumor immunity (38-40). Further research is necessary to investigate how STING signals are involved in regulating the immunogenicity of senescent cells. However, multiple cancer cell lines and tumors, such as gastric cancer, melanoma, colon cancer, lung cancer, and prostate cancer, have decreased STING expression via transcriptional or post-translational mechanisms (41-45). It has been demonstrated that downregulated STING is associated with poor outcomes for patients. In addition to contributing to cancer cell survival and proliferation, deficiencies in cGAS-STING signaling pathway also serve as an intrinsic mechanism for tumor

cells to escape immune surveillance, ultimately leading to treatment resistance. In light of this study showing that STING signals are necessary for tumor cell senescence-mediated immunostimulatory effects, determining how STING expression level contributes to immunogenic senescence may be an essential topic for future research. Furthermore, the development of tools for gene-editing protein expression may provide us with a promising strategy for restoring STING expression in cancer cells. In addition to the CRISPR-Cas system-based enhancement of gene transcription (46-48), other methods have been developed for activating mRNA translation, such as SINEUPs (49).

Interestingly, the surface expression of PD-L1 on DCs was also upregulated after being exposed to senescent cells, while senescence induced by IR+veliparib (a PARP inhibitor) displayed fewer effects on the expression of PD-L1, which is a well-known molecule that interacts with PD-1 on T cells and thus impedes T cell activity (50). Consistently, IR+veliparib induced senescent cells elicited the highest potency in stimulating T cell proliferation on their own. The expression of surface PD-L1 results from the coordinated action of extracellular signaling molecules, including EGF and IL-6, and intrinsic signals (34, 51). Considering that SASP composition includes both proinflammatory cytokines and growth factors, it is not surprising to see the senescence-mediated upregulation of PD-L1 on DCs after coculturing. However, the mechanisms about how veliparib triggers less PD-L1 upregulation is unclear. One possible explanation is that veliparib and other PAPR inhibitors have long been considered anti-inflammatory compounds (52-54), which might reprogram the constitution of SASP. Indeed, our studies have found that the addition of veliparib in irradiated cells decreases the secretion of IL-6 while increasing IFN- β (55). Other studies have also reported that veliparib enhances the expression of type I MHC molecules following radiation (55, 56). Thus, another explanation for

veliparib-mediated immunogenicity could be associated with antigen presentation, although the mechanisms are still to be clarified. As a non-trapping PAPR inhibitor, veliparib inhibits the parylation (also called polyADP-ribosylation) on proteins, which cross-talks with other post-translational modifications (PTMs), including phosphorylation, and therefore plays critical roles in modulating the activities and functions of proteins (57, 58). As the parylation process consumes NAD^+ (59), the addition of veliparib may also change the NAD^+/NADH ratio in cells, which plays a crucial role in regulating the redox state, mitochondria function, cell metabolism, and diverse signaling pathways (60-62). Further studies might be required to investigate how PARP proteins, particularly PARP 1, program the immunogenicity of senescent cells in terms of their effects on protein parylation and NAD^+ metabolism.

The *in vitro* examination of the immunogenicity of senescent cells in this thesis relies on coculturing them with bone marrow-derived dendritic cells (BMDCs), followed by the analysis of either the surface expression of activation markers on DCs or the T-cell priming capability of DCs. Plenty of protocols have been published to prepare BMDCs from mouse bone marrow, which usually supplements cytokines, including GM-CSF alone, GM-CSF+IL-4, or GM-CSF+Flt-3 ligand, into the cell culture medium to facilitate the differentiation of DCs. All these methods allow obtaining a high level of $CD11c^+$ DCs, but the high yield of $CD11c^+/CD103^+$ DCs can only be achieved with GM-CSF+Flt-3 ligand (63). After coculturing with senescent cells, both $CD11c^+$ DCs and $CD11c^+/CD103^+$ DCs displayed a comparable upregulation of the maturation/activation markers (CD80, CD86, H2-Kd, H2-Ld, and PD-L1 in this thesis, data not shown). However, compared to $CD11c^+/CD103^+$ DCs, $CD11c^+$ DCs showed much less capability in cross-presenting endogenous antigens to T cells and stimulating T cell proliferation (data not shown). Therefore, the studies in this thesis were all conducted using $CD11c^+/CD103^+$

DCs. In mice, the Batf3-dependent $CD103^+$ DCs are able to collect antigens from nonlymphoid tissues, including tumors, then migrate to lymph nodes and cross-present antigens during both steady-state and inflammation (64-66). The utilization of $CD103^+$ DCs may provide a better in vitro model representing tumor-infiltrating DCs and render an attractive strategy for vaccination against intracellular pathogens and tumors. Interestingly, $CD103^+$ DCs loaded with senescent cells displayed more potent effects on $CD8^+$ T cells than $CD4^+$ T cells. Further studies might be required to clarify whether the differentials are the consequences of the characteristics of $CD103^+$ DCs or senescent cells.

The senescent cells induced by IR+veliparib displayed the highest immunogenicity through in vitro experiments, so we utilized this specific type of senescent cells for in vivo investigation. Injection of senescent cells into WT BALB/c mice induced antigen-specific T cell response and protected animals from tumorigenesis. Treating tumor-bearing animals with senescent cells suppressed tumor growth, which synergized with radio- and immuno-therapy. Surprisingly, subcutaneous injection of senescent cells into mice also suppresses tumor metastasis, indicating an abscopal immune response elicited by tumor cell senescence. The conclusion of this study is consistent with the previous work from the Kron Lab, which reported that veliparib promoted tumor senescence in response to radiation, and these senescent cells serve as both traditional and in situ cancer vaccine (55). This prior art was conducted using mouse transgenic tumor cell lines expressing synthetic tumor antigens or rat antigens. The studies in this thesis utilized mouse cancer cell lines expressing endogenous but traceable tumor antigens, better imitating the actual tumor microenvironment in patients.

Our studies utilized veliparib in a concentration that displays no effects on DNA damage response, cell growth, or cellular senescence. However, veliparib delayed DNA damage repair

and sensitized tumor cells to radiation-associated growth arrest and senescence both in vitro and in vivo. These studies indicated that the immunogenic radiosensitization elicited by IR+veliparib might rely on the coordinance of DNA damage and PARP inhibition. As mentioned above, veliparib is considered a non-trapping PARP inhibitor, which is supposed to inhibit the catalytic activity of PARP1/2 by competitive inhibition of β-NAD^+ binding site of PARP-1 and PARP-2 (67). However, there are trapping PARP inhibitors (later referred to as PARP poisons), causing both catalytic inhibition and PARP trapping to form PARP-DNA complexes and eventually endogenous DNA breaks. The PARP poisons rucaparib, olaparib, niraparib, and talazoparib, which display increased trapping ability, are primarily used as single agents and have reached the clinic to treat multiple cancers, particularly those carries BRAC mutations (68-71). The recent pre-clinical and clinical studies have reported the combination of PARP poisons and immunotherapy as a promising strategy to improve patient outcomes (72-75). In light of the fact that PARP poison can effectively induce tumor cell senescence on its own (76-79), it may be worth investigating the immunogenicity of senescent cells induced by a single PARP poison, as well as their potential use as cancer vaccines.

As discussed in Chapter 4, the cancer vaccine has been resurging from the last decade (80). Among all the platforms for cancer vaccines, the whole cell-based vaccines offered the advantage of not requiring a search for the most potent tumor antigen, which might otherwise be a bottleneck in developing a cancer vaccine (80). Current whole tumor cell vaccines are intended to enhance immunogenicity by driving the expression of cytokines such as GM-CSF by gene editing, as well as to decrease proliferation by radiation (80-82). Senescent tumor cells, which already enter an irreversible cell cycle arrest and produce the SASP, including GM-CSF, might offer an all-in-one platform as whole tumor cell-based cancer vaccines. Our studies have

demonstrated the efficacy of the senescence vaccine in suppressing tumor growth and metastasis using synergic mouse tumor models. Meanwhile, our study indicated that the choice of senescence inducers and the timing and dosage for vaccination should be carefully examined before application in the clinic.

Although the reversibility of cellular senescence (78, 83-85), particularly therapy-induced senescence , remains controversial, this may draw concerns about the safety of using live senescent cells as cancer vaccines. As previous in vitro studies indicated that senescent cells mediate T cell response through DCs, this thesis also examined the potential of utilizing DCs stimulated by senescent tumor cells ex vivo as cancer vaccines. Consistent with the senescence vaccine, this DC vaccine displayed suppressive effects on local tumor growth and metastasis. One example of the DC-based cancer vaccines is Sipuleucel-T (86), the first therapeutic cancer vaccine approved by the FDA, proving DC vaccines' feasibility for cancer treatment. Multiple other DC vaccines are currently under pre-clinical and/or clinical investigation (87-89). Currently, tumor antigens can be loaded into DCs using tumor cell lysates, specific tumor antigens, or yeast wall particles carrying tumor antigens (87, 90). Then DCs might be exposed to specific cytokines such as GM-CSF to increase their immunogenicity further (87, 90). Coculturing with senescent cells provides a novel strategy for loading and activating DCs *ex vivo*. Moreover, the effects of senescence-loaded DC vaccine on tumor metastasis make it a promising candidate as adjuvant cancer therapy.

A large proportion of this thesis describes the beneficial impacts of therapy-induced senescence on cancer therapies. However, a growing number of studies have reported the detrimental roles of senescence in cancer, including promoting proliferating, facilitating metastasis, stimulating stemness, suppressing immunosurveillance, which contributes to the

resistance to therapy and cancer recurrence (91, 92). In order to alleviate the harmful effects of senescent cells, one strategy is to specifically eliminate senescent cells using senolytics, a class of compounds targeting the vulnerability of cellular senescence (93, 94). In cancer therapy, senolytic compounds have been used to eradicate senescent cells after primary therapy that leads to cell death and senescence (95-97). This approach has been described as "one-two punch" for cancer (98). One widely used senolytic compound is the BCL-2 inhibitor, ABT263 (99, 100). This thesis has compared the sensitivity of senescent cells induced by different methods to ABT263 induced apoptosis. Interestingly, this work demonstrated that DNA-damage-associated senescent cells appear to be more sensitive to ABT263 than DNA-damage-independent senescent cells. This observation is consistent with a recent study that suggested that radiation or olaparib but not anti-androgen enzalutamide-induced senescent cells are sensitive to ABT263 and A-1155463 (a specific BCL-xL inhibitor) (101). However, the molecular mechanisms regulating the senescence sensitivity to ABT263 remain unclarified. This thesis examined the association between ABT263 sensitivity and the expression of BH3 proteins (Bim, Bak, and NOXA) in senescent cells but was unable to determine a definitive pattern. The possibility of activated signals in DNA-damaged senescent cells also led me to investigate which signals might play an essential role in regulating the survival of senescent cells upon ABT263 treatment by using a small panel of inhibitors, including ATM inhibitor KU-55933, NF-kB inhibitor SC75741, STAT3 inhibitor stattic, STAT1 inhibitor Fludarabine, and cGAS inhibitor RU.521 (data not shown). The observations revealed that SC75741 significantly sensitizes senescent cells to ABT263-induced senolysis, whether they are DNA damage-dependent or not. However, SC75741 also sensitizes non-senescent cells to ABT263-induced apoptosis, which is consistent with NF-kB studies as a pro-survival signaling pathway. These results indicated that the effects

of NF-kB on ABT263 response are not restricted to senescent cells. The utilization of high-through omics studies in senescent cells might contribute to understanding the differences among senescence induced by various stimuli, which may also contribute to identifying the molecular mechanisms that control the cell fate of senescence in response to ABT263.

Another observation of this thesis study is that senescent cells appeared to increase the sensitivity of the neighboring non-senescent cells to ABT263 induced apoptosis in a SASP-dependent manner. As discussed in Chapter 1, SASP consists of diverse bioactive factors, including growth factors, cytokines, chemokines, proteases, DNA fragments, microRNA, and even exosomes (102). It is challenging to explore which SASP compounds are responsible for the bystander effects of senescent cells on ABT263 response. Alternatively, it may be possible to compare the SASP composition between senescent cells that induce greater or lesser bystander effects on non-senescent cells through proteomics and secretome studies. These studies may provide insight into the signaling pathways responsible for the senescence-associated bystander effects. Furthermore, the efficacy of "one-two punch" cancer therapy could be further enhanced if senescent cells could act as bystanders to prompt non-senescent tumor cells to respond to senolytic therapy. Future investigations on this topic might be required to maximize the utilization of senescence functions for improving clinical outcomes.

6.1 References

1. Liu Y, Efimova EV, Ramamurthy A, and Kron SJ. Repair-independent functions of DNA-PKcs protect irradiated cells from mitotic slippage and accelerated senescence. *J Cell Sci.* 2019;132(13).

2. Blackford AN, and Jackson SP. ATM, ATR, and DNA-PK: The Trinity at the Heart of the DNA Damage Response. *Molecular Cell.* 2017;66(6):801-17.

3. Zhou Y, Lee JH, Jiang W, Crowe JL, Zha S, and Paull TT. Regulation of the DNA Damage Response by DNA-PKcs Inhibitory Phosphorylation of ATM. *Mol Cell.* 2017;65(1):91-104.

4. Peng Y, Woods RG, Beamish H, Ye R, Lees-Miller SP, Lavin MF, et al. Deficiency in the catalytic subunit of DNA-dependent protein kinase causes down-regulation of ATM. *Cancer Res.* 2005;65(5):1670-7.

5. Huang B, Shang ZF, Li B, Wang Y, Liu XD, Zhang SM, et al. DNA-PKcs Associates With PLK1 and Is Involved in Proper Chromosome Segregation and Cytokinesis. *J Cell Biochem.* 2014;115(6):1077-88.

6. Lee KJ, Lin YF, Chou HY, Yajima H, Fattah KR, Lee SC, et al. Involvement of DNA-dependent Protein Kinase in Normal Cell Cycle Progression through Mitosis. *J Biol Chem.* 2011;286(14).

7. Douglas P, Ye R, Trinkle-Mulcahy L, Neal JA, De Wever V, Morrice NA, et al. Polo-like kinase 1 (PLK1) and protein phosphatase 6 (PP6) regulate DNA-dependent protein kinase catalytic subunit (DNA-PKcs) phosphorylation in mitosis. *Biosci Rep.* 2014;34(3).

8. Betori RC, Liu Y, Mishra RK, Cohen SB, Kron SJ, and Scheidt KA. Targeted Covalent Inhibition of Telomerase. *ACS Chem Biol.* 2020;15(3):706-17.

9. Greider CW, and Blackburn EH. Identification of a specific telomere terminal transferase activity in Tetrahymena extracts. *Cell.* 1985;43(2 Pt 1):405-13.

10. Feng J, Funk WD, Wang SS, Weinrich SL, Avilion AA, Chiu CP, et al. The RNA component of human telomerase. *Science.* 1995;269(5228):1236-41.

11. Kim NW, Piatyszek MA, Prowse KR, Harley CB, West MD, Ho PL, et al. Specific association of human telomerase activity with immortal cells and cancer. *Science.* 1994;266(5193):2011-5.

12. Thompson CAH, and Wong JMY. Non-canonical Functions of Telomerase Reverse Transcriptase: Emerging Roles and Biological Relevance. *Curr Top Med Chem.* 2020;20(6):498-507.

13. Chiodi I, and Mondello C. Telomere-independent functions of telomerase in nuclei, cytoplasm, and mitochondria. *Front Oncol.* 2012;2:133.

14. Segal-Bendirdjian E, and Geli V. Non-canonical Roles of Telomerase: Unraveling the Imbroglio. *Front Cell Dev Biol.* 2019;7:332.

15. Cao Y, Li H, Deb S, and Liu JP. TERT regulates cell survival independent of telomerase enzymatic activity. *Oncogene.* 2002;21(20):3130-8.

16. Yuan X, Larsson C, and Xu D. Mechanisms underlying the activation of TERT transcription and telomerase activity in human cancer: old actors and new players. *Oncogene.* 2019;38(34):6172-83.

17. Weinrich SL, Pruzan R, Ma L, Ouellette M, Tesmer VM, Holt SE, et al. Reconstitution of human telomerase with the template RNA component hTR and the catalytic protein subunit hTRT. *Nat Genet.* 1997;17(4):498-502.

18. Mouw KW, Goldberg MS, Konstantinopoulos PA, and D'Andrea AD. DNA Damage and Repair Biomarkers of Immunotherapy Response. *Cancer Discov.* 2017;7(7):675-93.

19. Deng L, Liang H, Xu M, Yang X, Burnette B, Arina A, et al. STING-Dependent Cytosolic DNA Sensing Promotes Radiation-Induced Type I Interferon-Dependent Antitumor Immunity in Immunogenic Tumors. *Immunity.* 2014;41(5):843-52.

20. Lhuillier C, Rudqvist NP, Elemento O, Formenti SC, and Demaria S. Radiation therapy and anti-tumor immunity: exposing immunogenic mutations to the immune system. *Genome Med.* 2019;11(1):40.

21. Golden EB, Pellicciotta L, Demaria S, Barcellos-Hoff MH, and Formenti SC. The convergence of radiation and immunogenic cell death signaling pathways. *Frontiers in Oncology.* 2012;2:1-13.

22. Low KC, and Tergaonkar V. Telomerase: central regulator of all of the hallmarks of cancer. *Trends Biochem Sci.* 2013;38(9):426-34.

23. Vonderheide RH. Telomerase as a universal tumor-associated antigen for cancer immunotherapy. *Oncogene.* 2002;21(4):674-9.

24. Godet Y, Fabre E, Dosset M, Lamuraglia M, Levionnois E, Ravel P, et al. Analysis of Spontaneous Tumor-Specific CD4 T-cell Immunity in Lung Cancer Using Promiscuous HLA-DR Telomerase-Derived Epitopes: Potential Synergistic Effect with Chemotherapy Response. *Clin Cancer Res.* 2012;18(10):2943-53.

25. Zanetti M. A second chance for telomerase reverse transcriptase in anticancer immunotherapy. *Nat Rev Clin Oncol.* 2017;14(2):115-28.

26. Ellingsen EB, Mangsbo SM, Hovig E, and Gaudernack G. Telomerase as a Target for Therapeutic Cancer Vaccines and Considerations for Optimizing Their Clinical Potential. *Front Immunol.* 2021;12.

27. Li T, Cheng H, Yuan H, Xu Q, Shu C, Zhang Y, et al. Antitumor Activity of cGAMP via Stimulation of cGAS-cGAMP-STING-IRF3 Mediated Innate Immune Response. *Sci Rep.* 2016;6:19049.

28. Barber GN. STING: infection, inflammation and cancer. *Nat Rev Immunol.* 2015;15(12):760-70.

29. Jiang M, Chen P, Wang L, Li W, Chen B, Liu Y, et al. cGAS-STING, an important pathway in cancer immunotherapy. *J Hematol Oncol.* 2020;13(1):81.

30. Chen Q, Sun L, and Chen ZJ. Regulation and function of the cGAS-STING pathway of cytosolic DNA sensing. *Nat Immunol.* 2016;17(10):1142-9.

31. Maekawa H, Inoue T, Ouchi H, Jao TM, Inoue R, Nishi H, et al. Mitochondrial Damage Causes Inflammation via cGAS-STING Signaling in Acute Kidney Injury. *Cell Rep.* 2019;29(5):1261-73 e6.

32. Mackenzie KJ, Carroll P, Martin CA, Murina O, Fluteau A, Simpson DJ, et al. cGAS surveillance of micronuclei links genome instability to innate immunity. *Nature.* 2017;548(7668):461-5.

33. Kitai Y, Kawasaki T, Sueyoshi T, Kobiyama K, Ishii KJ, Zou J, et al. DNA-Containing Exosomes Derived from Cancer Cells Treated with Topotecan Activate a STING-Dependent Pathway and Reinforce Antitumor Immunity. *J Immunol.* 2017;198(4):1649-59.

34. Dehkordi SK, Walker J, Sah E, Bennett E, Atrian F, Frost B, et al. Profiling senescent cells in human brains reveals neurons with CDKN2D/p19 and tau neuropathology. *Nature Aging.* 2021;1(12):1107-16.

35. Wan DS, Jiang W, and Hao JW. Research Advances in How the cGAS-STING Pathway Controls the Cellular Inflammatory Response. *Front Immunol.* 2020;11.

36. Lee S, and Schmitt CA. The dynamic nature of senescence in cancer. *Nat Cell Biol.* 2019;21(1):94-101.

37. Hopfner KP, and Hornung V. Molecular mechanisms and cellular functions of cGAS-STING signalling. *Nat Rev Mol Cell Biol.* 2020;21(9):501-21.

38. Leventhal DS, Sokolovska A, Li N, Plescia C, Kolodziej SA, Gallant CW, et al. Immunotherapy with engineered bacteria by targeting the STING pathway for anti-tumor immunity. *Nat Commun.* 2020;11(1):2739.

39. Lu CZ, Guan JH, Lu S, Jin QH, Rousseau B, Lu TS, et al. DNA Sensing in Mismatch Repair-Deficient Tumor Cells Is Essential for Anti-tumor Immunity. *Cancer Cell.* 2021;39(1):96-+.

40. Corrales L, Glickman LH, McWhirter SM, Kanne DB, Sivick KE, Katibah GE, et al. Direct Activation of STING in the Tumor Microenvironment Leads to Potent and Systemic Tumor Regression and Immunity. *Cell Rep.* 2015;11(7):1018-30.

41. Tan YS, Sansanaphongpricha K, Xie Y, Donnelly CR, Luo X, Heath BR, et al. Mitigating SOX2-potentiated Immune Escape of Head and Neck Squamous Cell Carcinoma with a STING-inducing Nanosatellite Vaccine. *Clin Cancer Res.* 2018;24(17):4242-55.

42. Kitajima S, Ivanova E, Guo S, Yoshida R, Campisi M, Sundararaman SK, et al. Suppression of STING Associated with LKB1 Loss in KRAS-Driven Lung Cancer. *Cancer Discov.* 2019;9(1):34-45.

43. Xia T, Konno H, Ahn J, and Barber GN. Deregulation of STING Signaling in Colorectal Carcinoma Constrains DNA Damage Responses and Correlates With Tumorigenesis. *Cell Rep.* 2016;14(2):282-97.

44. Xia T, Konno H, and Barber GN. Recurrent Loss of STING Signaling in Melanoma Correlates with Susceptibility to Viral Oncolysis. *Cancer Res.* 2016;76(22):6747-59.

45. Song S, Peng P, Tang Z, Zhao J, Wu W, Li H, et al. Decreased expression of STING predicts poor prognosis in patients with gastric cancer. *Sci Rep.* 2017;7:39858.

46. Rauch S, He C, and Dickinson BC. Targeted m(6)A Reader Proteins To Study Epitranscriptomic Regulation of Single RNAs. *J Am Chem Soc.* 2018;140(38):11974-81.

47. Bikard D, Jiang WY, Samai P, Hochschild A, Zhang F, and Marraffini LA. Programmable repression and activation of bacterial gene expression using an engineered CRISPR-Cas system. *Nucleic Acids Res.* 2013;41(15):7429-37.

48. Casas-Mollano JA, Zinselmeier MH, Erickson SE, and Smanski MJ. CRISPR-Cas Activators for Engineering Gene Expression in Higher Eukaryotes. *CRISPR J.* 2020;3(5):350-64.

49. Zucchelli S, Cotella D, Takahashi H, Carrieri C, Cimatti L, Fasolo F, et al. SINEUPs: A new class of natural and synthetic antisense long non-coding RNAs that activate translation. *RNA Biol.* 2015;12(8):771-9.

50. Iwai Y, Ishida M, Tanaka Y, Okazaki T, Honjo T, and Minato N. Involvement of PD-L1 on tumor cells in the escape from host immune system and tumor immunotherapy by PD-L1 blockade. *Proc Natl Acad Sci U S A.* 2002;99(19):12293-7.

51. Cha JH, Chan LC, Li CW, Hsu JL, and Hung MC. Mechanisms Controlling PD-L1 Expression in Cancer. *Mol Cell.* 2019;76(3):359-70.

52. Kovacs K, Vaczy A, Fekete K, Kovari P, Atlasz T, Reglodi D, et al. PARP Inhibitor Protects Against Chronic Hypoxia/Reoxygenation-Induced Retinal Injury by Regulation

of MAPKs, HIF1alpha, Nrf2, and NFkappaB. *Invest Ophthalmol Vis Sci.* 2019;60(5):1478-90.

53. Giansanti V, Dona F, Tillhon M, and Scovassi AI. PARP inhibitors: new tools to protect from inflammation. *Biochem Pharmacol.* 2010;80(12):1869-77.

54. Mabley JG, Jagtap P, Perretti M, Getting SJ, Salzman AL, Virag L, et al. Anti-inflammatory effects of a novel, potent inhibitor of poly (ADP-ribose) polymerase. *Inflamm Res.* 2001;50(11):561-9.

55. Meng Y, Efimova EV, Hamzeh KW, Darga TE, Mauceri HJ, Fu YX, et al. Radiation-inducible immunotherapy for cancer: senescent tumor cells as a cancer vaccine. *Mol Ther.* 2012;20(5):1046-55.

56. Seyedin SN, Hasibuzzaman MM, Pham V, Petronek MS, Callaghan C, Kalen AL, et al. Combination Therapy with Radiation and PARP Inhibition Enhances Responsiveness to Anti-PD-1 Therapy in Colorectal Tumor Models. *Int J Radiat Oncol Biol Phys.* 2020;108(1):81-92.

57. Alemasova EE, and Lavrik OI. Poly(ADP-ribosyl)ation by PARP1: reaction mechanism and regulatory proteins. *Nucleic Acids Res.* 2019;47(8):3811-27.

58. Morales J, Li L, Fattah FJ, Dong Y, Bey EA, Patel M, et al. Review of poly (ADP-ribose) polymerase (PARP) mechanisms of action and rationale for targeting in cancer and other diseases. *Crit Rev Eukaryot Gene Expr.* 2014;24(1):15-28.

59. Du L, Zhang X, Han YY, Burke NA, Kochanek PM, Watkins SC, et al. Intra-mitochondrial poly(ADP-ribosylation) contributes to NAD+ depletion and cell death induced by oxidative stress. *J Biol Chem.* 2003;278(20):18426-33.

60. Ying W. NAD+/NADH and NADP+/NADPH in cellular functions and cell death: regulation and biological consequences. *Antioxid Redox Signal.* 2008;10(2):179-206.

61. Srivastava S. Emerging therapeutic roles for NAD(+) metabolism in mitochondrial and age-related disorders. *Clin Transl Med.* 2016;5(1):25.

62. Amjad S, Nisar S, Bhat AA, Shah AR, Frenneaux MP, Fakhro K, et al. Role of NAD(+) in regulating cellular and metabolic signaling pathways. *Mol Metab.* 2021;49:101195.

63. Mayer CT, Ghorbani P, Nandan A, Dudek M, Arnold-Schrauf C, Hesse C, et al. Selective and efficient generation of functional Batf3-dependent CD103+ dendritic cells from mouse bone marrow. *Blood.* 2014;124(20):3081-91.

64. Merad M, Sathe P, Helft J, Miller J, and Mortha A. The Dendritic Cell Lineage: Ontogeny and Function of Dendritic Cells and Their Subsets in the Steady State and the Inflamed Setting. *Annu Rev Immunol.* 2013;31:563-604.

65. Henri S, Poulin LF, Tamoutounour S, Ardouin L, Guilliams M, de Bovis B, et al. CD207+ CD103+ dermal dendritic cells cross-present keratinocyte-derived antigens irrespective of the presence of Langerhans cells. *J Exp Med.* 2010;207(1):189-206.

66. Bedoui S, Whitney PG, Waithman J, Eidsmo L, Wakim L, Caminschi I, et al. Cross-presentation of viral and self antigens by skin-derived CD103+ dendritic cells. *Nat Immunol.* 2009;10(5):488-95.

67. Donawho CK, Luo Y, Luo Y, Penning TD, Bauch JL, Bouska JJ, et al. ABT-888, an orally active poly(ADP-ribose) polymerase inhibitor that potentiates DNA-damaging agents in preclinical tumor models. *Clin Cancer Res.* 2007;13(9):2728-37.

68. Thomas A, Murai J, and Pommier Y. The evolving landscape of predictive biomarkers of response to PARP inhibitors. *J Clin Invest.* 2018;128(5):1727-30.

69. Antolin AA, Ameratunga M, Banerji U, Clarke PA, Workman P, and Al-Lazikani B. The kinase polypharmacology landscape of clinical PARP inhibitors. *Sci Rep.* 2020;10(1):2585.

70. Paluch-Shimon S, and Cardoso F. PARP inhibitors coming of age. *Nat Rev Clin Oncol.* 2021;18(2):69-70.

71. Rose M, Burgess JT, O'Byrne K, Richard DJ, and Bolderson E. PARP Inhibitors: Clinical Relevance, Mechanisms of Action and Tumor Resistance. *Front Cell Dev Biol.* 2020;8:564601.

72. Jiao S, Xia W, Yamaguchi H, Wei Y, Chen MK, Hsu JM, et al. PARP Inhibitor Upregulates PD-L1 Expression and Enhances Cancer-Associated Immunosuppression. *Clin Cancer Res.* 2017;23(14):3711-20.

73. Lampert EJ, Zimmer A, Padget M, Cimino-Mathews A, Nair JR, Liu Y, et al. Combination of PARP Inhibitor Olaparib, and PD-L1 Inhibitor Durvalumab, in Recurrent Ovarian Cancer: a Proof-of-Concept Phase II Study. *Clin Cancer Res.* 2020;26(16):4268-79.

74. Palaia I, Tomao F, Sassu CM, Musacchio L, and Benedetti Panici P. Immunotherapy For Ovarian Cancer: Recent Advances And Combination Therapeutic Approaches. *Onco Targets Ther.* 2020;13:6109-29.

75. Vikas P, Borcherding N, Chennamadhavuni A, and Garje R. Therapeutic Potential of Combining PARP Inhibitor and Immunotherapy in Solid Tumors. *Front Oncol.* 2020;10:570.

76. Jia Y, Jin H, Gao L, Yang X, Wang F, Ding H, et al. A novel lncRNA PLK4 up-regulated by talazoparib represses hepatocellular carcinoma progression by promoting YAP-mediated cell senescence. *J Cell Mol Med.* 2020;24(9):5304-16.

77. Wang Z, Gao J, Zhou J, Liu H, and Xu C. Olaparib induced senescence under P16 or P53 dependent manner in ovarian cancer. *J Gynecol Oncol.* 2019;30(2):e26.

78. Fleury H, Malaquin N, Tu V, Gilbert S, Martinez A, Olivier MA, et al. Exploiting interconnected synthetic lethal interactions between PARP inhibition and cancer cell reversible senescence. *Nature Communications.* 2019;10.

79. Lombard AP, Armstrong CM, D'Abronzo LS, Ning S, Leslie AR, Sharifi M, et al. Olaparib Induced Senescence is Bypassed through G2/M Checkpoint Override in Olaparib Resistant Prostate Cancer. *Mol Cancer Ther.* 2022.

80. Vergati M, Intrivici C, Huen NY, Schlom J, and Tsang KY. Strategies for cancer vaccine development. *J Biomed Biotechnol.* 2010;2010.

81. Saxena M, van der Burg SH, Melief CJM, and Bhardwaj N. Therapeutic cancer vaccines. *Nat Rev Cancer.* 2021;21(6):360-78.

82. Melief CJM, van Hall T, Arens R, Ossendorp F, and van der Burg SH. Therapeutic cancer vaccines. *Journal of Clinical Investigation.* 2015;125(9):3401-12.

83. Hall BM, Balan V, Gleiberman AS, Strom E, Krasnov P, Virtuoso LP, et al. p16(Ink4a) and senescence-associated beta-galactosidase can be induced in macrophages as part of a reversible response to physiological stimuli. *Aging (Albany NY).* 2017;9(8):1867-84.

84. Krejci P, Prochazkova J, Smutny J, Chlebova K, Lin P, Aklian A, et al. FGFR3 signaling induces a reversible senescence phenotype in chondrocytes similar to oncogene-induced premature senescence. *Bone.* 2010;47(1):102-10.

85. Beausejour CM, Krtolica A, Galimi F, Narita M, Lowe SW, Yaswen P, et al. Reversal of human cellular senescence: roles of the p53 and p16 pathways. *EMBO J.* 2003;22(16):4212-22.

86. Cheever MA, and Higano CS. PROVENGE (Sipuleucel-T) in prostate cancer: the first FDA-approved therapeutic cancer vaccine. *Clin Cancer Res.* 2011;17(11):3520-6.

87. Ahmed MS, and Bae YS. Dendritic cell-based therapeutic cancer vaccines: past, present and future. *Clin Exp Vaccine Res.* 2014;3(2):113-6.

88. Saxena M, Balan S, Roudko V, and Bhardwaj N. Towards superior dendritic-cell vaccines for cancer therapy. *Nat Biomed Eng.* 2018;2(6):341-6.

89. Hu Z, Ott PA, and Wu CJ. Towards personalized, tumour-specific, therapeutic vaccines for cancer. *Nat Rev Immunol.* 2018;18(3):168-82.

90. Banchereau J, and Palucka AK. Dendritic cells as therapeutic vaccines against cancer. *Nature Reviews Immunology.* 2005;5(4):296-306.

91. Wang B, Kohli J, and Demaria M. Senescent Cells in Cancer Therapy: Friends or Foes? *Trends Cancer.* 2020;6(10):838-57.

92. Coppe JP, Desprez PY, Krtolica A, and Campisi J. The senescence-associated secretory phenotype: the dark side of tumor suppression. *Annu Rev Pathol.* 2010;5:99-118.

93. Dolgin E. Send in the senolytics. *Nat Biotechnol.* 2020;38(12):1371-7.

94. Kirkland JL, Tchkonia T, Zhu Y, Niedernhofer LJ, and Robbins PD. The Clinical Potential of Senolytic Drugs. *J Am Geriatr Soc.* 2017;65(10):2297-301.

95. Qing Y, Li H, Zhao Y, Hu P, Wang X, Yu X, et al. One-Two Punch Therapy for the Treatment of T-Cell Malignancies Involving p53-Dependent Cellular Senescence. *Oxid Med Cell Longev.* 2021;2021:5529518.

96. Wang C, Vegna S, Jin H, Benedict B, Lieftink C, Ramirez C, et al. Inducing and exploiting vulnerabilities for the treatment of liver cancer. *Nature.* 2019;574(7777):268-72.

97. Fletcher-Sananikone E, Kanji S, Tomimatsu N, Di Cristofaro LFM, Kollipara RK, Saha D, et al. Elimination of Radiation-Induced Senescence in the Brain Tumor Microenvironment Attenuates Glioblastoma Recurrence. *Cancer Res.* 2021;81(23):5935-47.

98. Prasanna PG, Citrin DE, Hildesheim J, Ahmed MM, Venkatachalam S, Riscuta G, et al. Therapy-Induced Senescence: Opportunities to Improve Anticancer Therapy. *J Natl Cancer Inst.* 2021;113(10):1285-98.

99. Saleh T, Carpenter VJ, Tyutyunyk-Massey L, Murray G, Leverson JD, Souers AJ, et al. Clearance of therapy-induced senescent tumor cells by the senolytic ABT-263 via interference with BCL-XL -BAX interaction. *Mol Oncol.* 2020;14(10):2504-19.

100. Zhu Y, Tchkonia T, Fuhrmann-Stroissnigg H, Dai HM, Ling YY, Stout MB, et al. Identification of a novel senolytic agent, navitoclax, targeting the Bcl-2 family of anti-apoptotic factors. *Aging Cell.* 2016;15(3):428-35.

101. Malaquin N, Vancayseele A, Gilbert S, Antenor-Habazac L, Olivier MA, Ait Ali Brahem Z, et al. DNA Damage- But Not Enzalutamide-Induced Senescence in Prostate Cancer Promotes Senolytic Bcl-xL Inhibitor Sensitivity. *Cells.* 2020;9(7).

102. Faget DV, Ren Q, and Stewart SA. Unmasking senescence: context-dependent effects of SASP in cancer. *Nat Rev Cancer.* 2019;19(8):439-53.